

TESIS DOCTORAL

EL PAPEL DE LA PROTEÍNA HSP90 EN EL  
MICROAMBIENTE TUMORAL

PhD THESIS

THE ROLE OF HSP90 IN SHAPING  
AGGRESSIVE TUMOR  
MICROENVIRONMENTS

AUTORA

SILVIA DOMÍNGUEZ GARCÍA

DIRECTORES

DR. FERNANDO CALVO GONZÁLEZ

DRA. ANA VICTORIA VILLAR RAMOS

UNIVERSIDAD DE CANTABRIA

Escuela de Doctorado de la Universidad de Cantabria

Santander 2024





El Dr. FERNANDO CALVO GONZÁLEZ, Investigador Principal del grupo Microambiente Tumoral en el Departamento de Señalización Molecular y Celular en el Instituto de Biomedicina y Biotecnología de Cantabria (IBBTEC)

CERTIFICA: que SILVIA DOMÍNGUEZ GARCÍA ha realizado bajo su dirección la presente Tesis Doctoral titulada “El papel de la proteína HSP90 en el microambiente tumoral” (“The role of HSP90 in shaping aggressive tumor microenvironments”).

Considero que este trabajo reúne los requisitos de originalidad y calidad científica necesarios para su presentación como Memoria de Doctorado al objeto de optar al grado de Doctor en Biología Molecular y Biomedicina por la Universidad de Cantabria, con mención internacional.

Y para que conste y surta los efectos oportunos, firmo el presente certificado en Santander a 4 de marzo de 2024.



Fdo: Dr. Fernando Calvo González



El presente trabajo de tesis titulado “El papel de la proteína HSP90 en el microambiente tumoral” (“The role of HSP90 in shaping aggressive tumor microenvironments”) fue realizado en el Instituto de Biología y Biomedicina de Cantabria (IBBTEC), en el laboratorio de Microambiente Tumoral, en Santander (Cantabria), gracias a la financiación y ayuda de los siguientes organismos:





*A mi familia*



# Resumen

Los Fibroblastos Asociados al Cáncer (CAFs) son componentes clave del microambiente tumoral (TME) con implicaciones importantes en cáncer, desempeñando funciones como la producción y remodelación de la matriz extracelular (ECM), angiogénesis, interacción con el sistema inmune y la promoción del crecimiento tumoral y la metástasis. Por lo general, tienen su origen en la activación patológica de sus precursores, cuando son expuestos a estímulos procedentes de las células cancerígenas. Sin embargo, sus posibles implicaciones terapéuticas aún no han sido exploradas. El análisis bioinformático de bases de datos públicas identificó a HSP90 como un regulador clave del TME. HSP90 es una proteína chaperona con dos isoformas, HSP90 $\alpha$  y HSP90 $\beta$ , cuya expresión generalmente se induce en condiciones estresantes, y que tiene implicaciones importantes en el cáncer y enfermedades fibróticas. Para investigar el posible papel de HSP90 en los CAFs, inhibimos la expresión de HSP90 $\alpha/\beta$  utilizando ARN interferente y realizamos una caracterización molecular y funcional extensa *in vitro* e *in vivo*. Nuestros datos demuestran que el silenciamiento de HSP90 $\alpha$  afecta específicamente varias características clave de los CAFs tales como su capacidad para remodelar la ECM, migración y la comunicación con células cancerígenas. Lo mismo sucede cuando tratamos fibroblastos normales con TGF $\beta$ , un conocido activador de estos mismos. Además, estudios de proteómica y RNAseq demuestran las implicaciones de HSP90 $\alpha$  en la modulación de procesos moleculares y celulares clave asociados con la regulación de los CAFs, incluyendo la actividad de YAP/TAZ. Asimismo, experimentos *in vivo* utilizando un modelo murino con delección específica de *Hsp90aa1* en el estroma demuestran el papel crítico de HSP90 $\alpha$  estromal en la promoción del crecimiento tumoral y la metástasis del cáncer de mama. En resumen, nuestros resultados describen una nueva función de HSP90 $\alpha$  en la modulación del fenotipo pro-tumoral de los CAFs, a través de la regulación de la actividad de YAP/TAZ.



# Abstract

Cancer Associated Fibroblasts (CAFs) are key components of the tumor microenvironment (TME) with important implications in all hallmarks of cancer, with functions such as Extracellular Matrix (ECM) production and remodeling, promotion of angiogenesis, immune crosstalk and induction of tumor growth and metastasis. CAFs generally originate from the pathological activation of normal precursors exposed to stressful insults emanating from the cancer cells, and are emerging as unexplored promising targets for anti-cancer therapies. Bioinformatic analysis of publicly available datasets identified HSP90 as a key regulator of the tumor stroma. HSP90 is a chaperone protein with two major isoforms, HSP90 $\alpha$  and HSP90 $\beta$ , whose expression is usually induced by stressful conditions, with important implications in cancer and fibrotic diseases. To investigate the possible role of HSP90 in CAFs, we depleted HSP90 $\alpha/\beta$  expression using siRNAs, and performed extensive molecular and functional characterization *in vitro* and *in vivo*. Our data demonstrates that the silencing of HSP90 $\alpha$  specifically impaired several key characteristics of CAFs, including ECM remodeling, migration and crosstalk with cancer cells. Similar results were obtained when treating normal fibroblasts with TGF $\beta$ , a well-known activator of fibroblasts. Further proteomics and RNAseq studies demonstrated HSP90 $\alpha$  implications in modulating key molecular and cellular processes associated with CAF regulation, including YAP/TAZ activities. In addition, *in vivo* experiments using a murine model with *Hsp90aa1* deletion in the stroma demonstrated a critical role of stromal HSP90 $\alpha$  in promoting breast cancer tumor growth and metastasis. Taken together, our results describe a novel function of HSP90 $\alpha$  in modulating the pro-tumoral phenotype of CAFs through regulation of YAP/TAZ activities.



# Abbreviations

ACN	Acetonitrile
apCAFs	Antigen-presenting CAFs
APS	Ammonium persulfate
BC	Breast Cancer
BSA	Albumin Bovine Fraction V
CAA	2-Chloroacetamide
CAF	Cancer Associated Fibroblast
CDM	Cell Derived Matrix
CHX	Cycloheximide
CR	Colorectal cancer
Ctrl	Control
Co-IP	Co-immunoprecipitation
DEGs	Differentially Expressed Genes
DEPs	Differentially Expressed Proteins
DIA	Data-Independent Acquisition
DMEM	Dulbecco's Modified Eagle Medium
DMSO	Dimethyl Sulfoxide
DTT	Dithiothreitol
ECL	Enhanced chemoluminescence
ECM	Extracellular Matrix
EDTA	Ethylene diamine tetra-acetic acid
EGF	Epithelial Growth Factor
eHSP90	Extracellular HSP90
EMT	Epithelial to mesenchymal transition
endEMT	Endothelial to mesenchymal transition
ER	Endoplasmic Reticulum
ERneg	Estrogen receptor negative
FAP	Fibroblast Activation Protein
FDR	False Discovery Rate
FXR	Farnesoid X Receptor
GFP	Green Fluorescent Protein
GO	Gene Ontology
GRP94	Glucose-Regulated Protein 94
GSEA	Gene-Set Enrichment Analysis
Gu-HCl	Guanidine Hydrochloride
H&E	Hematoxylin and Eosin
HE	Heterozygous
HeNe	Helium-Neon

HGF	Hepatocyte Growth Factor
HSF1	Heat Shock Factor 1
HSP90	Heat Shock Protein 90
HSP90i	HSP90 inhibitors
HSR	Heat Shock Response
iCAFs	Inflammatory CAFs
IF	Immunofluorescence
IHC	Immunohistochemistry
IL	Interleukin
ITS	Insulin Transferrin Selenium
KEGG	Kyoto Encyclopedia of Genes and Genomes
KO	Knock-out
LCM	Laser Capture Microdissection
LC-MS	Liquid Chromatography/Mass-spectrometry
LINCS	Library of Integrated Network-Based Cellular Signatures
LyC	Lysil Endopeptidase
MHC	Major Histocompatibility Complex
MLC2	Myosin Light Chain 2
MMP	Matrix Metalloproteinase
MMTV-PyMT	Mouse mammary tumor virus-polyoma middle tumor-antigen
NF	Normal Fibroblast
myCAFs	Myofibroblastic CAFs
NCE	Normalized Collision Energy
NES	Normalized Enriched Score
o/n	Overnight
OPN	Osteopontin
OV	Ovarian cancer
Padj	Adjusted P-value
PALM	Photoactivated Localization Microscopy
PBS	Phosphate Buffered Saline
PCA	Principal Component Analysis
PDGFR- $\alpha$	Platelet Derived Growth Factor Alpha
PDPN	Podoplanin
PFA	Paraformaldehyde
P/S	Penicillin/Streptomycin
rCAFs	Tumor Restraining CAFs
rlog	Regularized logarithm
RNAseq	RNA sequencing
ROS	Reactive Oxidative Species
RT	Room temperature

SDF-1	Stromal Cell-Derived Factor 1
scRNAseq	Single-cell RNA sequencing
siAA1	siRNA <i>Hsp90aa1</i> smart pool
siAB1	siRNA <i>Hsp90ab1</i> smart pool
siC	siRNA control
siRNA	Small interfering RNA
sp	Smart pool
ssGSEA	Single-sample GSEA
TAM	Tumor Associated Macrophage
TCA	Tricarboxylic Acid
TCEP	Tris (2-carboxyethyl) phosphine
TEC	Tumor Endothelial Cell
TEMED	N, N, N', N'-Tetramethyl-ethylenediamine
TFA	Trifluoroacetic Acid
TFE	Trifluoroethanol
TGFβ	Transforming Growth Factor β
TME	Tumor Microenvironment
TNF-α	Tumor Necrosis Factor α
tpm	Transcript per million
Treg	Regulatory T cells
UHPLC	Ultra High-Performance Liquid Chromatography
UMAP	Uniform Manifold Approximation and Projection
UMI	Unique Molecular Identifiers
vCAF	Vascular CAFs
VEGF	Vascular Endothelial Growth Factor
VEGFR	Vascular Endothelial Growth Factor Receptor
WB	Western Blot
WHO	World Health Organization
WT	Wild-type
αSMA	Alpha Smooth Muscle Actin



# Index

1. The tumor microenvironment	4
1.1. Tumor Endothelial cells (TECs)	6
1.2. Immune cells	7
1.3. Extracellular matrix (ECM)	8
2. The Cancer Associated Fibroblasts (CAFs)	9
2.1. CAFs activation, wound healing and the myofibroblastic phenotype	11
2.2. Origin of CAFs	13
2.3. CAFs contribution to cancer progression	16
2.3.1. <i>ECM generation and remodeling by CAFs</i>	17
2.3.2. <i>CAFs promote a pro-tumoral immune environment</i>	18
2.3.3. <i>Metabolic reprogramming of CAFs</i>	19
2.3.4. <i>Angiogenesis regulation by CAFs</i>	19
2.3.5. <i>CAFs promote cancer cell growth and malignancy</i>	20
2.4. Important signaling pathways dysregulated in CAFs	20
2.4.1. <i>The TGF<math>\beta</math> pathway</i>	20
2.4.2. <i>The Hippo pathway: YAP/TAZ</i>	22
2.5. Types of CAFs	24
2.5.1. <i>Myofibroblastic CAFs (myCAFs)</i>	25
2.5.2. <i>Pro-inflammatory CAFs (iCAFs)</i>	25
2.5.3. <i>Other CAF subtypes</i>	26
2.6. Therapeutic challenges of targeting CAFs	27
3. The Heat Shock Protein 90 (HSP90)	28
3.1. The HSP90 chaperone cycle	29
3.2. Other non-canonical HSP90 functions	31
3.3. HSP90 isoforms	32
3.3.1. <i>HSP90<math>\beta</math> (Hsp90ab1)</i>	33
3.3.2. <i>HSP90<math>\alpha</math> (Hsp90aa1)</i>	34
3.4. HSP90 clinical relevance	35
3.4.1. <i>The role of HSP90 in cancer</i>	35
3.4.2. <i>The role of HSP90 in fibrosis</i>	36
3.4.3. <i>HSP90 inhibitors</i>	36
<b>Materials</b>	
1. In vivo murine model description	41
2. Cell lines	41

3. Specialized materials, reagents lists and references	43
<b>Methods</b>	
1. In vivo procedures	53
2. Cell biology procedures	57
3. Molecular biology procedures	64
4. Molecular characterization approaches	68
5. Image processing and analysis	81
<b>Hypothesis and objectives</b>	<b>87</b>
<b>Results</b>	
1. Identification of HSP90 as a new regulator of the CAF pro-tumoral phenotype	89
1.1. Gene expression analysis of public datasets for the study of consistently dysregulated genes in the tumor stroma	91
1.2. Consistently upregulated genes in the tumor stroma correlate with myCAF signatures	94
1.3. Consistently upregulated genes in the tumor stroma are targets of HSP90	96
1.4. HSP90 inhibitors related signatures correlate with myCAF features in the tumor stroma	99
1.5. HSP90 inhibitors related signatures have prognostic value in cancer patients	102
1.6. scRNAseq analysis of public datasets correlates HSP90 and cancer stroma signatures with CAFs	103
1.7. HSP90 is equally expressed in CAFs and NFs	107
2. In vitro studies of HSP90 functions in CAFs	109
2.1. Specific modulation of HSP90 $\alpha$ / $\beta$ expression by siRNAs in murine NFs and CAFs	111
2.2. Analysis of gene and protein expression of CAF markers affected by Hsp90aa1/ab1 silencing	114
2.3. Role of HSP90 $\alpha$ in modulating the contractile capacity of CAFs	117
2.4. Role of HSP90 $\alpha$ in controlling motility and migration capacities in fibroblasts	119

2.5. HSP90 $\alpha$ promotes the generation of altered cytoskeletal phenotypes in CAFs	123
2.6. HSP90 $\alpha$ regulates the architecture of CAF-derived ECMs and its influence over cancer cell behavior	129
2.7. HSP90 $\alpha$ regulation in CAFs impairs cancer cell growth in restrictive conditions in vitro	140
2.8. HSP90 $\alpha$ regulates CAF secreted factors	143
2.9. HSP90 $\alpha$ functions in NFs from wild-type and Hsp90 $\alpha$ 1-knock out mice	145
2.10. HSP90 $\alpha$ functions are independent of TGF $\beta$ in CAFs	147
3. Role of HSP90 $\alpha$ in tumoral processes in vivo	149
3.1. Stromal <i>Hsp90<math>\alpha</math>1</i> knock-out impairs E0771 breast tumor growth in vivo	151
3.2. Stromal <i>Hsp90<math>\alpha</math>1</i> knock-out affects collagen deposition in E0771 breast tumor	154
3.3. Stromal <i>Hsp90<math>\alpha</math>1</i> knock out impairs in vivo lung metastasis from E0771 cells	156
4. Molecular processes underlying HSP90 functions in CAFs and TGF $\beta$ -stimulated NFs	159
4.1. <i>Hsp90<math>\alpha</math>1</i> silencing induces a specific gene expression program in CAFs	161
4.2. Gene ontology analysis of differential gene expression profiles altered by Hsp90 $\alpha$ 1/ <i>ab1</i> silencing in CAFs	163
4.3. Gene set enrichment analysis of differential gene expression profiles altered by <i>Hsp90<math>\alpha</math>1/ab1</i> silencing in CAFs	167
4.4. <i>Hsp90<math>\alpha</math>1</i> -silencing induces significant gene expression alterations in TGF $\beta$ -stimulated NFs	170
4.5. Gene ontology analysis of differential gene expression profiles altered by <i>Hsp90<math>\alpha</math>1/ab1</i> silencing in TGF $\beta$ -stimulated NFs	172
4.6. GSEA of differential gene expression profiles altered by <i>Hsp90<math>\alpha</math>1/ab1</i> silencing in TGF $\beta$ -stimulated NFs	176
4.7. Proteomic analysis of <i>Hsp90<math>\alpha</math>1/ab1</i> -depleted CAFs and TGF $\beta$ -stimulated NFs	178

4.8. Integrated analysis of transcriptomic and proteomic datasets for the understanding of the HSP90 $\alpha$ -YAP regulatory mechanisms in CAFs and TGF $\beta$ -stimulated NFs	182
5. HSP90 $\alpha$ regulates CAF pro-tumoral functions through YAP signaling	187
5.1. HSP90 effects over cell cycle and proliferation	189
5.2. Modulation of Yap1 expression by HSP90 $\alpha$ in CAFs and TGF $\beta$ -stimulated NFs	190
5.3. HSP90 $\alpha$ controls Yap1 protein stability	193
5.4. YAP as a "client" protein of HSP90 $\alpha$	194
5.5. Effects of anti-HSP90 drugs over CAF functions and YAP expression	198
5.6. Modulation of YAP/TAZ upstream regulators by HSP90 $\alpha/\beta$	203
5.7. HSP90 controls YAP expression and function in YAP-overexpressing NFs	205
5.8. Correlation of YAP and HSP90 $\alpha$ signatures with human scRNAseq datasets	207
<b>Discussion</b>	<b>213</b>
<b>Conclusions</b>	<b>227</b>
<b>Bibliography</b>	<b>231</b>

*“Nothing in life is to be feared,  
it is only to be understood.”*

*Marie Curie*







# Introduction



In the last few decades, advances in early diagnosis, treatment, prevention and in-depth understanding of cancer have greatly improved cancer survival<sup>1</sup>. In Spain, the five-year survival rate increased by 3.3% in men and 2.5% in women between 2002 and 2013<sup>2</sup>. Despite these efforts, according to the World Health Organization (WHO), cancer remains the leading cause of death worldwide, comprising one of every six deaths<sup>3</sup>. Cancer research is ever evolving, but the fight against cancer remains quite challenging. Several important questions remain unanswered, particularly those related to prevention, metastasis and therapy resistance.

Cancer research has traditionally focused on understanding the molecular signaling pathways driving the malignant behavior of cancer cells, enabling the design of therapies directed specifically to them<sup>4</sup>. Despite the great knowledge gathered during the last few decades on this matter, there are still important deficiencies in the effectiveness and specificity of most current anti-cancer therapies<sup>5</sup>. Thus, it is crucial to continue exploring cancer biology to search for new therapeutic strategies that will ultimately improve cancer prognosis and the life of cancer patients. In this sense, it will be useful to focus on cancer research, not only in the study of cancer cells themselves, but also in understanding the cellular and molecular context in which they thrive and exert their malignant functions.

# 1. The tumor microenvironment

Cancer originates from the accumulation of genetic alterations that result in the excessive growth and increased survival of cancer cells<sup>4,6</sup>. However, they are not the only elements found within tumors. The aberrant behavior of cancer cells is generally accompanied by the influence of a pro-tumoral environment that promotes their malignant features and constantly evolves with them offering support over time<sup>7</sup>. Thus, cancer progression is the consequence of the crosstalk between the cancer cells and their tumor microenvironment (TME).

The TME, which is also usually referred to as “tumor stroma”, comprises all non-malignant cellular and molecular components within tumors. This includes several different cell types, such as Cancer Associated Fibroblasts (CAFs), endothelial cells and immune cells; but it also includes the Extracellular Matrix (ECM) and all the cytokines, chemokines and growth factors that are secreted as the result of all the interactions between cancer cells and the rest of the TME<sup>8</sup> (**Figure 1**). Importantly, the composition of the TME may vary depending on the tissue of origin and anatomical localization, and can incorporate specialized cells specific from those areas, such as adipocytes, neurons, osteoblasts, etc<sup>9</sup>. These differences significantly contribute to the tumor heterogeneity, having a significant impact over the behavior and evolution of solid tumors<sup>10</sup>.

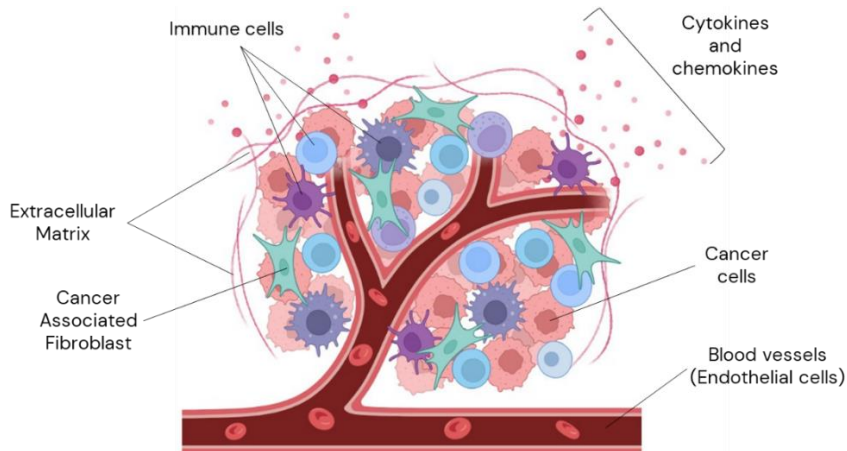


**Figure 1. Principal components of the TME.** The TME is composed of several different cell types and molecules that interact with each other and with cancer cells. These include CAFs, endothelial cells, immune cells, ECM components, and different cytokines and chemokines. *Created on Biorender.com.*

Most of the components of the TME are originally present in the host tissue before the malignancy appears. The emerging tumor is able to influence these normal non-tumoral components and transform them at the molecular and functional level, using them to its advantage and inducing the emergence of malignant behaviors<sup>11,12</sup>. The pro-tumoral TME components then acquire malignant capacities that will ultimately promote tumor progression. Thus, the tumor establishes a reciprocal relationship between cancer cells and the TME in which each one of these elements interacts with the other, creating a complex and ever-evolving environment that progresses with the tumor itself<sup>8,13</sup>. Importantly, the TME exerts its influence during all stages of the tumor progression: from the initial lesion to more mature and bigger tumors, to the metastatic niche. In fact, each component of the TME contributes significantly and in their unique way to tumor progression.

## 1.1. Tumor Endothelial cells (TECs)

Endothelial cells are the constitutors of the tissue vasculature in normal conditions, in which they are specialized in providing oxygen and nutrients to the surrounding cells<sup>14</sup>. Tumors have very high energy requirements to support their continuous growth, for which cancer cells have the capacity to induce the generation of new blood vessels through process such as angiogenesis<sup>4</sup>. However, the tumor vasculature has different characteristics than the normal vasculature. Tumors have an aberrant vasculature formed by immature and hyper-permeable blood vessels<sup>15</sup>. In addition, the Tumor Endothelial Cells (TEC) that constitute the tumor vasculature also have specific independent functions. In fact, TEC have been reported to be key modulators of the immune population in the TME by regulating their transmigration through the vessels and even activating T cells<sup>16-18</sup>. Given these key pro-tumoral functions, TECs serve as a promising target for anti-cancer therapies, and many anti-angiogenic treatments have been developed. Most of them have been directed against the Vascular Endothelial Growth Factor (VEGF) – VEGF receptor (VEGFR) axis. However, these approaches have traditionally failed in successfully eliminating malignant tumors. On one hand, the aberrant tumor vasculature severely impedes the correct distribution of the anti-angiogenic agents. On the other hand, the elimination of blood vessels leads to the emergence of hypoxia in the tumor, which is an important driver of pro-tumoral processes, leading to the emergence of resistances<sup>15,19</sup>.

## 1.2. Immune cells

Immune cells in the TME can act both as tumor-suppressor or tumor-promoter agents, and each of them has specific functions in the TME. The tumor-suppressor cells can act either by improving the visibility of the cancer cells to the rest of the immune system, so that they can be more easily detected; or directly eliminating cancer cells. Among this last group, the main cancer cell killers in the TME are the CD8<sup>+</sup> T cells, as they have cytotoxic capacities<sup>20,21</sup>. On the other hand, the tumor-promoting group include cells such as the regulatory T cells (Treg) or Tumor Associated Macrophages (TAM). The role of Tregs in the TME is complex. Although they mainly function as immune suppressors, preventing the immune response over the cancer cells<sup>20,22</sup>, they can also act as tumor suppressors, as their ability to reduce the activation of the immune system reduces inflammation in the TME<sup>23</sup>. In fact, they have also been pointed out as promising targets for anti-cancer therapies<sup>22,24</sup>. Similarly, the TAMs also promote an immune suppressive environment, blocking anti-tumor immune responses by the secretion of different cytokines<sup>25,26</sup>. In addition, they have the capacity to influence other cells in the TME, including TECs<sup>27</sup>. Thus, the immune system has also been proposed in the last few decades as a promising target for anti-cancer treatments. Some of these new approaches, such as the immune checkpoint blockade strategies, have demonstrated to be very useful. However, they still present unexpected secondary effects for patients, and some of them are even non-responsive to these treatments<sup>28</sup>.

### 1.3. Extracellular matrix (ECM)

The ECM constitutes a complex three-dimensional molecular network that supports the cellular components in tissues and confers mechanical properties. It is typically composed of collagens, proteoglycans, elastin and glycoproteins (mostly fibronectin and laminins)<sup>29,30</sup>. However, in the context of cancer, the ECM is not only a physical scaffold for tumors, but an important dynamic element of the TME with additional pro-tumoral functions. Although cancer cells are known to secrete ECM molecules, and this feature is considered a hallmark of cancer<sup>31</sup>, this characteristic is shared with other members of the TME, which collaborate together in creating tumor-specific ECMs<sup>32</sup>.

Both cancer cells and the TME can modulate the proportion of structural proteins in the ECM<sup>33,34</sup>, changing its mechanical properties. In fact, tumoral ECMs are characterized by increased collagen content<sup>35,36</sup>. Furthermore, the specific organization of the collagen fibers also influences tumor behavior. Thus, organized and aligned collagen fibers create molecular roadways that increase cancer cell motility and dissemination<sup>37</sup>.

In addition, the ECM also constitutes an important reservoir of molecules such as cytokines, chemokines and growth factors, that get released with the secretion of ECM remodeling enzymes from cancer cells and other components of the TME<sup>38</sup>. Some are bioactive molecules that directly originate from the cleavage of some of the major molecular components of the ECM. As an example, fibronectin

derivatives have largely been associated with the activation of growth factor receptors, directly contributing to cancer cell growth<sup>39</sup>.

Given the previously described importance of each of the TME components for cancer progression, the TME has been explored in the last few decades as a promising new source of cancer biomarkers and therapeutic targets. These new approaches have opened the door to the design of therapies for cancer types that have never been specifically targeted. Although some of these new approaches have already showed important limitations, targeting the TME could still become the only possibility for the treatment of some cancer types for which traditional strategies have so far been unsuccessful. In addition, it could provide new combinations with traditional treatments in order to overcome resistance to therapy.

## 2. The Cancer-Associated Fibroblasts

The term “fibroblast” typically involves a heterogeneous population of cells usually found in normal healthy tissues, whose main function is to maintain tissue structure by generating and organizing connective tissue and orchestrating chemical and mechanical cues among the different cellular components of the organ<sup>40,41</sup>. Fibroblasts are usually spindle-shaped, most of them have a mesenchymal origin, and are defined as non-immune, non-endothelial, and non-epithelial cells<sup>41</sup>.

This definition of fibroblasts is quite broad and non-specific. Fibroblasts are easily found throughout the human body, participate in the homeostasis of many different organs and tissues, and are easy to isolate and maintain in cell culture. These features have made them one of the most studied cells *in vitro*. Despite these advantages, the establishment of a true fibroblast definition remains a challenge owing to the lack of specific biomarkers exclusive to this cell type<sup>42</sup>.

Cancer Associated Fibroblasts (CAFs) are pathologically activated fibroblasts that differ phenotypically from the normal ones and actively participate in all hallmarks of cancer<sup>4,6</sup>. They are one of the most important components of the TME, representing the major proportion of non-tumoral cells in solid cancers<sup>40</sup>.

Despite the lack of specific biomarkers to distinguish CAFs, some proteins that have been usually associated with this particular cell type are  $\alpha$ -Smooth Muscle Actin ( $\alpha$ SMA), Fibroblast Activated Protein (FAP), Platelet-derived growth factor receptor- $\alpha$  (PDGFR- $\alpha$ ) and S100A4, among others<sup>40,43,44</sup>

CAFs are also differentiated from normal fibroblasts (NFs) by their exclusive characteristics and functions. They are usually spindle-shaped<sup>40</sup> and have enhanced expression of cytoskeleton proteins and cytoskeleton-related structures, such as stress-fibers and focal adhesions<sup>45,46</sup>. CAFs are not only the main producers of ECM components in the TME, with increased collagen production<sup>32</sup>, but they modulate the ECM through the secretion of Matrix Metalloproteinases (MMPs)<sup>44</sup>. In addition, CAFs exert their influence

over cancer cells and the TME by secreting several different cytokines, chemokines and growth factors<sup>47,48</sup>. Taken together, all these characteristics allow CAFs to have an important influence over all the components of the TME and cancer cells.

Given their key prominent role in tumor progression, CAFs have gained increasing attention over the last few decades, and extensive research has been conducted on their origin and the molecular mechanisms controlling their pro-tumoral behavior<sup>49</sup>. Consequently, CAFs constitute a promising targetable option for the treatment of solid tumors, but their vast heterogeneity in both origin and function makes this possibility still challenging<sup>50,51</sup>.

## **2.1. CAFs activation, wound healing and the myofibroblastic phenotype**

In normal tissue, fibroblasts are usually found in a quiescent state. When the tissue homeostasis is compromised, they become activated in order to quickly repair cellular damage and resolve the injury, in a process known as “wound healing”<sup>41,52–54</sup>. The activated fibroblasts that participate in this process are mainly characterized by their ability to produce and remodel the ECM, as well as enhanced contractile capacities, and they are commonly known as “myofibroblasts”<sup>55</sup>. The activation of the myofibroblast phenotype is mediated by Transforming Growth Factor  $\beta$  (TGF $\beta$ ) signaling, which induces the expression of myofibroblastic markers such as  $\alpha$ -SMA<sup>55</sup>. Once the injury is resolved, the myofibroblasts abandon their activated state and return to their original quiescent phenotype.

However, if the damage persists, fibroblasts eventually become pathologically activated, causing fibrosis<sup>56,57</sup>. Traditionally, tumors have been described as “wounds that do not heal”<sup>58</sup>. They present a continuous source of stress signals to their surrounding cells, creating a permanently unresolved situation. Similar to the wound healing process, as soon as a tumor appears, tissue-resident fibroblasts are recruited to the TME and become activated due to the stressful signals emanating from the cancer cells. These include changes in ECM stiffness, TGF $\beta$  signaling, hypoxia, inflammation and the direct stimulation from different chemokines secreted by the cancer cells (**Figure 2**)<sup>53,57</sup>. The combination of all these stimuli induce a permanent activation state over the fibroblasts, inducing a series of phenotypic modifications that lead to the emergence of CAFs<sup>40</sup>. Thus, CAFs are the consequence of an exaggerated wound healing response activated against the tumor “wound”. In fact, CAFs share common features with the myofibroblasts from wound healing, including some of their mechanisms of activation, their ability to remodel the ECM, and the expression of the  $\alpha$ -SMA marker, among others.

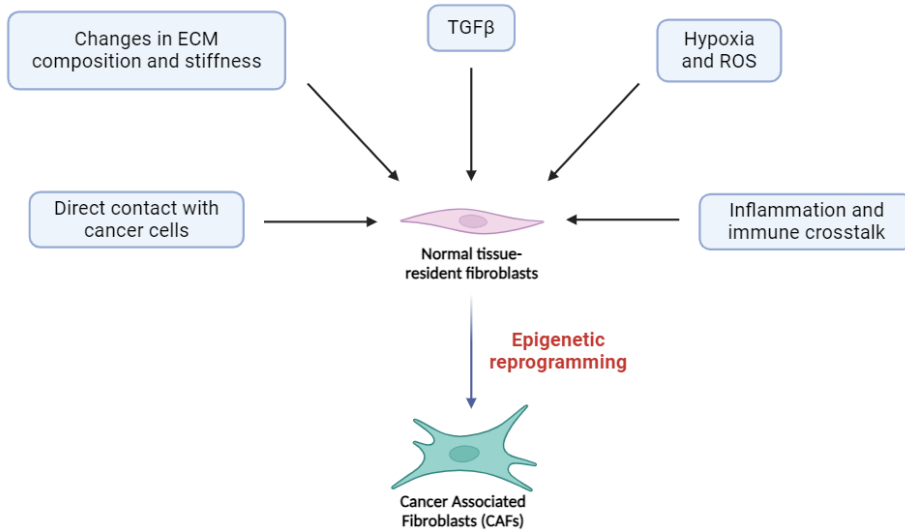


**Figure 2. CAFs activation due to different stressful stimuli.** Fibroblasts get continuously exposed to the stressful TME caused by the emerging tumor, which leads to the acquisition of CAF phenotypes. ROS: reactive oxygen species. *Created on Biorender.com.*

## 2.2. Origin of CAFs

Considering that NFs are ubiquitously distributed throughout the human body, it is not surprising that the same variability is also found when studying the origin of CAFs<sup>52,59</sup>. This, together with the fact that fibroblasts are also very plastic cells that can transform into different cell types<sup>41</sup>, has historically made it particularly difficult to establish a “canonical CAF lineage” that could predict the original cell type that generated a specific CAF. However, recent advances in single-cell RNA sequencing (scRNAseq) and other molecular and biological techniques have helped clarify this issue. There is evidence supporting that CAFs can originate from pericytes<sup>40,60</sup>, adipocytes<sup>61</sup>, bone marrow-derived mesenchymal stem cells<sup>62</sup>, pancreatic or hepatic stellate cells<sup>52,63</sup>, endothelial cells<sup>64</sup> and epithelial cells<sup>65</sup>

(Figure 3). However, the most widely studied possibility is the origin of CAFs from normal tissue-resident fibroblasts, which become pathologically activated as previously described, as soon as a tumoral process colonizes the healthy tissue.

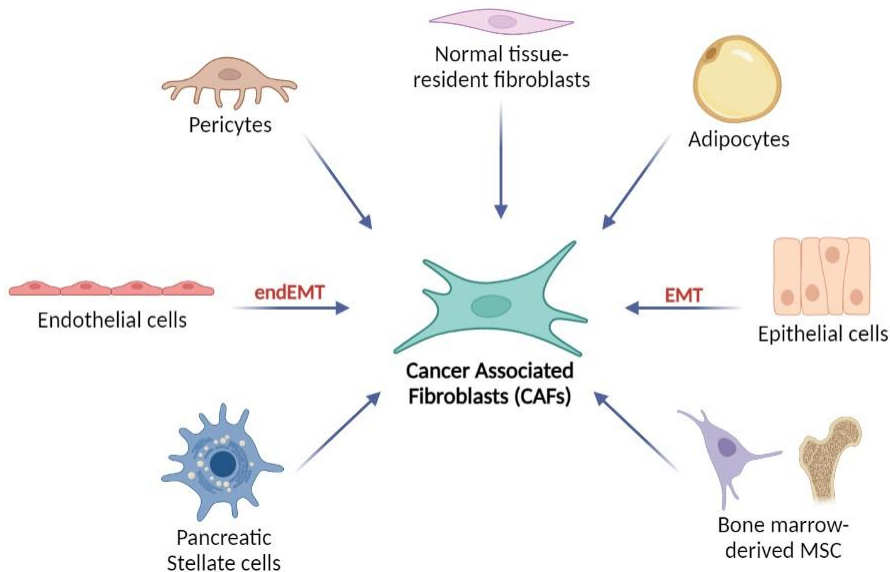


**Figure 3. Different origins of Cancer Associated Fibroblasts (CAFs).** Although the cellular origin of CAFs in tumors is still not well understood, it has been demonstrated that cells from multiple origins can acquire phenotypes associated with CAFs. Most of these cells are mesenchymal in nature. EMT: epithelial-to-mesenchymal transition; endEMT: endothelial-to-mesenchymal transition. Created on Biorender.com.

There are several different molecular pathways in the emergence of CAFs. One of the most important drivers of fibroblasts activation is the TGF $\beta$  protein family. In the context of wound healing, TGF $\beta$  controls the necessary activation of normal fibroblasts into myofibroblasts, inducing increased migration, contractility and ECM remodeling capacities<sup>55</sup>. Cancer cells, on the other hand, are known to secrete TGF $\beta$  into the TME<sup>66,67</sup>, which has been reported to activate normal tissue-resident fibroblasts into CAFs in various cancer

types<sup>68-70</sup>. Another important event that happens during wound healing is inflammation, which involves the secretion of specific cytokines and chemokines, as well as the recruitment of the immune system to the injury. During this process, the recruited immune cells further contribute with their secretome to the inflammatory process, participating in the crosstalk with the tissue-resident fibroblasts. In tumors, CAFs activation can also emerge as a consequence of this crosstalk, as their stimulation with cytokines such as Interleukin-1 $\beta$  (IL-1 $\beta$ ) and Tumor Necrosis Factor  $\alpha$  (TNF- $\alpha$ ) induces the activation of the NF- $\kappa$ B signaling pathway<sup>71-73</sup>. Other interleukins, including IL-6, IL-10 and IL-11 induce CAFs activation through JAK/STAT<sup>73</sup>.

As previously mentioned, the emergence of a tumor consequently results in the generation of a stressful environment that influences tissue-resident cells. In fact, cancer cells promote hypoxia in the TME due to their excessive growth and the lack of a proper functional vasculature system<sup>4</sup>. Thus, cancer cells increase the presence of reactive oxygen species (ROS) in the TME<sup>74</sup>, which can also drive the activation of fibroblasts into the CAF phenotype<sup>75,76</sup>. In addition, acute stress is known to activate the heat shock response (HSR) in cells, orchestrated by the transcription factor Heat Shock Factor 1 (HSF1). In cancer, HSF1 has been described to participate in growth and metastasis, among other malignant functions<sup>77</sup>. In addition, HSF1 has been found to participate in CAF activation and promote its malignant phenotype in multiple cancer types<sup>78,79</sup>.

Moreover, CAFs activation may also occur as a result of the direct interaction between cancer cells and fibroblasts<sup>80</sup>, most probably through cell-surface adhesion molecules<sup>81</sup>. In fact, in some cancer types, including breast cancer, it has been described that CAF activation occurs via Notch signaling after direct contact with malignant cells<sup>82</sup>. However, this may not apply to all cancer types, in which other signaling pathways may be the mediators of these interactions.

### **2.3. CAFs contribution to cancer progression**

CAFs actively participate in all stages of tumor development, and they have been described to have a direct or indirect role in all hallmarks of cancer (**Figure 4**). These pro-tumoral effects depend on specific CAF functions, including their ability to produce and remodel the ECM; their influence over the immune system in order to promote a pro-tumoral immune environment; their capacity to undergo important metabolic changes to support tumor growth; their influence over angiogenesis; and the secretion of different molecules that directly influence cancer cells<sup>43,53</sup>.

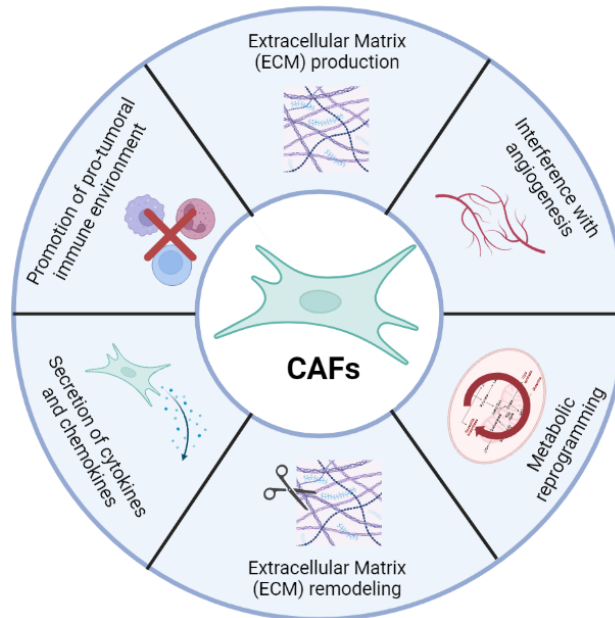


**Figure 4. The different CAF functions contribute to tumor progression and metastasis.** CAFs exert a great variety of functions in the TME, all of which have direct or indirect consequences for the cancer cells and ultimately contribute to cancer progression, dissemination and response to therapy. *Created on Biorender.com.*

### 2.3.1 ECM generation and remodeling by CAFs

The ECM in the TME becomes aberrant in both its composition and architecture due to the activity of CAFs<sup>83,84</sup>. As previously mentioned, CAFs are the main producers of ECM components in the TME, as they secrete most collagens, fibronectin, glycoproteins and proteoglycans<sup>44,84</sup>. But not only they produce *de novo* ECM components, they also have the capacity to modify the existing ECM. In fact, CAFs are able to modulate collagen crosslinking, which has a direct impact in ECM stiffness and can stimulate cancer cell migration and invasion<sup>85</sup>. In addition, they secrete MMPs promoting ECM degradation<sup>44,86</sup>.

The physical properties of the ECM (stiffness) directly influence the behavior of the cancer cells and other cells in the TME by mechanotransduction processes. In addition, it has been described that the architecture of the ECM can influence the motility and invasion capacity of cancer cells<sup>87</sup>. As previously mentioned, anisotropic ECMs, characterized by being well-organized and structured, are used by cancer cells as molecular roadways, facilitating their migration and invasion<sup>88</sup>. Furthermore, the structure and composition of the ECM can also influence immune infiltration into the TME, and an increase in ECM stiffness has been reported to reduce angiogenesis and increase hypoxia in the TME<sup>44,53,89</sup>.

### ***2.3.2. CAFs promote a pro-tumoral immune environment***

As previously discussed, CAFs secrete cytokines and chemokines to the TME that promote an immune-suppressive environment, facilitating tumor progression<sup>53</sup>. This immune-suppressive response consists mostly in reducing the presence of CD8<sup>+</sup> T lymphocytes in the TME in favor of other more cancer-permissive populations, such as regulatory T cells (Treg) and CD4<sup>+</sup> T cells<sup>90</sup>. In fact, CAFs are known to secrete TGF $\beta$ , which is known to interfere with CD8<sup>+</sup> T cells cytotoxic activities<sup>91,92</sup>. Importantly, CAFs have been reported to recruit and activate TAMs by secretion of SDF-1, which further contributes to the generation of an immune suppressive TME and cancer progression<sup>93</sup>.

### ***2.3.3. Metabolic reprogramming of CAFs***

Increasing evidence suggests that CAFs undergo a metabolic reprogramming to adapt to the restrictive nutrient-deprived environment caused by the excessive growth of cancer cells<sup>53,94,95</sup>. As a consequence, CAFs experience increased autophagy<sup>96</sup> and activate their catabolic metabolic pathways to increase the secretion of nutrients, growth factors and other molecules to support cancer cell growth<sup>94</sup>. In this sense, CAFs perform the “reverse Warburg effect” to undergo aerobic glycolysis and secrete high-energy metabolites that are then incorporated into the tricarboxylic acid (TCA) cycle in the cancer cells<sup>97</sup>. These metabolic changes in CAFs may also be driven by the crosstalk with other components of the TME. Importantly, the ECM has been recently proposed as a key regulator of these metabolic changes in both CAFs and cancer cells<sup>94</sup>, creating a positive feedback loop in which CAFs modulate and at the same time are influenced by the ECM to ultimately contribute to tumor growth and progression.

### ***2.3.4. Angiogenesis regulation by CAFs***

Hypoxia is a characteristic of the TME, but it is also a well-known driver of angiogenesis. CAFs, induced by this stressful environment, are able to promote the production of new vasculature in the TME by secreting several pro-angiogenic molecules, including VEGF<sup>47</sup>. In breast cancer and lung squamous cell carcinoma, CAFs have been described to express podoplanin (PDPN), which promotes angiogenesis by downregulating VEGF-C<sup>98,99</sup>. Secretion of Stromal

Cell-Derived Factor 1 (SDF-1) by CAFs has also been reported to induce angiogenesis in pancreatic cancer<sup>100</sup>.

### ***2.3.5. CAFs promote cancer cell growth and malignancy***

The secretome of CAFs includes a wide range of molecules that actively promote tumor growth and malignant features. CAFs induce cancer cell growth through secretion of growth factors such as TGF $\beta$ , PDGF, Hepatocyte Growth Factor (HGF), or Osteopontin (OPN), among many others<sup>101</sup>. All of these molecules stimulate different molecular pathways in the cancer cells related with growth and survival, such as PI3K/AKT and MAPK. In addition, CAFs are also able to induce other pathways in cancer cells related with migration and invasion. For example, CAFs secrete Wnt ligands that activate canonical and non-canonical Hippo pathway in cancer cells to promote migration and invasion<sup>102</sup>. Furthermore, other CAF-derived factors have been related with increased chemotherapy resistance. This is the case of HGF, which has been reported to be implicated in resistance to anti-RAF therapies<sup>103</sup>.

## **2.4. Important signaling pathways dysregulated in CAFs**

### ***2.4.1 The TGF $\beta$ pathway***

As previously mentioned, TGF $\beta$  is one of the most important drivers of CAF activation, and it can be secreted by cancer cells or CAFs themselves. The canonical TGF $\beta$  pathway starts with the binding of one of TGF $\beta$  family ligands to its corresponding TGF $\beta$  receptor, causing the phosphorylation and activation of Smad2/3

and their hetero-trimerization with Smad4. The newly formed complex translocates into the nucleus, where it functions as a transcription factor and induces the activation of their target genes (Figure 5). In CAFs, canonical TGF $\beta$  pathway induces the expression of important factors, including  $\alpha$ SMA and FAP<sup>104,105</sup> and the acquisition of myofibroblast characteristics.

In addition, although it may not be the main mechanism of activation, non-canonical TGF $\beta$  pathway can also induce other molecular pathways that play important roles in the induction of the CAF phenotype. TGF $\beta$  can phosphorylate and activate ERK1/2, which are kinases that belong to the MAP pathway, with implications in CAF metabolism<sup>106</sup>, proliferation and migration<sup>107,108</sup>. The activation of RhoA/ROCK by non-canonical TGF $\beta$  induces the expression of markers related with ECM remodeling and CAF contractility, such as Snail1 and Twist1<sup>109</sup>. In addition, JAK1 can also be activated by TGF $\beta$ , which cooperates with ROCK to mediate CAFs actomyosin-driven contractility by regulating the phosphorylation of Myosin Light Chain II (MLC2)<sup>110</sup>. Finally, non-canonical TGF $\beta$ , together with growth factors such as VEGF or Endothelial Growth Factor (EGF), induce the activation of the PI3K/Akt/mTOR pathway. While this pathway is mostly implicated in cell growth and survival, in CAFs it has also been reported to affect motility through regulation of Farnesoid X receptor (FXR)<sup>111,112</sup>.

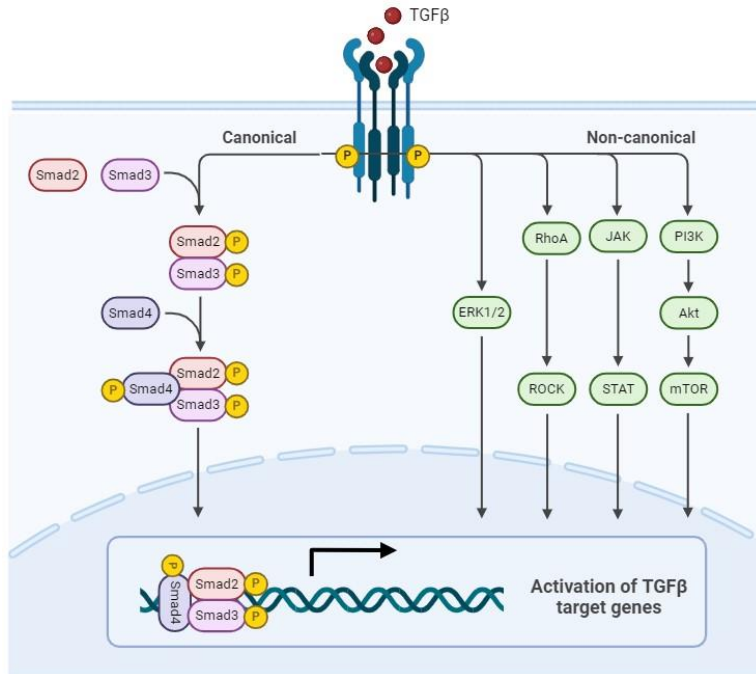


**Figure 5. Canonical and non-canonical TGFβ pathway in CAFs.** In the canonical TGFβ pathway, the phosphorylated SMAD proteins get translocated into the nucleus and activate the transcription of important drivers of the CAF phenotype. Non-canonical TGFβ pathway can also induce the expression of important CAF effectors by the activation of alternative pathways, including ERK1/2, RhoA/ROCK, JAK/STAT, and PI3K/mTOR. *Created on Biorender.com.*

### 2.4.2 The Hippo pathway: YAP/TAZ

Fibroblasts are also known to have the capacity to sense and react to physical changes in their surroundings. That is, they are able to respond to changes in the stiffness and composition of the ECM<sup>113</sup>. This function is crucial for their role in wound healing<sup>113,114</sup>, but it is also an important driver of the CAF phenotype in the TME<sup>41</sup>. The mechanical forces caused by changes in ECM stiffness are sensed by focal adhesions and integrins, creating a link between the ECM and the fibroblast cytoskeleton that translates into a series of biochemical signals inside the fibroblasts in a process known as

mechanotransduction<sup>115,116</sup>. In CAFs, this process has been described to be orchestrated by YAP and TAZ<sup>105</sup>. YAP/TAZ are essential CAFs effectors. When they are activated by molecular and mechanical signals, they promote the transcription of ECM-related genes and regulate the expression of cytoskeletal regulators. Thus, YAP/TAZ activities in CAFs promote ECM remodeling, cancer cell invasion and angiogenesis<sup>79,105</sup>.

YAP/TAZ were first identified as the most important effectors of the Hippo signaling pathway during embryonic development<sup>117</sup>, although there is also plenty of evidence that describe the Hippo pathway as an important driver of tumorigenic processes in cancer<sup>118,119</sup>. This pathway consists of a cascade of protein kinases whose function ultimately leads to the inhibition of YAP/TAZ impeding their translocation into the nucleus, where they will bind the TEAD family of transcription factors and activate specific transcriptional programs related to cell proliferation and survival<sup>117,120</sup> (**Figure 6**). In addition, YAP/TAZ have also been found to be activated by Wnt3a signaling through non-canonical Wnt signaling pathway<sup>121,122</sup>, which is particularly interesting in the TME context due to Wnt3a being also an important driver of the CAF phenotype<sup>73</sup>. Importantly, Wnt ligands are also well-known activators of  $\beta$ -catenin, which has also been recently related with CAF functions such as migration and ECM remodeling<sup>73,79</sup>. In CAFs, as previously mentioned, YAP/TAZ mechanoactivation can occur independently of the Hippo pathway, and is usually related to changes in the actin cytoskeleton, where increased actin fiber formation and actomyosin contractility promote YAP/TAZ nuclear translocation<sup>105</sup>.

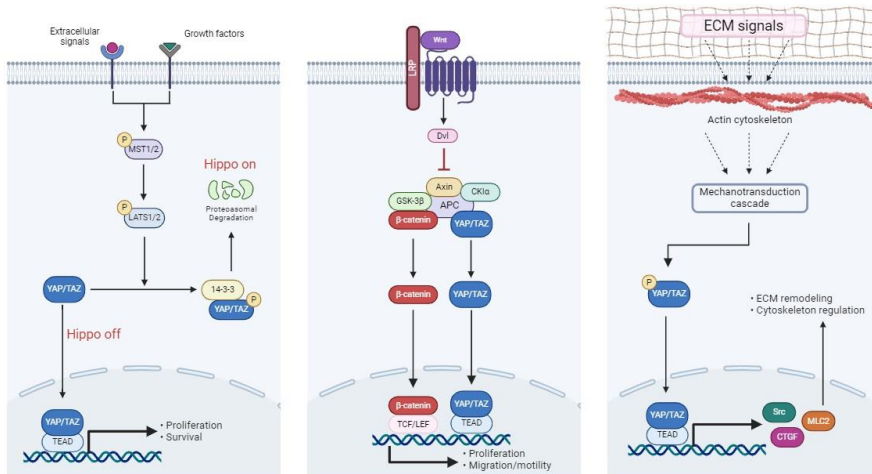


**Figure 6. Canonical and non-canonical Hippo pathway and YAP/TAZ regulation in CAFs.** In the canonical Hippo pathway, when the pathway is activated, YAP/TAZ are translocated into the nucleus to control the transcription of genes related to proliferation and survival (left panel). In the non-canonical Hippo pathway, Wnt ligands can also induce YAP/TAZ translocation into the nucleus through activation of various kinases (center panel). Similarly, Wnt ligands can activate  $\beta$ -catenin, which is also transported into the nucleus and work in coordination with YAP/TAZ to regulate important CAF functions such as migration and motility. In CAFs, ECM remodeling signals are sensed in the intracellular compartment by actin fibers that activate the mechanotransduction cascade, leading to YAP/TAZ activation (right panel). *Created on Biorender.com.*

## 2.5. Types of CAFs

CAF heterogeneity, both intra-tumoral and between cancer types, has historically complicated CAF research and makes it difficult to characterize CAF subpopulations. Recently, this paradigm has completely changed with the introduction of scRNA-seq techniques for the study of CAFs<sup>123</sup>, which has facilitated the identification of particular CAF subsets with shared characteristics, even between different cancer types. In particular, two main CAF subtypes have been commonly found in diverse tumors: myofibroblastic CAFs (myCAF) and inflammatory CAFs (iCAF).

However, these do not exclude the possibility of finding CAF subpopulations specific of certain tumors and organs<sup>124,125</sup>. Importantly, it is still not known if these different phenotypes are permanent, or if they can be interchanged and CAFs can move from one subtype to another depending on the circumstances.

### ***2.5.1. Myofibroblastic CAFs (myCAFs)***

This particular CAF subtype is very similar to the myofibroblasts that can be found during wound healing processes<sup>123</sup>. They are highly responsive to TGF $\beta$ , as they have increased expression of TGF $\beta$  receptors<sup>123,126</sup>. Similar to the myofibroblasts, myCAFs are characterized by the expression of  $\alpha$ SMA and have enhanced cytoskeleton activity. Thus, this particular CAF subset has been specially related to the ECM remodeling and contractility functions<sup>55,126–128</sup>.

### ***2.5.2. Pro-inflammatory CAFs (iCAFs)***

Unlike the myCAFs, these fibroblasts usually do not have contractile functions and have lower  $\alpha$ SMA expression. Instead, they are characterized by the expression of IL-6<sup>126,129</sup> and being highly responsive to IL-1R<sup>128</sup>. These CAFs are specifically in charge of the immune system reconfiguration in the TME, as they are able to recruit specific immune cells into the tumor stroma to increase their presence in detriment of other immune populations that could be more aggressive towards the cancer cells<sup>80,123</sup>. They also secrete chemokines and cytokines that ultimately induce an inflammatory

state in the tumor stroma beneficial for cancer cell growth. However, although pro-inflammatory CAFs have been found in several different cancer types with similar functions, their secretome has been found to be variable between them, making them difficult to classify under the same subtype<sup>123</sup>.

### ***2.5.3. Other CAF subtypes***

In the last few years, single-cell technologies have significantly increased the information about the numerous CAF identities that can be found in different cancer types, and had help identify additional CAF subtypes whose functions may differ from those previously described<sup>123</sup>. This is the case of the antigen-presenting CAFs (apCAF), characterized by the expression of MHC class II at the cell surface and have been reported to be capable of activating T-cells in the TME<sup>130</sup>. In some murine models such as the MMTV-PyMT, a subpopulation of CAFs was found to be specifically associated with endothelial cells and blood vessels. This population, designated as vascular CAFs (vCAF) were characterized by an overexpression of angiogenic genes<sup>131</sup>. Further studies are needed to confirm the presence of these and other potential CAF specialized subtypes in other types of cancer, as well as to further understand their role in the TME.

## 2.6. Therapeutic challenges of targeting CAFs

Because of all their implications in cancer development and their pro-tumoral functions, CAF represent a promising target for new anti-cancer therapies that could complement and improve other traditional approaches. This could be particularly helpful in scenarios in which targeting cancer cells alone is not effective or has failed over time, for example when they have already developed resistance to the treatment, or in the case of metastasis.

However, targeting CAFs has proven to be challenging for different reasons. Despite the identification of biomarkers that are known to be expressed by some CAFs subtypes, these are not exclusive of CAFs and can even be found expressed by other cells in the tumor stroma. In fact, there has not been found a common biomarker for all CAF subtypes yet that can specifically identify this population and differentiate it from others in the TME. Thus, there is a lack of clinical biomarkers that could potentially be used as clinical targets for specifically designed drugs.

Nevertheless, some strategies have been developed *in vivo* to eliminate CAFs from the TME. In some cases, these strategies were effective and there was a reduction in tumor size<sup>132,133</sup>. But in others, the elimination of CAFs accelerated tumor progression and aggravated the prognosis<sup>134</sup>. This effect is thought to be a consequence of the double nature of CAFs as tumor suppressors or tumor promoters.

Although the total elimination of CAFs from the tumor stroma appears to be counterproductive for tumor suppression, there may be other therapeutic strategies regarding CAFs that could still be beneficial. The plastic nature of fibroblasts together with the fact that the CAF phenotype is due to epigenetic alterations, points out to the possibility of CAFs being reprogrammed to a more “normal” phenotype. Thus, instead of completely removing CAFs from the tumor stroma, research efforts are now directed to identify strategies to re-program CAFs back into their original quiescent state so that they could stop providing support to the cancer cells. However, this is still only a promising possibility, but more research is needed to explore its viability.

### 3. The Heat Shock Protein 90 (HSP90)

The Heat Shock Protein 90 (HSP90) is a molecular chaperone that controls the proper folding and stability of a great number of proteins, usually referred to as “clients”. It was first described as part of the Heat Shock Response (HSR)<sup>135</sup>, as its expression was found to be increased under extreme heat conditions, and it is highly evolutionary conserved from bacteria to humans<sup>136</sup>. Despite this, HSP90 is also known to be essential for some cellular processes under physiological conditions, representing between 1–2% of all the cytosolic proteins within a cell<sup>137</sup>. This percentage comes up to around 10% when the cells are experiencing some kind of stress, as HSP90 is in charge of maintaining protein homeostasis in order for

the cells to effectively adapt to adverse environments<sup>138</sup>. In addition, more than 300 proteins have been described to directly interact with HSP90 so far<sup>139</sup>. Thus, it is not surprising that HSP90 has been related with a number of different diseases, including cancer, neurodegenerative processes, infection, and fibrotic diseases.

### 3.1. The HSP90 chaperone cycle

As a chaperone, HSP90 uses ATP to change its conformation in a cyclic manner in order to bind to its client protein and release it once it has been folded properly<sup>140</sup>. This ATPase activity is essential for its chaperone role. However, HSP90 does not function alone: it needs the cooperation of different co-chaperones that bind reversibly to HSP90 and whose combination is specific for each client protein<sup>141</sup>. Thus, HSP90 is the main piece of a protein complex dedicated to facilitate the correct assembly of proteins, which is regulated by the participation of the corresponding co-chaperones and post-transcriptional modifications that can affect all the different components of the complex<sup>142</sup>.

In order to perform this chaperone function, HSP90 needs to form a homodimer<sup>143</sup>. Each HSP90 monomer is comprised of three different conserved domains: the amino-terminal (N-terminal) ATP binding domain; the middle domain, which includes the ATP hydrolysis enzymatic activity and binds the client proteins<sup>144</sup>; and the carboxy-terminal domain (C-terminal), important for the dimerization and the interaction with the different co-chaperones<sup>145</sup>. The chaperone cycle of HSP90 begins when the homodimer takes a

V form in the absence of ATP, considered as the “open” conformation (Figure 7). When the ATP binds its corresponding site, a series of complex rearrangements involving all three domains takes place, for which the interaction with the specific co-chaperones is essential. These will ultimately lead to the “closed” state and the ATP hydrolysis take place. Once the ADP and inorganic phosphate are liberated, HSP90 comes back to their open state, completing the cycle<sup>137,146</sup>.

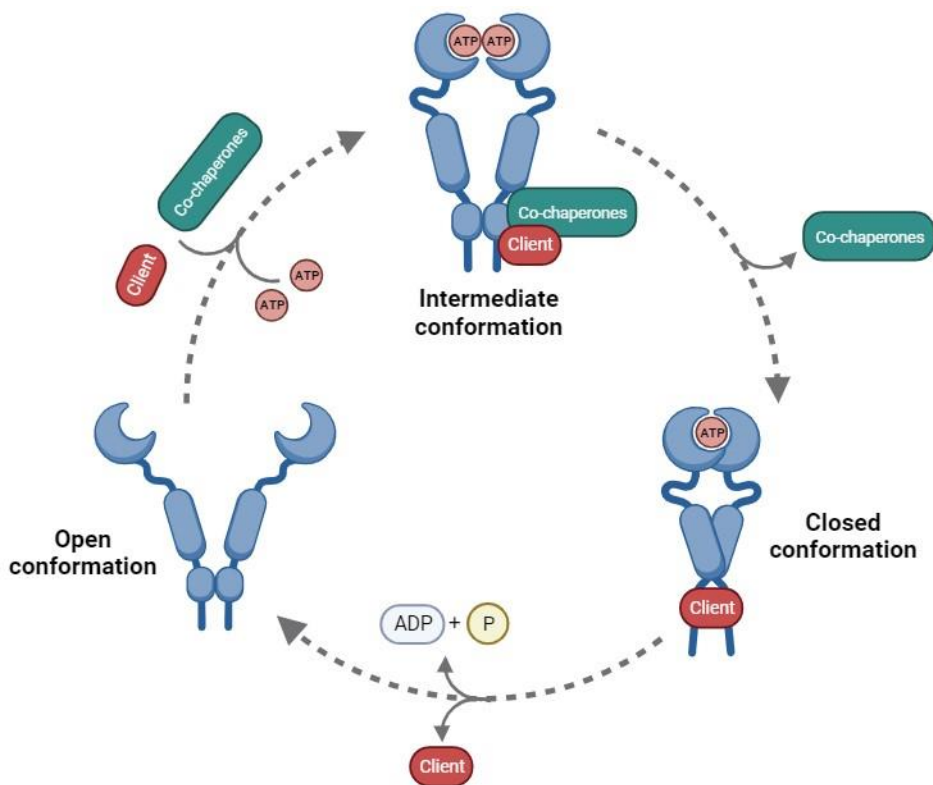


**Figure 7. The HSP90 chaperone cycle.** In order to exert its chaperone function, HSP90 needs ATP and various client-specific co-chaperones to change its conformation from a V-shaped open state to a closed one in a cyclic manner. Created on Biorender.com.

### 3.2. Other non-canonical HSP90 functions

Although the intra-cellular chaperone function of HSP90 has traditionally been the most studied and it is already well characterized, the study of HSP90 in different diseases and contexts has revealed additional important roles that are not necessarily related with maintaining cellular proteostasis. For example, HSP90 has been found to stabilize different signaling pathways by binding several receptors in the cell membrane. The most studied case in this sense, which is also correlated with the importance of HSP90 in stress responses, is the implications in controlling the activity of steroid hormone receptors<sup>147</sup>. This is the case of the TGF $\beta$  pathway, as HSP90 has been described to directly bind both TGF $\beta$  receptors (T $\beta$ RI and T $\beta$ RII) and be essential for maintaining minimum activity of the pathway<sup>148</sup>. Not only that, extracellular HSP90 (eHSP90) has also been found to bind the TGF $\beta$  receptors with similar consequences<sup>149</sup>. Thus, HSP90 can also be found in the extracellular compartment both as a secreted protein and as a membrane-associated protein. Other functions described for these particular HSP90 role include, on one hand, the participation of secreted eHSP90 in the regulation of the assembly and stability of some ECM components such as fibronectin, both in normal and pathological situations<sup>150</sup>. On the other hand, membrane-associated eHSP90 has been found to be implicated in the transduction of extracellular signals into the intracellular compartment<sup>142</sup>, as well as in cell migration and motility through binding to its main receptor: LRP1<sup>151,152</sup>. How HSP90 is secreted into the extracellular compartment remains undetermined, as HSP90 lacks all of the known peptide sequences needed for

protein secretion<sup>136</sup>, although it has been found in exosomes<sup>153</sup>. Altogether, this heterogeneity in functions and implications suggests that HSP90 complexity goes beyond its chaperone nature and ATP dependency.

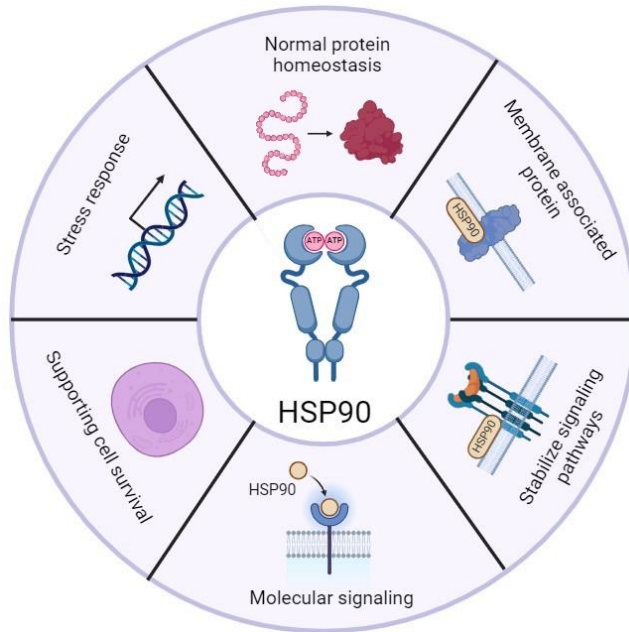


**Figure 8. HSP90 functions.** Besides the canonical chaperone function, which is mostly implicated in maintaining normal protein homeostasis of the cell, HSP90 has other non-canonical functions. *Created on Biorender.com.*

### 3.3. HSP90 isoforms

The HSP90 chaperone family in mammals consists of four different isoforms: the cytosolic forms HSP90 $\alpha$  and HSP90 $\beta$ <sup>154</sup>; the endoplasmic reticulum (ER) form GRP94<sup>155</sup>; and the mitochondrial form Trap-1<sup>156</sup>. Whereas the two cytosolic isoforms are mostly in charge of normal proteostasis in the cell, the other two act more like quality control checkpoints in their respective compartments. In fact, HSP90 $\alpha$  and HSP90 $\beta$  are largely the most abundant isoforms,

and share approximately 96% homology as well as more than 84% sequence identity<sup>136,157</sup>. Despite their similarities, each isoform has been reported to have some preferred client proteins to be chaperoned, although the isoform specificity of all the identified HSP90 client proteins has yet to be thoroughly studied<sup>136,157</sup>. In addition, HSP90 isoforms have even been reported to react differently to anti-HSP90 inhibitors, with consequent independent roles in anti-stress responses<sup>136,158</sup>.

### **3.3.1. HSP90 $\beta$ (*Hsp90ab1*)**

This isoform is constitutively expressed under normal conditions<sup>136,157</sup>, but its expression can also be increased under certain stresses, as described in some types of cancer<sup>159,160</sup>. In mice, and similarly in humans, HSP90 $\beta$  can mostly be found expressed in heart, liver, spleen, lungs, intestine, muscles, brain, testicles and kidneys<sup>157</sup>. Its constitutive expression leads to the idea of HSP90 $\beta$  being essential for cells, and the most important isoform for the maintenance of normal cellular functions and proteostasis. In fact, the knock-out (KO) of this isoform in mice leads to embryonic lethality<sup>161</sup>, supporting an essential role for HSP90 $\beta$  in early embryonic mammalian development. However, the exact cellular or biological process affected is yet to be determined, but it has been certainly attributed only to this particular isoform. Despite the enormous similarity with its homologous isoform HSP90 $\alpha$ , which makes them particularly difficult to study independently, other cellular functions have been attributed exclusively to HSP90 $\beta$ . It has been described to have an exclusive role in the differentiation of some cell types,

including murine muscle cells and hepatocytes<sup>162,163</sup>. Furthermore, HSP90 $\beta$  is also known to have essential roles in metabolism of the cell. In fact, HSP90 $\beta$  is essential for normal lipid homeostasis, as it controls fatty acids and cholesterol metabolism<sup>164</sup>. Altogether, HSP90 $\beta$  appear to be in charge of more structural and essential tasks for the normal behavior of the cells.

### ***3.3.2. HSP90 $\alpha$ (Hsp90aa1)***

The expression of this isoform is usually dependent on various different stress signals, including hypoxia, nutrient-deprived environments, inflammation and of course heat, among other stimuli that have not even been fully characterized yet<sup>165</sup>. Thus, most of the functions attributed exclusively to this isoform are related with stress responses and signaling pathways. That is why, unlike the HSP90 $\beta$ , complete deletion of HSP90 $\alpha$  in mice is not lethal<sup>166</sup>. HSP90 $\alpha$  is particularly abundant in some organs, including brain and reproductive organs. Consequently, complete elimination of HSP90 $\alpha$  in mice has been reported to have notable effects in their reproductive capacity, as HSP90 $\alpha$ -KO male mice are sterile<sup>166</sup>. In addition, HSP90 $\alpha$  has also been reported to play an important role in the DNA damage response, where it is phosphorylated and accumulated in double strand break sites to promote their repair<sup>167,168</sup>. Interestingly, the previously mentioned stress signals induce not only its expression, but also the secretion of this particular isoform<sup>169,170</sup>. Thus, the above-mentioned eHSP90 functions would correspond mostly with the HSP90 $\alpha$  effects specifically. Importantly, eHSP90

was recently found to specifically bind the TGF $\beta$  receptor I (TGF $\beta$ RI), enhancing and stabilizing the activation of the pathway<sup>149</sup>.

### 3.4. HSP90 clinical relevance

#### 3.4.1. *The role of HSP90 in cancer*

Cancer cells need to survive and proliferate in highly stressful environments. In addition, they suffer the intracellular stress resulting from their numerous mutations and aberrant protein expression. Thus, cancer cells are highly dependent on the activity of chaperones for their malignant functions<sup>171</sup>. HSP90 $\alpha$ , both cytosolic and extracellular, has been largely described as an important facilitator of all hallmarks of cancer<sup>157,169</sup>. In fact, it has been found to be overexpressed in different cancer types, where it also can be used as a biomarker for poor cancer prognosis<sup>172</sup>. In the cytosolic compartment, HSP90 $\alpha$  stabilizes and assist the activation of numerous client oncoproteins<sup>171</sup>. In the extracellular compartment, the HSP90 $\alpha$  functions are more variable, mostly promoting cancer invasiveness and metastasis through interactions with the ECM and other cells in the stroma<sup>142,169</sup>. On the other hand, although HSP90 $\beta$  is the constitutively expressed isoform, it has also been found significantly overexpressed in some types of cancer, and it has been described to be particularly important for drug resistance in lung cancer<sup>173</sup>. With all this evidence, HSP90 has been considered a promising candidate for the development of new anti-cancer therapies, and some anti-HSP90 drugs have already been developed and tested in clinical trials<sup>174</sup>. However, all anti-HSP90 therapeutic

efforts so far have been directed specifically to the elimination of cancer cells, but whether anti-HSP90 therapies could also be beneficial when used against TME components remains to be explored.

### ***3.4.2. The role of HSP90 in fibrosis***

Fibrotic disorders consist on the pathologic accumulation of ECM components (mostly collagens) in response to tissue damage<sup>175</sup>. In these processes, the healthy tissue is progressively replaced by a fibrotic scar in a process that is driven by permanently activated fibroblasts in a TGF $\beta$ -dependent manner. Interestingly, HSP90 has been found to be upregulated in many fibrotic disorders, in which it is mostly in charge of maintaining TGF $\beta$  signaling either intracellularly, by stabilizing TGF $\beta$  effectors, or extracellularly, by stabilizing TGF $\beta$  receptors<sup>149,176,177</sup>. Thus, the above-mentioned anti-HSP90 drugs are also thought to be potentially beneficial for the treatment of fibrotic disorders. It has already been proved that anti-HSP90 treatment in fibrosis drastically reduces TGF $\beta$  activity and improves patient prognosis<sup>176,178,179</sup>.

### ***3.4.3. HSP90 inhibitors (HSP90i)***

Given the implications of HSP90 in driving important processes not only in cancer, but also in other diseases, many efforts have been made in the last few decades to design specific HSP90 inhibitors (HSP90i) that could potentially be used in the clinic. Due to the previously mentioned great similarity between the different

HSP90 isoforms, most of the compounds that have been found or designed to target HSP90 are pan-inhibitors<sup>180</sup>. As previously mentioned, HSP90 is expressed all over the human anatomy. Thus, pan-HSP90 inhibitors have enormous consequences for patients, showing severe secondary effects. In fact, none of these compounds have been approved to be used in the clinic so far<sup>180</sup>.

The majority of HSP90i bind the ATP pocket at the N-terminal domain, inhibiting its ATPase activity and thus impeding its dimerization and normal chaperone function. This is the case of the HSP90i Geldanamycin and Tanespimycin (17-AAG). Geldanamycin was one of the first HSP90i to be identified, and it was tested as an anticancer drug with very promising results<sup>181</sup>. Although its derivative, Tanespimycin, also showed similar results in pre-clinical studies, both failed in clinical trials due to solubility and toxicity problems<sup>180</sup>. Importantly, the inhibition of HSP90 with N-terminal inhibitors was observed to induce the HSR in cancer, leading to an increase in other proteins of the system such as HSP70 or HSF1, which is also the reason of their failure in clinical trials<sup>180,182,183</sup>.

To overcome these issues, other HSP90i have been discovered more recently to target the opposite C-terminus instead. These compounds represent a more promising strategy for HSP90 inhibition in the clinic, as these do not activate the HSR. However, clinical trials are still ongoing for these compounds to test their toxicity and efficacy.

In addition, although some of these HSP90i have been tested for the treatment of fibrosis<sup>176,184</sup>, in the context of cancer they have only been tested their efficacy in cancer cells. Little is known about their possible effect over other components in the TME, including CAFs.

# Materials



## 1. *In vivo* murine model description

C57BL/6 *Hsp90aa1<sup>+/+</sup>* (wild-type, WT), *Hsp90aa1<sup>-/-</sup>* (knock-out, KO) and *Hsp90aa1<sup>+/-</sup>* (heterozygous, HE) mice were kindly provided by the lab of Dr. Ana Victoria Villar (IBBTEC, Spain)<sup>149</sup> and kept in a pathogen-free animal facility unit. Mice were exposed to a 12 h light and darkness photoperiod and kept at a constant temperature of approximately 22 °C and 10% of relative humidity, with *ad libitum* food and water accessibility. Due to *Hsp90aa1<sup>-/-</sup>* males being sterile, female *Hsp90aa1<sup>-/-</sup>* mice were usually mated with *Hsp90aa1<sup>+/-</sup>* males to maximize the number of *Hsp90aa1<sup>-/-</sup>* mice obtained. Mating couples were established between 2.5 and 9 months old. WT, KO and HE female mice were employed for *in vivo* tumor analyses.

## 2. Cell lines

### *Fibroblast cell lines*

Murine NFs (NF1, NF5) and CAFs (CAF1, CAF2, CAF5) cell lines were previously established by the Calvo lab<sup>185</sup>. They were derived from the mouse mammary tumor virus-polyoma middle tumor-antigen (MMTV-PyMT) breast cancer model and the corresponding normal mammary gland counterparts. Briefly, fibroblasts were isolated and expanded *in vitro*, and immortalized by the expression of the *HPV-16 E6* gene during the first 5 passages<sup>186</sup>. Murine mammary fibroblasts were also isolated and established from the healthy mammary glands of *Hsp90aa1<sup>+/+</sup>*, *Hsp90aa1<sup>-/-</sup>* and *Hsp90aa1<sup>+/-</sup>* mice (see “Isolation and immortalization of mammary gland fibroblasts from murine model” section below).

To enable the immunoprecipitation of endogenous YAP and its targeted degradation, genetically-modified versions of NF1 and CAF1 generated by the lab were also employed. These modified cell lines contain a V5-dTAG sequence in frame at the 5' extreme of one of the endogenous *Yap1* alleles (NF1-V5-dTAG and CAF1-V5-dTAG). As a result, these cells express a copy of the wild-type *Yap1* and one copy of *Yap1-V5-dTAG*. The product of this modified version can therefore be detected and immunoprecipitated with V5 antibodies. The dTAG sequence is FKBP12-F36V. Addition of the targeted degrader dTAG in these cell lines results in the targeted degradation of the chimeric Yap1-V5-dTAG, remaining the wild-type version unaltered. As a result, YAP activity is reduced but cell viability is not compromised. The dTAG treatment (300 nM) was maintained for 24 h prior performing the experiments.

For the generation of NF1 cells overexpressing a constitutive active version of YAP (NF1-YAP<sup>MUT</sup>), NF1 were infected with the pLL3.7-EF-EYFP-YAP1\_5SA-PolyA plasmid (#112285, Addgene). This YAP mutant presents the substitution of 5 Serine residues (Ser61, Ser109, Ser127, Ser164 and Ser397) by Alanine. These substitutions impede the phosphorylation of YAP and its consequent inactivation/degradation, resulting on its stabilization in the cytoplasm and its overactivation.

### *Cancer cell lines*

D2A1 (Cellosaurus CVCL\_OI90) murine breast cancer cells were derived from spontaneous mammary tumors in BALB/c mice, which originated from a D2 hyperplastic alveolar nodule in. These

cells were a kind gift from Dr. Erik Sahai (Crick Institute, UK), and were used in *in vitro* experiments. E0771 (Cellosaurus CVCL\_GR23) murine breast cancer cells were originally isolated from a spontaneous tumor in C57BL/6 mouse. They were a kind gift from Dr Kristian Pietras (Lund University, Sweden), and were used to generate syngeneic tumors in our murine *in vivo* model. Where indicated, both cancer cell lines were labeled with Green Fluorescent Protein (GFP) using the EGFP-CAAX pCSII-IRES2-hygro lentiviral vector.

PY8119 cells are murine breast cancer cells isolated from the MMTV-PyMT *in vivo* model. They were a kind gift from the lab of Dr. Hector Peinado (Spanish National Cancer Research Centre, CNIO) and originally isolated by Dr. Daniela Quail lab (Goodman Cancer Institute, Canada).

### 3. Specialized materials, reagents lists and references

#### *Cell culture reagents*

- DMEM High Glucose: Dulbecco's Modified Eagle's Medium – High Glucose (#D5671, Sigma)
- F-12K Nut Mix medium (#21127-022, Gibco)
- FBS: Fetal Bovine Serum (#10270106, Gibco)
- GlutaMAX™: GlutaMAX™-I (100X) (#35050-061, Gibco)
- Trypsin: 0.05% Trypsin-EDTA 1X (#253000-062, Gibco)
- PBS: Dulbecco's Phosphate Buffered Saline (#D8537, Sigma)

### *Cell culture treatments*

- TGF $\beta$ : Human TGF- $\beta$ 1 (#100-21C-10UG, Peprotech)
- Geldanamycin (#S2713, Selleckchem)
- Tanespimycin (17-AAG) (#S1141, Selleckchem)
- Cycloheximide (CHX) (C7698, Sigma)
- dTAG: dTAGV-1 (#6914, Tocris)
- DMSO: Dimethyl Sulfoxide (#D8418, Sigma)

### *Gel contraction materials*

- Matrigel: ECM Gel From Engelbreth-Holm-Swarm Murine Sarcoma (#E1270, Sigma-Aldrich).
- Collagen: Collagen I, High Concentration, Rat Tail (#354249, Corning).
- FBS: Fetal Bovine Serum (#10270106, Gibco)
- 5X coll DMEM: 2.5 g DMEM high glucose powder (#12800-058, Gibco), 5 mL 1 M HEPES pH 7.5, 1 g NaHCO<sub>3</sub>, H<sub>2</sub>O up to 50 mL.

### *Cell-Derived Matrices materials*

- 12 well glass-bottom plates: 12-well | No. 1.0 Coverslip | 14 mm Glass Diameter | Uncoated (#2547, Mattek)
- Gelatin: Gelatin from bovine skin (#G9391, Sigma)
- Glutaraldehyde: Glutaraldehyde solution 25% in H<sub>2</sub>O (#G5882, Sigma)
- Glycine (#MBO1401, NZYTech)
- Ascorbic acid: L-Ascorbic Acid (#A92902, Sigma)
- NH<sub>4</sub>OH: Ammonium hydroxide solution (#221228, Sigma)
- Triton X-100: Triton™ X-100 (#X100, Sigma)
- Extraction Buffer: 500  $\mu$ L NH<sub>4</sub>OH, 125  $\mu$ L Triton X-100, 24.38  $\mu$ L PBS

\*All reagents used for CDM experiments were filtered–sterilized using 0.45  $\mu\text{m}$  pore size filters, except for the gelatin, which needed a 0.2  $\mu\text{m}$  pore size filter.

### *Co-culture experiments materials*

- 24 well glass–bottom plates: 24–well | No. O Coverslip | 13 mm Glass Diameter | Uncoated (#P24G–O–13–F, Mattek)
- Mitomycin–C: Mitomycin–C from *Streptomyces caespitosus* (#M4287–2G, Sigma)
- Growth Factor Reduced Matrigel®: Matrigel® Basement Membrane Matrix, Growth Factor Reduced (#354230, Corning)
- Low Glucose DMEM: (#D5546, Sigma)
- Green fluorescent dye: DiO solution from the Vybrant™ Multicolor Cell–Labeling kit (#V22889, Invitrogen)

### *Histology reagents*

- Hematoxylin: Papanicolaou's solution 1a Harris' hematoxylin solution (#1092531000, Sigma)
- Eosin: Eosin Y (yellowish), C.I. 45380 (#1159350025, Sigma)
- Xylene: Xylene mixt. Of isomers (#VWRC28975.360, Avantor)
- Ponceau Fuchsin Masson: 0.1 g Acid Fuchsin (#F8129, Sigma), 0.2 g Ponceau Red (#09189, Fluka), 0.6 mL Acetic Acid, 300 mL Distilled H<sub>2</sub>O.
- Light Green Masson: 0.24g Light Green (1159410025, Sigma), 0.24mL Acetic Acid, 120mL Distilled H<sub>2</sub>O
- Acetic Acid (A6283, Sigma)
- Picrosirius Red (#SRS500, Quimigen)

### *Immunoprecipitation*

- Lysis buffer: 1% Triton X-100, 20 mM Tris-HCl pH 7.5, 50 mM NaCl, 50 mM NaF, 15 mM Na<sub>4</sub>P<sub>2</sub>O<sub>7</sub>, 2 mM Na<sub>3</sub>VO<sub>4</sub>,
- Leupeptin 50 mg (#11034626001, Roche), Aprotinin from bovine lung 50 mg (#10981532001, Roche)
- Washing buffer: 50 mM Tris-HCl pH 7.5, 150 mM NaCl, 5% Glycerol, 0.05% IGEPal-CA-630 (#18896, Sigma).
- Anti-V5 conjugated beads: Anti-V5 Agarose Affinity Gel Antibody Produced in Mouse (#A7345, Sigma).
- Protein G: Pierce™ Protein G Agarose (#20398, Thermo)

### *Western Blot reagents*

- Acrylamide: 30% Acrylamide Bis Solution 37.5:1 (#1610158, Bio-Rad).
- TEMED: N, N, N', N'-Tetramethyl-ethylenediamine (#110-18-9, Sigma)
- Stacking gel: 4% Acrylamide, 125 mM Tris-HCl pH 6.8, 0.4% SDS, 0.1% APS and 0.1% TEMED in H<sub>2</sub>O.
- Resolving gel: 10% acrylamide, 375 mM Tris-HCl pH 8.8, 0.4% SDS, 0.1% Ammonium persulfate (APS, #17874, Thermo Scientific) and 0.1% TEMED in H<sub>2</sub>O.
- Running SDS-Page buffer: 880 mL Milli-Q H<sub>2</sub>O, 20mL SDS 10%, 100mL Tris-Glycine 10x.
- Transference SDS-Page Buffer: 800 mL Milli-Q H<sub>2</sub>O, 100 mL Tris-Glycine 10x, 100 mL methanol.
- BSA: Albumin Bovine Fraction V (BSA) MB Grade (#MBO4602, NZYTech)

### *Proteomics reagents*

- Gu-HCl: Guanidium Hydrochloride (#G3272, Sigma)
- CAA: 2-Chloroacetamide (#C0267, Sigma)
- TCEP: Tris(2-carboxyethyl)phosphine (#C4706, Sigma)
- LyC: Lysil Endopeptidase (#121-05063, Waiko)

- Trypsin: MS-Grade Trypsin (#XJ354843, Pierce)
- TFA: Trifluoroacetic Acid (In house production)
- C18 disks: Empore™ C18 SPE disks (#66883-U, Merck)
- ACN: Acetonitrile (#34998, Honeywell)
- LC-MS H<sub>2</sub>O (#Z0687333 042, Supelco)
- Benzonase: Benzonase® nuclease (#70746, Merck)
- TFE: 2,2,2-Trifluoroethanol (#8.08259, Sigma)

### Primers for *in vivo* genotyping

Genotype	Primer sequence
Forward primer	GCTGTTATGGAAGCCTCAGC
<i>Hsp90aa1</i> <sup>+/-</sup> Reverse primer	CACTCCAACCTCCGCAAACCTC
<i>Hsp90aa1</i> <sup>-/-</sup> Reverse primer	AGGGTTGTTCTCGGGACTTT

**Table M1. Primers used for mice genotyping.** A combination of the 3 different primers at the same time is added to each reaction for the amplification of the corresponding fragment.

### siRNAs references

Name	Gene	Species	Reference	Company
siHsp90aa1 (siAA1)	<i>Hsp90aa1</i>	Murine	D-055680-01	Dharmacon™
	<i>Hsp90aa1</i>	Murine	D-055680-02	
	<i>Hsp90aa1</i>	Murine	D-055680-03	
	<i>Hsp90aa1</i>	Murine	D-055680-04	
siHsp90ab1 (siAB1)	<i>Hsp90ab1</i>	Murine	D-050742-01	Dharmacon™
	<i>Hsp90ab1</i>	Murine	D-050742-02	
	<i>Hsp90ab1</i>	Murine	D-050742-03	
	<i>Hsp90ab1</i>	Murine	D-050742-04	
All Star negative control	-	-	1027281	Qiagen
DharmaFECT® 1	-	-	T-2001-03	Dharmacon™

**Table M2. siRNA sequences used for the silencing of *Hsp90aa1* and *Hsp90ab1* respectively.** A combination of the 4 different siRNAs for each isoform was used to create a “smart pool” for their effective silencing.

*Primers for mycoplasma detection*

Genotype	Primer sequence
Myco A	GGCGAATGGGTGAGTAACACG
Myco B	CGGATAACGCTTGCGACCTATG

**Table M3. Primers used to detect mycoplasma through PCR.**

*Antibodies for Western Blotting*

Protein	Dilution	Company	Reference
HSP90 (1)	1:1000	Abcam	ab2928
HSP90 (2)	1:1000	Invitrogen	PA3-013
HSP90 (3)	1:1000	Synaptic Systems	380003
GAPDH	1:5000	Cell signaling	#3683
YAP/TAZ	1:1000	Santa Cruz	sc-101199
Src	1:1000	Cell signaling	#2109
Yes1	1:1000	Abcam	ab109265
$\beta$ -catenin	1:1000	Cell signaling	#8480
Non-Phospho (Active) $\beta$ -catenin	1:1000	Cell signaling	#8814
$\alpha$ SMA	1:5000	Sigma Aldrich	A5228
SMAD2/3	1:1000	Cell signaling	#8685S
Phospho-Smad2 (Ser465/467)/ Smad3 (Ser423/425)	1:0000	Cell signaling	#8828S
FAK	1:1000	Cell signaling	#3285
Phospho-FAK (Tyr397)	1:1000	Cell signaling	#8556
MLC2	1:1000	Cell signaling	#3672
Phospho-MLC2 (Ser19)	1:1000	Cell signaling	#3671
MYH10	1:1000	Sigma	M7939
Fibronectin	1:1000	Sigma	F3648
HSF1	1:1000	Cell signaling	#4356
Phospho-HSF1 (Ser326)	1:1000	Bioss	bsm-52166R
V5-Tag	1:1000	Invitrogen	R960-25
Polyclonal Goat Anti-Rabbit Secondary Antibody	1:10000	Agilent Technologies	PO448
Polyclonal Goat Anti-Mouse Secondary Antibody	1:10000	Agilent Technologies	PO447

**Table M4. Antibodies used for Western Blotting.** All antibody dilutions were prepared in 4% BSA.

### *Antibodies for Immunofluorescence*

Antibody	Dilution	Company	Reference
DAPI	1:500	Millipore	90229
Phospho-PAX (Tyr118)	1:500	Invitrogen	44-722G
Fibronectin	1:500	Sigma	F3648
Phalloidin-TRITC	1:1000	Sigma	P1951
Alexa Fluor 488	1:500	Invitrogen	A11008
Alexa Fluor 594	1:500	Invitrogen	A-11012

**Table M5. Primary and secondary antibodies used for immunofluorescence.** All antibodies were diluted in PBS.

### *RT-qPCR primers sequence*

Gene	Forward primer	Reverse primer
<i>Gapdh</i>	GTGCAGTGCCAGCCTCGTCC	GCCACTGCAAATGGCAGCCC
<i>Hsp90aa1</i>	ACTCTGCCTAATTTGGTTGCTG	CTTTGTTCCACGACCCATTG
<i>Hsp90ab1</i>	TACTCGGCTTTCCCGTCAAG	TTAGAAGGGTCCGTCAGGCT
<i>Yap1</i>	AACATGGCAGGACCCCGGA	TGGAGCATTTGCTGTGCTGGG
<i>Wwtr1</i> (TAZ)	GAGAGGATTAGGATGCGTCAA	GGATCTGAGCTACTGTTGGTG

**Table M6. Primers used for the RT-qPCR experiments.** All of them are murine genes.

### *Antibodies for Immunoprecipitation*

Antibody	Dilution	Company	Reference
HSP90 (3)	1:1000	Synaptic Systems	380003
YAP/TAZ	1:1000	Santa Cruz	sc-101199
LATS1	1:1000	Cell signaling	3477P
14-3-3	1:1000	Santa Cruz	sc-1657
Anti-V5	1:1000	Millipore	A7345

**Table M7. Antibodies used for immunoprecipitation.** All antibody dilutions were prepared in 4% BSA.



# Methods



## 1. In vivo procedures

All in vivo experiments were approved by the relevant Authority and performed according to the guidelines of the Committee of Animal Experimentation of the University of Cantabria (Project “Caracterización molecular y celular del papel del microambiente tumoral y los CAFs en la progresión tumoral, metástasis y resistencia a terapias (antiCAFing)”, References: PI/O5/19 and PI-O2-23). All in vivo experiments were performed by qualified personnel with the relevant authorizations.

### *In vivo genotyping*

In order to check the genotype of the newborn mice, DNA from ear samples was extracted by incubation with a digestion buffer containing 0.1 M Tris-HCl pH 8, 5 mM ethylene diamine tetra-acetic acid (EDTA), 0.2 M NaCl, 1:50 (v:v), 10% SDS and 10 mg/mL Proteinase K. Samples are then incubated for 3 h at 55 °C, followed by subsequent addition of isopropanol, centrifugation and addition of 70% ethanol before leaving samples to dry overnight (o/n). The following day, samples were resuspended in RNase free H<sub>2</sub>O and a PCR was run to amplify for the corresponding *Hsp90aa1* region. PCR was performed using the Supreme NZYtaq II 2x Green Master Mix (NZYTech) with a combination of all three primers in **Table M1** for each sample (see *Primers for in vivo genotyping* in the Materials section above for details). PCR products were then run in a 1% agarose gel containing 2 µL of GreenSafe Premium (NZYTech), and the corresponding bands were scanned in a Chemidoc XRS scan system (Bio-Rad).

### *Orthotopic injection of breast cancer cells in vivo*

C57BL/6 *Hsp90aa1<sup>+/+</sup>*, *Hsp90aa1<sup>-/-</sup>* and *Hsp90aa1<sup>+/-</sup>* mice were subjected to orthotopic injection of syngeneic murine breast cancer cells.  $2.5 \times 10^5$  E0771 breast cancer cells were injected directly into the 4<sup>th</sup> mammary fat pad of 6–8 weeks old mice by performing small surgery. The induction of anesthetized mice was performed using inhaled 2% isoflurane at a flow rate of 0.8 L/min and reduced down to a flow rate of 0.4 L/min to maintain the anesthesia. Then, a small incision was performed in the 4<sup>th</sup> mammary fat pad and the mammary gland was exposed to the exterior. Cells were then injected, and wound was closed with suture. Tumor growth was monitored every other day using palpation and calipers until their length or width was no bigger than 2 cm in average. Tumor volume was calculated for each time point using the formula:  $(4\pi/3) \times (\text{width}/2)^2 \times (\text{length}/2)$ . When the final point was reached, mice were sacrificed and tumors were extracted, weighted, fixed for 24 h in 4% formaldehyde and paraffin-embedded for further histological studies in our lab and by the pathology services at the Hospital Universitario Marqués de Valdecilla (HUMV).

### *Isolation and immortalization of mammary gland fibroblasts from murine model*

At the same time that the above-mentioned primary breast cancer tumors were extracted, we also extracted the opposite healthy mammary gland to isolate *Hsp90aa1<sup>+/+</sup>*, *Hsp90aa1<sup>-/-</sup>* and *Hsp90aa1<sup>+/-</sup>* fibroblasts, following the protocol previously published by Calvo, et al<sup>186</sup>. Briefly, tissue was mechanically disaggregated in cell culture plates, covered with coverslips to avoid fatty tissue floating,

and cell culture media was added. Tissue was maintained in culture and media was changed every day until fibroblasts could be observed leaving the tissue and attached to the plate. Fibroblasts were then transferred to a new cell culture plate, expanded, and immortalized by infection with HPV-E6-puromycin retroviruses<sup>186</sup>.

#### *In vivo breast cancer metastasis experiment*

C57BL/6 *Hsp90aa1<sup>+/+</sup>*, *Hsp90aa1<sup>+/-</sup>* and *Hsp90aa1<sup>-/-</sup>* mice were subjected to tail vein injection of syngeneic murine breast cancer cells for metastasis assays. Briefly, mice were restrained using appropriate clamps and the tail was pre-warmed in hot water to allow venous dilation.  $2.5 \times 10^5$  E0771 breast cancer cells were injected via the lateral tail vein. Mice weight was monitored every two days until weight loss started. Mice were then sacrificed approximately 2 months after the procedure, when no more than 20% of their weight was lost. Lungs were then extracted, fixed in 4% Formol for 24 h and prepared for further histological studies by the pathology services at HUMV.

#### *Histology techniques, Immunohistochemistry (IHC) and Immunofluorescence (IF)*

Fixed tissues were paraffin-embedded and cut in 5  $\mu$ m sections. For tissue staining with the different techniques, samples were first de-paraffined by inclusion into a Xylene solution for 10 min, followed by washing with decreasing concentrations of ethanol to rehydrate the tissue.

For Hematoxylin and Eosin (H&E) staining, samples were then incubated in Hematoxylin for 10 min and included into a differentiation solution of 100% ethanol and 1% HCl to remove the excess of Hematoxylin. Then, samples were incubated in 1 g/L Eosin-H<sub>2</sub>O for 12 min and treated in 100% ethanol to remove the excess of Eosin and de-hydrate the samples. After a final inclusion in Xylene to remove all excess reagents, coverslips were placed on top of the tissue with glue to make them ready for analysis.

For Masson's Trichrome staining, de-paraffined tissue was first stained with Hematoxylin similar as described above, followed by incubation for 2 min in Ponceau Fuchsin Masson solution and 5 min in Light Green Masson (see *Materials* section for recipes). Slides were washed with 1% Acetic Acid-H<sub>2</sub>O and 5% Phosphomolybdic Acid in between incubations. Finally, tissue was dehydrated in 100% ethanol, Xylene-washed and mounted for histology imaging as previously described.

For Picrosirius Red staining, de-paraffined samples were first stained for 8 min with Hematoxylin, followed by incubation in Picrosirius Red for 1 h (see *Materials* section for recipe). The staining was washed with 0.5% Acetic Acid-H<sub>2</sub>O, de-hydrated and mounted for imaging as previously described.

Glass slides were scanned using Axio Scan.Z1 Slide Scanner (ZEISS).

## 2. Cell biology procedures

### *Cell culture conditions*

All cell lines were cultured in High Glucose Dulbecco's Modified Eagle Medium, except the PY8119 cancer cells, which were cultured in F-12K Nut Mix medium. All media were supplemented with 10% FBS, 1% Penicillin/Streptomycin (P/S), and 1% GlutaMAX, and cells were maintained at 37°C in a humidified atmosphere containing 5% CO<sub>2</sub> (see *Materials* section for references). For certain experiments, FBS concentration was reduced to 2%. All cell lines were maintained in cell culture for no longer than 10 passages, and used at below 80% confluence, unless indicated otherwise. Cells were also regularly tested for mycoplasma (see *Molecular biology procedures* below for details). For cryopreservation, 5x10<sup>5</sup> cells were centrifuged and resuspended in 1 mL FBS containing 10% Dimethyl Sulfoxide (DMSO) and kept at -80 °C for no longer than 2 months using a Mr. Frosty™ freezing container (Nalgene). For long-term storage, cells were kept up to 6 months at -140 °C and then transferred into liquid nitrogen. Cells were quickly thawed by heating vials at 37 °C for few seconds and transferring them immediately into cell culture flasks with fresh complete media.

### *Cell treatments*

For those experiments that required this stimulation, TGFβ was added to a final concentration of 5 ng/mL into the cell culture media 5 h after transfection, and the stimuli was maintained throughout the whole experiment. Cells were typically used after 24h of TGFβ stimulation.

HSP90 inhibitors Geldanamycin and Tanespimycin (17-AAG) were used to block HSP90 activity in our in vitro experiments (see *Specialized materials and reagents lists* section above for drug references). The 0.01  $\mu\text{M}$  concentration employed for both drugs was decided by performing alamarBlue™ proliferation assays and comparing the obtained results with the literature. This concentration was the highest one that did not have significant effects in fibroblasts proliferation. Controls were always treated with the same concentration of DMSO, as this was the solvent used to dissolve drugs stocks (vehicle). Cells were left for 24 h with the drug treatment prior use in any experiment.

#### *Transfection with siRNAs*

Transfection was performed using the DharmaFECT® transfection reagent according to manufacturer instructions. Briefly,  $3 \times 10^5$  fibroblasts per well were seeded 24h before transfection in a 6 well plate. Media was changed for 1 mL of Opti-MEM cell culture media (Gibco) and transfected with 64 nM of siRNA and 4.5  $\mu\text{L}$  of DharmaFECT for 5h. After that, media was supplemented with 1 mL of complete DMEM. Individual siRNAs or smart-pool (sp) siRNAs were employed for these analyses. sp-siRNAs were generated by combining the 4 different siRNAs available for each one of the specific HSP90 isoforms, respectively (**Table M2**). In addition, All-Star siRNA was used as a negative control, which has no homology to any known mammalian gene (**Table M2**). Fibroblasts were then used 24 h or 48 h after transfection for subsequent cellular or molecular analysis.

### *Gel contraction assay*

Gel contraction experiments were performed in standard 48 well plates. The day before the experiment, the plates were incubated o/n with 1% BSA in PBS at 37 °C in sterile conditions. Right before the experiment, the BSA was removed from the wells. Then,  $1 \times 10^5$  fibroblasts were mixed with 100  $\mu$ L per well of an artificial matrix made of Matrigel® (final concentration ~2.2 mg/mL), Collagen I (final concentration ~4.6 mg/mL), 10% FBS and cell culture media (see *Specialized materials and reagents lists* above for details). The mix was plated in triplicates and incubated 1 h at 37 °C to allow for gel solidification. Once the gel was solid, complete culture media was added on top, including TGF $\beta$  or other factors when indicated. The gels were scanned every 24 h and images analyzed in Fiji (Image J) to measure the percentage of gel contraction for each condition (see *Image processing and analysis* section below). Unless stated otherwise, results show the percentage of gel contraction after 48 h.

### *Generation of Cell Derived Matrices (CDM)*

CDMs were generated as described in the protocol by Kaukonen, R. et al<sup>187</sup>. Briefly, glass-bottom 12-well plates were coated with 0.2% (w/v) gelatin o/n at 37 °C and cross-linked with 1% (v/v) Glutaraldehyde for 1 h. After washing with PBS, 1 M Glycine was added for 1 h, and washed again with PBS prior fibroblasts seeding. Then, fibroblasts were seeded into a confluent monolayer and culture media was supplemented with 5 ng/mL of TGF $\beta$  and 50  $\mu$ g/mL ascorbic acid to promote ECM deposition. Cells were then maintained in culture for 5 days and media was changed every other

day due to the instability of the ascorbic acid. TGF $\beta$  was also added every time the media was changed, to maintain the stimulation.

For the experiments in which fibroblasts were not removed, plates were directly fixed with 4% PFA for 30 min at room temperature and further processed for immunofluorescence analyses (see *Immunofluorescence* section below). For the experiments in which the fibroblasts were removed, plates were incubated with Extraction Buffer containing NH<sub>4</sub>OH and Triton X-100 (see *Specialized materials and reagents lists* above for details) at 37 °C, until no intact cells were observed. The resulting CDMs were used right away or stored with 1 mL of PBS at 4 °C until further use.

See *Specialized materials and reagents lists* section above for details about the reagents used for this experiment.

#### *Cancer cells cultured over CDMs*

5x10<sup>3</sup> D2A1-GFP cells were seeded on top of the fibroblast-cleaned CDMs in low serum media (2% FBS) and maintained in culture for 4 days (final time point represented in results section). To monitor cancer cell growth, GFP-fluorescence images were taken every day with an Eclipse TS100 (Nikon) microscope. After that, the experiment was fixed in 4% PFA to prepare for immunofluorescence (see *Immunofluorescence* section below). Images were taken using confocal microscopy and analyzed using Fiji (see *Image processing and analysis* section below). Cells and CDM at endpoint were washed with PBS, fixed in 4% PFA for 30 min and further processed for immunofluorescence analysis.

### *Cancer cell spheroids timelapse over CDMs*

D2A1-GFP spheroids were generated by plating 100 cells per well in a low-adherence curved-bottom 96 well plate for 48h. Then, 4 spheroids per condition were transferred directly over the already-made CDMs and 1 mL of complete cell culture media was added. Images were then taken every hour for 3 days using confocal microscopy in a Nikon Eclipse Ci2 microscope coupled to a closed chamber in which environmental conditions were kept similar to the usual cell culture conditions, so that the cells stay alive during the whole experiment.

### *Wound Healing assay*

$4 \times 10^5$  fibroblasts were seeded per well in a 6-well plate to form a confluent monolayer, and a straight scratch was made in the center of the well using a 200  $\mu$ L pipette tip. Then, cell migration was monitored, and images of the scar were taken every 2 h using the bright field mode in an Eclipse TS100 (Nikon) microscope with the 4X objective, until one of the conditions completely closed the wound. The closed wound area was then measured using Fiji.

### *Transwell assay*

For this experiment, 24 well plate/12 insert chambers with 8  $\mu$ m pore (#3422, Costar<sup>®</sup>) were used to study the migration of the cells in different conditions. The lower chamber was filled with 500  $\mu$ L of complete cell culture media and  $1 \times 10^4$  transfected fibroblasts were seeded per well in 200  $\mu$ L of complete cell culture media, on top of the membrane in the upper chamber. In the case of the TGF $\beta$ -stimulated conditions, the total concentration in the well (upper and

lower chamber together) was 5 ng/mL. The following day, the media was carefully aspirated, and cells were removed from the upper part of the membrane by carefully rubbing with a cotton swab. Next, the membranes were stained using Crystal Violet staining solution for 20 min, carefully washed with MilliQ H<sub>2</sub>O and dried o/n. The following day, images were taken at 4X and analyzed using a specific Macro in Fiji (Image J).

### *2D co-culture experiments*

3x10<sup>5</sup> siRNA-transfected fibroblasts were seeded per well in a 6-well plate to form a confluent monolayer. The next day, 10 µg/mL of Mitomycin-C was added for 3 h. Cells were washed with PBS and DMEM supplemented with low serum media (2.5% FBS) was added.

In an alternative approach, to perform the same experiment in a more restrictive environment, 2 x 10<sup>3</sup> fibroblasts (siRNA-transfected or *in vivo*-derived) were seeded per well in a 24 well plate containing low glucose DMEM media supplemented with 2% FBS.

On top of the fibroblasts, 1.5 x 10<sup>4</sup> D2A1-GFP or PY8119-GFP cells were seeded per well. Cancer cell growth was monitored by taking images in the fluorescent microscope every 24 h up to 7 days. Images were then analyzed using Fiji (see *Image processing and analysis* section below). Graphs and images show results after 48 h, 120 h or 7 days.

### *3D co-culture experiments in Matrigel*

150  $\mu\text{L}$  of a mix of 1:1 Growth Factor Reduced Matrigel<sup>®</sup>:PBS were added per well of a 24 well glass-bottom plate, and left to solidify at 37 °C for 2 h. Next,  $1.5 \times 10^4$  transfected fibroblasts and  $5 \times 10^3$  D2A1-GFP cells were seeded together at the same time on top of the Matrigel<sup>®</sup>, in 700  $\mu\text{L}$  of low glucose DMEM supplemented with 2.5% FBS, 1% GlutaMAX and 1% P/S. Then, cancer cell growth was monitored by taking images in the fluorescent microscope every 24 h up to 3 days. Images were then analyzed using Fiji (see *Image processing and analysis* section below). Graphs and images show results after 48 h.

### *Cell cycle experiments*

$2 \times 10^5$  cells were plated for each condition in P60 plates for transfection as previously described, including a control condition with DharmaFECT<sup>®</sup> alone (and no siRNA) to confirm that this reagent does not affect cell proliferation. Cell culture medium was changed 24 h after transfection, and at this point  $2 \times 10^5$  non-transfected fibroblasts were plated as an additional control. After additional 24 h, cells from all conditions were collected and fixed in 70% ethanol o/n at 4 °C. The following day, cells were centrifuged at 1,000 rpm for 5 min, washed with PBS and resuspended in 100  $\mu\text{L}$  of PBS containing RNase and Propidium Iodide (except for the non-transfected controls, that will only contain the RNase). Samples were then analyzed by the cytometry service at Instituto de Investigación Valdecilla (IDIVAL), in which cells were separated by cell cycle stage and the percentage of cells in each one of them was analyzed.

### 3. Molecular biology procedures

#### *Mycoplasma test*

1.5 x 10<sup>5</sup> cells are plated in a P60 cell culture plate and left for 48 h in normal cell culture media without antibiotics. After this incubation, 1 mL of media is collected and centrifuged, and the resulting supernatant is incubated at 95 °C for 10 min. The PCR is then conducted by mixing the Supreme NZYtaq II 2 x Green Master Mix (NZYTech) with 1 µL of primer Myco A, 1 µL of primer Myco B, 1 µL of the sample and up to 20 µL of RNase free H<sub>2</sub>O, and carried out as follows: denaturalization step at 94 °C for 6 min; annealing step at 60 °C for 1 min; extension step at 72 °C for 1 h 35 min; with 35 cycles of amplification. PCR products were then run in a 1% agarose gel containing 2 µL of GreenSafe Premium (NZYTech), and the corresponding bands were scanned in a Chemidoc XRS scan system (Bio-Rad).

#### *Western Blotting (WB)*

Unless stated otherwise, cells were lysed directly in 2X Laemmli Buffer, which was prepared by diluting 4X Laemmli Sample Buffer (Bio-Rad) with Tris HCl 1M pH 6.8 in a 1:1 proportion, and adding 0.07 g/mL of dithiothreitol (DTT) 4.5 M. Lysed samples were then sonicated for 5 min at the highest power and boiled at 95 °C for 10 min. Protein lysates were resolved by standard SDS-PAGE electrophoresis and proteins were then transferred into nitrocellulose membranes, followed by 1 h of blockage with 4% BSA. Incubation with the corresponding primary antibody was performed o/n at 4 °C. After that, incubation with the corresponding secondary

antibody was performed for 1 h at RT. Dilutions and references for antibodies can be found in **Table M3** of the *Materials* section. For protein detection, the Enhanced Chemoluminescence (ECL) reaction was performed, and proteins were detected using the Amersham ImageQuant 800 (Cytiva). For the statistical analysis, intensity of the bands was measured using Fiji, and normalized to GAPDH as loading control.

#### *Protein stability experiments*

5 x 10<sup>4</sup> fibroblasts were plated in 6-well plates and treated with 10 µg/mL of cycloheximide (CHX) to stop the production of new proteins. Cells were then lysed in 100 µL 2X Laemmli Buffer at 0 h, 1 h, 2 h and 3 h after the treatment, and WB was performed following the above-described protocol.

#### *Immunoprecipitation*

Cells were collected using lysis buffer suitable for immunoprecipitation (see *Materials* section above for recipe details). Lysed samples were then centrifuged at 17,000 g for 15 min at 4 °C, and a small aliquot of the supernatant for each condition was diluted in 4X SDS-PAGE sample buffer and kept for subsequent immunoblot analysis (total lysate). The rest of the supernatant was incubated at 4 °C for 4 h with the anti-V5 antibody conjugated to agarose beads, or anti-HSP90 antibody conjugated to Protein G (see *Materials* section above for reference details). The beads were next washed three times with washing buffer (see *Materials* section above for recipe details). Finally, beads were diluted in 2X Laemmli Buffer

and the WB protocol was carried out. A list of used antibodies can be found in **Table M6**, in the *Materials* section.

### *Immunofluorescence*

Fibroblasts were seeded in sterilized cover glass slides placed into a 24-well plate. After 24 h, cells were fixed in 4% paraformaldehyde (PFA) for 10 min. Cells were then permeabilized with 0.2% Triton X-100 for 7 min, followed by blockade in 3% BSA 0.1% Tween for 1 h. After that, cells are incubated with the corresponding primary antibody o/n at RT in a humidified chamber. The following day, the primary antibody was washed with PBS and cells are incubated with the corresponding secondary antibody for 1 h at RT. After washing the secondary antibody with PBS, glass covers were mounted in slides and imaged using a confocal microscope (See below)

For the observation of the ECM by immunofluorescence, previously fixed CDMs were permeabilized with a 0.5% PBS-Triton solution for 10 min at RT. After washing with PBS, CDMs were blocked o/n at RT with 3% BSA. The following day, BSA was washed and CDMs were incubated with 0.1% PBS-Tween for few seconds prior incubation with the primary antibody for 3 h at RT. Next, the primary antibody was washed with PBS and CDMs were incubated with the corresponding secondary antibody for 1h at RT. Antibodies, references and dilutions used for immunofluorescence can be found in **Table M4**, in *Antibodies for Immunofluorescence* in the Materials section above.

Immunofluorescence images were obtained using a TCS SP5 Confocal Microscope (Leica). For in vitro cell imaging, images were taken using the 40X oil immersion objective. For CDM imaging, the 20X objective was used. Lasers of 405 Diode UV, Argon Helium–Neon (HeNe) 543 and HeNe 633 were used for the excitation of the corresponding fluorophores, and fluorescence was captured in the following wave lengths: blue fluorescence, between 420 nm and 480 nm; green fluorescence, between 500 nm and 540 nm; red fluorescence, between 606 nm and 656 nm.

#### *RNA extraction and RT-qPCR*

RNA extraction was performed using the NZY Total Isolation Kit (NZYTech), according to manufacturer's instructions. RNA quality and concentration were measured using the Nanodrop 2000 spectrophotometer (ThermoFisher Scientific). Reverse transcription was performed using the NZY First-Strand cDNA Synthesis Kit (NZYTech). RT-qPCR was carried out in triplicates for each sample, using the NZYSpeedy qPCR Green Master Mix 2X ROX plus (NZYTech), according to the manufacturer's instructions. The RT-qPCR reaction was performed in a StepOnePlus real-time PCR system (Applied Biosystems). *Gapdh* was used as the housekeeping gene for the normalization of the data, and the quantification and comparison were obtained using the  $\Delta\Delta C_t$  method. Primers used and their corresponding sequence can be found in **Table M5**, in *RT-qPCR primers sequence* in the Materials section above.

## 4. Molecular characterization approaches

### *Proteomic studies of in vitro cell lysates*

1 x 10<sup>5</sup> fibroblasts were transfected as previously explained (see *Transfection with siRNAs* section) and lysed with 6M Gu-HCl, 1 mg/mL 2-CAA and 1.5 mg/mL TCEP. Cell lysates were then boiled for 5 min at 95 °C, followed by incubation with 1 µL of LyC (Waiko) at 37 °C in a shaking heat block for 2 h. After that, 1 µL of MS-Grade Trypsin (Pierce) was added per sample and incubated o/n at 37 °C for protein digestion. The following day, 5 µL of 10% TFA was added per sample to ensure the acidification of the sample. To obtain the supernatant with the corresponding digested peptides, samples were centrifuged for 5 min at 17,000 g prior stage-tipping step. Stage tips were prepared by placing two Empore™ C18 extraction disks into a 200 µL pipette tip. C18 disks were then activated by adding 15 µL methanol and washed with 0.1% TFA by centrifuging 1 min at 500 Relative Centrifugal Force (rcf). Samples were then centrifuged through the disks 5 min at 500 rcf and disks were washed again with 0.1% TFA prior elution of the samples using 10% ACN and 0.05% TFA onto a 96-well plate. Samples were vacuum dried and reconstituted in LC-MS-grade H<sub>2</sub>O, and peptide content was estimated at 280 nm absorption using a Nanodrop 2000 spectrophotometer (ThermoFisher Scientific). For LC-MS analysis of the samples, 1 µg of peptides was injected and separated on an UltiMate™ 3000 RSLCnano UHPLCsystem (ThermoFisher Scientific), using an Aurora C18 packed emitter (IonOpticks), with a gradient from 4% to 29% ACN in 90 min and a 10 min 80% ACN wash. 0.5 % acetic acid was present throughout. The UHPLC system was coupled online with an Orbitrap

Fusion™ Lumos™ Tribrid™ mass spectrometer (ThermoFisher Scientific) operated in Data-Independent Acquisition (DIA) mode, acquiring a MS 350–1650 Da at 120 k resolution followed by MS/MS on 45 windows with 0.5 Da overlap (200–2000 Da) at 30 k with a Normalized Collision Energy (NCE) setting of 27.

### *Proteomic studies of CDMs*

After the generation of CDMs using the above-mentioned protocol, these were carefully cleaned by washing several times with PBS and incubated with a mix of 1  $\mu$ L Benzonase® nuclease (Merck), 1 M Mg and Triton X-100, to avoid contamination of our proteomic data with other intracellular components. Then, CDMs were lysed using the above-described lysis buffer (see *Generation of Cell Derived Matrices (CDM)* for details), and the same above-described protocol was followed to process the CDM samples through the mass-spectrophotometer.

### *Proteomic data analysis*

The raw spectra files were searched using DIA-NN software (version 1.8.1, Demichev, Ralser and Lilley labs) against the UPO00000589 *Mus musculus* database, using the default setting for library-free search. Protein and peptides expression ratios were obtained and normalized using Perseus software (version 2.0.11, MaxQuant), as well as performance of the corresponding statistical t-tests for comparison between conditions. This way, we generated an expression matrix of total lysates for NFs and CAFs after modulation of *Hsp90* genes. For the analysis of proteins in CDMs, a similar approach was performed, and intracellular proteins were

removed from the analysis. Unless stated otherwise, expression values for each protein represented in the figures or tables were z-score normalized from the normalized data.

### *RNA-sequencing (RNAseq) processing and analysis*

1.5x10<sup>5</sup> CAF1 and TGFβ-stimulated NFs were transfected in triplicates and RNA was extracted as previously described (see *RNA extraction and RT-qPCR* section above). RNA quality was checked performing an RNA ScreenTape analysis in an Agilent TapeStation system (Agilent Technologies). Samples were then sent to the Centro Nacional de Análisis Genómico (CNAG) for RNA sequencing analysis. Samples were first quality checked and transformed into a library of stranded mRNA molecules using the TrueSeq® Stranded mRNA library preparation kit (Illumina). The stranded mRNA library was then sequenced at a depth of 40 million reads per sample, with a total read length of 150 paired-ended base pairs (bp), using a NovaSeq 6000 S4 system (Illumina). Sequencing gave an output of approximately 12Gb per sample.

RNA sequencing data analysis was performed using the following workflow by the bioinformatician in our group: (1) The quality of the samples was verified using FastQC software (<https://www.bioinformatics.babraham.ac.uk/projects/fastqc/>). (2) Trim Galore! was used for trimming ends and adapters (<https://github.com/FelixKrueger/TrimGalore>). (3) Genome contaminants and ribosomal RNA were removed with BBSplit and SortMeRNA<sup>188</sup> software, respectively. (4) The alignment of reads to the mouse genome (Genome Reference: GRCm38) was performed

using STAR<sup>189</sup>. (5) Gene expression quantification using read counts of exonic gene regions was carried out using Salmon<sup>190</sup>. (6) UMI-tools<sup>191</sup> and Picard (<http://broadinstitute.github.io/picard/>) were used for Unique Molecular Identifiers (UMI)-based deduplication and marking, respectively. (7) Differential expression statistical analysis was performed using DESeq2<sup>192</sup>, and figures and statistics were performed in R software.

Subsequent analyses were performed using either 'count' or 'tpm' (Transcript Per Million) matrix datasets. Principal Component Analysis (PCA) and hierarchical clustering were performed using pre-filtered datasets (removing rows with no counts, or with only a single count across all samples) after 'regularized logarithm' (rlog) transformation.

DESeq2 software was used to identify the Differentially Expressed Genes (DEGs, cutoff:  $P_{adj} < 0.05$ ) and fold changes between experimental conditions, following the program guidelines. This dataset was also employed to derive gene signatures (genesets) associated with either *Hsp90aa1* or *Hsp90ab1* silencing in CAFs or NFs, that were employed in subsequent analyses. Unless stated otherwise, expression values for each gene represented in the figures or tables were z-score normalized from the 'tpm' matrix dataset.

#### *Gene-Set Enrichment Analysis (GSEA)*

For transcriptomic analyses by GSEA, gene count RNAseq data was first preprocessed using the 'Voom Normalization' from the GenePattern platform, following the program guidelines (expression value filter threshold=1). This module preprocesses RNA-Seq data

into a form suitable for use in this type of analysis. Preprocessed data was then run through GSEA software (Broad Institute of MIT and Harvard, USA, [www.broadinstitute.org](http://www.broadinstitute.org)) following the program guidelines. The specific settings applied in all analyses were: Number of Permutations: 1000; Permutation Type: Gene set; Enrichment statistic: Weighted; Metric for ranking genes: T Test. Analyzed genesets were retrieved from the Molecular Signatures Database (MSigDB) from the Broad Institute of MIT and Harvard (USA) (<https://www.gsea-msigdb.org/gsea/msigdb/index.jsp>). In addition, in-house manually curated genesets or genesets from specific publications were employed and are available upon request. Results were represented using an in-house adapted script from GSEA Multi-sample Running Enrichment plots (<https://github.com/GryderArt/VisualizeRNAseq>). Similar approaches were employed to analyze proteomics datasets using normalized proteomic data, using the gene name for the analysis.

To calculate the gene-signature score in each individual sample, we used single sample Gene Set Enrichment Analysis (ssGSEA) Projection Software from the GenePattern platform, following the programs guidelines. This analysis calculates separate enrichment scores for each pairing of sample and gene set. Each ssGSEA enrichment score represents the degree to which the genes in a particular gene set are co-ordinately up- or downregulated within a sample. ssGSEA scores were z-score normalised.

Similar approaches (GSEA and ssGSEA) were employed to investigate the enrichment and/or expression of particular gene signatures in stromal datasets (*see below - Gene expression analyses of clinical datasets*).

#### *Gene expression analyses of clinical datasets*

Gene expression analyses of human tumor stroma were retrieved from NCBI Gene Expression Omnibus (GEO). Datasets include: Finak (GSE9014, Breast), Yeung (GSE40595, Ovary), and Nishida (GSE35602, Colon). These datasets were employed to identify consistent differentially expressed genes (DEGs) in cancer stroma vs normal stroma (cutoff  $\text{Padj} < 0.05$ ) and common up- and downregulated genes, that were employed in subsequent analyses. Additional datasets include two independent datasets of breast cancer stroma suitable for ssGSEA analyses: GSE8977 and GSE26910. In addition, the dataset describing the expression profiles of cell populations purified from human colorectal cancer (GSE39396) was also used. All these datasets were also employed in other bioinformatics approaches including DESeq2, GSEA and ssGSEA, following methodology explained before. ssGSEA analysis of GSE8977, GSE26910 and GSE39396 was employed to investigate the Person correlation coefficient between gene signatures of interest or the normalized expression of gene signatures in each individual sample. For representation purposes, ssGSEA and gene expression values were z-score normalized. GSEA was employed in GSE9014, GSE40595 and GSE35602 to confirm the enrichment of HSP90i signatures. GSE20086 (human breast NF and CAFs), GSE70468 (human colon NF and CAFs), GSE35250 (human ovarian NF and

CAFs) and GSE45256 (murine breast NF and CAFs) were also employed to assess the enrichment of HSP90i signatures in CAFs by GSEA. Finally, a HSP90i gene signature in murine embryonic fibroblasts (MEFs) was generated by identifying the top 500 downregulated DEGs after incubation with 200nM of NVP-AUY922 (HSP90 inhibitor) for 16h (GSE125161). For microarray-based datasets, probe-to-gene collapsing was performed using the highest variance probe.

#### *Unbiased chemical genomics approach*

To identify drug treatments that could potentially regulate the expression of DEGs consistently upregulated in cancer stroma, we interrogated the gene list through the Library of Integrated Network-based Cellular Signatures (LINCS) database using the “Enrichr” platform (<https://maayanlab.cloud/Enrichr/>). The LINCS library has gene-expression profiles induced by over 20,000 compounds, shRNAs, and kinase inhibitors in the L1000 platform, and we specifically interrogated the “LINCS\_L1000\_Chem\_Pert\_down” database (i.e. drug treatments that reduce the expression of our genes of interest), using the “combined score” metric rank in the results.

#### *Enrichment analysis*

DEGs and other gene signatures obtained from previous differential analyses were also processed for enrichment analyses using online platforms such as “DAVID” (<https://david.ncifcrf.gov/>) and “g:Profiler” (<https://biit.cs.ut.ee/gprofiler/gost>). Briefly, “DAVID” was employed to perform functional enrichment analysis (over-

representation analysis) of candidate gene lists over Gene Ontology datasets such as KEGG, GOTERM\_BP and GOTERM\_MF. “g:Profiler” was employed to perform functional enrichment analysis of candidate gene list over manually curated-user provided datasets, provided as “.gmt” files. Adjusted p values were employed for representation.

### *Integrative analysis of proteomics and transcriptomics datasets*

For the integrative analysis of proteomics and transcriptomic datasets to identify HSP90 $\alpha$  effector proteins that may be modulating YAP activity, we first generated a gene list of HSP90 $\alpha$  interactors and YAP-related proteins. The list of HSP90 $\alpha$  interactors was obtained from the BioGRID database<sup>193</sup> (<https://thebiogrid.org/>) on September 2023, obtaining 1,156 interactors. For the list of YAP-related proteins, we first obtained a similar list from BioGRID to identify all proteins reported to interact with YAP (766 proteins). This list was expanded by including all known factors associated with YAP by adding genes contained in the following gene signatures obtained from MSigDB (<https://www.gsea-msigdb.org/gsea/msigdb>): “GOBP HIPPO SIGNALING”, “GOBP NEGATIVE REGULATION OF HIPPO SIGNALING”, “GOBP POSITIVE REGULATION OF HIPPO SIGNALING”, “GOBP REGULATION OF HIPPO SIGNALING”, “REACTOME SIGNALING BY HIPPO”, “WP HIPPO SIGNALING REGULATION PATHWAYS”, “WP LEUKOCYTEINTRINSIC HIPPO PATHWAY FUNCTIONS”, “WP MECHANOREGULATION AND PATHOLOGY OF YAP/TAZ VIA HIPPO AND NONHIPPO MECHANISMS” (917 proteins). Finally, we obtained the intersection between both lists (HSP90 $\alpha$  interactors and YAP-related proteins) to obtain a list of 233 common elements, of which 147 were

represented in the proteomics dataset and were subjected to further analysis. The proteomics expression data of those proteins was first averaged between the different replicates and z-score normalized. In addition, the ssGSEA score for the signature “NON\_PROLIF\_B\_CAF\_YAPTAZ\_ALL\_UP”<sup>79</sup> obtained from the transcriptomics data for each sample was also averaged between the different replicates and z-score normalized. Finally, the Pearson correlation coefficient between the z-score normalized expression of each protein and the z-score normalized ssGSEA score from all samples was calculated. For the analysis with TAZ signatures, the signature “ZHANG\_TAZ\_GENES\_NOT\_YAP” was assessed in the transcriptomics data as the “NON\_PROLIF\_B\_CAF\_YAPTAZ\_ALL\_UP” signature. This signature contains genes induced by TAZ but not YAP in MCF10A cells<sup>194</sup>.

### *Survival analysis*

Analysis of clinical relevance of specific genes or geneset expression was assessed using publicly available data from the Kaplan–Meier Plotter platform for breast, colon and ovarian cancer (www.kmplot.com)<sup>195–197</sup>. Probe-to-gene mapping was performed using Jetset. For survival analysis of ER negative breast (recurrence-free survival) and colon (disease-specific survival) cancer datasets the highest tertial of gene expression was used to dichotomise the different tumors into high and low groups; for ovarian cancer (progression-free survival), “autoselect best cut-off” was selected.

### *Single cell RNAseq (scRNAseq) processing and analysis*

scRNAseq analysis was performed from public datasets of breast and bladder human cancers by the bioinformatician in our lab. Breast scRNAseq data was obtained from the European Genome-Phenome Archive, reference E-MTAB-1060 (<https://www.ebi.ac.uk/biostudies/arrayexpress/studies/E-MTAB-10607>)<sup>198</sup> and consists of 14 fresh human breast tumor tissue samples dissociated into single cells and viably frozen, 7 exhausted and 7 non-exhausted, without prior cell type enrichment. Bladder scRNAseq data was obtained from the China National Center for Bioinformation, reference GSA-Human HRA000212 (<https://ngdc.cncb.ac.cn/gsa-human/browse/HRA000212>)<sup>199</sup>, and consists of tumor and normal mucosa samples processed immediately after being obtained from bladder cancer patients of the study. Our analyses included only the ones with publicly uploaded metadata, remaining 5 tumor samples and 2 mucosae: ("BC1", "BC2", "BC4", "BC5", "BC7", "Mucosa1", "Mucosa3").

Each sample was preprocessed individually following the exact methodology of their original publication, with some changes in software versions in R.

For Breast cancer from Cords 2023: This dataset was generated using the 10x Genomics platform, and the raw data pre-processing, quality control steps, and main cell type annotation have been described. Briefly, gene-by-cell matrices were generated from the raw sequencing data using CellRanger (10x Genomics, v3.0.1) and subsequently transformed into Seurat objects (Seurat v3.0.2). After

removing high-confidence doublets using the DoubletFinder Package, all Seurat objects were merged, and single cells with >7500 or <200 genes, with >75000 read counts, or with >20% of reads mapping to mitochondrial RNA were excluded. Highly variable genes were identified by the sctransform wrapper in Seurat and used to construct principal components. The principal components covering the highest variance in the dataset were used as input for graph-based clustering. Differential gene expression analysis was performed for the resulting clusters, and main cell types were annotated based on the cluster expression of established marker genes (EPCAM and CDH1 for epithelial cells, PECAM1 and VWF for endothelial cells, PDGFRB and FAP for fibroblasts, CD3, CD4, CD8, and NCR1 for the T and NK cell fraction, CD14, ITGAX and HLA-DRA for myeloid cells, MS4A2 for mast cells and basophils, MS4A1 for B cells, and immunoglobulin-encoding genes for plasma cells). For the present study, all clusters annotated as "fibroblasts" in the original dataset were used for downstream analysis. All scRNA-seq analyses were done using R version 4.3.2. We used the Seurat package (5.0.1) function sctransform to normalise and scale the data, using the variables "percent.mt" (mitochondrial genes), "percent.krt", and "percent.MGP" for regression (KRT and MGP were detected across all cell types in some samples due to contamination originating from apoptotic tumor cells). After running principal component analysis, the first 25 components were used for both graph-based clustering using the Seurat functions FindNeighbours and FindClusters as well as dimension reduction analysis such as UMAP.

Bladder samples form Chen 2020: Cell Ranger (version 2.2.0) was used to process the raw data, demultiplex cellular barcodes, map reads to the transcriptome, and down-sample reads (as required to generate normalized aggregate data across samples). These processes produced a raw unique molecular identifier (UMI) count matrix, which was converted into a Seurat object by the R 4.2.2 package Seurat (version 5.0.1). Cells with UMI numbers <1000 or with over 10% mitochondrial-derived UMI counts were considered low-quality cells and were removed. In order to eliminate potential doublets, single cells with over 6000 genes detected were also filtered out. Finally, 52721 single cells remained, and they were applied in downstream analyses. After quality control, the UMI count matrix was log normalized. Since sample from eight patients were processed and sequenced in batches, patient number was used to remove potential batch effect. Then, for each tumor type, all samples were merged together. We used `SelectIntegrationFeatures` to find 2000 most variable genes to perform the integration and minimise batch effect, and `FindIntegrationAnchors` to perform the integration of the samples. `IntegrateData` function was used to integrate data and create a new matrix, in which potential batch effect was regressed out. Integrated datasets were again scaled, linear (PCA) and non-linear (UMAP) dimensional reductions calculated, and clusters discovered with `FindNeighbours` and `FindClusters` at 0.5 resolution using the Louvain algorithm. SingleR 2.2.0 was used in conjunction with `celldex's HumanPrimaryCellAtlasData` to assign cell type to each individual cell. The fibroblasts populations were extracted from the merged datasets at this point filtering the cells

assigned as “fibroblasts”. These new datasets were again scaled, dimensionally reduced, and clustered as the previous ones.

Once all these processes were performed and individual cells were assigned to specific clusters/cell types, we could assign the expression of normalized gene counts to each cell. Individual cell gene signature expression of indicated gene signatures was calculated with Seurat’s AddModuleScore function. Either target gene or gene signature were projected on the UMAP graphs to obtain a visualization of gene expression per cluster. In addition, matrices of gene/gene signature expression per cell were further processed for additional analyses. Briefly, for correlation analyses, the Pearson coefficient between the expression of particular genes/gene signatures was calculated for each identified cell type. For analyses of expression in each cell cluster, the average expression per cell type was calculated and then scaled within a 1 to 0 range (1 high expression, 0 no expression). For genes, where the lowest value was always 0, average values were scaled by dividing by the highest average value. For gene signatures, where certain cell types might contain negative values, average values were scaled by subtracting the minimum average value and dividing by the total range (maximum average value minus minimum average value). For certain analyses, cell types were further stratified depending on the tissue of origin (mucosal or tumor in the BLCA dataset).

## 5. Image processing and analysis

### *Western Blot quantification*

Protein expression from all WB conditions was quantified by measuring the intensity of the bands using the 'Analyze Gels' tool in Fiji. Protein expression was then referred to their corresponding loading control (GAPDH or Actin) and normalized to their corresponding control condition to obtain the fold change and be able to compare between conditions. For analysis of protein stability with CHX, the relative levels of the target protein were calculated for each condition (0 and 3 h after CHX treatment) by normalizing to GAPDH levels. Then, the stability value was calculated as the fold change between the normalized values after 3 h of CHX treatment in comparison with 0 h of CHX treatment.

### *Cell immunofluorescence analysis*

For analysis of focal adhesions, cells were stained with phalloidin and pY118-Paxillin antibodies, and individual cells were imaged using a 63×/1.40 NA oil immersion objective lens (TCS SP8 microscope; Leica). For these analyses that rely on fluorescence intensity differences, microscope settings were kept constant and independent replicates imaged on the same day. Using phalloidin-TRITC staining and ImageJ software, individual cells were selected and analyzed to obtain the whole cell area. Next, the same cell was analyzed to determine the focal adhesion parameters based on pY118-Paxillin staining. A specific threshold was applied in 8-bit converted images and the average size and total area of pY118-Paxillin positive regions was obtained. All images were subjected to the same

threshold parameters to obtain the positive regions, and regions with areas smaller than 10 square pixels were discarded. The pY118-Paxillin-positive area relative to the whole cell area (as determined by phalloidin staining), number of pY118-Paxillin-positive areas and their average size was then calculated for each individual cell.

#### *Gel contraction analysis*

Using Fiji, total area of the well and relative area of each gel are measured. Area of the gel is then referred to the total area of the well and the % of contraction is measured by:

$$\% \text{ Contraction} = \frac{(\text{Well area} - \text{Gel area})}{\text{Gel area}} \times 100$$

#### *CDM architecture analysis*

We used a Fiji macro called TWOMBLI to analyze the architecture of the CDMs, as described by Wershof, E. et al<sup>200</sup>. This software is able to measure the following parameters: lacunarity, fractal dimension, alignment of the fibers, % of High-Density Matrix, Curvature of the fibers, and number of endpoints and branchpoints.

Only the parameters that presented significant differences between the studied conditions were shown in this work.

#### *Analysis of cancer cell growth in co-culture assays*

Images were processed and analyzed using Fiji. A specific threshold was defined to identify GFP positive areas, and the same threshold was maintained for all images. To calculate cancer cell growth index, the area covered by cancer cells in each field of view

was calculated and referred to the corresponding control condition to obtain the fold change used to compare between them.

#### *Analysis of cancer cell behavior over CDMs*

Images were processed and analyzed using Fiji. A specific threshold was defined to identify GFP positive areas, and the same threshold was maintained for all images. To study cancer cell behavior *in vitro*, we used the 'Analyze particles' tool from Fiji to measure the angles in which the cancer cells were disposed on top of the CDMs generated by our fibroblasts. Then, the distribution of those angles was analyzed in order to find the most abundant angle range for each experimental point. This represented a quantitative measure of how the cells were distributed in each condition. In addition, total GFP area was calculated for each image and CDM parameters were calculated as described before. For the analysis of clusters, the area and shape features of endpoint clusters were analyzed using Fiji.

#### *Statistical significance*

Unless specified otherwise, all statistical analysis, graphs and heatmaps were performed and generated using GraphPad Prism software (GraphPad Software, Inc.). Firstly, data was tested for Gaussian distribution using the D'Agostino–Pearson normality test. For those experiments that came out positive for normal distribution, unpaired two-tailed Student's t-test was performed. For non-Gaussian distributions, Mann–Whitney's test was the chosen one. Unless stated otherwise, mean values and standard errors (SEM) are shown. Survival curves were estimated based on the Kaplan–Meier

method and compared using a log-rank test. Significance of the results was stated as follows: \*P < 0.1; \*\*P < 0.01; \*\*\*P < 0.001; #P < 0.0001; ns: non-significant. GraphPad Prism was also used to generate graphs and heatmaps.

### *Diagrams and images*

All drawings and diagrams were generated using Biorender (Biorender.com) or Microsoft PowerPoint (Microsoft Office 2019 version).

# Hypothesis and objectives



The hypothesis of this project is that **HSP90 activities control the tumor promoting behavior of CAFs**. Thus, targeting HSP90 in CAFs may block their capacity to shape aggressive environments and significantly affect tumor progression, offering a novel approach to reprogram the TME with strong therapeutic potential in cancer. To test this hypothesis, the following objectives will be addressed:

- 1. Ascertain the relevance of HSP90 activities in CAF functions**
  - 1.1. Performing comprehensive analysis of the tumor-promoting functions of HSP90 in CAFs.
  - 1.2. Determining the role of HSP90 in the pro-tumorigenic activity of CAFs *in vivo*.
  - 1.3. Assessing stromal changes and therapeutic potential after HSP90 inhibition *in vivo* and *in vitro*.
  
- 2. Investigate the molecular mechanisms whereby HSP90 exert their functions**
  - 2.1. Identification of potential molecular mechanisms downstream of HSP90 in CAFs.
  - 2.2. Delineation of mechanism of action through epistasis analysis.
  
- 3. Extend key findings to human disease**
  - 3.1. Investigate associations using publicly available datasets.



# Results

1. Identification of HSP90 as a new regulator of the CAF pro-tumoral phenotype



## 1.1. Gene expression analysis of public datasets for the study of consistently dysregulated genes in the tumor stroma

There is an increasing interest in studying the molecular mechanisms underlying the configuration of the TME to increase the fundamental understanding of the disease and identify new promising targets for therapeutic approaches that could benefit cancer patients. In recent years, several studies have leveraged on clinical specimens to perform in-depth molecular characterization of the stromal compartment in different tumor types in comparison with normal tissue counterparts. These studies can be exploited to study the differences between the tumor and the healthy stroma, and identify consistent patterns of expression that may be relevant in establishing pathological TMEs.

Using this methodology, our lab previously investigated the stroma of breast, colon and ovarian cancers and identified Dickkopf-3 (*DKK3*) as a consistently upregulated gene in the tumor stroma<sup>79</sup>. Further functional, biological and clinical validation informed that DKK3 was a key regulator of tumor promoting functions in CAFs and delineated its mechanism of action. This study underlined that the identification of consistently dysregulated genes in the tumor stroma across different cancer types is a valid approach for the identification of new CAF-driving mechanisms that could potentially serve as new therapeutic targets in the clinic.

Here, we designed an approach to harness available gene expression datasets to generate signatures of consistently dysregulated genes in tumor stroma across different tumor types. Subsequently, these signatures would be interrogated using an unbiased chemical genomics approach to identify perturbations that affect the expression of the dysregulated genes. The goal was to identify new regulators of tumoral processes in the stroma, focusing in factors that can be specifically modulated with available small molecule inhibitors and that may present therapeutic value. Top candidates would be further characterized to understand their target cell, mechanism of action and anti-cancer potential (**Figure I-1, A**).

Following the above-described workflow, we first performed a gene expression analysis on publicly available tumor stroma datasets from breast, colorectal and ovarian cancer, as well as normal tissue counterparts (**Figure I-1, B**). These datasets were obtained by performing microdissection of the stromal component in normal and cancerous tissues, followed by gene expression analysis. In all three cases, there was a significant amount of differentially expressed genes (DEGs), both upregulated and downregulated in cancer stroma. From all the DEGs, we found 209 consistently upregulated genes in all studied cancer types, and 83 genes that were commonly downregulated (**Figure I-1, C**). Since our aim was to identify strategies that could block pro-tumoral functions in the TME we focused on the list of 209 upregulated genes, that we called “CANCER STROMA HIGH” signature.

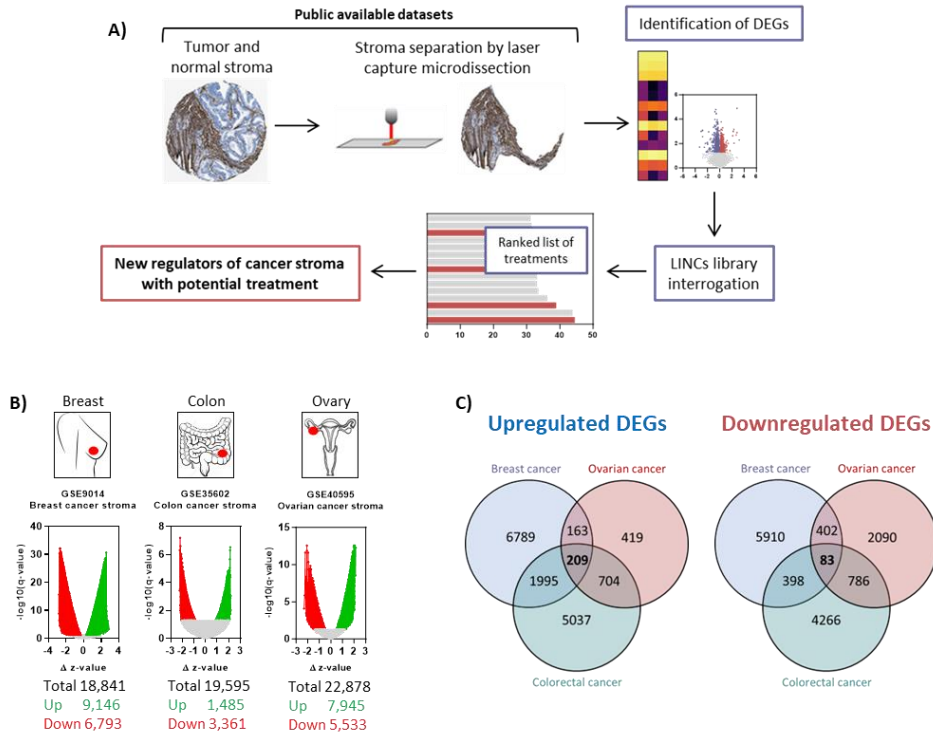


**Figure I-1. Identification of consistently dysregulated genes in the tumor stroma vs normal tissue.** **A.** Schematic representation of the workflow for the identification of new regulators of cancer stroma with potential therapeutic potential. **B.** Graphs showing DEGs resulting from the gene expression analysis in breast (GSE9014), colorectal (GSE35602) and ovarian (GSE40595) databases (tumor stroma vs normal stroma). Graphs show adjusted p-value (q-value) and difference in z-score between cancer and normal samples. Each point represents an individual gene. Upregulated genes are shown in green, whereas downregulated genes are shown in red. **C.** Schematic representation of consistently upregulated (left) and downregulated (right) DEGs in the stroma of breast, colorectal and ovarian cancer. Overlapping areas include the number of commonly upregulated or downregulated genes for each combination. *BC: Breast cancer. CR: colorectal cancer. OV: ovarian cancer.*

## 1.2. Consistently upregulated genes in the tumor stroma correlate with myCAF signatures

Focusing on the genes found to be commonly upregulated in the three cancer types explored (“CANCER STROMA HIGH” signature), we performed enrichment analyses in order to study its potential implications and associations with other tumoral parameters. Using single-sample Gene Set Enrichment Analysis (ssGSEA) in independent datasets of breast cancer stroma, we could obtain a value of expression for the “CANCER STROMA HIGH” signature and other signatures related to tumoral characteristics for each individual sample. First, we confirmed that the “CANCER STROMA HIGH” signature was also enriched in cancer stroma samples in these datasets (**Figure I-2, A**), suggesting that the upregulated expression of these particular genes is a common feature of cancer stroma. Furthermore, our analysis revealed a positive correlation between the “CANCER STROMA HIGH” signature and signatures related with poor prognosis in breast cancer, chemotherapy resistance and metastasis (**Figure I-2, B**). Of note, our signature also strongly correlated with CAF-related signatures, including TGF $\beta$  signaling and matrix remodeling. On the other hand, correlations with signatures related to other stromal components such as endothelia, angiogenesis and immune cells were less relevant, with the exception of macrophage signatures related to M2 and tumor-associated phenotypes.

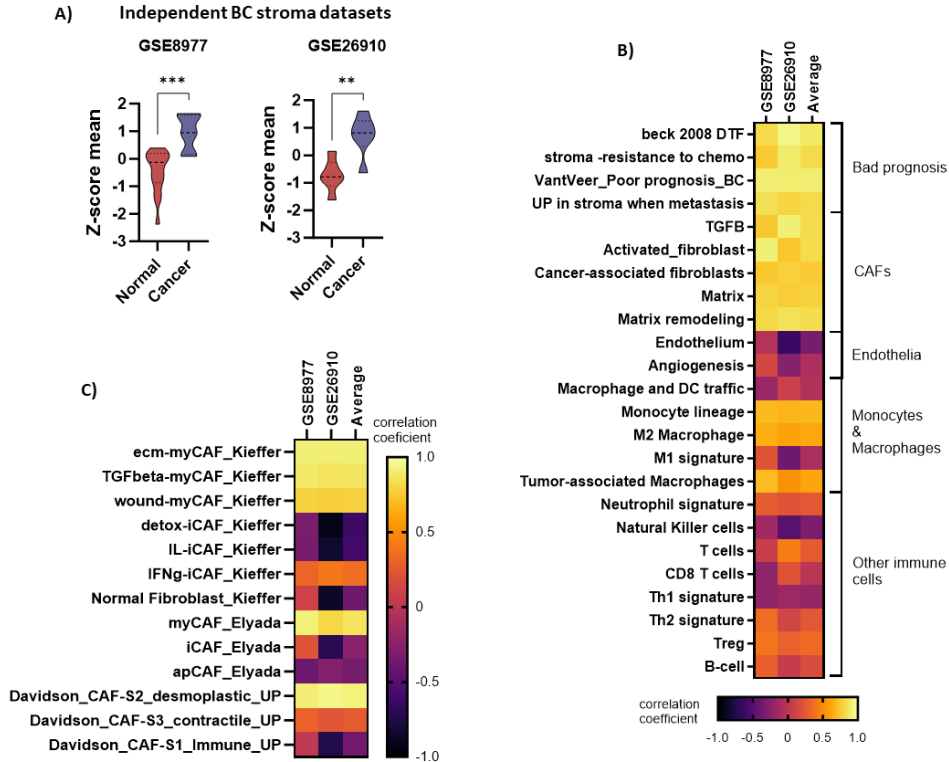


**Figure I-2. Correlation of consistently upregulated genes in the tumor stroma with the different components of the TME.** **A.** Graphs showing the Z-score mean of the ssGSEA value for the “CANCER STROMA HIGH” signature in normal and cancer stroma samples from breast cancer patients. Datasets GSE8977 (left, P-value = 0.0008) and GSE26910 (right, P-value = 0.0087). **B.** Heatmap showing the correlation coefficient between the “CANCER STROMA HIGH” signature and signatures related to immune cells, endothelia, CAFs and bad prognosis in the breast cancer stroma datasets GSE8977 and GSE26910, as informed by ssGSEA analysis. **C.** Heatmap showing the correlation coefficient of the “CANCER STROMA HIGH” signature and signatures related to different CAF subtypes in the breast cancer stroma datasets GSE8977 and GSE26910, as informed by ssGSEA analysis.

Given the positive correlation observed between the “CANCER STROMA HIGH” signature and CAFs signatures, we decided to further explore its potential association with signatures ascribed to different CAF subtypes. The ssGSEA analysis showed a strong positive correlation between the “CANCER STROMA HIGH” signature with myCAF and desmoplastic signatures. On the other hand,

correlations with iCAFs and immune-associated CAFs were mostly negative. These results suggested that myCAFs may be the main contributors to the molecular features associated with the “CANCER STROMA HIGH” signature (**Figure I-2, C**). Noteworthy, original datasets employed to delineate this signature (GSE9014, GSE35602, GSE40595) were not suitable for ssGSEA, so they could not be used to confirm these findings.

### **1.3. Consistently upregulated genes in the tumor stroma are targets of HSP90**

The next step in our approach was to perform an unbiased chemical genomics approach to identify perturbations that negatively affect the expression of the “CANCER STROMA HIGH” genes. For that, we interrogated the LINCS library, a collection of gene expression data coming from cell biology experiments in which a specific perturbation (mainly incubation with small molecules, such as inhibitors, soluble factors or cytokines and chemokines) was applied, and the top dysregulated genes were identified. This computational approach aims to provide a list of potential perturbations that could affect the expression of the genes contained in any given signature.

Among the 15 signatures that were more strongly associated with the “CANCER STROMA HIGH” signature, 4 of them corresponded to signatures obtained from the treatment of different cellular models with the HSP90 inhibitors radicicol, geldanamycin and tanespimycin (**Figure I-3, A**). In fact, this positive correlation was

consistent for breast, colorectal and ovarian cancer, as the HSP90 inhibitors related signatures (“HSP90i signatures”) were significantly enriched in the stroma of these cancer types in comparison with the normal counterparts, as informed by GSEA analysis (Figure I-3, B). These findings suggest that the genes included in the “CANCER STROMA HIGH” signature are mostly HSP90 target genes and that blocking HSP90 activity may target cancer stromal features.

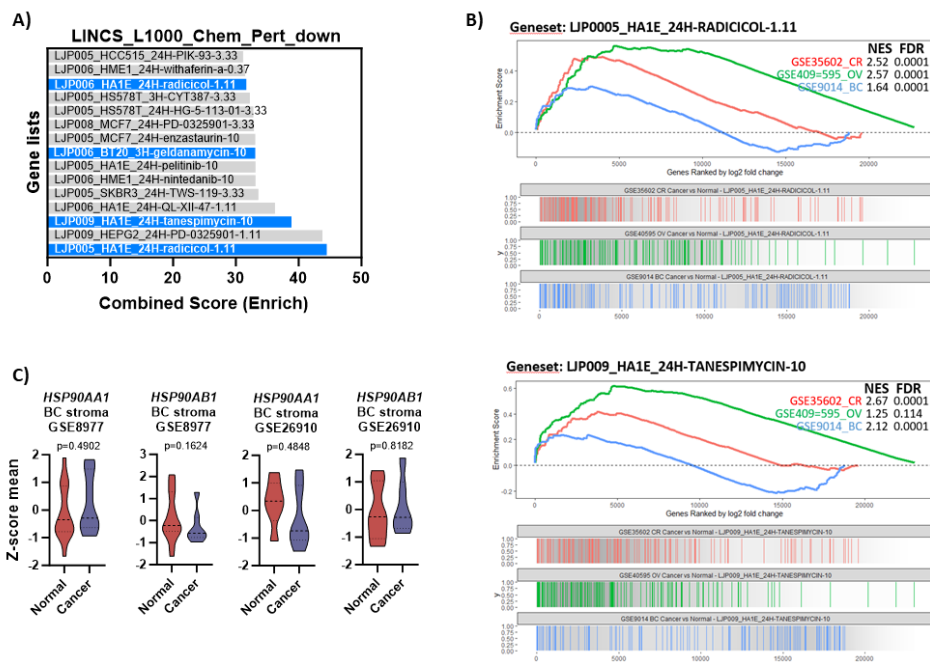


**Figure I-3. Correlation of consistently upregulated genes in the tumor stroma with HSP90 inhibitor signatures.** **A.** Graph showing the 15 signatures with higher combined score (as provided by Enrich analysis of the LINC L100 Chem Pert down database) of enrichment for the “CANCER STROMA HIGH” signature. Signatures related with HSP90 inhibitors are shown in blue. **B.** Graphs showing GSEA plots of HSP90i signatures LJP0005\_HA1E\_24H-RADICICOL-1.11 (upper graph) and LJP009\_HA1E\_24H-TANESPIMYCIN (lower graph) in colorectal (GSE35602), ovarian (GSE 40595) and breast (GSE9014) cancer stroma datasets. Normalized Enriched Score (NES) and False Discovery Rate (FDR) coefficients are also shown. *CR: colorectal cancer. OV: ovarian cancer. BC: breast cancer.* **C.** Graphs showing the z-score value for the gene expression of HSP90AA1 and HSP90AB1 in cancer and normal stroma of the breast cancer patient datasets GSE8977 and GSE26910.

Notably, none of the most abundant HSP90 isoforms (*HSP90AA1* and *HSP90AB1*) were found to be differentially expressed in the analyzed breast cancer datasets (Figure I-3, C). Nonetheless, despite the gene expression analysis not showing any significant variations in HSP90 expression, there could still be differences in HSP90 activities at the functional level.

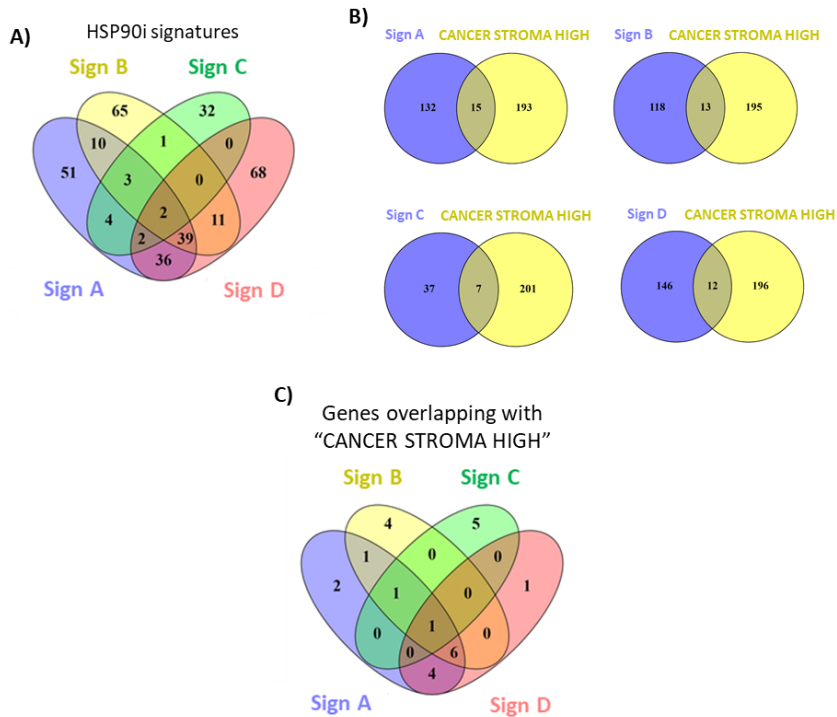


**Figure I-4. Overlap between “HSP90i” and “CANCER STROMA HIGH” signatures.** **A.** Diagram showing the number of genes contained in each “HSP90i” signature and how they overlap between them. **B.** Diagram showing the number of genes from each individual “HSP90i” signature and how they overlap with the “CANCER STROMA HIGH” signature. **C.** Diagram showing the number of genes found to overlap in (B) that are found in each of the “HSP90i” signatures individually and how they overlap between them.

To validate the independency of the “HSP90i” signatures as well as the “CANCER STROMA HIGH” signature and corroborate that there is no overlapping in gene content between them, we studied the genes included in each one of them. Firstly, we studied the gene content of all “HSP90i” signatures and found that there were only two genes that overlap between all of them, indicating that there was minimum overlapping between these signatures (**Figure I-4, A**). Next, we explored the possible coincidences between each “HSP90i” signature and the “CANCER STROMA HIGH” signature, and we also found minimum overlapping in all cases (**Figure I-4, B**). Finally, we studied the possible coincidences of these previously found overlapping genes with the “CANCER STROMA HIGH” signature in all the “HSP90i” ones and found only one coincidence between all of them (**Figure I-4, C**). These results indicate that the follow up analyses of all these signatures and the possible correlations that can be found will not be a consequence of them having the same gene content.

#### **1.4. HSP90 inhibitors related signatures correlate with myCAF features in the tumor stroma**

The previous findings from the LINCx library interrogation showed an enrichment of HSP90i signatures in the tumor stroma of different cancer types. Next, we studied which of the TME components was preferentially associated with these signatures. The ssGSEA analysis of the two breast cancer datasets indicated that the identified HSP90i signatures strongly correlated with signatures related to poor breast cancer prognosis, as well as CAF-related

signatures (**Figure I-5, A**). There was also some positive correlation of the HSP90i signatures with monocytes and macrophages signatures, but no correlation with other cells in the TME, including endothelial cells and other immune cells. Notably, these results resemble those obtained from the ssGSEA analysis of the “CANCER STROMA HIGH” signature in correlation with the different components of the TME.

To further investigate which of the cellular components of the TME were more associated with the HSP90i signatures, we analyzed an independent public dataset of different tumoral components (cancer cells, immune cells, endothelial cells and fibroblasts) isolated from human colon cancer samples (GSE39396). ssGSEA analysis revealed that the HSP90i signatures were preferentially expressed by FAP<sup>+</sup> fibroblasts among the different cellular components of the TME (**Figure I-5, B**).

Furthermore, ssGSEA analysis informed that the HSP90i signatures correlated with myCAF features, including ECM, TGF $\beta$  and wound healing signatures (**Figure I-5, C**), for which there was a significant strong positive correlation (**Figure I-5, D**). On the contrary, no correlation was found with other CAF subtypes related signatures, including iCAFs (**Figure I-5, C-D**).

Taken together, these results indicate that the HSP90 target genes are enriched in cancer stroma and preferentially expressed by the myCAF subtype.

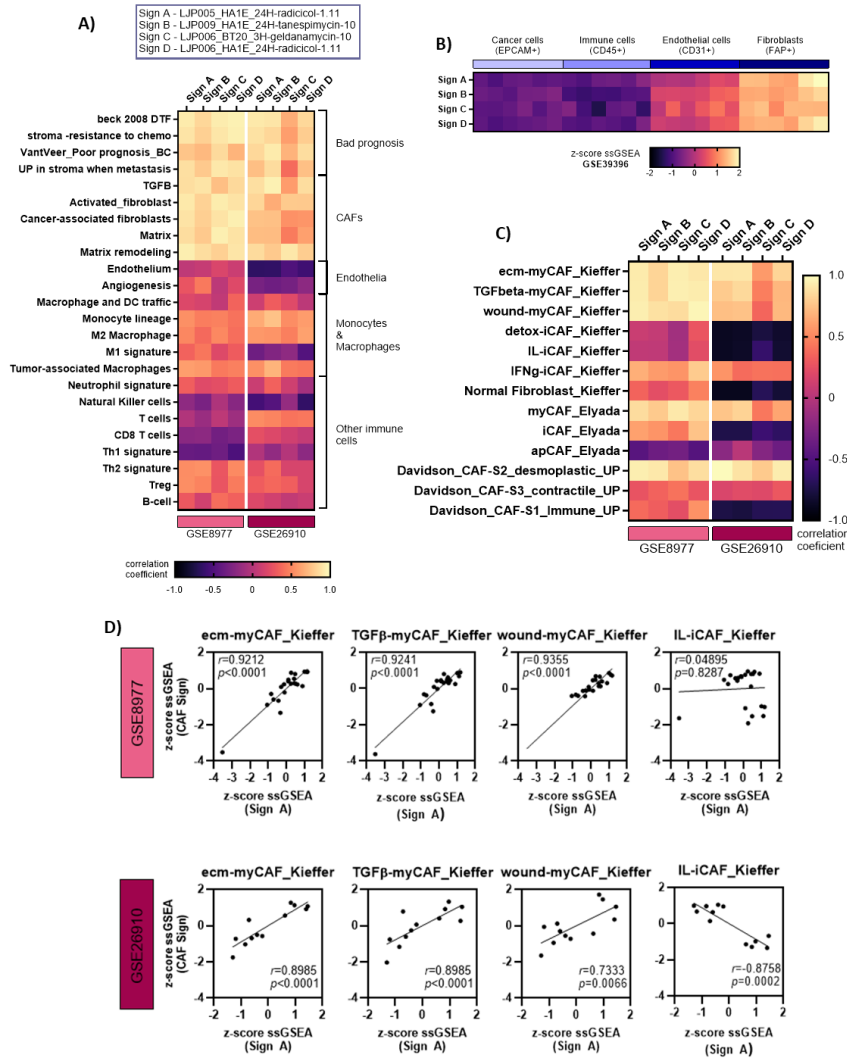


**Figure I-5. Correlation of HSP90i signatures with the different components of the TME, including CAFs.** **A.** Heatmap showing the correlation coefficient between the HSP90i signatures and signatures related to immune cells, endothelia, CAFs and bad prognosis in the breast cancer stroma datasets GSE8977 and GSE26910, as informed by ssGSEA analysis. The corresponding signature abbreviations are detailed on top. **B.** Heatmap showing the z-score of the enrichment of the HSP90i signatures in cancer cells (EPCAM<sup>+</sup>), immune cells (CD45<sup>+</sup>), endothelial cells (CD31<sup>+</sup>) and fibroblasts (FAP<sup>+</sup>) in human colon cancer samples (GSE39396). **C.** Heatmap showing the correlation coefficient between the HSP90i signatures and signatures related with the different CAF subtypes in the breast cancer datasets GSE8977 and GSE26910. **D.** Graphs showing an example of the correlation analysis shown in (C) between the indicated signatures and breast cancer stroma datasets (GSE8977 and GSE26910). Values represent the z-score normalized ssGSEA value and each point is an individual sample. *Sign A*, LJP005\_HA1E\_24H\_radicicol-1.11.

## 1.5. HSP90 inhibitor related signatures have prognostic value in cancer patients

Our data indicated that HSP90i signatures were preferentially expressed by CAFs, particularly the aggressive myCAF phenotypes, in different tumor types. To elucidate the potential clinical implications of the HSP90i signatures we studied datasets from patients from ER negative breast cancer, colon cancer and ovarian cancer with clinical data and whole tumor gene expression information available. Patients from these datasets were divided into two groups based on the expression levels of the genes included in the HSP90i signatures. Then, their progression-free survival was studied in correlation with this stratification. The data showed a significant lower survival rate in the case of the patients in the “high” group in comparison with the “low” group for the three cancer types tested (Figure I-6). These results indicate that the HSP90 target genes found consistently upregulated in the tumor stroma have clinical value and correlate with poorer patient prognosis.

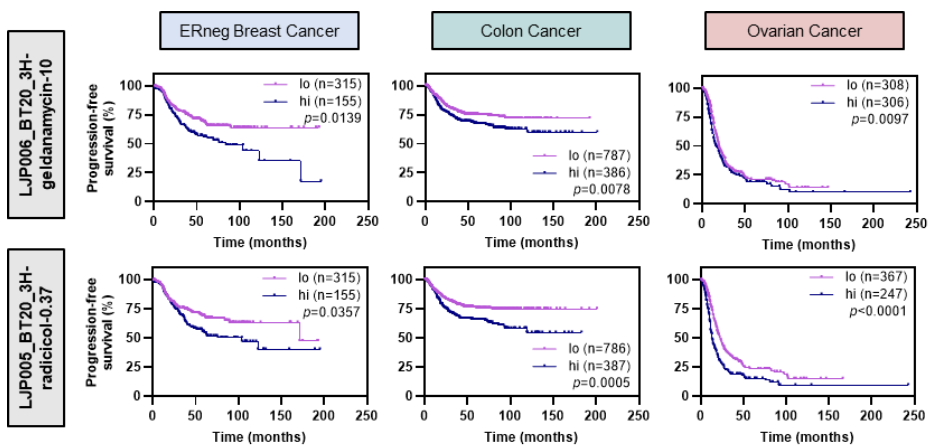


**Figure I-6. Cancer patients enriched in HSP90i signatures significantly correlate with poorer prognosis.** Graphs showing the percentage of progression-free survival patients with high (purple) or low (green) enrichment in the genes included in the LP006\_BT20\_3H-geldanamycin-10 (top) and LJP005\_BT20\_3H-radical-0.37 (bottom) signatures, for the ER negative breast, colon and ovarian cancer datasets. The level of significance (p -value) for each dataset and number of patients in each group is included in the corresponding graph. *ERneg*: Endocrine receptors negative. *Lo*: low enriched patients. *Hi*: high enriched patients.

## 1.6. scRNAseq analysis of public datasets correlates HSP90 and cancer stroma signatures with CAFs

To further confirm previous correlations found between HSP90 activities and CAFs, we performed scRNAseq analysis of publicly available datasets and studied the expression of the “HSP90i” and “CANCER STROMA HIGH” signatures in the different components of the TME. First, the different TME cellular components from a breast cancer scRNAseq database<sup>198</sup> were separated, in order to identify which populations expressed the previously studied signatures (**Figure I-7, A**). We found that all “HSP90i” and the “CANCER STROMA HIGH” signatures were mostly expressed by CAFs (**Figure I-7, A-B**). However, no differences were found in the gene expression levels of both *HSP90AA1* and *HSP90AB1* genes or their co-chaperones (*HSPA1A* and *HSPA1B*, respectively) between the different TME components (**Figure I-7, B**). In addition, the highest correlation between the “HSP90i” and the “CANCER STROMA HIGH” signatures was exclusively found in CAFs (**Figure I-7, C**).

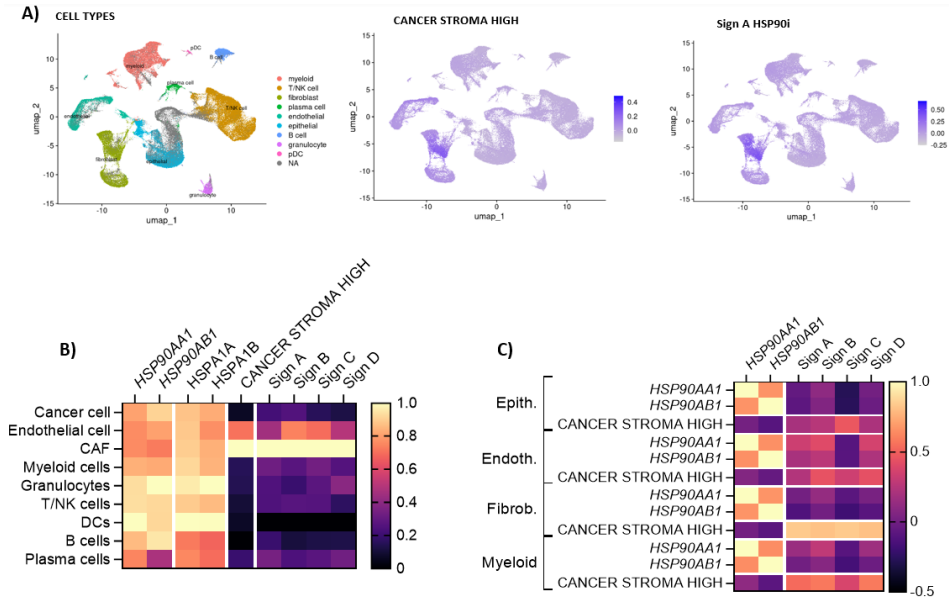


**Figure I-7. Correlation of stromal and HSP90i signatures with TME components through scRNAseq analysis of a breast cancer database.** **A.** UMAP of all TME cell types found in the studied breast cancer database<sup>198</sup> as informed by scRNAseq analysis (left panel) and plots showing the expression levels of the “CANCER STROMA HIGH” (middle panel) and HSP90i signature A (right panel) for each cell. **B.** Heatmap showing scaled values of gene expression levels of each HSP90 isoform (*HSP90AA1* and *HSP90AB1*), HSP90 isoform-specific clients (*HSPA1A* and *HSPA1B*, respectively), “CANCER STROMA HIGH” and all four “HSP90i” signatures in each TME cell type. **C.** Heatmap showing correlation coefficients of *HSP90AA1*, *HSP90AB1* and the “CANCER STROMA HIGH” signatures with all four “HSP90i” signatures for the indicated cell types. *Sign A*: *LJP005\_HA1E\_24H-radicicol-1.11*. *Sign B*: *LJP009\_HA1E\_24H-tanespimycin-10*. *Sign C*: *LJP006\_BT20\_3H-geldanamycin-10*. *Sign D*: *LJP006\_HA1E\_24H-radicicol-1.11*. *Epith*: epithelial cells. *Endoth*: endothelial cells. *Fibrob*: fibroblasts.

A similar analysis was conducted using a human bladder cancer scRNAseq dataset<sup>199</sup>, in which we also identified the different TME cellular components and studied the expression of the same signatures in them. In this case, the “CANCER STROMA HIGH” and “HSP90i” signatures were mostly expressed by fibroblasts and CAF precursors, such as smooth muscle cells and chondrocytes (Figure I-8, A-B). However, similar to the previously obtained results, there were

no differences in the gene expression of the HSP90 isoforms or their isoform-specific clients between the different TME components.

When the cells were separated based on its tumoral or non-tumoral (mucosa) origin, we found that the expression of all tested signatures was significantly increased in fibroblasts and smooth muscle cells with tumor origin (**Figure I-8, C**). In addition, similar to the previous findings from the breast cancer dataset, the highest correlation between the “CANCER STROMA HIGH” and the “HSP90i” was specifically found in fibroblasts (**Figure I-8, D**). Finally, we focused only in fibroblast cells in both breast and bladder datasets and investigated specific associations (**Figure I-8, E**). This analysis informed that HSP90i signatures (but not *HSP90AA1* or *HSP90AB1*) present a high correlation with myCAF signatures and TGF $\beta$  responses in fibroblasts (F-TBRS signature), as well with the expression of certain CAF markers such as *PDPN* and *INHBA*.

Taken together, these results indicate that HSP90 activities correlate with the expression of CAF pro-tumoral signatures in the TME of breast and bladder cancer. These findings suggest a possible role of HSP90 in modulating myCAF phenotypes in the TME.

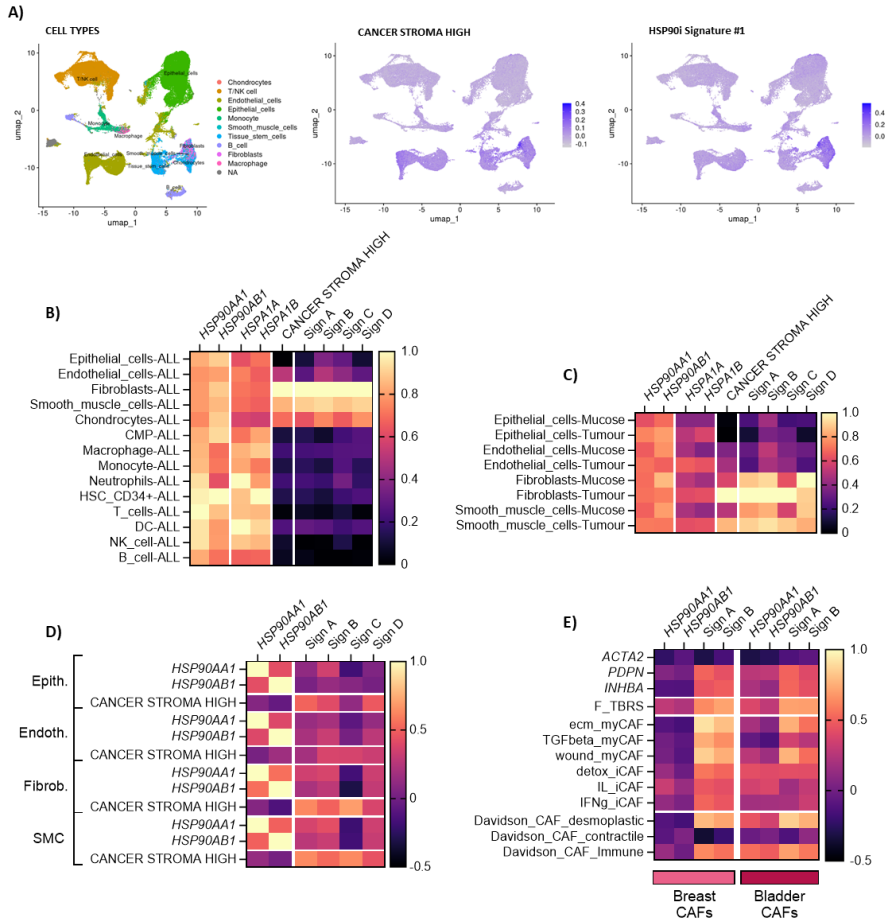


**Figure I-8. Correlation of HSP90 related signatures with different stromal cells in human bladder cancer.** **A.** UMAP of all TME cell types found in the studied bladder cancer database<sup>199</sup> as informed by scRNAseq analysis (left panel) and plots showing the expression levels of the "CANCER STROMA HIGH" (middle panel) and HSP90i signature A (right panel) for each cell. **B-C.** Heatmap showing scaled values of gene expression levels of each HSP90 isoform (*HSP90AA1* and *HSP90AB1*), HSP90 isoform-specific clients (*HSPA1A* and *HSPA1B*, respectively), "CANCER STROMA HIGH" and all four "HSP90i" signatures in each TME cell type (B) and indicated cell types with tumoral and non-tumoral (mucosa) origin (C). **D.** Heatmap showing correlation coefficients of *HSP90AA1*, *HSP90AB1* gene expression and the "CANCER STROMA HIGH" signatures with all four "HSP90i" signatures for the indicated cell types found in the bladder cancer dataset. **E.** Heatmap showing correlation coefficients of *HSP90AA1*, *HSP90AB1*, and HSP90i signatures A and B with indicated genes (*ACTA2*, *PDPN* and *INHBA*) and different CAF-related signatures in fibroblasts/CAFs from both breast and bladder datasets. *Sign A*: *LJP005\_HA1E\_24H-radicicol-1.11*. *Sign B*: *LJP009\_HA1E\_24H-tanespimycin-10*. *Sign C*: *LJP006\_BT20\_3H-geldanamycin-10*. *Sign D*: *LJP006\_HA1E\_24H-radicicol-1.11*. *Epith*: epithelial cells. *Endoth*: endothelial cells. *Fibrob*: fibroblasts. *SMC*: smooth muscle cells.

## 1.7. HSP90 is equally expressed in CAFs and NFs

The enrichment of HSP90i signatures in the tumor stroma, and more specifically in CAFs, in comparison to normal healthy tissue, suggests an increase in HSP90 activities in the TME and CAFs. To further explore the possible differences in HSP90 expression in CAFs vs. NFs, we studied the enrichment of our HSP90i signatures together with other signatures related with HSP90 inhibition in Mouse Embryonic Fibroblasts (MEFs, “HSP90I SIGNATURE MEF GSE126151 TOP 500\_UP”) in the CAFs and NFs from breast, colorectal and ovarian cancer (**Figure I-9, A**). The analysis showed a significant enrichment of the three HSP90i signatures tested in CAFs from these cancer types, even in CAFs from murine breast cancer (**Figure I-9, B-C**), which further confirms a major presence of HSP90 functions in CAFs in comparison with NFs. In addition, we explored if these observations were due to differences in the gene expression levels of HSP90. Gene expression analysis of HSP90 and related genes in CAFs vs. NFs of murine and human breast cancer showed no significant differences at the gene expression level (**Figure I-9, D-E**). Thus, these results indicate that the differences in HSP90 activity between CAFs and NFs must be due to differences at the functional level.

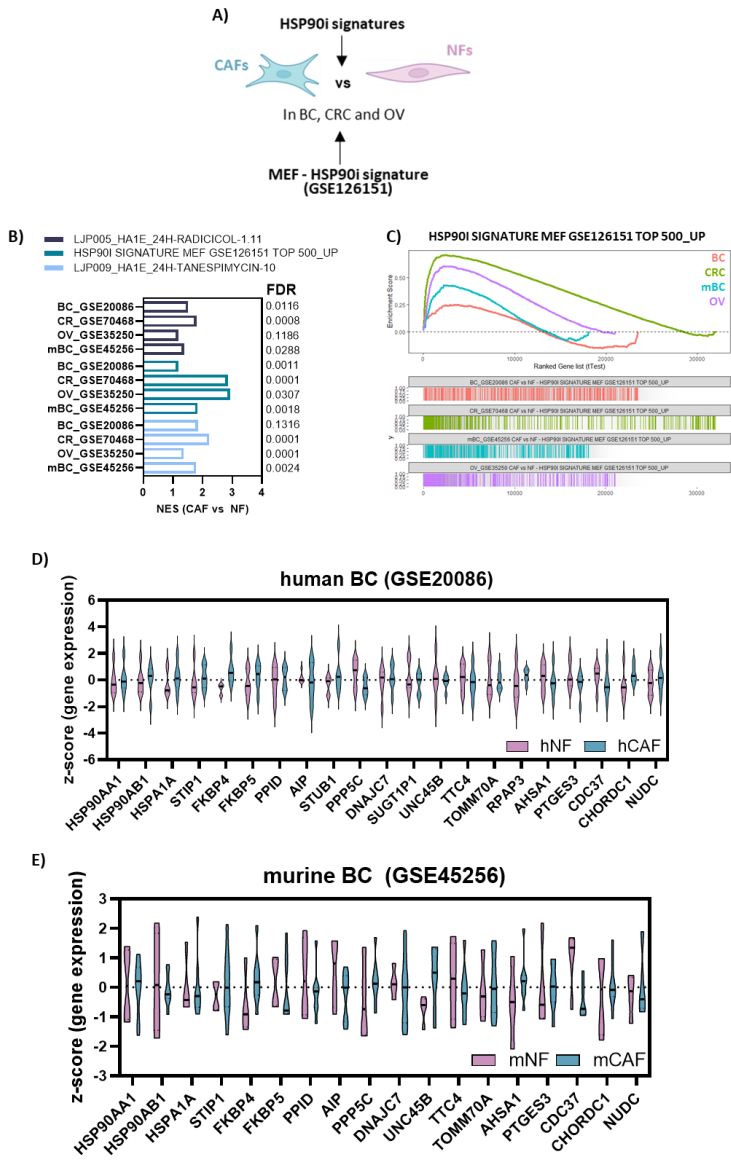


**Figure I-9. HSP90 gene expression and activity differences in CAFs vs NFs. A.** Schematic representation of our approach to study the differences in HSP90 activity in CAFs vs. NFs of breast, colorectal and ovarian cancer. **B.** Graph showing the NES and FDR scores for the enrichment of the above indicated HSP90i signatures in the CAFs vs. NFs of human breast cancer (GSE20086), human colorectal cancer (GSE70468), human ovarian cancer (GSE35250) and murine breast cancer (GSE45256) as informed by GSEA analysis. **C.** GSEA plot showing the activity of the indicated HSP90i signature in the different databases explored in (B). **D-E.** Graphs showing the z-score of the gene expression of the different indicated genes in human breast cancer (D) and murine breast cancer (E). *BC: Breast cancer. CR: colorectal cancer. OV: ovarian cancer. m: murine.*

# Results

## 2. *In vitro* studies of HSP90 functions in CAFs



The bioinformatic analysis of public datasets revealed HSP90 as a key regulator of upregulated genes in tumor stroma vs. non-malignant samples, indicating a potential role in tumorigenesis. In addition, HSP90 activity was found upregulated in the tumor stroma, where it was strongly correlated with pro-tumorigenic CAF programs, including myCAFs signatures. However, little is known about the role of HSP90 in the tumor stroma or more specifically in CAFs.

## 2.1. Specific modulation of HSP90 $\alpha$ / $\beta$ expression by siRNAs in murine NFs and CAFs

To investigate which CAF functions could potentially be modulated by HSP90 and the molecular mechanisms behind them, a battery of different *in vitro* phenotypic and functional analyses was performed using two different systems with murine fibroblasts derived from the MMTV-PyMT spontaneous breast cancer model (**Figure II-1, A**). In order to do so, HSP90 expression was depleted in murine breast cancer CAFs by transfecting them with a smart pool (sp) of siRNAs for the two most important isoforms respectively: HSP90 $\alpha$  (*Hsp90aa1*) and HSP90 $\beta$  (*Hsp90ab1*). In parallel, NFs derived from normal murine mammary glands were activated by stimulation with TGF $\beta$  and transfected with siRNAs against *Hsp90aa1/ab1*. The first approach will enable us to investigate the role of HSP90 in pathologically activated CAFs whereas the second will inform of its involvement in fibroblast activation. As previously mentioned in the introduction, TGF $\beta$  is a well-known activator of fibroblasts into myfibroblast phenotypes. Thus, it is expected that these stimulated

NFs present enhanced activities in the different functional experiments performed. Both models were then tested for well-known CAF features including CAF marker expression, ECM generation and remodeling, invasion and promotion of cancer cell growth.

The efficacy and specificity of the corresponding siRNA sp for each isoform was verified by qPCR in both CAFs and NFs. The qPCR analysis showed a reduction in the expression of both HSP90 $\alpha$  (*Hsp90aa1*) and HSP90 $\beta$  (*Hsp90ab1*) when CAFs were transfected with the corresponding siRNA sp (**Figure II-1, B**). The efficacy of the different siRNAs was also confirmed when tested individually, where all 4 different siRNAs potently reduced the expression of their target (**Figure II-1, D-E**). In both approaches, siRNAs demonstrated to be specific for their corresponding HSP90 isoform, as the expression of the *Hsp90ab1* gene was not significantly affected by the siRNAs for *Hsp90aa1*, and vice versa (**Figure II-1, B**). Similar results were obtained in the case of the transfected TGF $\beta$ -stimulated NFs, for which the siRNA sp also demonstrated to be effective and specific for their corresponding isoform (**Figure II-1, C**). Interestingly, the stimulation with TGF $\beta$  did not induce the gene expression of any of the two HSP90 isoforms.

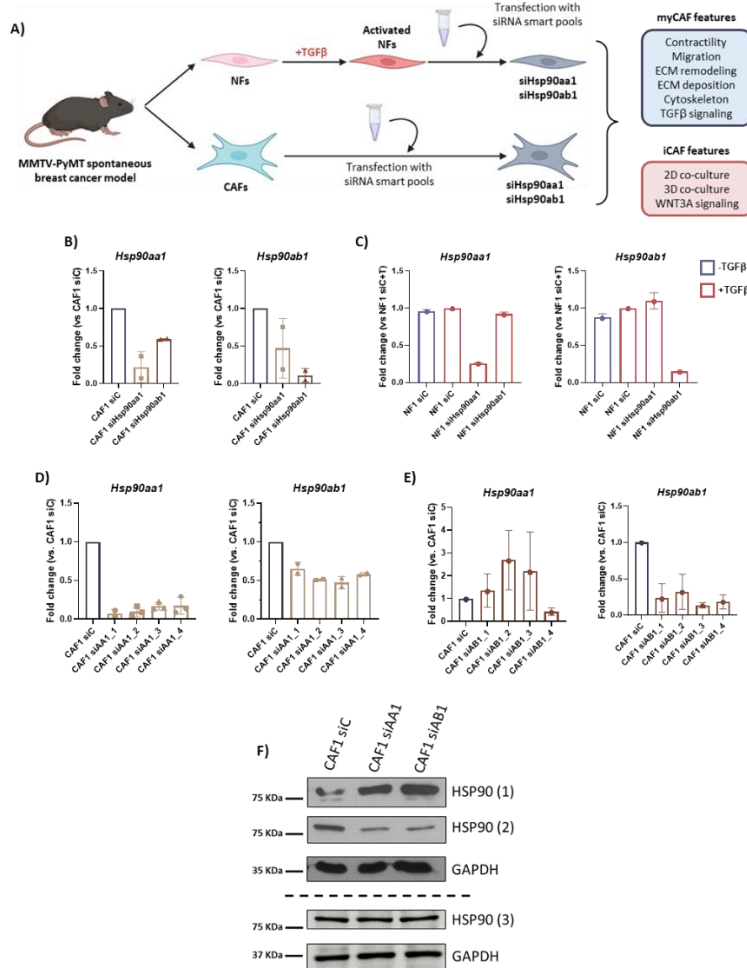


**Figure II-1. Specific modulation of HSP90 $\alpha$ / $\beta$  expression by siRNA in murine models of NF/CAFs.** A. Schematic representation of our *in vitro* system. All *in vitro* experiments were performed using mCAFs and TGF $\beta$ -stimulated mNFs, transfected with the corresponding *Hsp90aa1/ab1* siRNA sp. Created on Biorender.com. B-C. Graphs showing the fold change in gene expression of *Hsp90aa1* and *Hsp90ab1* respectively, in comparison with the control condition, after transfection with control or *Hsp90aa1/ab1* siRNAs in CAF1 (B, n=2) and TGF $\beta$ -stimulated NF1 (C, n=1), tested by qPCR. D-E. Graphs showing the fold change in gene expression of *Hsp90aa1* and *Hsp90ab1* respectively in comparison with the control condition, after transfecting CAF1 with the individual siRNAs for both *Hsp90aa1* (D, n=2-3) and *Hsp90ab1* (E, n=1). All qPCR experiments were performed in technical triplicates. F. Representative WB experiment for the expression of Hsp90 in control and *Hsp90aa1/ab1*-silenced CAFs, using different anti-HSP90 antibodies. GAPDH was used as loading control. The dash line separates different WB, each one of them with its corresponding loading control. Where indicated, 5 ng/mL of TGF $\beta$  was added for 24 h. siC: siRNA control. siAA1: siHsp90aa1. siAB1: siHsp90ab1. \*\*: P-value < 0.01. \*\*\*: P-value < 0.001. \*\*\*\*: P-value < 0.0001.

We aimed to confirm these results at the protein level, for which several different anti-HSP90 antibodies were tested in order to study the differences in the protein expression of each HSP90 isoform individually after siRNA transfection. However, given the great similarity between the two HSP90 isoforms, none of the antibodies was able to properly distinguish between them despite being claimed to be isoform-specific (**Figure II-1, D**). With the HSP90(1) antibody, we unexpectedly observed increased expression of HSP90 after siRNA transfection. With the HSP90(2) antibody, we observed reduced expression after transfection with either *Hsp90aa1* or *Hsp90ab1* siRNAs in CAFs. And with the HSP90(3) one, no differences were detected in HSP90 expression levels in CAFs after siRNA transfection.

In conclusion, the siRNAs used for the *in vitro* model can effectively and specifically silence both *Hsp90* isoforms, at least at gene level, which makes this siRNA-based *in vitro* model suitable for the study of HSP90 functions in CAFs.

## **2.2. Analysis of gene and protein expression of CAF markers affected by *Hsp90aa1/ab1* silencing**

To explore the potential implications of HSP90 $\alpha/\beta$  in CAFs, different factors and phenotypes associated with the CAF emergence and pro-tumoral functions were investigated at the gene and protein expression levels, both in *Hsp90aa1/ab1*-silenced CAFs and TGF $\beta$ -stimulated NFs.

As previously discussed in the introduction, there are no specific markers to identify CAFs in the TME. However, there are some genes whose expression is known to be increased in CAFs in comparison with NFs.

One important CAF marker whose expression is particularly enhanced in the myCAF phenotype is the *Acta2* gene, which encodes for  $\alpha$ -SMA protein. This is a cytoskeleton protein that plays an important role in the ability of myCAF s to contract and remodel the ECM<sup>201</sup>. The protein expression analysis by WB showed that the stimulation of NFs with TGF $\beta$  induced the protein expression of  $\alpha$ -SMA in these cells, but the silencing of *Hsp90aa1/ab1* was not able to revert this phenotype (**Figure II-2, A**). Furthermore, the protein levels of  $\alpha$ -SMA also remained unaltered in *Hsp90aa1/ab1*-silenced CAFs (**Figure II-2, B**), indicating that  $\alpha$ -SMA expression in CAFs is independent of HSP90 $\alpha/\beta$  expression. Similar findings were obtained for S100A4, which is another well-known CAF marker, whose expression also remained invariable after *Hsp90aa1/ab1* silencing in CAFs (**Figure II-2, B**).

These results prompted us to investigate the gene and protein expression levels of other factors associated with CAFs or myCAF s using RNAseq and proteomics approaches. These analyses confirmed that  $\alpha$ -SMA (*Acta2*) and S100A4 (*S100a4*) were not altered by *Hsp90aa1/ab1* depletion in our systems.

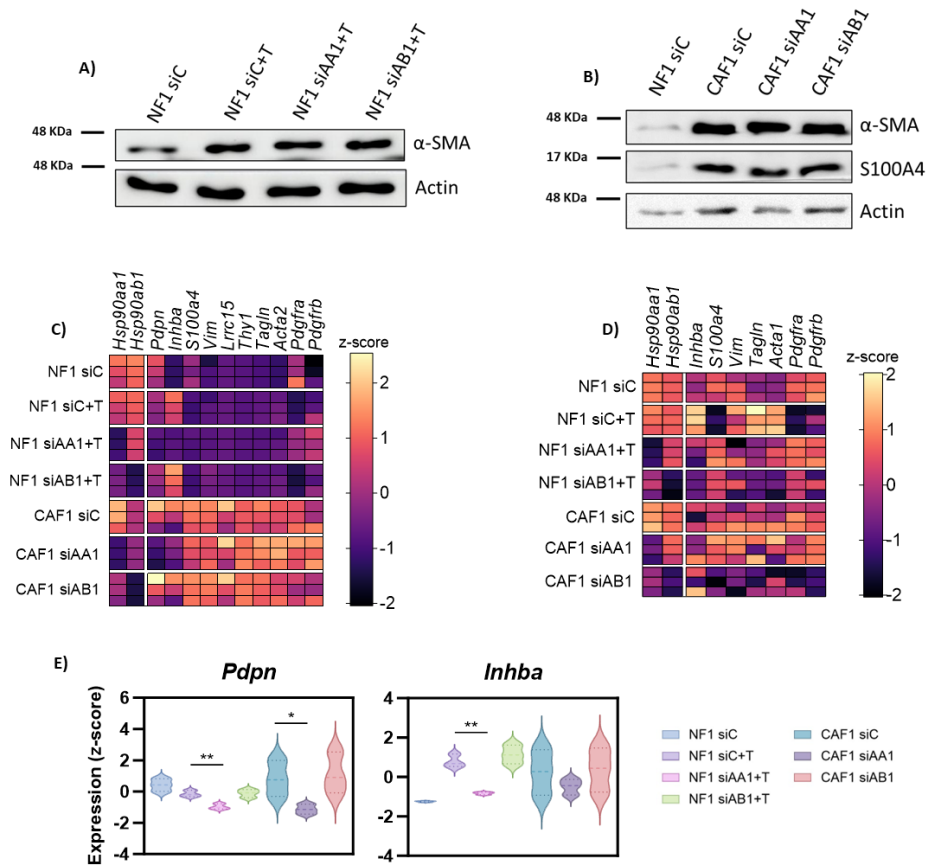


**Figure II-2. Gene and protein expression profile of relevant CAF markers in *Hsp90aa1/ab1*-silenced CAFs and NFs.** A-B. Representative WB experiments for the expression of  $\alpha$ -SMA, S100A4 and Actin in control and *Hsp90aa1/ab1* silenced TGF $\beta$ -stimulated NF1 (A) and CAF1 cells (B). Protein weight markers are also shown. C. Heatmap of the z-score value of indicated genes in CAF1 and TGF $\beta$ -stimulated NF1 after transfection with control, *Hsp90aa1* or *Hsp90ab1* siRNAs. Data extracted from RNAseq analysis (triplicates). D. Heatmap of the z-score value of indicated proteins in CAF1 and TGF $\beta$ -stimulated NF1 after transfection with control, *Hsp90aa1* or *Hsp90ab1* siRNAs, as informed by the proteomic analysis (triplicates). E. Graphs showing z-score of gene expression of *Pdpn* and *Inhba* in CAF1 and TGF $\beta$ -stimulated NF1 cells after transfection with control, *Hsp90aa1* or *Hsp90ab1* siRNAs. Data extracted from RNAseq analysis (n=3, from 3 independent experiments). Where indicated, 5 ng/mL TGF $\beta$  was added for 24 h. siC: siRNA control. siAA1: si*Hsp90aa1*. siAB1: si*Hsp90ab1*. +T: +TGF $\beta$ .

In fact, the gene expression analysis of RNAseq data showed that only *Pdpn* and *Inhba* were significantly downregulated only after *Hsp90aa1* silencing in both CAFs and TGF $\beta$ -stimulated NFs (Figure II-

2, C-E), although the reduction in the expression of *Inhba* was only significant in the case of the *Hsp90aa1*-silenced TGF $\beta$ -stimulated NFs (Figure II-2, E). Similarly, the proteomic analysis showed a reduction in the protein levels of *Inhba* in *Hsp90aa1*-silenced TGF $\beta$ -stimulated NFs, but not in CAFs (Figure II-2, D), indicating that HSP90 $\alpha$  may control different expression programs in both systems.

Taken together, these results suggest that HSP90 genetic modulation does not appear to modulate in great extent the expression of CAF markers, with the exception of *Pdpr* and *Inhba*.

### 2.3. Role of HSP90 $\alpha$ in modulating the contractile capacity of CAFs

Analysis of CAF markers may be useful to determine particular cellular states, but they are not consistent readouts of CAF behavior. Thus, we next planned to investigate whether modulation of HSP90 activity affected specific CAF functions.

As mentioned in the introduction, one of the most characteristic functions of myCAF is their ability to remodel the ECM in the TME. One in vitro experiment that is typically performed to study this function is the gel contraction assay (Figure II-3, A). In this experiment, the fibroblasts are embedded in a mix of Collagen I and Matrigel™ and the gel size is monitored over time, as it will decrease according to the contraction ability of the fibroblasts. This experiment was performed using both siRNA transfected CAFs and TGF $\beta$ -stimulated NFs to explore the possible HSP90 implications in both systems.

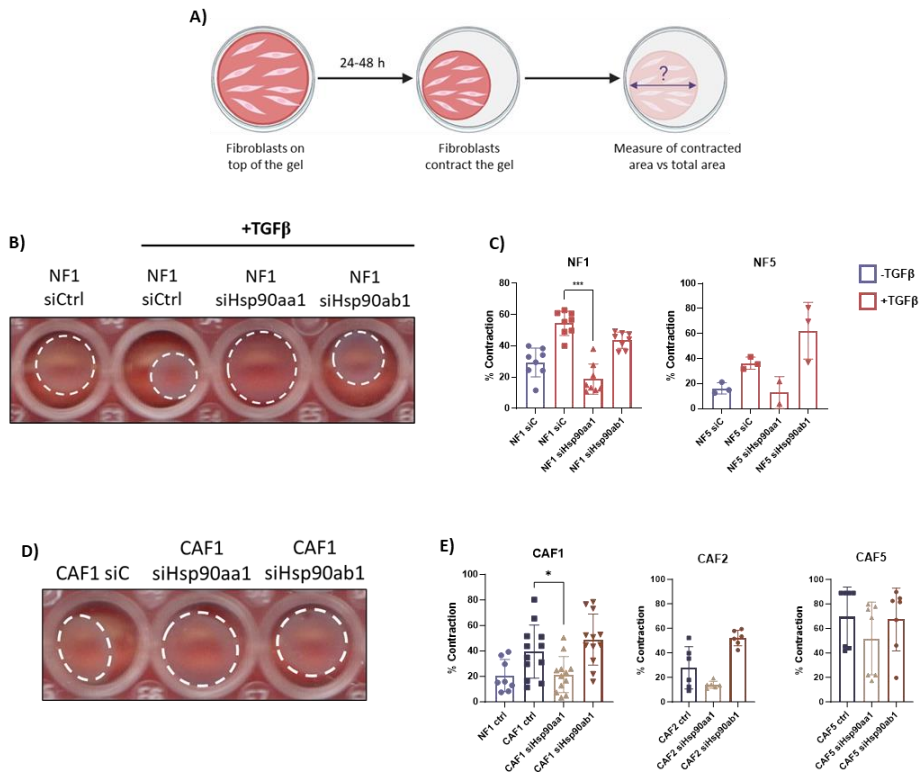


**Figure II-3. siRNA depletion of HSP90 $\alpha$  impedes the gel contraction capacity of TGF $\beta$ -stimulated NFs and CAFs.** **A.** Schematic representation of a gel contraction experiment. *Created on Biorender.com.* **B.** Representative images of a gel contraction experiment with control unstimulated NF1 and TGF $\beta$ -stimulated NF1 cells after transfection with control, *Hsp90aa1* or *Hsp90ab1* siRNAs. **C.** Graphs showing percentage of gel contraction of indicated experimental points for NF1 (n=8, from 3 independent experiments) and NF5 (n=3, from 1 experiment). **D.** Representative images of a gel contraction experiment with CAF1 cells after transfection with control, *Hsp90aa1* or *Hsp90ab1* siRNAs. **E.** Graphs showing percentage of gel contraction of indicated experimental points for CAF1 (n=12, from 4 independent experiments), CAF2 (n=6, from 2 independent experiments) and CAF5 (n=7, from 3 independent experiments). Where indicated, fibroblasts were stimulated with 5 ng/mL of TGF $\beta$  for 24 h. *siCtrl/siC*: siRNA control.

In the case of the NFs, their stimulation with TGF $\beta$  induced an increase in their gel contraction capacity, consistent with previous literature (Figure II-3, B-C). Interestingly, the depletion of *Hsp90aa1* expression in TGF $\beta$ -stimulated NFs resulted in a significant decrease in their gel contraction ability. The depletion of *Hsp90ab1* did not have any consequences. Results with a similar trend were obtained

with an alternative NF cell line, although the observed differences were not significant (**Figure II-3, C**). Thus, these results indicate that the silencing of the *Hsp90aa1* isoform specifically was able to impair the gel contraction capacity of TGF $\beta$ -activated fibroblasts.

As expected, control transfected CAFs had increased contraction capacity in comparison with the control non-stimulated NFs (**Figure II-3, D-E**). However, similarly to the case of the TGF $\beta$ -stimulated NFs, the silencing of *Hsp90aa1* significantly impaired the gel contraction ability of CAFs. Importantly, the silencing of *Hsp90ab1* had not observable effect. Similar results were obtained with alternative CAF lines CAF2 and CAF5. All together, these observations suggest that HSP90 $\alpha$  significantly impairs the capacity of CAFs and activated fibroblasts to contract collagen gels. On the other hand, the HSP90 $\beta$  isoform, did not appear to play any role in this particular myCAF function.

#### **2.4. Role of HSP90 $\alpha$ in controlling motility and migration capacities in fibroblasts**

CAFs have increased migration and invasion capacities in comparison to NFs and can promote cancer invasion. These characteristics, that have been usually attributed to the myCAF phenotype, are correlated with pro-tumoral outcomes in the tumor stroma and, similar to the gel contraction/ECM remodeling ability, is highly dependent on the characteristic enhanced cytoskeleton of CAFs/myCAFs. Thus, it is also of interest to study whether HSP90 may also play a role in the regulation of these capacities.

To investigate if HSP90 could control the migration abilities of the fibroblasts, wound healing experiments were performed using both CAFs and TGF-stimulated NFs. In the case of the TGF $\beta$ -stimulated NFs, the *Hsp90aa1*-silenced condition closed the wound more slowly in comparison with the control condition (**Figure II-4, A**). Similar results were obtained with CAFs, as the wound had only closed around 50% at 8 h (**Figure II-4, B**). In fact, in both CAFs and NFs, the percentage of closed wound for the HSP90 $\alpha$ -depleted fibroblasts was similar to that observed in the non-stimulated NF condition, suggesting that the silencing of *Hsp90aa1* is able to revert the enhanced migratory capabilities characteristic of CAFs and TGF $\beta$ -stimulated NFS. On the other hand, silencing of *Hsp90ab1* did not affect wound closure in CAFs or TGF $\beta$ -stimulated NFs.

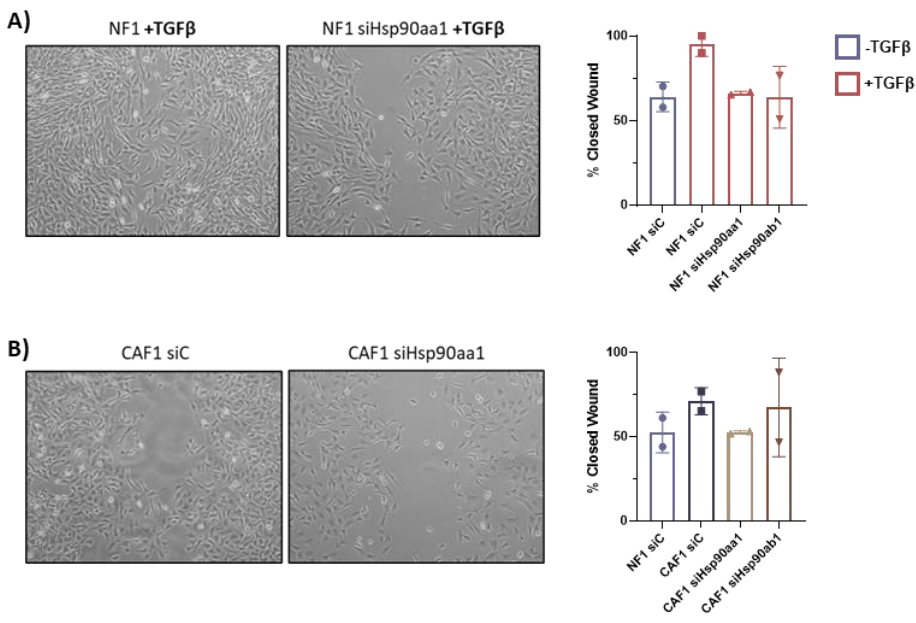


**Figure II-4. Wound healing experiment with *Hsp90aa/ab1* silenced CAFs and TGF $\beta$ -stimulated NFs.** **A.** Representative images of wound healing experiments at 8 h with TGF $\beta$ -stimulated NF1 after transfection with control and *Hsp90aa1* siRNAs. Graph on the right show percentage of wound healing on indicated experimental points (n=2). **B.** Representative images of wound healing experiments at 8 h with after transfection with control and *Hsp90aa1* siRNAs. Graph on the right show percentage of wound healing on indicated experimental points (n=2). Where indicated, fibroblasts were stimulated with 5 ng/mL of TGF $\beta$  for 24 h. Each experiment was performed in technical triplicates.

The wound healing approach is also influenced by the proliferating capacity of the system under study, whereby proliferating cells can close the wound independently of their migratory potential. To confirm that HSP90 $\alpha$  was indeed affecting cell migration, an alternative transwell-based approach was employed using the same previous conditions with CAFs and stimulated NFs. In this particular set up, in which only the intrinsic invasion capacity of the fibroblasts themselves is studied, without the influence of any external stimuli, the lower chamber was simply filled with full cell culture media, supplemented with TGF $\beta$  in the case of NFs.

In the case of the stimulated NFs, there was considerably smaller stained area for the *Hsp90aa1*-transfected condition than in the TGF $\beta$ -stimulated control (**Figure II-5, A**), indicating that less cells were able to pass through the pores. On the other hand, silencing of *Hsp90ab1* did not affect the capacity of the cells to get to the opposite side of the membrane. Similar results were obtained in the case of the CAFs, where the silencing of *Hsp90aa1* severely impeded the migration of the fibroblasts in comparison with the control condition (**Figure II-5, B**). Although the silencing of *Hsp90ab1* also affected the migration capacities of CAFs, the observed effect was not as strong as in the case of the *Hsp90aa1* silencing. In conclusion,

these results indicate that HSP90 $\alpha$  activities control the migration capacity of activated fibroblasts.

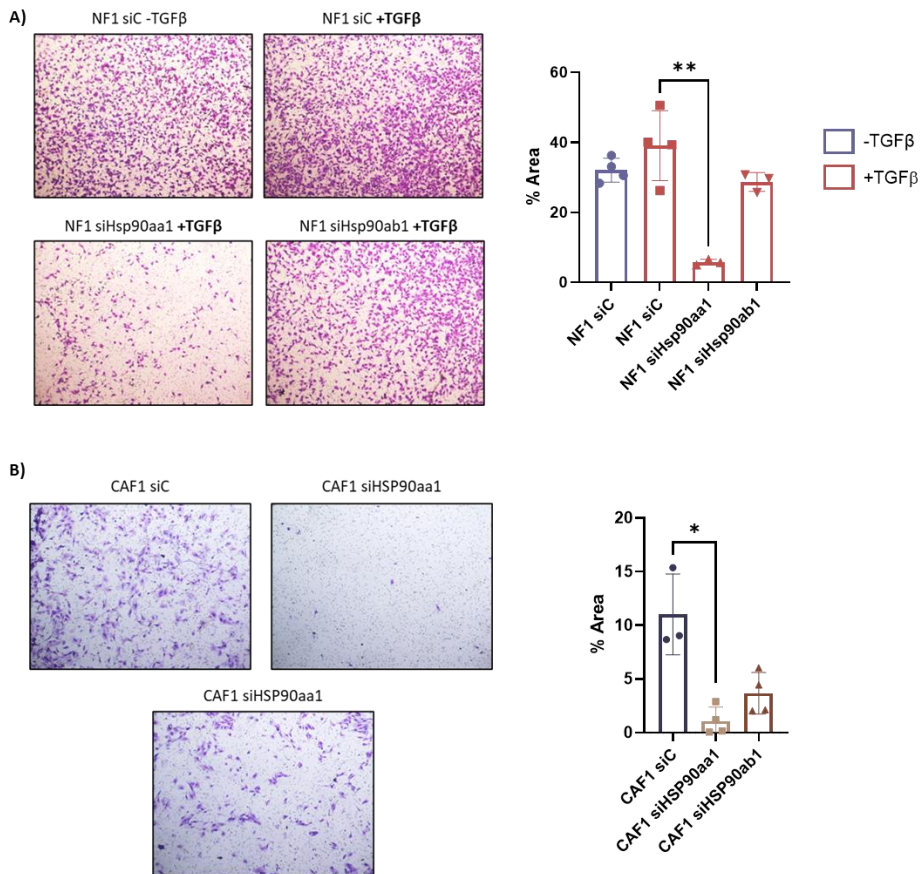


**Figure II-5. Study of the migration capacity of *Hsp90aa1/ab1*-silenced CAFs and TGF $\beta$ -stimulated NFs. A-B.** Representative images of control and *Hsp90aa1/ab1* silenced TGF $\beta$ -stimulated NFs (A) and CAFs (B) 24 h after plating the cells in the upper chamber of the transwell (left). Graphs on the right show the corresponding percentage of area occupied by the cells in the membrane. Where indicated, fibroblasts were stimulated with 5 ng/mL of TGF $\beta$  for 24 h before the experiment, and 5 ng/mL TGF $\beta$  was added to the transwell media (n=3-4, from 1 experiment).

## 2.5. HSP90 $\alpha$ promotes the generation of altered cytoskeletal phenotypes in CAFs

Our functional analyses suggested a potential role of HSP90 $\alpha$  in modulating CAF behavior associated to increased migration and ECM remodeling. These functions in CAFs are strongly dependent on particular enhanced cytoskeleton characteristics, such as stress fiber formation, focal adhesion formation and actomyosin contractility<sup>55</sup>. Thus, we next explored the expression of particular genes and proteins that may be involved in these processes. Gene expression analysis revealed that there is a different cytoskeleton gene expression profile in both TGF $\beta$ -stimulated NFs and CAFs after *Hsp90aa1/ab1* modulation, that was specially marked in *Hsp90aa1*-silenced conditions (**Figure II-6, A**). Thus, there was a significant decrease in the expression of genes such as *Rock1* and *Sept9*, which are typically related to the establishment of an actomyosin contractile cytoskeleton, in both *Hsp90aa1*-silenced TGF $\beta$ -stimulated NFs and CAFs (**Figure II-6, B**).

Interestingly, there were other cytoskeleton related genes whose gene expression levels remained invariable but behave differently at the level of protein expression. This is the case of Myosin Heavy Chain 10 (Myh10), whose protein levels decreased after *Hsp90aa1* and *Hsp90ab1* silencing in TGF $\beta$ -stimulated NFs in comparison with the stimulated control, although there was no significant variation at the gene expression level (**Figure II-6, A-C-D**). Similar results were found in the case of the CAFs, in which the silencing of both *Hsp90aa1* and *Hsp90ab1* decreased the protein

expression of Myh10 while maintaining its gene expression profile (Figure II-6, A-C-E).

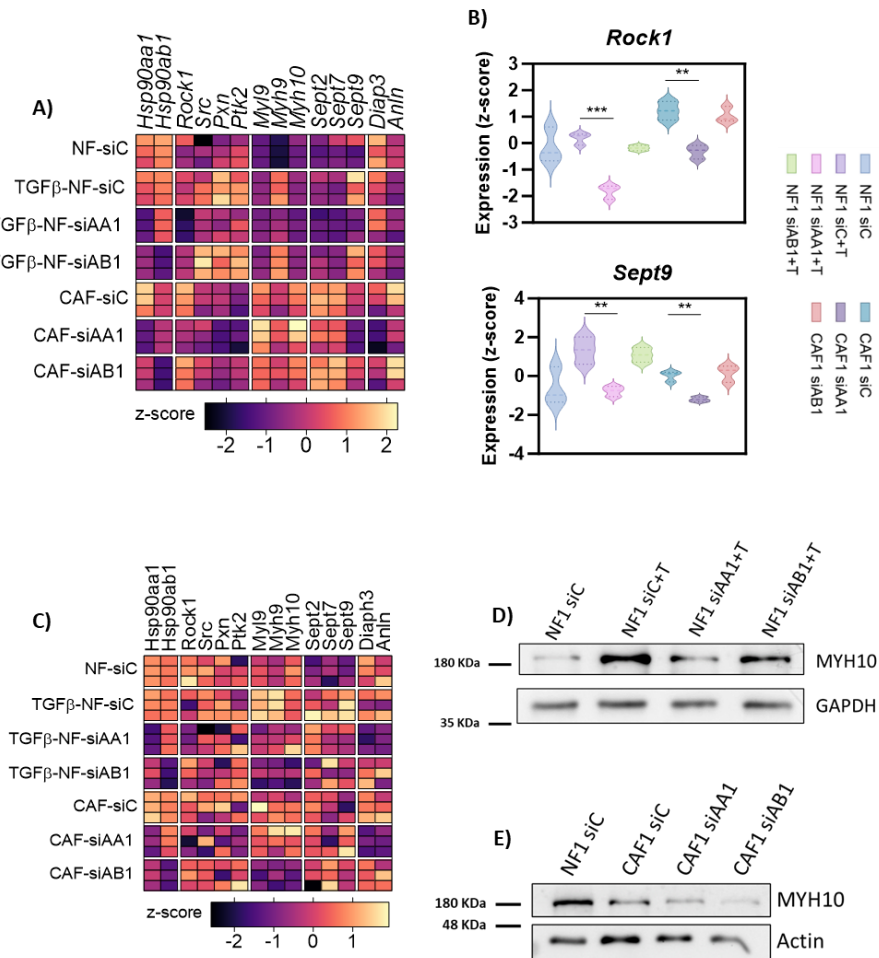


**Figure II-6. Gene and protein expression profile of cytoskeleton markers in *Hsp90aa1/ab1*-silenced CAFs and NFs.** **A.** Heatmap of the z-score value of indicated genes in CAF1 and TGFβ-stimulated NF1 after silencing of *Hsp90aa1* or *Hsp90ab1* respectively. Data extracted from RNAseq analysis (triplicates). **B.** Graphs showing z-score of gene expression of *Rock1* and *Sept9* in transfected CAF1 and TGFβ-stimulated NF1 cells. Data extracted from RNAseq analysis (n=3 from 3 independent experiments) **C.** Heatmap of the z-score value of indicated proteins in CAF1 and TGFβ-stimulated NF1 after silencing of *Hsp90aa1* or *Hsp90ab1* respectively, as informed by the proteomic analysis (triplicates). **D-E.** Representative WB experiments for the expression of MYH10 in *Hsp90aa1/ab1* silenced TGFβ-stimulated NF1 (**D**) and CAF1 cells (**E**). Actin or GAPDH were used as loading controls. Protein weight markers are also shown. Where indicated, 5 ng/mL TGFβ was added for 24 h. siC: siRNA control. siAA1: siHsp90aa1. siAB1: siHsp90ab1. +T: +TGFβ.

Thus far, all the genes and proteins that were downregulated after *Hsp90aa1* depletion presented a direct association with the establishment of an enhanced actomyosin cytoskeleton. In fact, ROCK1 is the main kinase promoting the phosphorylation and activation of myosin light chain (MLC2), with is involved in actomyosin fiber contraction<sup>110</sup>. In addition, MYH10 is necessary to generate the very same actomyosin fibers within the cell, which are also supported and stabilized by Septin cytoskeleton elements, such as Sept9<sup>45</sup>. These particular rearrangements result in the stabilization of cytoskeletal features, with include the formation and stabilization of focal adhesions and the activation of downstream signaling cascades.

To further investigate the cytoskeletal phenotype resulting from *Hsp90aa1/ab1* modulation in our *in vitro* systems, we performed immunofluorescence experiments to study the expression of F-actin (through Phalloidin staining) and focal adhesions (through phospho-Paxillin staining) in NFs and CAFs subjected to TGF $\beta$  stimulation. In the case of the NFs, the stimulation with TGF $\beta$  induced the formation of focal adhesions, as shown by an increase in the focal adhesion area per cell and average size, as well as an increase in the total number of focal adhesions (**Figure II-7, A**).

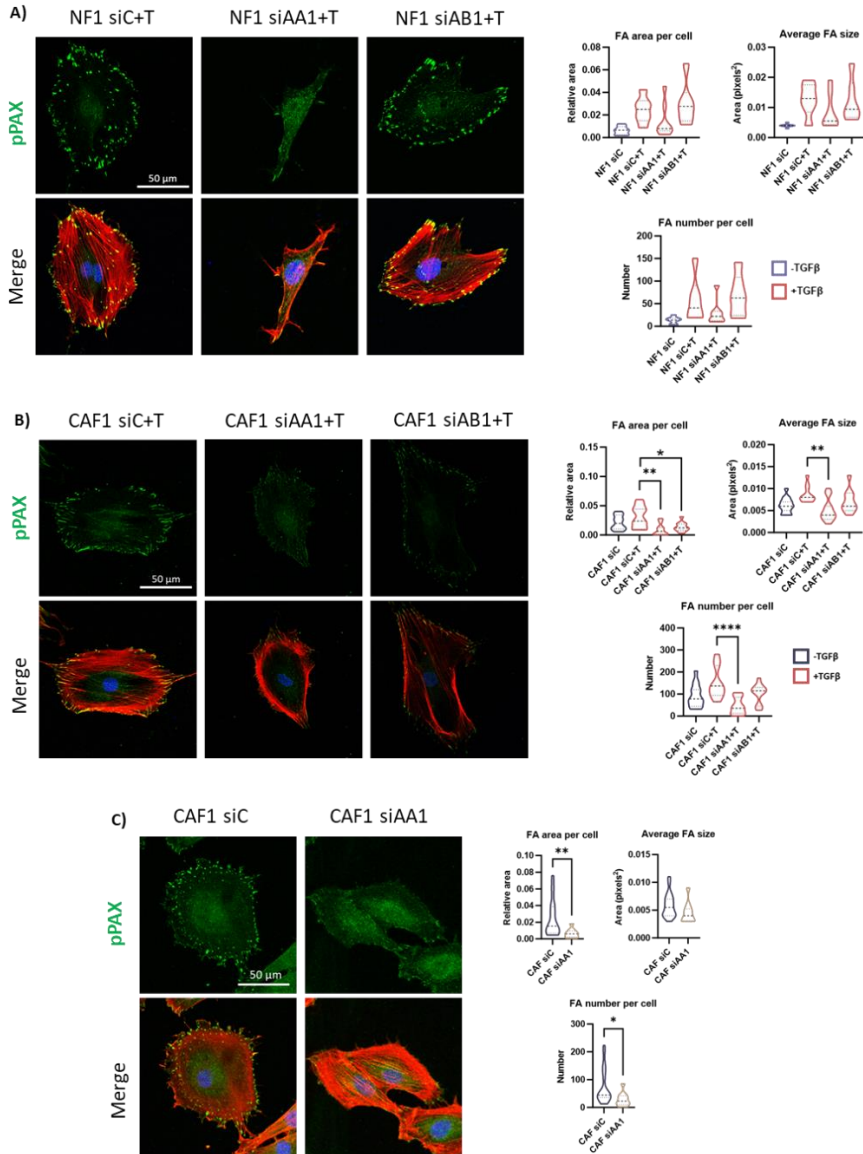


**Figure II-7. Immunofluorescence of focal adhesions in control and *Hsp90aa1/ab1*-silenced TGF $\beta$ -stimulated CAFs and NFs. A-B.** Representative images of immunofluorescence staining (left) with Phalloidin (red), phospho-Paxillin (Tyr118, green) and DAPI (blue) in control and *Hsp90aa1/ab1*-silenced TGF-stimulated NFs (**A**) and TGF-stimulated CAFs (**B**). Graphs on the right show the corresponding quantification of FA area per cell, average size and FA number. **C.** Representative images of phalloidin (red), phospho-Paxillin (Tyr188, green) and DAPI (blue) staining in control and *Hsp90aa1* silenced unstimulated CAF1. Graphs on the right show quantification of indicated FA parameters. Where indicated, fibroblasts were stimulated with 5 ng/mL of TGF $\beta$  for 24 h. siC: *siRNA control*. siAA1: *siHsp90aa1*. siAB1: *siHsp90ab1*. +T: +TGF $\beta$ . pPAX: phospho-Paxillin. FA: Focal Adhesions. \*: P-value < 0.1. \*\*: P-value < 0.01. \*\*\*\*: P-value < 0.0001.

Importantly, the silencing of *Hsp90aa1* caused a decrease in focal adhesion formation in comparison with the TGF $\beta$ -stimulated control, as shown by a reduction in all these parameters (**Figure II-7, B**), although the differences were not significant. In the case of the TGF $\beta$ -stimulated CAFs, the silencing of *Hsp90aa1* also resulted in a significant decrease in focal adhesion area per cell, average size and number (**Figure II-7, B**). Depletion of *Hsp90ab1* in TGF $\beta$ -stimulated CAFs also resulted in a decrease in all these parameters, but it was only significant in the case of the focal adhesion area per cell (**Figure II-7, B**). Similar results were obtained in the case of the non-stimulated CAFs, in which the silencing of *Hsp90aa1* also resulted in a significant decrease of focal adhesion formation (**Figure II-7, C**). Thus, these results indicate that the silencing of *Hsp90aa1* severely affects the ability of activated fibroblasts to produce focal adhesions.

The formation of an actomyosin cytoskeleton and focal adhesions involves the activation of associated signaling cascades<sup>202,203</sup>. Thus, we performed WB analysis to explore if HSP90 modulation affected them in our systems. As expected, TGF $\beta$  stimulation in NFs induced the protein expression of both Focal Adhesion Kinase (FAK) and Myosin Light Chain 2 (MLC2), as well as their respective phosphorylated activated forms (pFAK and pMLC2, respectively, **Figure II-8, A**). The silencing of *Hsp90aa1* reverted this phenotype, as it reduced the expression of both the total and active form of these proteins. Interestingly, this effect was exclusive to the *Hsp90aa1* siRNA transfected condition, as the TGF $\beta$ -induced expression levels were maintained after *Hsp90ab1* silencing.

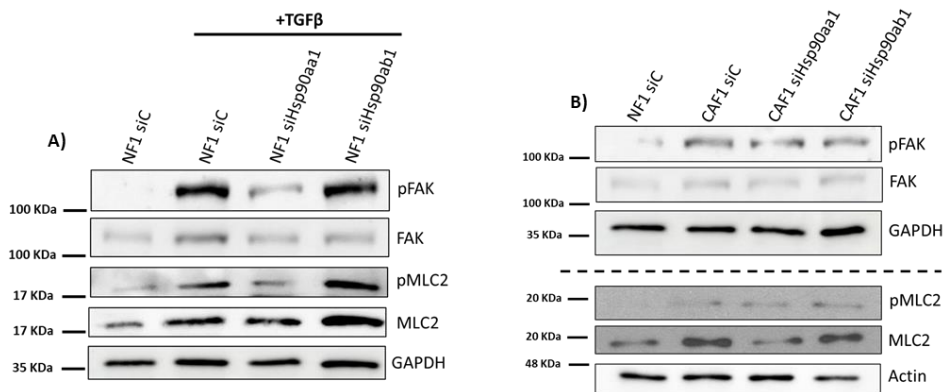


**Figure II-8. A-B. Expression of cytoskeleton related proteins after *Hsp90aa1/ab1* silencing in CAFs and TGFβ-stimulated NFs.** Representative WB experiments showing the expression of total FAK and MLC2 and their corresponding active forms pFAK (Tyr397), and pMLC2 (Ser19) in transfected TGFβ-stimulated NFs (A) and CAFs (B) after transfection with control, *Hsp90aa1* and *Hsp90ab1* siRNAs. Actin or GAPDH were used as loading control for all WB experiments. Dashed lines separate independent WB experiments, each one of them with their corresponding loading control. Protein weight markers are also shown. Where indicated, fibroblasts were stimulated with 5 ng/mL of TGFβ for 24 h. *siC*: siRNA control. *siAA1*: si*Hsp90aa1*. *siAB1*: si*Hsp90ab1*. *+T*: +TGFβ.

In the case of the CAFs, the silencing of *Hsp90aa1/ab1* did not affect the total expression of FAK, although some reduction in their active phosphorylated form was observed (Figure II-8, B). In addition, *Hsp90aa1* silencing depleted the total protein levels of MLC2, although no reduction of its active form pMLC2 was observed. Again, this effect was exclusive to the *Hsp90aa1* isoform.

Altogether, these observations confirmed the implications of HSP90, in regulating the cytoskeleton of CAFs and TGFβ-stimulated NFs.

## 2.6. HSP90 $\alpha$ regulates the architecture of CAF-derived ECMs and its influence over cancer cell behavior

CAFs, and more specifically myCAFs, are also known to be the main producers of ECM components in the TME as well as ECM-remodeling enzymes. Thus, we next aimed at investigating whether HSP90 affects these functions in CAFs.

Gene expression analysis revealed that *Hsp90aa1/ab1* silencing in TGF $\beta$ -stimulated NFs or CAFs did not appear to have any impact in the expression levels of ECM genes in general, including Fibronectin (*Fn1*, **Figure II-9, A**). Although the proteomic analysis suggested a decrease in Fibronectin expression in *Hsp90aa1*-silenced TGF $\beta$ -stimulated NFs in comparison with the control (**Figure II-9, C**), the WB analysis showed no differences in Fibronectin levels after *Hsp90aa1/ab1* silencing in TGF $\beta$ -stimulated NFs, nor in CAFs (**Figure II-9, D-E**). The only ECM genes whose expression was affected by *Hsp90aa1/ab1* silencing were *Has2* and *Tnc* (**Figure II-9, B**) although these differences were only significant in the case of the TGF $\beta$ -stimulated NFs.

However, the molecular composition is not the only ECM characteristic that is typically modulated by CAFs in the TME, as they are also known to influence ECM architecture and structure. The ECM is known to have different patterns in pathological tissue vs healthy tissue. In cancer, the ECM presents a more linear and aligned structure that typically serves as molecular roadways for the migration of malignant cells<sup>204</sup>. This ECM structure is known as “anisotropic” (**Figure II-10, A**). On the other hand, when the ECM is

composed by curvier, non-linear, and disorganized structures, the cells are not able to migrate as easily as in an anisotropic context. This last type of ECM structure is known as “isotropic”.

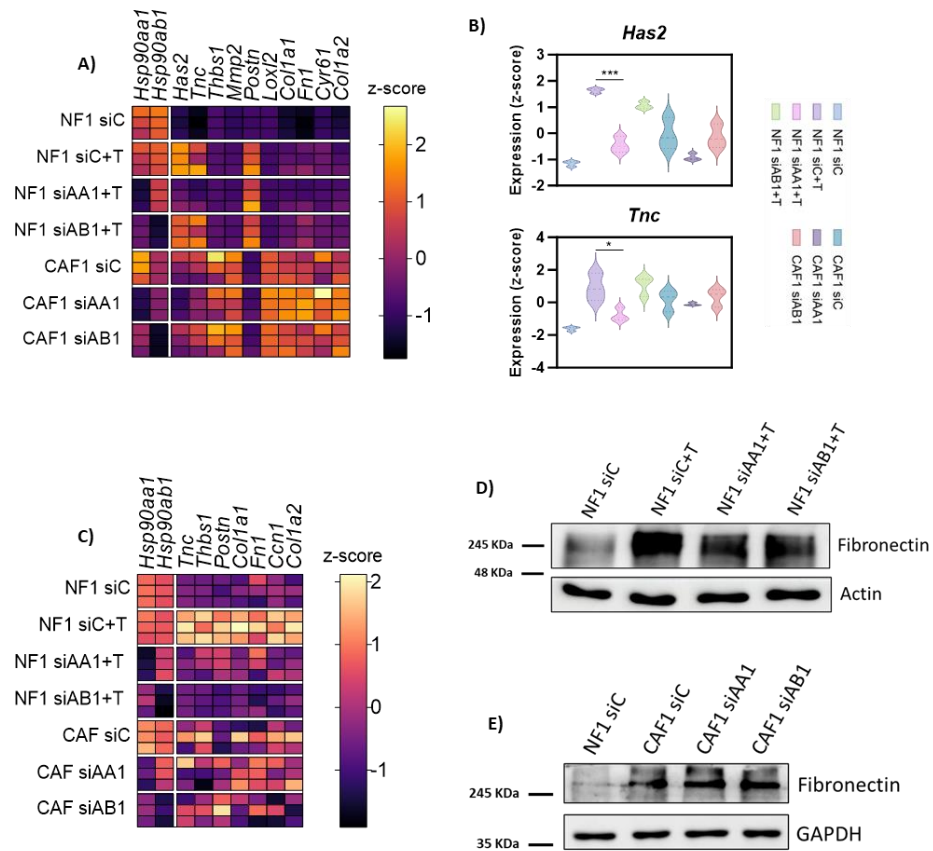


**Figure II-9. Gene and protein expression profile of ECM-related factors in *Hsp90aa1/ab1*-silenced CAFs and TGFβ-stimulated NFs.** **A.** Heatmap of the z-score value of indicated genes in CAF1 and TGFβ-stimulated NF1 after transfection with control, *Hsp90aa1* or *Hsp90ab1* siRNAs. Data extracted from RNAseq (triplicates). **B.** Graphs showing z-score of gene expression of *Has2* and *Tnc* in the indicated experimental points. Data extracted from RNAseq analysis analysis (n=3 from 3 independent experiments). **C.** Heatmap of the z-score value of indicated proteins in CAF1 and TGFβ-stimulated NF1 after silencing of *Hsp90aa1* or *Hsp90ab1* respectively, as informed by the proteomic analysis (triplicate). **D-E.** Representative WB experiments for the expression of Fibronectin in *Hsp90aa1/ab1* silenced TGFβ-stimulated NFs (**D**) and CAF1 cells (**E**). GAPDH or Actin were used as loading control. Protein weight markers are also shown. Where indicated, 5 ng/mL TGFβ was added for 24 h. siC: siRNA control. siAA1: si*Hsp90aa1*. siAB1: si*Hsp90ab1*. +T: +TGFβ. \*: P-value < 0.1. \*\*\*: P-value < 0.001.

To study the possible implications of HSP90 in ECM architecture and composition, a protocol for obtaining Cell Derived Matrices (CDMs) was performed with the siRNA transfected CAFs and TGF $\beta$ -stimulated NFs (Figure II-10, B). Briefly, this protocol enables the generation of ECM by plating fibroblasts in pre-coated glass-bottom plates and maintaining them for over 5–7 days with L-Ascorbic Acid, a stimulator of collagen production. Then, the resulting CDM can consequently be investigated by conventional immunofluorescence and microscopy approaches. In addition, the resulting CDM can be further processed to remove the cells, leaving it free of fibroblasts for posterior molecular, phenotypic and functional analyses.

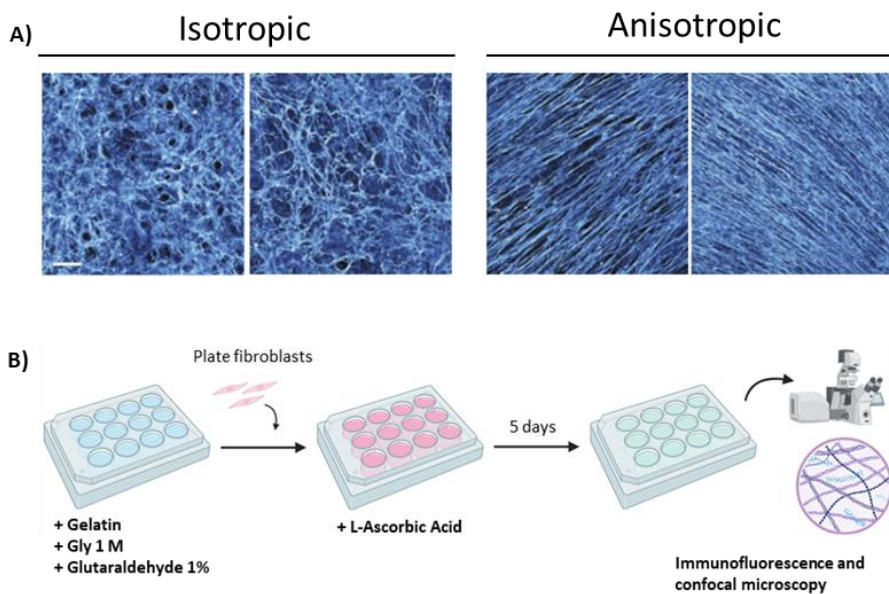


**Figure II-10. Generation of Cell Derived Matrices (CDMs) for the study of ECM structure *in vitro*.** A. Representative images of isotropic (disorganized) and anisotropic (aligned) CDMs derived from different types of CAFs. Extracted from Wershof E. et al<sup>200</sup>. B. Schematic representation of the protocol for generating CDMs. The fibroblasts are plated in a confluent monolayer over a pre-treated cell culture plate and left in cell culture for 5 days with L-Ascorbic Acid (25  $\mu\text{g}/\text{mL}$ ) to induce ECM production. Created on Biorender.com.

First, we investigated the composition of the CDMs derived from *Hsp90aa1/ab1*-silenced CAFs and NFs by proteomic analysis. Importantly, our murine CAF model does not produce anisotropic CDMs unless it is stimulated with TGF $\beta$  (not shown), in line with previous results from other laboratories<sup>204</sup>. Thus, for all CDM analyses we used TGF $\beta$ -stimulated CAFs. The proteomic analysis revealed that there were few significant changes in CDM composition in both CAFs and NFs after *Hsp90aa1/ab1*-silencing (**Figure II-11, A-B**).

Among the proteins whose expression was altered, we found that the silencing of *Hsp90aa1* downregulated the expression of Prolyl 4-hydroxylase subunit alpha 3 (P4ha3) in both CAFs and NFs, which is a key enzyme for collagen biosynthesis<sup>205</sup> (**Figure II-11, C-D**). In addition, *Wnt5a*, an important secreted factor by CAFs which regulates the cancer stroma<sup>206,207</sup>, was found to be significantly downregulated after *Hsp90aa1/ab1* silencing in CAFs, but only after *Hsp90ab1* silencing in NFs (**Figure II-11, C-D**).

The silencing of *Hsp90aa1* in both CAFs and NFs also caused the upregulation of proteins such as Type II Collagen alpha-1 (Col2a1, **Figure II-11, C-D**). Other proteins were only affected in one of the systems. This is the case of the proteoglycan Decorin (Dcn), whose expression decreased only after *Hsp90aa1* silencing in NFs, but not in CAFs (**Figure II-11, C-D**). Furthermore, proteins such as Fibronectin (Fn1) were differentially modulated by the HSP90 isoforms, as the silencing of *Hsp90aa1* in NFs induced its upregulation, but the silencing of *Hsp90ab1* caused its downregulation in this same system (**Figure II-11, C-D**).

Taken together, this analysis confirmed our previous RNAseq-based results, as no relevant trends in composition changes in the ECM were observed after *Hsp90aa1/ab1* silencing in NFs or CAFs (Figure II-11). Thus, HSP90 does not appear to particularly influence the CAF-derived ECM composition.

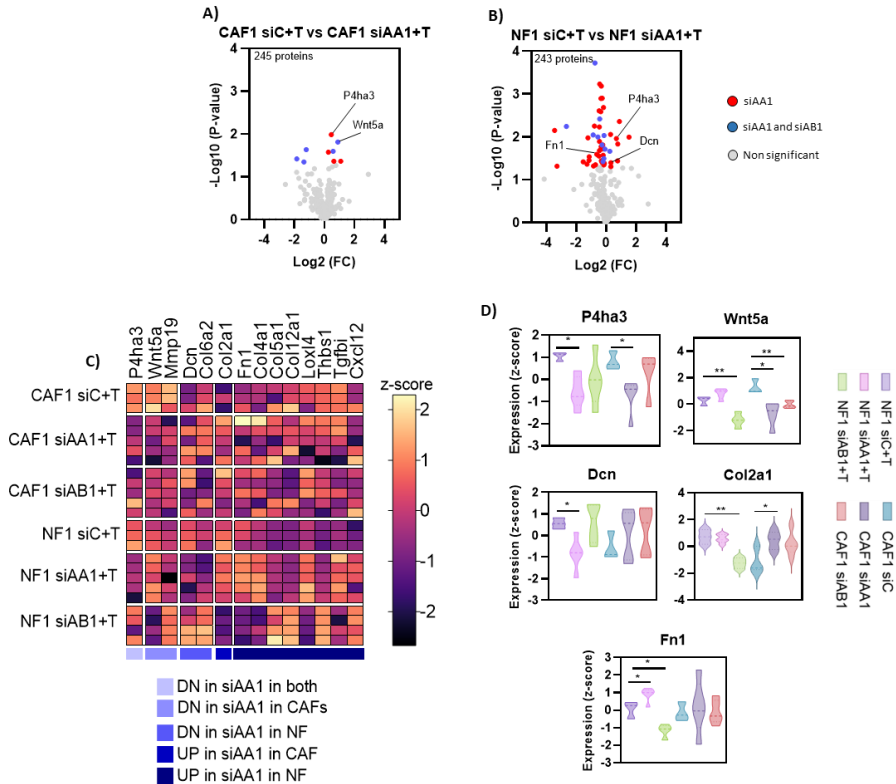


**Figure II-11. Proteomic analysis of ECM components in *Hsp90aa1/ab1* silenced CDMs.** **A-B.** Graphs showing the Differentially Expressed Proteins (DEPs), as determined by their  $-\text{Log}_{10}$  P-value and the  $\text{Log}_2$  fold change, found in CAF-derived (**A**) and NF-derived (**B**) CDMs, after silencing of *Hsp90aa1* in each system. DEPs significantly altered in the *siHsp90aa1* condition are indicated in red; DEPs significantly altered in both *Hsp90aa1/ab1* conditions are indicated in blue. Non-significant DEPs are also shown in grey. **C.** Heatmap of the z-score value of indicated proteins for all CDMs derived from transfected TGF $\beta$ -stimulated CAF1 and NF1 cells. **D.** Graphs showing z-score of protein expression of P4ha3, Wnt5a, Dcn, Col2a1 and Fn1 in CDMs derived from transfected TGF $\beta$ -stimulated CAF1 and NF1 cells (n=3, from 3 independent experiments for siC; n=5 from 5 independent experiments for siAA1; n=5 from 5 independent experiments for siAB1). *siC*: siRNA control. *siAA1*: *siHsp90aa1*. *siAB1*: *siHsp90ab1*. +T: +TGF  $\beta$ . \*: P-value < 0.1. \*\*: P-value < 0.01.

Next, we investigated the structure of the CDMs by fibronectin immunofluorescence focusing in CAFs. We observed that the ECM produced by TGF $\beta$ -stimulated CAFs is highly anisotropic, represented by a high percentage of alignment of the fibronectin fibers (Figure II-12, A-B). However, when *Hsp90aa1* expression is silenced, the organization of the fibronectin fibers is lost and the ECM becomes more isotropic, as there is a significant increase in the percentage of curvature and a significant reduction in the percentage of alignment of the fibers. This effect was exclusive to the HSP90 $\alpha$  isoform, as the silencing of *Hsp90ab1* did not affect the fibronectin structure of the ECM. Interestingly, there was no significant changes in the percentage of high-density matrix, which is a measure of the fibronectin content of the matrix, confirming that HSP90 $\alpha$  only influences the architecture of the ECM and not its actual composition or density.

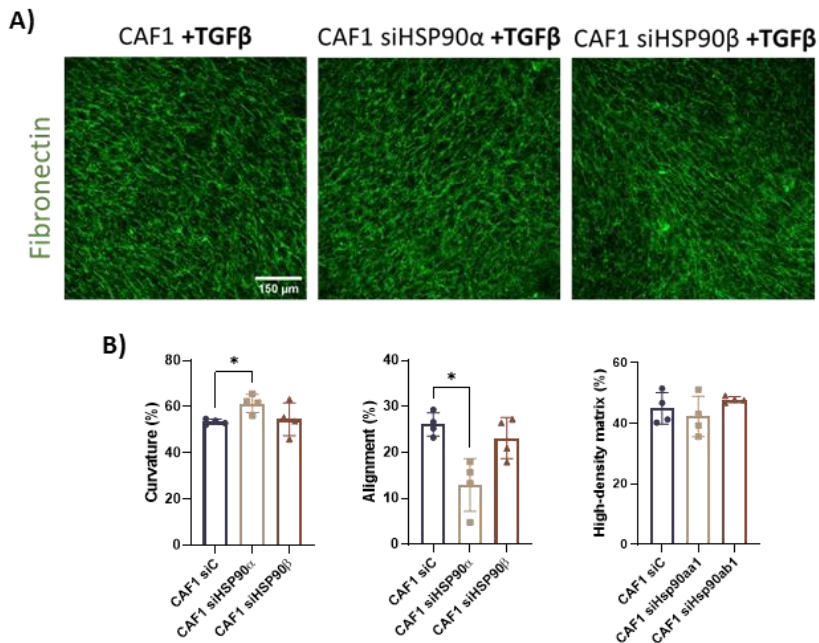


**Figure II-12. CDMs derived from *Hsp90aa1/ab1*-depleted CDMs. A.** Representative images of CDMs derived from TGF $\beta$ -stimulated CAFs after transfection with control, *Hsp90aa1* and *Hsp90ab1* siRNAs (5 ng/mL). **B.** TWOMBLI parameters (curvature, alignment and high-density matrix) for the study of the ECM structure and measurement of its anisotropic features, extracted from CDMs from (A) (n=5-6, from 1 experiment). \*: P-value < 0.1

As previously mentioned, the architecture of the ECM directly influences the migration capacities of the malignant cells that are disposed directly on top of them. To elucidate if the changes in ECM structure induced by the specific inhibition of HSP90 $\alpha$  have any consequences over the behavior of the cancer cells, D2A1-GFP murine breast cancer cells were plated on top of fibroblast-free CDMs, in which the fibroblasts have previously been lysed and removed (**Figure II-13**). The D2A1-GFP cells were monitored for 4 days, and then fixed for immunofluorescence analyses.

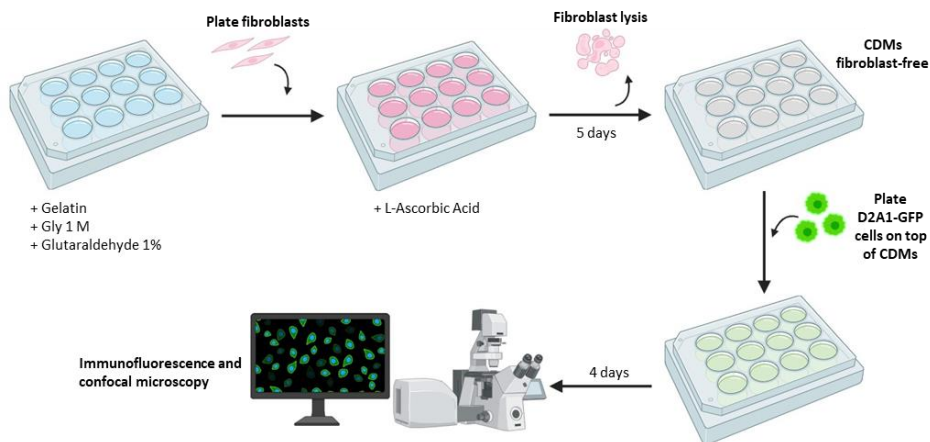
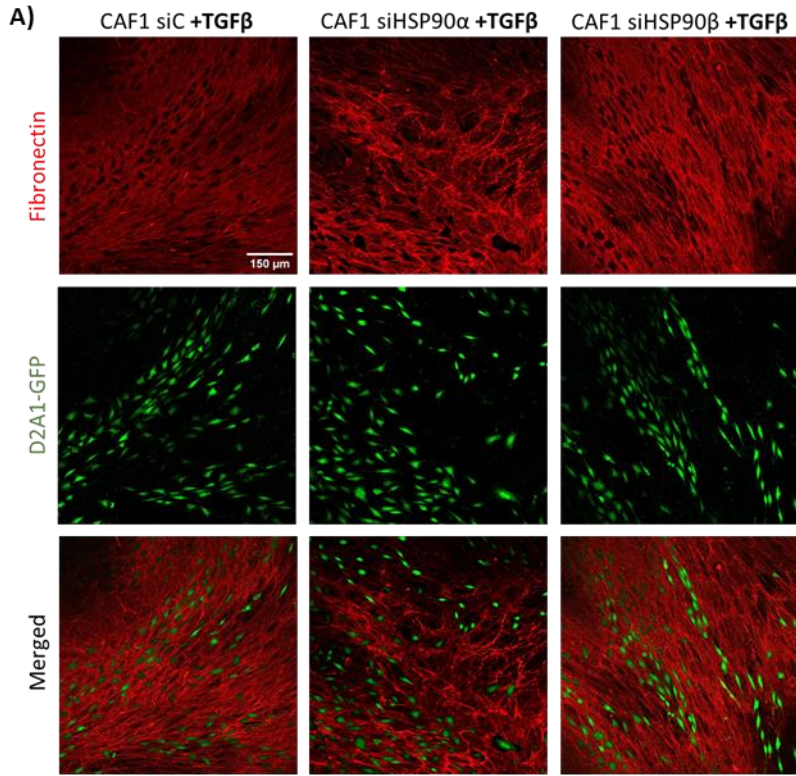
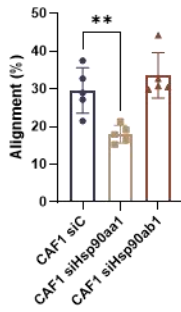


**Figure II-13. Protocol for the study of cancer cell behavior over CDMs.** Schematic representation of the protocol for plating cancer cells on top of fibroblast-free CDMs. The fibroblasts are removed in order to study the real influence of the CDM alone over the cancer cells. *Created on biorender.com.*

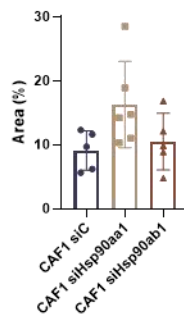
The CDM structures after removing the CAFs were similar to those observed in the case of the cell-containing CDMs: the silencing of *Hsp90aa1* specifically transforms the CDM into more isotropic, as there was a significant decrease in the percentage of alignment of the fibers (**Figure II-14, A-B**). It was also observed an increase in the GFP area in the case of the *Hsp90aa1*-depleted CDMs, but that difference was not significant (**Figure II-14, C**). However, although there was no significant effect of the CDMs over cancer cell growth, there was a significant difference in the behavior of the D2A1-GFP cells, that correlated with the CDM structure below them. In the case of control and *Hsp90ab1*-depleted CAFs, the D2A1-GFP cells were specifically distributed in angles between 80°–100° (**Figure II-14, A-D-E**). Thus, there was a correlation between the organization of the CDM fibers and the D2A1-GFP cell distribution, as cancer cells aligned with the fibronectin fibers below them. On the other hand, in the *Hsp90aa1*-depleted condition, the D2A1-GFP cells were evenly distributed all over the CDM, taking a wider angle range (**Figure II-14, E**). In fact, there was a significant reduction in the number of cells that were disposed in angles between 80° and 100° (**Figure II-14, D**). These results confirm the literature observations that describe a direct relationship between the CDM architecture and cancer cell orientation. Thus, the modulation of the CAF-derived CDM structure by HSP90 $\alpha$  directly influences cancer cell behavior.



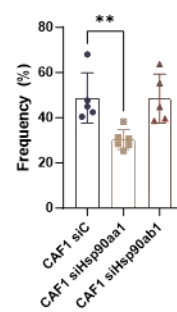
**B) Alignment of CDM fibers**



**C) % GFP Area**



**D) Angle Frequency (80°-100°)**



**E) Angle Frequency Distribution**

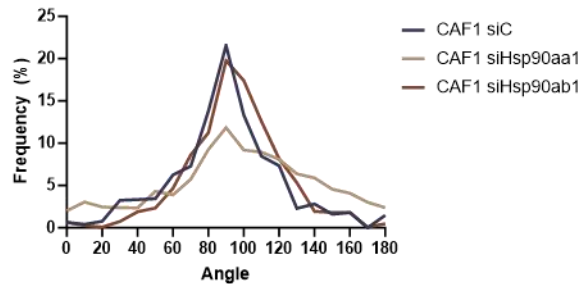


**Figure II-14. Study of cancer cell behavior over *Hsp90aa1/ab1*-depleted CDMs.** **A.** Representative endpoint images of the D2A1-GFP (green) cell disposition on top of CDMs generated by CAFs after transfection with control, *Hsp90aa1* and *Hsp90ab1* siRNAs. CDMs were visualized by fibronectin staining (red). **B.** Percentage of alignment of the fibers of indicated CDMs from (A), delivered by the TWOMBLI software (n=5, from 1 experiment). **C.** Percentage of GFP Area as a measure of cancer cell growth in each condition (n=5, from 1 experiment). **D.** Percentage of D2A1-GFP cells that were distributed in angles between 80° and 100° (perpendicular to the observed plane) (n=5, from 1 experiment). **E.** Frequency distribution of the different orientation angles in which the cancer cells were disposed. \*\*: P-value < 0.01.

To test if the observed differences in the disposition of the D2A1-GFP cells over different CDM structures were the consequence of differences in their migratory capacity and directionality, timelapse experiments were performed to monitor cancer cell motility over the different CDMs. The CDMs were generated following the same protocol, but in this experiment, the D2A1-GFP cells were plated in spheroid form. The spheroids were then monitored for 3 days and images were taken every hour. The main aim of this experiment was to monitor whether cancer cells migrated in a preferred direction depending on the underlying ECM structure: i.e. cancer cells on anisotropic ECMs may migrate preferentially within the angles of the fibers, whereas cancer cells on isotropic ECMs may migrate in several different angles<sup>204,208</sup>.

Endpoint analyses showed that the D2A1-GFP spheroids on top of CDMs generated by CAF controls had a significantly increased aspect ratio and significantly less roundness than the spheroids on top of CDMs generated by HSP90 $\alpha$ -silenced CAFs (Figure II-15, A-B). These parameters indicate that the D2A1-GFP cells were able to migrate in a particular direction more easily when plated on top of the control-derived CDMs in comparison with the ones plated on top of

the HSP90 $\alpha$ -depleted CDMs. In the latter condition, cells had no preferred migratory direction and therefore had substantial differences in shape parameters. Importantly, there was no significant differences in growth index, suggesting that the D2A1-GFP cells were able to grow equally in both CDMs (Figure II-15, A-B). Thus, the observed differences in the migration capacities are the consequence of the differences in CDM architecture below them exclusively. Taken together, our experiments confirmed the particular role of HSP90 $\alpha$  in controlling the ECM architecture by CAFs, promoting phenotypes associated with increased directed cancer cell migration.

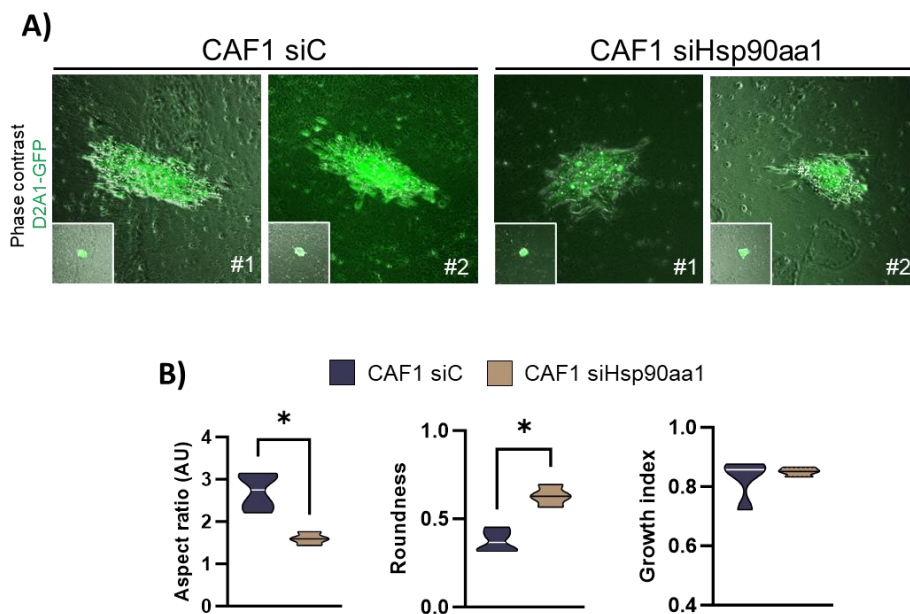


**Figure II-15. Cancer cell migration over *Hsp90aa1*-depleted CDMs. A.** Representative images of two different D2A1-GFP cell (green) spheroids at the final point (big image) and starting point (small image) for each indicated condition. Phase contrast images show both cancer cells and underlying ECM. **B.** Quantification of the aspect ratio and roundness of the spheroids at endpoint, as a measure of directed migration, as well as growth index of the D2A1-GFP cells from (A) (n=4, from one independent experiment). *siC*: *siCtrl*. \*: P-value < 0.01.

## 2.7. HSP90 $\alpha$ regulation in CAFs impairs cancer cell growth in restrictive conditions *in vitro*

Another important pro-tumoral function of CAFs is their ability to induce cancer cell growth. Although myCAF<sub>s</sub> also have this capacity, this function is more typically attributed to the iCAF phenotype. In the lab, the study of this particular characteristic is assessed by performing co-culture experiments of CAFs and cancer cells together.

The co-culture experiments of HSP90-transfected CAFs together with D2A1-GFP cells in full media showed no significant differences in cancer cell growth when HSP90 $\alpha/\beta$  are silenced (**Figure II-16**), indicating that the depletion of HSP90 in CAFs does not impede their influence over cancer cell growth.

The TME, as previously discussed in the introduction, is typically a stressful environment in which there is lack of nutrient availability, and these stressful conditions shape the TME changing the behavior of all the players as the tumor progresses. Thus, changing the cell culture conditions in the co-culture experiments into more restrictive ones will better resemble the physiological environment typically found in TMEs.

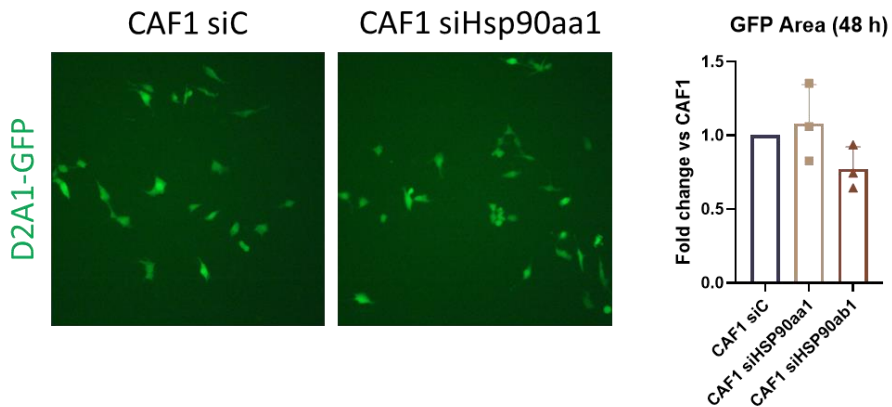


**Figure II-16. Co-culture of cancer cells and Hsp90aa1/ab1 silenced CAFs.** *Left.* Representative images of D2A1-GFP cells (green) in co-culture with CAF1 (not shown) after transfection with control or Hsp90aa1 siRNAs at 48 h. *Right.* Graph shows fold change of GFP area in comparison to the siRNA control transfected CAFs at 48 h for the indicated conditions. The experiments were performed in normal cell culture conditions (high glucose DMEM supplemented with 10% FBS). (n=3, from 3 independent experiments). *siC:* *siCtrl*.

A similar co-culture experiment as the one previously described was performed, this time using low glucose supplemented only with 2% FBS. In this new set up, the co-culture with control transfected CAFs increased the GFP area in comparison with the culture of the D2A1 cells alone (**Figure II-17, A**). Interestingly, there was a reduction in the GFP area when the D2A1-GFP cells were plated together with *Hsp90aa1*-silenced CAFs. Although this observation was not significant, it was exclusive to the HSP90 $\alpha$  isoform, as the GFP area in the case of the HSP90 $\beta$ -depleted CAFs co-culture remained similar to the control CAF.

Another component of the TME that also directly influences cancer cell growth is the ECM, which is also transformed by CAFs. To better resemble the physiological conditions that can be found in the

TME, the co-culture experiment was reproduced in the presence of Matrigel, creating a 3D set up and maintaining the more restrictive starving conditions with low glucose media supplemented with 2.5% FBS. In this system, there was also a trend for more cancer cell growth (as measure by GFP positive area, although not significant) when they were co-cultured with control CAFs and *Hsp90ab1*-depleted cells, in comparison with *Hsp90aa1*-silenced (Figure II-17, B).

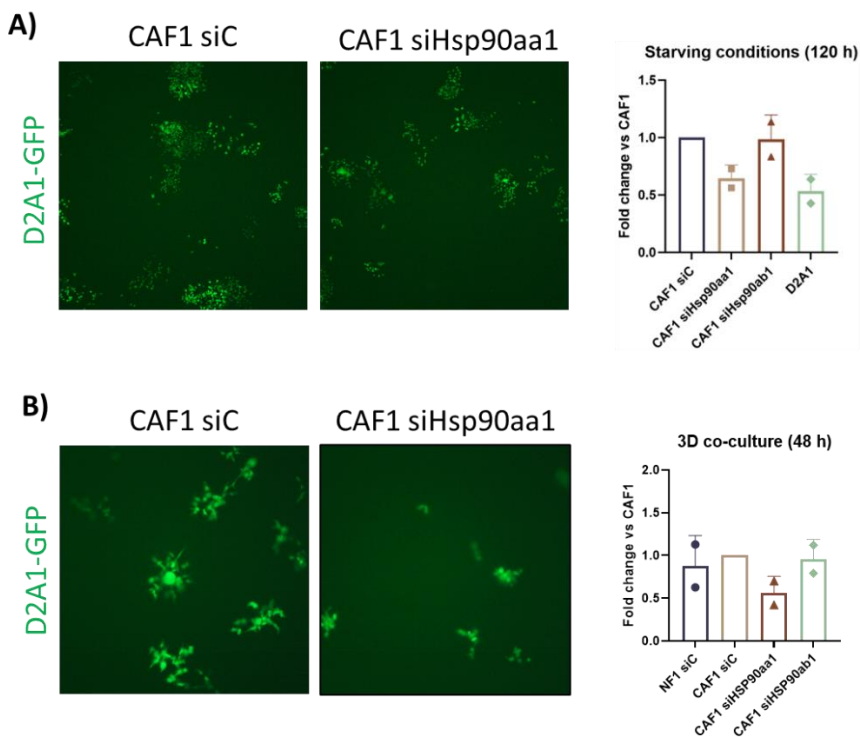


**Figure II-17. HSP90 $\alpha$  may modulate the ability of CAFs to support cancer cell growth in restricted conditions.** **A.** Representative images (left) of D2A1-GFP cells (green) in co-culture with siRNA transfected CAFs (not shown) at 120 h, and quantification (right) of fold change in GFP area for each tested condition. Cells were maintained in low glucose media supplemented with 2% FBS. (n=2). **B.** Representative images (left) of D2A1-GFP (green) cells in co-culture with siRNA transfected CAFs (not shown) on top of matrigel, at 48 h, and quantification (right) of fold change in GFP area for each tested condition. Cells were maintained in low glucose media supplemented with 2.5% FBS (n=2). *siC*: *siCtrl*.

These results indicate a possible role of HSP90 $\alpha$  in the capacity of the CAFs to support cancer cell growth in nutrient restricted conditions, but more work is needed in this direction to further elucidate the importance of these findings.

## 2.8. HSP90 $\alpha$ regulates CAF secreted factors

CAF $s$  are also known to secrete diverse factors to exert their influence over the remaining components of the TME and shape the pro-tumoral environment. In the case of the TGF $\beta$ -stimulated NF $s$ , the silencing of *Hsp90aa1* significantly altered the gene expression of growth factors such as TGF $\beta$  (*Tgfb1*); and Fibroblast Growth Factor 2 (FGF-2, *Fgf2*), whose expression is regulated by TGF $\beta$ <sup>209</sup> (**Figure II-18, A-B**). Similar results were obtained in the proteomic analysis, which indicated a decrease on both proteins after *Hsp90aa1/ab1* silencing (**Figure II-18, C**). On the other hand, in the case of the CAF $s$ , no differences were found in the gene expression profile of these secreted factors (**Figure II-18, A-B-C**).

Taken together, these results show that the silencing of HSP90 does not appear to affect CAF marker expression, albeit it may modulate genes and proteins required to sustain specific pro-tumoral CAF functions. Furthermore, HSP90 silencing, and specially *Hsp90aa1*, appears to affect cytoskeletal components in CAF $s$  and TGF $\beta$ -stimulated NF $s$ , whilst it may also influence secreted factor production in TGF $\beta$ -stimulated NF $s$ .

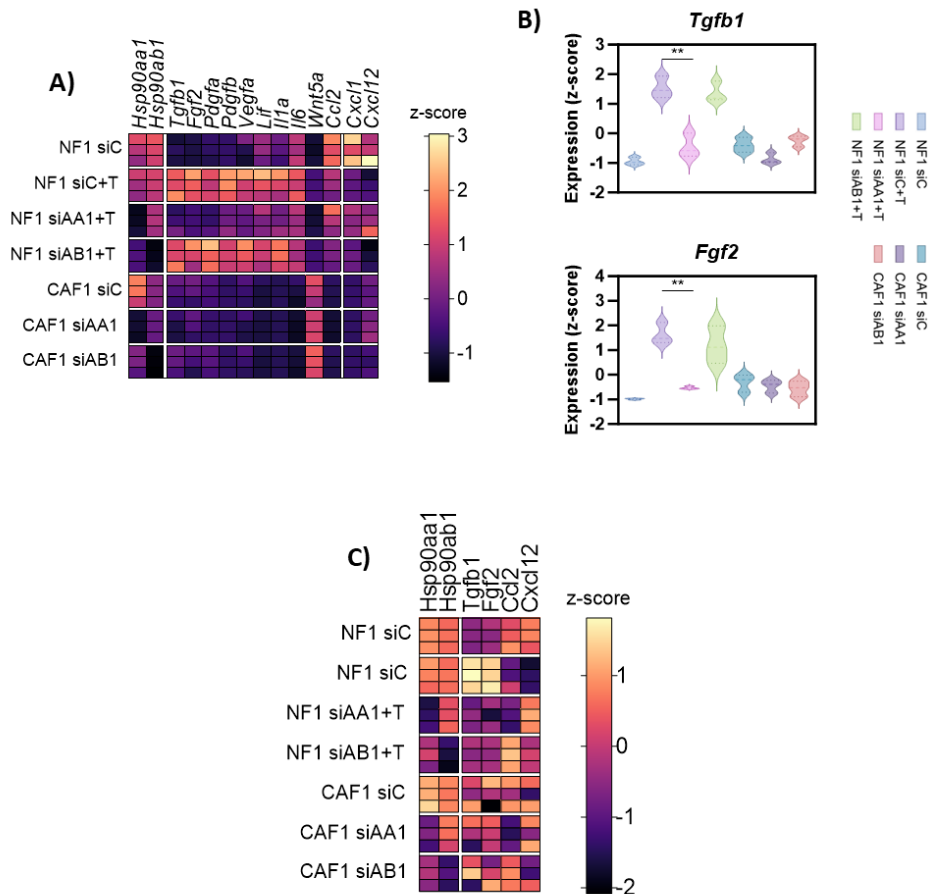


**Figure II-18. Gene and protein expression profile of *Hsp90aa1/ab1*-silenced CAFs and NFs.** **A.** Heatmap of the z-score value of indicated genes in CAF1 and TGF $\beta$ -stimulated NF1 after silencing of *Hsp90aa1* or *Hsp90ab1* respectively. Data extracted from RNAseq analysis (triplicates). **B.** Graphs showing z-score of gene expression of *Tgfb1* and *Fgf2* in transfected CAF1 and TGF $\beta$ -stimulated NF1 cells. Data extracted from RNAseq analysis (n=3 from 3 independent experiments). **C.** Heatmap of the z-score value of indicated proteins in CAF1 and TGF $\beta$ -stimulated NF1 after silencing of *Hsp90aa1* or *Hsp90ab1* respectively, as informed by the proteomic analysis (triplicates). Where indicated, 5 ng/mL TGF $\beta$  was added for 24 h. *siC*: siRNA control. *siAA1*: si*Hsp90aa1*. *siAB1*: si*Hsp90ab1*. *+T*: +TGF $\beta$ .

## 2.9. HSP90 $\alpha$ functions in NFs from wild-type and *Hsp90aa1*-knock out mice

To further validate the observed effects of silencing *Hsp90aa1*, we also studied *Hsp90aa1* functions in *Hsp90aa1*<sup>+/+</sup> and *Hsp90aa1*<sup>-/-</sup> murine breast NFs obtained from our *in vivo* model (Figure II-19, A-B). In this system, similar to the silencing with siRNA, the *Hsp90aa1*<sup>-/-</sup> fibroblasts also showed a reduction in their gel contraction capacity in comparison with the *Hsp90aa1*<sup>+/+</sup> fibroblasts (Figure II-19, C). In addition, the co-culture of these cells with the breast cancer cell line PY8119 showed that the absence of HSP90 $\alpha$  in fibroblasts affects their capacity to support cancer cell growth *in vitro* (Figure II-19, D).

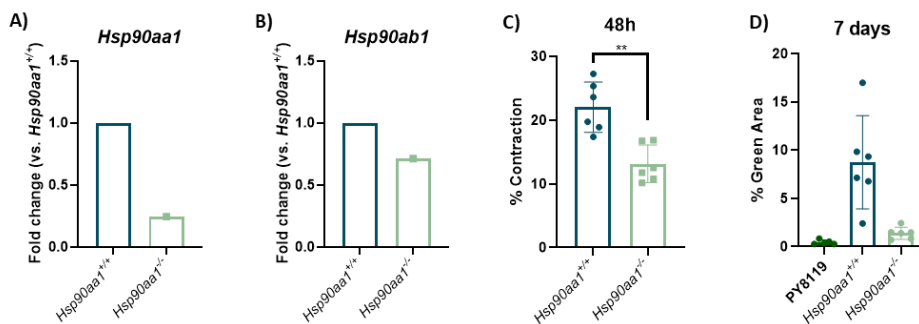


**Figure II-19. Functional characterization of wild-type and *Hsp90aa1* knock-out normal murine mammary gland fibroblasts.** A-B. Graphs showing the fold change in gene expression of *Hsp90aa1* (A) and *Hsp90ab1* (B) respectively in *Hsp90aa1*<sup>-/-</sup> fibroblasts in comparison with *Hsp90aa1*<sup>+/+</sup> (n=1). qPCRs were performed in technical triplicates. C. Graph showing percentage of gel contraction of *Hsp90aa1*<sup>-/-</sup> and *Hsp90aa1*<sup>+/+</sup> fibroblasts after 48 h (n=6, from 2 independent experiment performed in technical triplicates). D. Graph showing percentage of green area of PY8119 alone or in co-culture with *Hsp90aa1*<sup>-/-</sup> or *Hsp90aa1*<sup>+/+</sup> fibroblasts, respectively, after 7 days. \*\*: *P*-value < 0.01.

## 2.10. HSP90 $\alpha$ functions are independent of TGF $\beta$ in CAFs

Thus far, our *in vitro* results show effects of silencing HSP90 $\alpha$  in CAFs and in TGF $\beta$ -stimulated NFs. To further elucidate the potential role of HSP90 $\alpha$  in the TGF $\beta$  pathway as a possible explanation of the observed effects, WB experiments were performed to check the protein expression and activated status of SMAD proteins after *Hsp90aa1/ab1* silencing, which are the most important effectors of the TGF $\beta$  pathway.

The WB for the protein expression of the total amount of SMAD proteins and their active phosphorylated form in transfected CAFs showed that there was no difference between the control and the *Hsp90aa1/ab1*-silenced CAFs (**Figure II-20, A**). These results indicate that HSP90 $\alpha$  functions in CAFs would be independent of the TGF $\beta$  pathway.

In CAFs, the TGF $\beta$  pathway is not the only one modulating all the pro-tumoral characteristics of CAFs. To explore the implications of this pathway in the functional *in vitro* experiments previously presented, a gel contraction assay was performed with CAFs treated with the TGF $\beta$  inhibitor SB431542 (**Figure II-20, C**). In this experiment, the inhibitor did not have any effect on the gel contraction capacity of the CAFs, even after further TGF $\beta$  stimulation, indicating that these characteristics are independent of the TGF $\beta$  pathway in CAFs. Given the previously presented results, in which the silencing of HSP90 $\alpha$  resulted in impaired contractile capacity of CAFs, these observations further suggested that HSP90 $\alpha$  may operate independently of the TGF $\beta$  pathway in CAFs.

On the other hand, a different outcome resulted from the WB experiment with the TGF $\beta$ -stimulated NFs (Figure II-20, B). In this case, the silencing of *Hsp90aa1* decreased the expression of both the total amount of SMAD proteins and their corresponding phosphorylated forms. Thus, HSP90 $\alpha$  functions in this particular setting appear to actually modulate the TGF $\beta$  pathway. This result may explain, at least in part, some of the molecular differences obtain by *Hsp90aa1/ab1* silencing in both systems (CAFs and TGF $\beta$ -stimulated NFs).

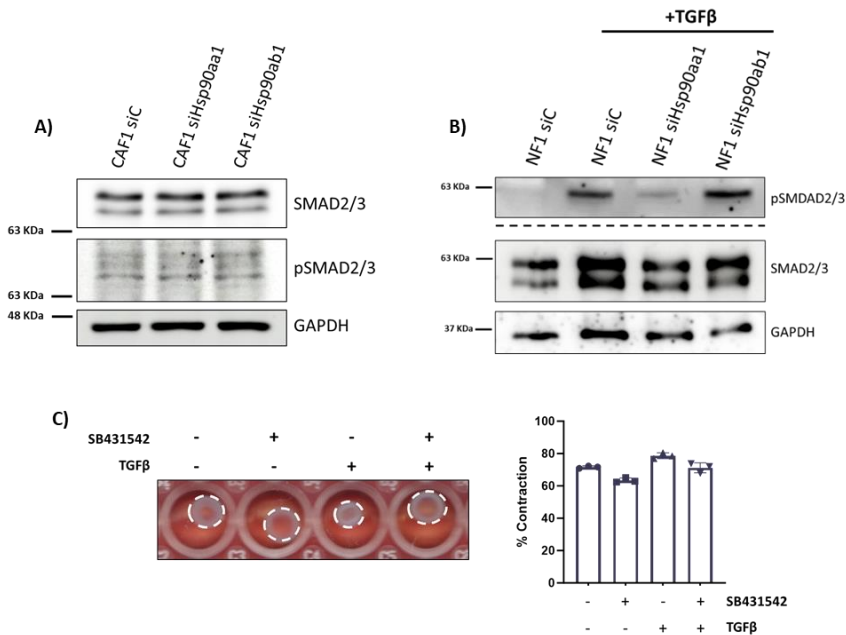


**Figure II-20. HSP90 $\alpha$  functions in CAFs are independent of the TGF $\beta$  pathway.** A-B. Representative WB experiments for the expression of SMAD proteins and their corresponding active phosphorylated forms (pSMAD2: Ser465/467; pSMAD3: Ser423/425) in control and *Hsp90aa1/ab1*-silenced CAFs (A) or TGF $\beta$ -stimulated NFs (B). GAPDH was used as loading control for all WB experiments. Dashed lines separate independent WB experiments, each one of them with their corresponding loading control. Protein weight markers are also shown. C. Representative image of a gel contraction experiment (left) with CAFs treated with TGF $\beta$  and the TGF $\beta$  inhibitor (SB431542, 5  $\mu$ M) as indicated, and graphs showing percentage of contraction (right) (n=3, from one experiment). *siC*: *siCtrl*.



# Results

## 3. Role of HSP90 $\alpha$ in tumoral processes *in vivo*



### 3.1. Stromal *Hsp90aa1* knock-out impairs E0771 breast tumor growth *in vivo*

Our bioinformatic analysis revealed HSP90 as a possible driver of pro-tumoral programs in the TME. Additionally, our *in vitro* characterization showed a specific role of HSP90 $\alpha$  in regulating CAF emergence and behavior. To further explore the implications of stromal HSP90 in tumor development, we performed *in vivo* experiments using the *Hsp90aa1* knock-out (KO) murine model kindly provided by Dr. Ana Victoria Villar at the IBBTEC. This mutant was first generated and characterized by Dr. Picard and colleagues<sup>210</sup>. There are no phenotypic differences described for KO mice for *Hsp90aa1* in comparison with the wild-type (WT) mice, except for the fact that male *Hsp90aa1*-KO mice are sterile. This mice also show the same HSP90 $\beta$  expression levels as the WT mice<sup>210</sup>. As previously mentioned, mice without expression of *Hsp90ab1* are not viable and therefore not suitable for this type of experiments.

The *in vivo* studies of HSP90 implications in tumor stroma were carried out by orthotopically injecting syngeneic E0771 murine breast cancer cells into immunocompetent WT (*Hsp90aa1*<sup>+/+</sup>), heterozygous (HE, *Hsp90aa1*<sup>+/-</sup>) and KO (*Hsp90aa1*<sup>-/-</sup>) C57BL/6 mice. In this context, the potential tumors generated by the E0771 cells will have wild-type expression of HSP90 $\alpha$  in all malignant cells, as they do not present any perturbation related to HSP90 expression.

However, the expression of HSP90 $\alpha$  in the stroma of those tumors will vary according to the genetic background of the host mouse (Figure III-1, A). The experimental mice were first genotyped for HSP90 $\alpha$  by PCR prior injection of the cancer cells (Figure III-1, B).

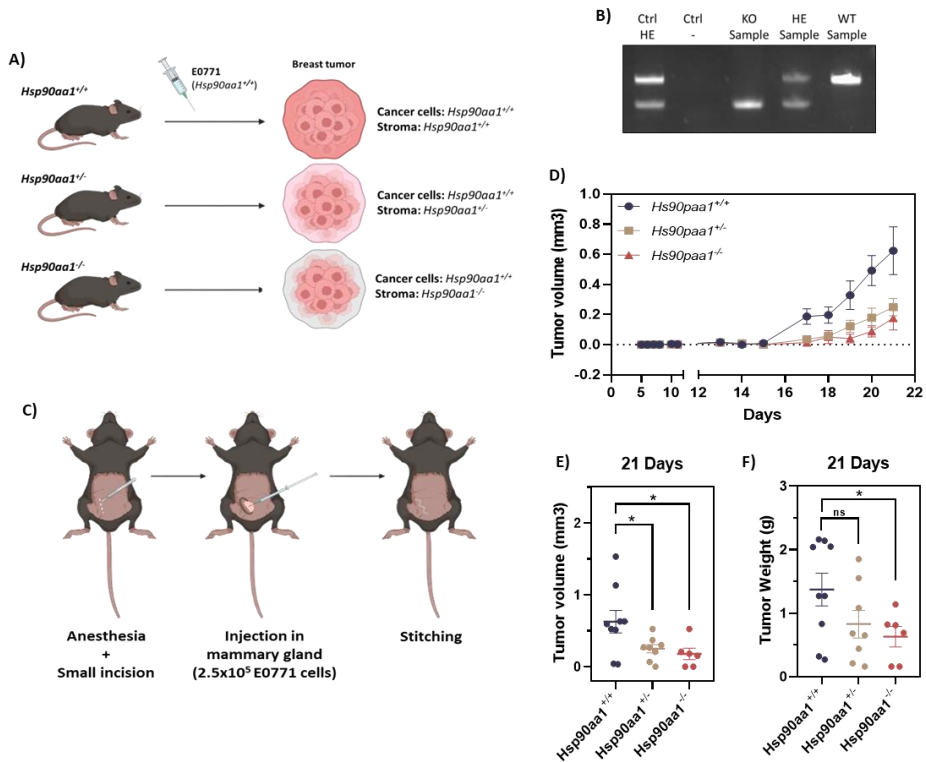


**Figure III-1. Orthotopic injection of syngeneic E0771 murine breast cancer cells in HSP90 $\alpha$  deficient mice.** **A.** Experimental design for the study of stromal HSP90 $\alpha$  in E0771 breast cancer tumors. *Created on Biorender.com.* **B.** Example of an agarose gel showing the PCR for genotyping mice employed in the analyses. Ctrl HE: positive control for both bands (WT and deleted). *Ctrl -*: negative control. **C.** Experimental procedure for the injection of the E0771 cells directly into the 4<sup>th</sup> mammary fat pad of the mice. *Created on Biorender.com.* **D.** Tumor volume (mm<sup>3</sup>) of experimental orthotopic tumors in the indicated mice strains. Volume was measured periodically until they reached the final endpoint (day 21). **E-F.** Tumor volume (mm<sup>3</sup>, **E**) and tumor weight (g, **F**) measured at 21 days post-injection (final endpoint, tumor extraction day). \*: *P*-value < 0.01.

To generate the breast cancer tumors,  $2.5 \times 10^5$  E0771 cells were injected directly into the fourth mammary fat pad of the mice by performing small surgery, in order to avoid possible experimental mistakes and ensure the correct placement of the cancer cells (**Figure III-1, C**). Tumors were measured consistently throughout the experiment, and tumor growth was monitored by calculating tumor volume for each experimental point (**Figure III-1, D**). When the mice reached the final point, at 21 days post-injection, they were sacrificed and tumors were extracted, weighted and processed for further histopathology analysis.

Differences in tumor volume were observed as soon as 17 days post-injection between the different genotypes, suggesting a delay in tumor development in the *Hsp90aa1<sup>+/-</sup>* and *Hsp90aa1<sup>-/-</sup>* mice in comparison with the *Hsp90aa1<sup>+/+</sup>*, which grew faster (**Figure III-1, D**). At day 21 post-injection, *Hsp90aa1<sup>+/-</sup>* and *Hsp90aa1<sup>-/-</sup>* tumors were significantly smaller than the *Hsp90aa1<sup>+/+</sup>* in volume (**Figure III-1, E**). There was also a significant difference in tumor weight at 21 days between *Hsp90aa1<sup>-/-</sup>* and *Hsp90aa1<sup>+/+</sup>* tumors (**Figure III-1, F**). Altogether, these results indicate that there is a defect in tumor growth when HSP90 $\alpha$  is not expressed in host tissues, suggesting a critical role of stromal HSP90 $\alpha$  in tumorigenesis *in vivo*.

### 3.2. Stromal *Hsp90aa1* knock-out affects collagen deposition in E0771 breast tumors

To study possible differences in tumor structure and cellular composition between *Hsp90aa1<sup>+/+</sup>* and *Hsp90aa1<sup>-/-</sup>* breast tumors, H&E, Picrosirius Red and Masson's trichrome staining were performed in histopathology slides (**Figure III-2**). No differences were observed at the macroscopic level in any of the different staining between *Hsp90aa1<sup>+/+</sup>* and *Hsp90aa1<sup>-/-</sup>* tumors. Macroscopic analysis of Hematoxylin-Eosin (H&E) staining of *Hsp90aa1<sup>+/+</sup>* and *Hsp90aa1<sup>-/-</sup>* tumors showed no significant changes in tumor architecture or cellular and nuclear morphology (**Figure III-2, A**). Of note, *Hsp90aa1<sup>-/-</sup>* tumors presented a slight increase in necrotic areas in comparison with the *Hsp90aa1<sup>+/+</sup>*, albeit these differences were not significant (not shown).

Our previous analyses suggested an association between desmoplastic responses and HSP90 activity. As previously described in the introduction, CAFs are the main producers of ECM components in the TME, especially collagen. Thus, the abundance of collagen in histopathology slides can be used to evaluate the presence and activity of CAFs in tumors. To evaluate the collagen content in the extracted murine breast tumors, slides were stained with Picrosirius Red and Masson's trichrome, two different approaches to analyze collagen fibers and fibrosis (**Figure III-2, B-C**).

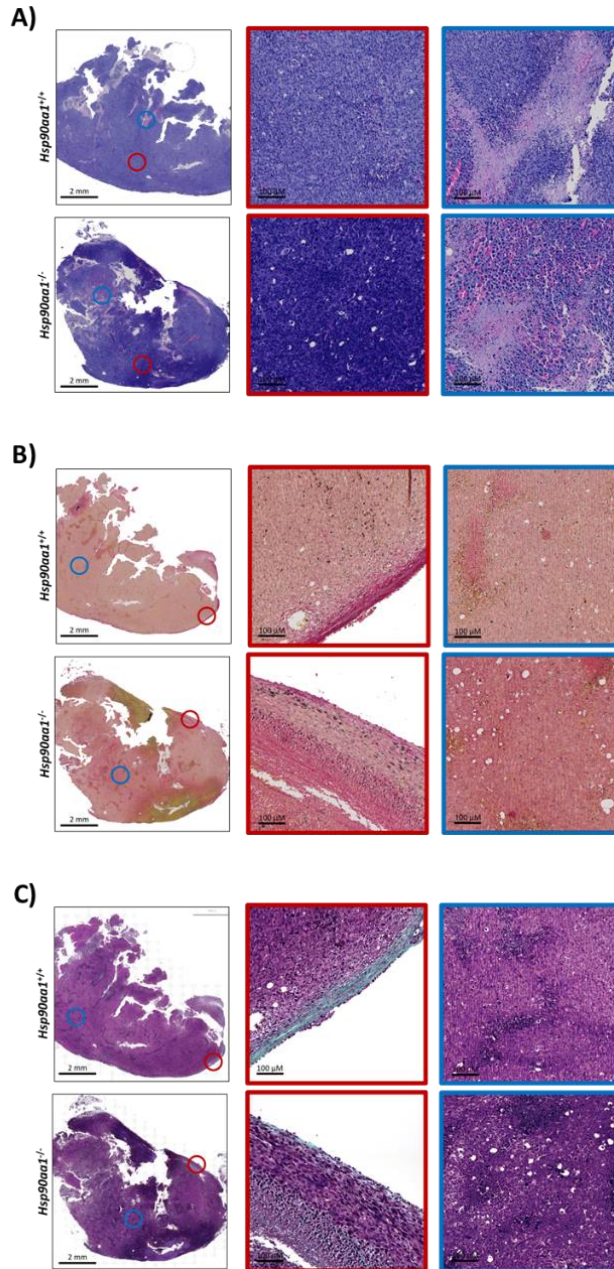


**Figure III-2. Histopathology studies of architecture and collagen content of *in vivo* murine breast tumors.** **A.** Representative images of hematoxylin-eosin (H&E) staining and closeup images of cellular architecture of the tumor (red circle, red frame) and necrotic areas (blue circle, blue frame) of E0771 tumors grown in *Hsp90aa1*<sup>+/+</sup> and *Hsp90aa1*<sup>-/-</sup> mice. **B-C.** Representative images of Picrosirius Red staining (**B**) and Masson's trichrome staining (**C**) of E0771 tumors grown in *Hsp90aa1*<sup>+/+</sup> and *Hsp90aa1*<sup>-/-</sup> mice. Right panels show zoom up areas at the periphery of the tumors (red frame) and at central areas (blue frame).

We noticed that orthotopic tumors generated by the EO771 model presented a limited desmoplastic response in general, with central regions devoid of relevant collagen content and positivity restricted to peripheral areas. Both stains revealed an accumulation of collagen specifically in the peripheral areas of the tumor in *Hsp90aa1<sup>+/+</sup>* animals. In those areas, there was a reduction in the collagen content in the case of the *Hsp90aa1<sup>-/-</sup>* in comparison with the *wild-type*. These observations showed that the accumulation of collagen in the TME is dependent on stromal HSP90 $\alpha$  expression. Since collagen production is primarily associated with CAFs, these results suggested a role of HSP90 $\alpha$  in controlling the pro-tumoral activities of CAFs *in vivo*.

### **3.3. Stromal *Hsp90aa1*<sup>-</sup> knock out impairs *in vivo* lung metastasis from EO771 cells**

Given the observed effect of stromal HSP90 $\alpha$  over tumor growth, questions emerged on whether stromal HSP90 $\alpha$  could also play an important role in the development of metastasis. To answer this, the same EO771 breast cancer cells were injected into the tail vein of WT and KO mice (**Figure III-3, A**). This cell line is known to be very aggressive and to generate lung metastasis when injected directly into the bloodstream of the mice. If stromal HSP90 $\alpha$  has any relevance in metastasis formation, we would expect less overt metastases in KO mice.

After injection of  $2.5 \times 10^5$  E0771 directly in the tail vein, the weight of the mice was periodically monitored (Figure III-3, B), as the development of lung metastases can cause severe weight loss. All mice were sacrificed at the same time as soon as one of them reached the final endpoint. Lungs were extracted, visually inspected for metastasis and fixed for further histopathology analysis. The H&E staining analysis revealed that the *Hsp90aa1*<sup>-/-</sup> lungs had significantly less metastasis than the *Hsp90aa1*<sup>+/+</sup> (Figure III-3, C).

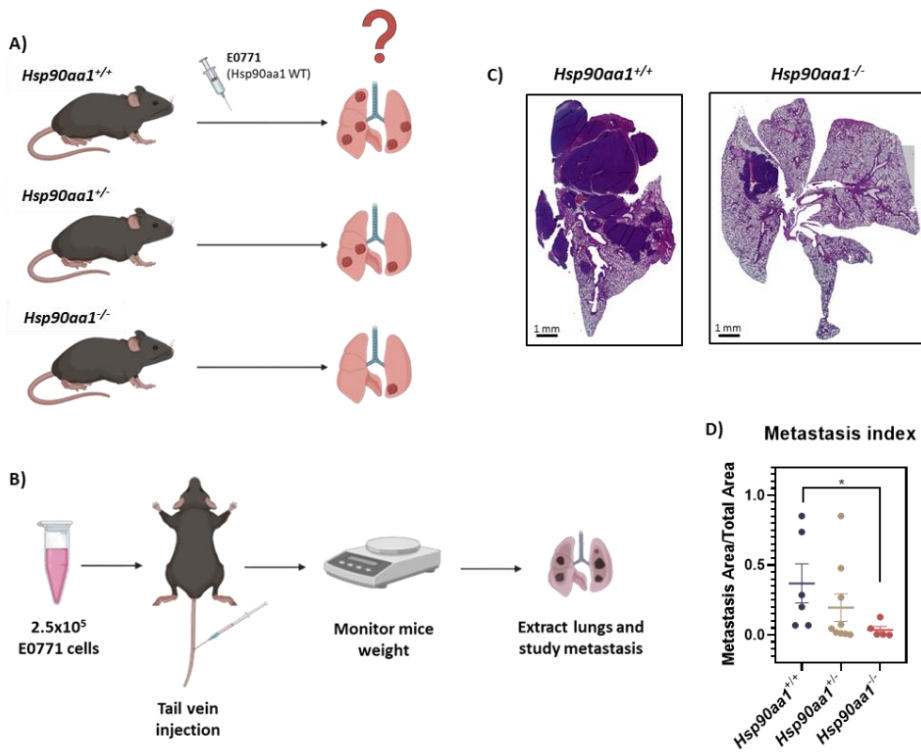


**Figure III-3. Tail vein injection of syngeneic E0771 murine breast cancer cells for disseminated metastasis studies.** A. Experimental design for the study of stromal HSP90 $\alpha$  in metastasis development. Created on Biorender.com. B. Experimental procedure for the tail vein injection of the E0771 breast cancer cells and monitoring of the mice. C. Representative images of H&E staining of metastatic lungs from *Hsp90aa1*<sup>+/+</sup> and *Hsp90aa1*<sup>-/-</sup> mice. D. Metastasis index (metastasis area/total area) of the H&E-stained lungs from experiments as described in (A). \*: P-value < 0.01.

There were no significant differences in metastasis index between the *Hsp90aa1*<sup>+/-</sup> and the *Hsp90aa1*<sup>+/+</sup> mice (**Figure III-3, D**). These results indicate that stromal HSP90 $\alpha$  not only plays an important role in primary tumor growth, but also in generating pro-survival/proliferative cues to promote the establishment of metastases *in vivo*.

# Results

## 4. Molecular processes underlying HSP90 functions in CAFs and TGF $\beta$ -stimulated NFs



The *in vitro* functional experiments with *Hsp90aa1/ab1*-transfected CAFs and TGF $\beta$ -stimulated NFs demonstrated a role of HSP90, and particularly HSP90 $\alpha$ , in modulating important pro-tumoral functions. However, the first *in vitro* exploratory studies of the possible implications of HSP90 in modulating the TGF $\beta$  pathway did not fully explain the molecular mechanisms underlying the functional effects of HSP90 $\alpha/\beta$  in both systems. In particular, *Hsp90aa1*-silencing affected different functions without influencing TGF $\beta$  pathway activation in CAFs, suggesting additional mechanisms at play. To further elucidate the molecular mechanisms and pathways responsible for HSP90 pro-tumoral functions in CAFs, in-depth molecular characterization (transcriptomics and proteomics) was performed in both *Hsp90aa1/ab1*-silenced CAFs and TGF $\beta$ -stimulated NFs.

#### 4.1. *Hsp90aa1* silencing induces a specific gene expression program in CAFs

For the gene expression characterization of *Hsp90aa1/ab1*-silenced CAFs, we performed RNAseq analysis in CAFs transfected with control, *Hsp90aa1* and *Hsp90ab1* siRNAs. Principal component analysis (PCA) of transcriptomics data showed that CAFs transfected with control siRNA and *Hsp90ab1*-silenced CAFs clustered more closely in comparison with *Hsp90aa1*-silenced CAFs, which formed a separated cluster (**Figure IV-1, A**).

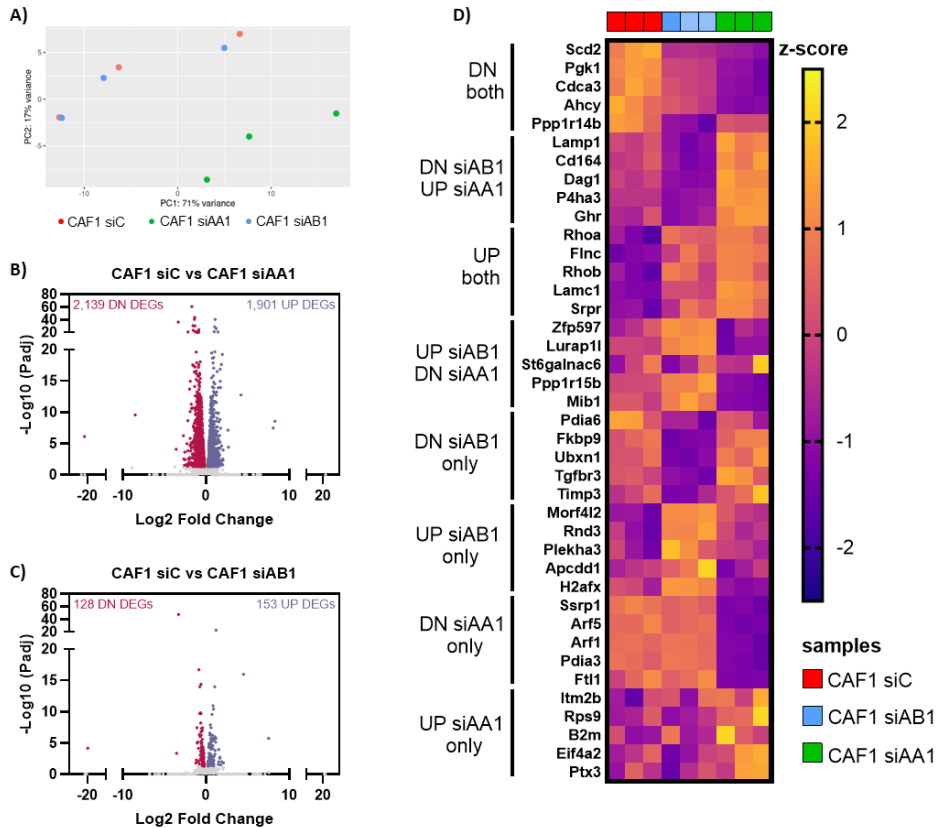


**Figure IV-1. Gene expression analysis of *Hsp90aa1/ab1* silenced CAFs and TGF $\beta$ -stimulated NFs.** **A.** Graph showing PCA of control, *Hsp90aa1* and *Hsp90ab1* siRNA transfected CAF1 cells (n=3, from 3 independent experiments). **B-C.** Graphs showing the upregulated (blue dots) and downregulated (red dots) DEGs as determined by their  $-\text{Log}_{10}$  P adjusted value (Padj) and the  $\text{Log}_2$  fold change, for the *Hsp90aa1*-silenced (B) and *Hsp90ab1*-silenced (C) CAF1 cells, in comparison with siRNA control transfected CAF1. Every dot in the graphs is an individual gene. **D.** Heatmap showing the z-score normalized value of the expression of the top 5 most upregulated or downregulated DEGs in the three CAF1 transfected conditions clustered in the indicated categories (left), as informed by the RNAseq data (n=3, from 3 independent experiments). *DN*: downregulated. *UP*: upregulated. *siC*: siRNA control. *siAA1*: si*Hsp90aa1*. *siAB1*: si*Hsp90ab1*.

In addition, there were more differentially expressed genes (DEGs) in the *Hsp90aa1*-silenced than in the *Hsp90ab1*-silenced CAFs, both upregulated and downregulated (Figure IV-1, B-C). When focusing on the top 5 DEGs in all three transfected conditions, we observed that the silencing of each isoform (*Hsp90aa1* or *Hsp90ab1*)

resulted in disparate molecular responses in CAFs. Namely, we could observe genes that were modulated in the same direction when either isoform was targeted, but also several genes that were only modulated by one of them. In addition, we observed certain genes that were modulated in different directions in response to either *Hsp90aa1* or *Hsp90ab1* silencing. Altogether, these analyses demonstrated that silencing of *Hsp90aa1* induces a more distinct phenotype in CAFs than the silencing of *Hsp90ab1*, affecting the expression of a bigger number of genes (Figure IV-1, D).

#### 4.2. Gene ontology analysis of differential gene expression profiles altered by Hsp90aa1/ab1 silencing in CAFs

To gain insights into the biological and molecular processes controlled by each HSP90 isoform in CAFs, we performed a gene ontology (GO) enrichment analysis of common and specific DEGs, both upregulated and downregulated, in *Hsp90aa1/ab1*-silenced CAFs.

Firstly, we performed a global enrichment analysis using the Gene Ontology Term (GOTERM) databases, which categorizes genes based on three different groups depending on their typical function: Biological Processes (BO), Cellular Component (CC) and Molecular Function (MF). The enrichment analysis of the common DEGs found in both *Hsp90aa1* and *Hsp90ab1*-silenced CAFs when compared to the control CAFs showed very small enrichment values (Figure IV-2, A). Similar results were obtained in the case of the HSP90 $\beta$  specific DEGs. These results suggested that perturbing HSP90 $\beta$  has very little

effect in altering the expression of genes associated with critical biological or molecular functions in CAFs.

On the other hand, the enrichment analysis of the specific DEGs found in the *Hsp90aa1*-silenced CAFs showed a significant enrichment in multiple processes, in line with the observed effects on CAF behavior for this specific experimental point. In particular, gene sets associated with cell cycle, DNA repair and protein binding signatures presented an important enrichment score in downregulated DEGs, suggesting a defect on these biological processes in *Hsp90aa1*-silenced CAFs. The upregulated DEGs in this same condition were significantly enriched in other signatures such as vacuole organization and catabolic processes (**Figure IV-2, A**). Similar findings were obtained when the same DEGs were interrogated using the Kyoto Encyclopedia of Genes and Genomes (KEGG) database. Again, DEGs common to *Hsp90aa1* and *Hsp90ab1*-silenced CAFs presented low enrichment scores. When focusing on HSP90 $\alpha$  specific DEGs, the analysis showed a significant enrichment in pathways related to cell cycle, nucleocytoplasmic transport, DNA repair and proteasome for the downregulated DEGs (**Figure IV-2, B**). In addition, there was a significant enrichment for upregulated DEGs in molecular pathways related to lysosomes, the mTOR signaling pathway and fatty acid degradation, among others processes. These results indicate that *Hsp90aa1*-silencing in CAFs, unlike *Hsp90ab1*, affects several molecular and biological processes.

In order to elucidate which molecular pathways associated with CAF functions or their emergence were affected by *Hsp90aa1*-

silencing, we performed an enrichment analysis using a list of curated gene sets that include relevant molecular and biological processes related to the CAF phenotype (“Curated genesets”). This analysis revealed that the most significant enriched signatures in the downregulated DEGs were those related to the activation of YAP/TAZ in CAFs (Figure IV-2, C; “CAF\_YAPTAZ\_ALL\_UP”).

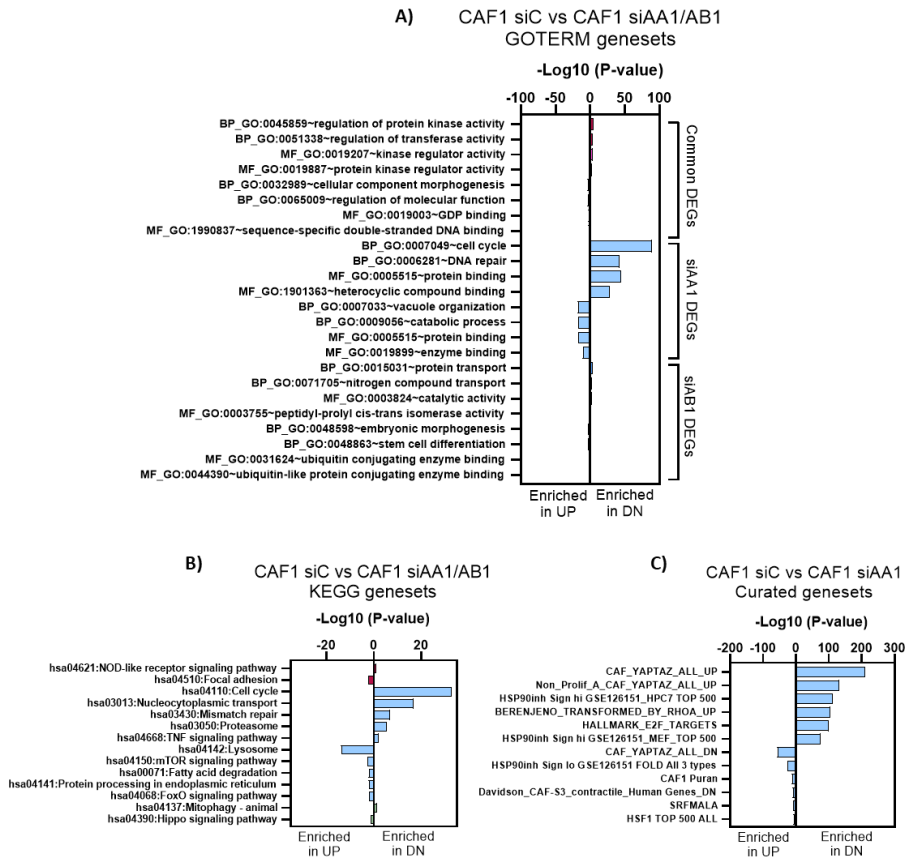


**Figure IV-2. Specific gene expression dysregulation caused by *Hsp90aa1*-silencing in CAFs has significant biological and molecular consequences. A-B.** Graphs showing the enrichment score (represented as  $-\text{Log}_{10}$  of the P-value) in GOTERM genesets (A) and KEGG genesets (B) in the common DEGs found in both *Hsp90aa1* and *Hsp90ab1* silenced CAF1 (red bars), specific *Hsp90aa1*-silencing DEGs (blue bars) and specific *Hsp90ab1*-silencing DEGs (green bars). C. Graph showing the enrichment score (represented as  $-\text{Log}_{10}$  of the P-value) in signatures from curated CAF-related genesets in the specific downregulated and upregulated DEGs resulting from *Hsp90aa1* silencing in CAFs. DN: downregulated. UP: upregulated. siC: siRNA control. siAA1: si*Hsp90aa1*. siAB1: si*Hsp90ab1*.

YAP/TAZ are transcriptional regulators with important roles in development and cancer<sup>211</sup>. In CAFs, they promote the activation of transcriptional programs that enhance ECM remodeling and cancer cell invasion<sup>79,105</sup>. Importantly, the downregulated DEGs were found to be also significantly enriched in signatures related to cell cycle, including E2F signatures (**Figure IV-2, C**). In addition, and in correlation with the results obtained for the downregulated DEGs, the most significantly enriched signature in the upregulated DEGs in *Hsp90aa1*-silenced CAFs was associated with YAP/TAZ inactivation (**Figure IV-2, C**; "CAF\_YAPTAZ\_ALL\_DN").

In different systems, YAP activity has been shown to be associated with cell cycle progression, as it promotes the expression of cell cycle-related genes<sup>212,213</sup>. Since our results indicated an enrichment of genes related to cell cycle in downregulated DEGs from the HSP90 $\alpha$ -silenced condition, there was a possibility that the score for the YAP/TAZ signatures was just reflecting changes in expression in cell cycle genes contained in it, and not actual changes in YAP/TAZ activity. To correct for this possibility, we investigated the enrichment score of the "Non\_Prolif\_A\_CAF\_YAPTAZ\_ALL\_UP" signature, which contains all the genes included in the "CAF\_YAPTAZ\_ALL\_UP" signature, minus those associated with cell proliferation. Notably, the score of this signature was also particularly high, suggesting a dysregulation of YAP/TAZ activity after *Hsp90aa1*-silencing in CAFs independent of cell cycle alterations. In addition, signatures related to HSP90 inhibition in different systems ("Hsp90inh Sign hi GSE126151\_HCP7 TOP 500" and "Hsp90inh Sign hi GSE126151\_MEF TOP 500"), as well as signatures associated with

cytoskeletal signaling (“BERENJERO\_TRANSFORMED\_BY\_RHOA\_UP”) were also enriched in downregulated DEGs from the *Hsp90aa1*-silenced CAFs.

Altogether, these results indicate that the most important consequence derived from *Hsp90aa1*-silencing in CAFs is the dysregulation of YAP/TAZ related signatures.

#### 4.3. Gene set enrichment analysis of differential gene expression profiles altered by *Hsp90aa1/ab1* silencing in CAFs

To further understand the molecular mechanisms whereby HSP90 exerts its functions in CAFs, the same RNAseq dataset obtained from siRNA transfected CAFs was interrogated using Geneset enrichment analysis (GSEA). For this analysis, we focused on the signatures from the “Curated genesets” dataset (that showed particularly high enrichment scores in the previous analysis) and analyzed the different expression programs resulting from *Hsp90aa1* or *Hsp90ab1* silencing in CAFs. Focusing first in genesets that were common for both perturbations, we observed a significant downregulation of signatures related to cell cycle progression (“E2F\_TARGETS”; **Figure IV-3, A-B**). This result further suggests a possible defect in cell proliferation when either HSP90 $\alpha$  or HSP90 $\beta$  is inhibited. Thus, this effect cannot fully explain the functional perturbations associated specifically to HSP90 $\alpha$  silencing.

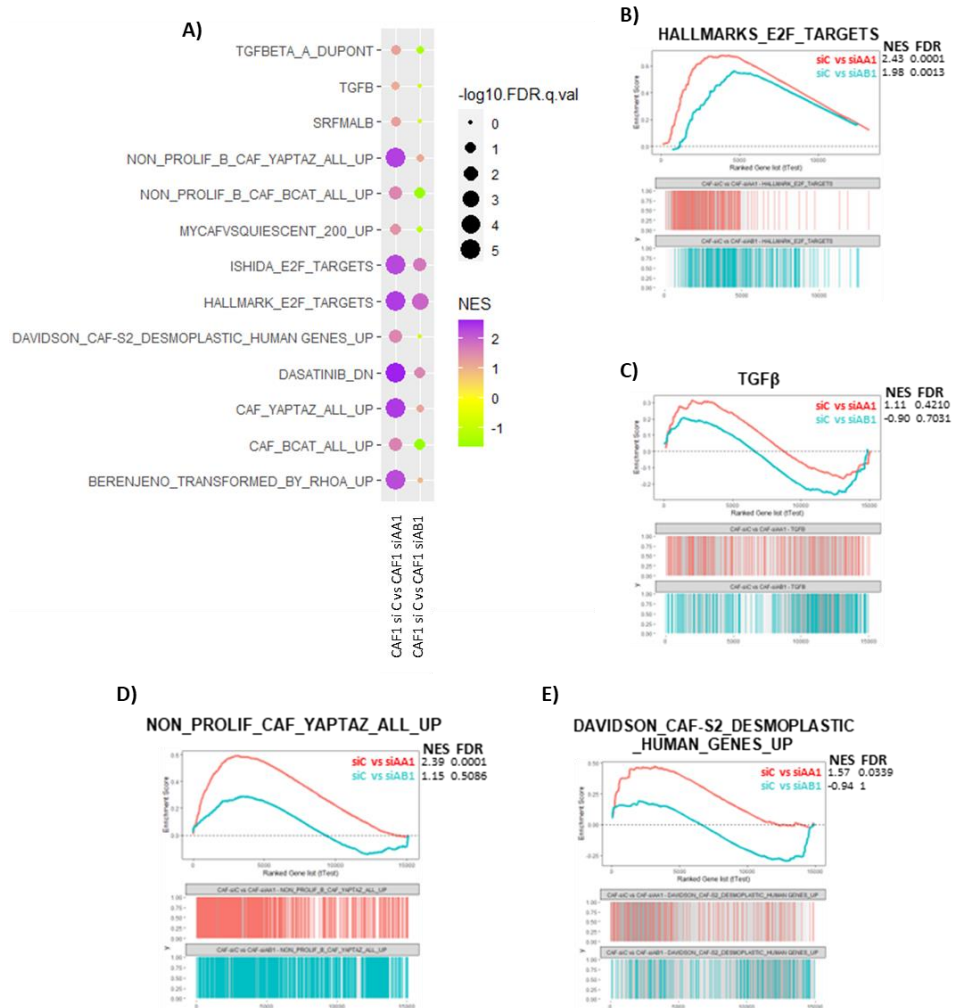


**Figure IV-3. GSEA analysis of transcriptional programs affected by *Hsp90aa1* and *Hsp90ab1* silencing in CAFs. A.** Bubble plot summarizing GSEA results of “curated genesets” when comparing CAF1 control (siC) vs *Hsp90aa1*-silenced or *Hsp90ab1*-silenced CAF1. The size of the bubbles represents the level of significance of the signature (-log<sub>10</sub> FDR), and their color represents the level of enrichment (purple: high NES; green: low NES). A positive NES represents signatures enriched in CAF1 control, whereas a negative NES represents signatures enriched in *Hsp90aa1* or *Hsp90ab1*-silenced CAFs respectively. **B-E.** GSEA plots showing the activity of the indicated signatures in both *Hsp90aa1*-silenced (red line) and *Hsp90ab1*-silenced CAF1 (blue line) when compared to the control CAF1 condition. NES and FDR coefficients are also indicated. siC: siRNA control. siAA1: si*Hsp90aa1*. siAB1: si*Hsp90ab1*. NES: Normalized Enrichment Score. FDR: False Discovery Rate.

On the other hand, silencing of neither *Hsp90aa1* nor *Hsp90ab1* appeared to significantly affect TGF $\beta$ -signaling related gene signatures in CAFs (**Figure IV-3, A-C**), which confirms that the *Hsp90aa1* silencing effects observed *in vitro* are independent of the TGF $\beta$  signaling pathway in CAFs.

Similar to the previous GO enrichment analysis, the GSEA of signatures only affected by HSP90 $\alpha$ -depletion showed that there was a significant enrichment in signatures related to YAP/TAZ in CAF control when compared to HSP90 $\alpha$ -silenced CAFs (**Figure IV-3, A**). YAP/TAZ related signatures that do not include cell cycle regulating genes (“NON\_PROLIF\_CAF\_YAPTAZ\_ALL\_UP”, **Figure IV-3, A-D**) were also significantly downregulated after *Hsp90aa1* depletion in CAFs. In addition, a significant enrichment in desmoplastic signatures (“DAVIDSON\_CAF-S2\_DESMOPLASTIC\_HUMAN\_GENES\_UP”), signatures associated with RhoA (“BERENJERO\_TRANSFORMED\_BY\_RHOA UP”) and SRC signaling (“DASATINIB\_DN”) were also significantly enriched in CAF control when compared to *Hsp90aa1*-silenced CAFs, (**Figure IV-3, A-E**).

Taking all these results together, our gene expression analyses suggest that HSP90 $\alpha$  silencing has a more profound effect in than HSP90 $\beta$  depletion in CAFs. They also informed of a new potential role of HSP90 $\alpha$  in modulating CAF activities through YAP/TAZ.

#### 4.4. *Hsp90aa1*-silencing induces significant gene expression alterations in TGF $\beta$ -stimulated NFs

The protein expression analysis of the SMAD proteins in *Hsp90aa1*-depleted TGF $\beta$ -stimulated NFs suggested a possible role in regulating the TGF $\beta$  pathway in this particular system. To further confirm this relationship and elucidate the molecular mechanisms behind HSP90 functions in TGF $\beta$ -stimulated NFs, a similar gene expression analysis was performed using RNAseq data derived from control and *Hsp90aa1/ab1*-silenced NF1 after stimulation with TGF $\beta$ .

The PCA analysis showed that the *Hsp90ab1*-silenced TGF $\beta$ -activated NF clustered near the TGF $\beta$ -stimulated control, whereas the *Hsp90aa1*-silenced samples and the non-treated NFs clustered independently of the rest of the groups (**Figure IV-4, A**). In addition, the silencing of *Hsp90aa1* induced a higher amount of DEGs in TGF $\beta$ -stimulated NFs (**Figure IV-4, B-C**). Amongst the top 5 DEGs downregulated in si*Hsp90aa1* and si*Hsp90ab1* conditions were *Timp3* and *Sdc2*, genes associated with ECM remodeling and cell-ECM crosstalk, respectively (**Figure IV-4, D**). *Timp2* was also downregulated in si*Hsp90ab1* conditions but not after *Hsp90aa1* depletion. In the case of top 5 DEGs only downregulated after *Hsp90aa1*, we observed *Actg1* and *Actb*, both associated with the actin cytoskeleton. Thus, this first exploratory analysis indicates that the silencing of *Hsp90aa1* in TGF $\beta$ -stimulated NFs results in a complete switch on the phenotype of these fibroblasts, as it happened with CAFs.

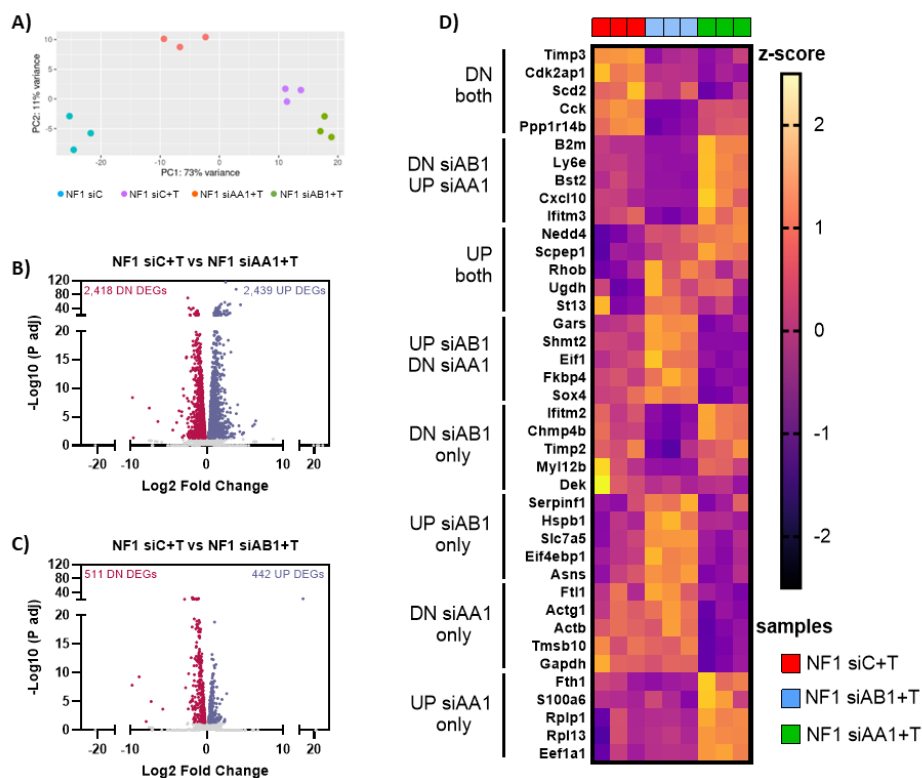


**Figure IV-4. Silencing of *Hsp90aa1* in TGF $\beta$ -stimulated NFs, unlike *Hsp90ab1*, induces a distinct gene expression profile.** **A.** Graph showing the PCA of control, *Hsp90aa1* and *Hsp90ab1* siRNA transfected TGF $\beta$ -stimulated NF1 (n=3, from 3 independent experiments). **B-C.** Graphs showing the upregulated (blue) and downregulated (red) DEGs as determined by their  $-\text{Log}_{10}$  P adjusted value (Padj) and the  $\text{Log}_2$  fold change, for the *Hsp90aa1*-silenced (B) and *Hsp90ab1*-silenced (C) TGF $\beta$ -stimulated NF1, in comparison with the siRNA control transfected condition (siC). Every dot in the graphs represents an individual gene. **D.** Heatmap showing the z-score normalized value of the expression of the top 50 most upregulated or downregulated DEGs in the three TGF $\beta$ -stimulated conditions clustered in the indicated categories (left), as informed by the RNAseq data. (n=3 from 3 independent experiments). Where indicated, 5 ng/mL of TGF $\beta$  was added for 24h. *DN*: downregulated. *UP*: upregulated. *siC*: siRNA control. *siAA1*: si*Hsp90aa1*. *siAB1*: si*Hsp90ab1*. *+T*: +TGF $\beta$ .

#### 4.5. Gene ontology analysis of differential gene expression profiles altered by *Hsp90aa1/ab1* silencing in TGFβ-stimulated NFs

Following a similar strategy to the one employed with the CAF system, we performed a GO enrichment analysis of all common and specific DEGs found after silencing *Hsp90aa1/ab1* in TGFβ-stimulated NFs.

The global analysis with the GOTERM datasets revealed that there was a low enrichment in signatures related to DNA replication, cell cycle and nucleotide binding in the DEGs commonly found in both *Hsp90aa1/ab1*-silenced TGFβ-stimulated NFs (**Figure IV-5, A**). The analysis of the specific *Hsp90ab1*-depleted DEGs also showed very low enrichment values, indicating that the silencing of *Hsp90ab1* has minimal effect in altering the molecular characteristics of TGFβ-stimulated NFs.

On the contrary, the global enrichment analysis of the specific DEGs for the *Hsp90aa1*-silencing condition revealed a significant enrichment in signatures related to cellular components organization, metabolism of nitrogen compounds, protein binding and RNA binding in the case of the downregulated DEGs (**Figure IV-5, A**). In the case of the upregulated DEGs, there was a relevant enrichment in signatures related to various metabolic processes, including fatty acid metabolism. Some of these signatures were also found enriched in the *Hsp90ab1*-depleted CAF DEGs, showing common defects associated to the silencing of *Hsp90aa1* in both systems and suggesting a role of HSP90α in fibroblast activation.

Similar results were obtained when analyzing the same common DEGs from both *Hsp90aa1/ab1*-silenced TGF $\beta$ -stimulated NFs but interrogating the KEGG database. There was a small enrichment in signatures related with cell cycle and DNA replication in the case of the commonly downregulated DEGs (**Figure IV-5, B**). Low enrichment values were also found for inositol phosphate metabolism and cytokine-cytokine receptor mechanisms signatures in the commonly upregulated DEGs. Focusing in the specific *Hsp90aa1*-silencing derived DEGs, some of the most highly enriched signatures were also found in the case of the transfected CAFs, and included the nucleocytoplasmic transport and proteasome signatures enriched in downregulated DEGs, and signatures related to lysosomes and fatty acid degradation in the upregulated DEGs (**Figure IV-5, B**). Other signatures exclusively found enriched in the *Hsp90aa1*-silenced TGF $\beta$ -stimulated NFs aligned with the pro-tumoral functions affected by HSP90 $\alpha$  in vitro, including signatures related to the Hippo signaling pathway (in which YAP/TAZ participates) and the regulation of the actin cytoskeleton, both found significantly enriched in the downregulated DEGs. Importantly, there was also a high enrichment in the TGF $\beta$  signaling pathway signature in the downregulated DEGs dataset.

When interrogating the specific *siHsp90aa1* DEGs obtained in the TGF $\beta$ -stimulated NFs system with the “Curated genesets”, we found that among the top most enriched signatures in the downregulated DEGs were again those related with YAP/TAZ: “CAF\_YAPTAZ\_ALL\_UP” and “Non\_Prolif\_A\_CAF\_YAPTAZ\_ALL\_UP” (**Figure IV-5, C**). Importantly, the most significantly enriched

signature in the downregulated DEGs was “BERENJENO\_TRANSFORMED\_BY\_RHOA\_UP”, which is related to cytoskeleton remodeling. Also, there was a significant enrichment in the signature “myCAFvsQUIESCENT\_200\_UP”, indicating a significant downregulation of genes related to the myCAF phenotype when *Hsp90aa1* is silenced in TGF-stimulated NFs. Given that myCAFs are characterized by the activation of the TGF $\beta$  pathway, this signature constitutes another evidence of the relationship between the activity of this signaling pathway and HSP90 $\alpha$ . In the case of the upregulated DEGs, the most enriched signature was again related with YAP/TAZ inactivation (**Figure IV-5, C**). Other enriched signatures associated with the upregulated DEGs included signatures found silenced in contractile CAFs (“Davidson\_CAF-S3\_contractile\_Human\_Genes\_DN”) suggesting alterations in cell contractility, as well as signatures associated with immunomodulatory CAFs (“Davidson\_CAF-S1\_Immune\_Human\_Genes UP”).

Taken together, these results indicate that the particular gene expression program elicited by *Hsp90aa1*-silencing in TGF $\beta$ -stimulated NFs differs slightly from that found in the case of the *Hsp90aa1*-silenced CAFs, and confirms the role of HSP90 $\alpha$  in regulating the TGF $\beta$ -pathway in this specific system, unlike CAFs. In addition, our data suggests that HSP90 $\alpha$  also modulates an unexpected set of transcriptional programs associated with YAP/TAZ, SRC and RhoA in CAFs and in TGF $\beta$ -activated NFs.

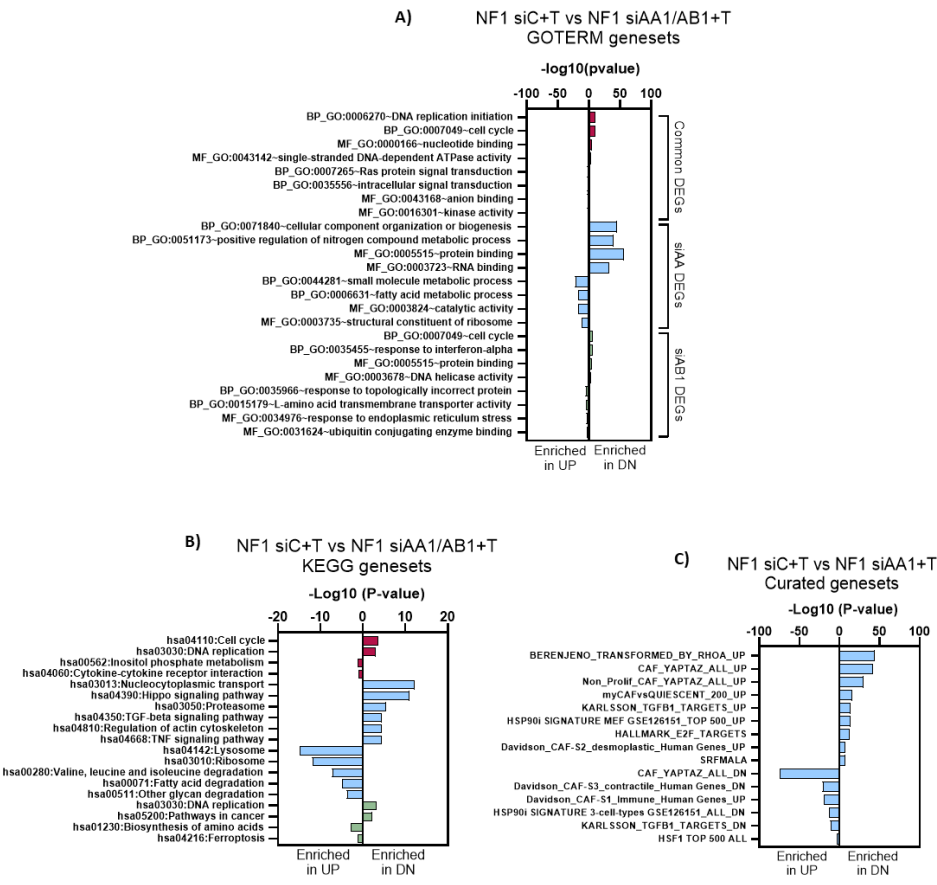


**Figure IV-5. Biological and molecular associations of gene expression dysregulation caused by *Hsp90aa1*-silencing in TGFβ-stimulated NFs. A-B.** Graphs showing the enrichment score (represented as  $-\text{Log}_{10}$  of the P-value) in GOTERM genesets (A) and KEGG genesets (B) in common DEGs after *Hsp90aa1* and *Hsp90ab1* silencing (red bars), and in DEGs specific for *Hsp90aa1* silencing (blue bars) or specific *Hsp90ab1* silencing (green bars) in TGFβ-stimulated NF1. **C.** Graph showing the enrichment score (represented as  $-\text{Log}_{10}$  of the P-value) in signatures from “Curated genesets” for upregulated and downregulated DEGs after silencing of *Hsp90aa1* in TGFβ-stimulated NF1. Where indicated, 5 ng/mL of TGFβ was added for 24h. *DN*: downregulated. *UP*: upregulated. *siC*: siRNA control. *siAA1*: si*Hsp90aa1*. *siAB1*: si*Hsp90ab1*. *+T*: +TGFβ.

#### 4.6. GSEA of differential gene expression profiles altered by *Hsp90aa1/ab1* silencing in TGF $\beta$ -stimulated NFs

Next, we performed a GSEA focused in the “Curated signatures” and analyzed the differences in molecular and functional programs resulting from silencing *Hsp90aa1* or *Hsp90ab1* in TGF $\beta$ -stimulated NFs. As in the case of CAFs, there was a significant enrichment in cell cycle related signatures (“E2F\_TARGETS”, **Figure IV-6, A-B**) in the control setting when compared to both *Hsp90aa1* and *Hsp90ab1* silencing. Thus, in the TGF $\beta$ -stimulated NFs system, the effects observed *in vitro* after HSP90 $\alpha$ -depletion cannot be the consequence of cell cycle defects in these cells. Importantly, TGF $\beta$  signatures were specifically downregulated in *Hsp90aa1*-depleted TGF $\beta$ -stimulated NFs but not after *Hsp90ab1* silencing (**Figure IV-6, A-C**), further confirming the importance of HSP90 $\alpha$  for the activity of this signaling pathway in this system. Consistent with the previous findings in CAFs, there was also a significant enrichment in YAP/TAZ signatures in control TGF $\beta$ -stimulated NFs when compared to *Hsp90aa1*-depleted TGF $\beta$ -stimulated NFs, including the YAP/TAZ signature lacking genes related to cell proliferation (“NON\_PROLIF\_CAF\_YAPTAZ\_ALL\_UP”, **Figure IV-6, A-D**). Altogether, these results further confirm the previous findings and in general resemble the results obtained in the case of the transfected CAFs. Thus, HSP90 $\alpha$  appears to control pro-tumoral functions in TGF $\beta$ -stimulated NFs by regulating YAP/TAZ activities. Contrary to CAFs, in the TGF $\beta$ -stimulated NF system HSP90 $\alpha$  also potentiates the TGF $\beta$ -pathway and therefore may be associated with the establishment of myCAF gene expression programs.

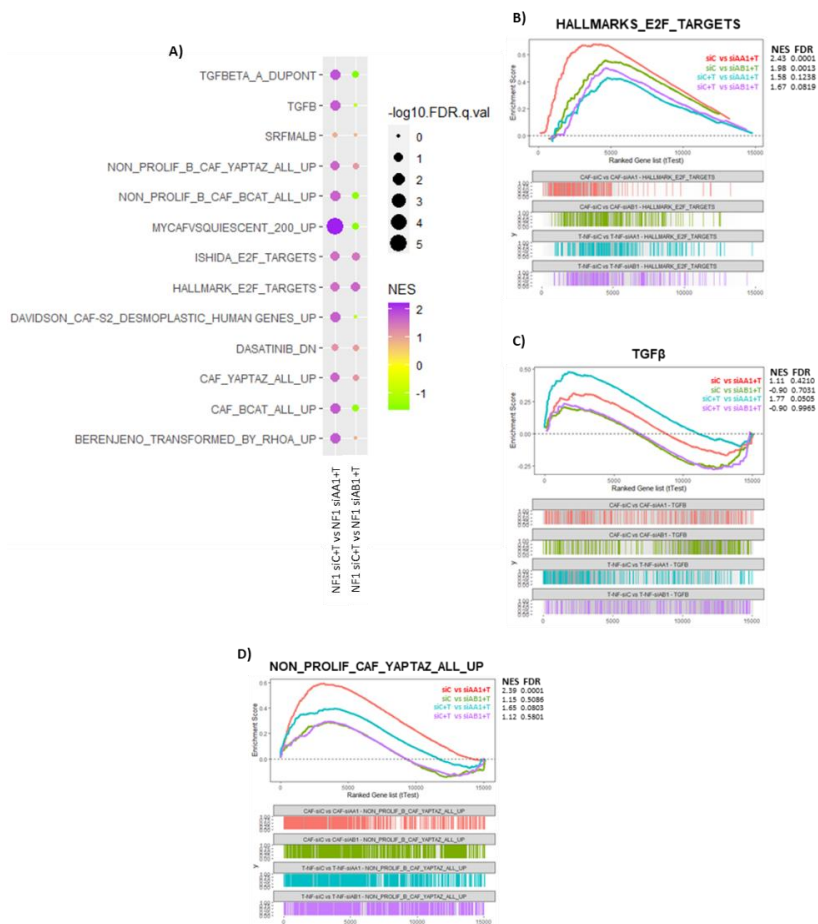


**Figure IV-6. GSEA analysis of transcriptional programs affected by *Hsp90aa1* and *Hsp90ab1* silencing in TGFβ-stimulated NFs.** **A.** Bubble plot summarizing GSEA results of “Curated datasets” when comparing control vs *Hsp90aa1*-silenced or *Hsp90ab1*-silenced TGFβ-stimulated NFs. The size of the bubbles represents the level of significance of the signature (-log<sub>10</sub> FDR), and their color represents the level of enrichment of the signature (purple: high NES; yellow: low NES). A positive NES represents signatures enriched in the stimulated control, whereas a negative NES represents signatures enriched in the corresponding transfected condition. **B-E.** GSEA plots show the level of activity of the indicated signatures in *Hsp90aa1*-silenced CAF1 compared with CAF1 control (red line), *Hsp90ab1*-silenced CAF1 compared with the CAF1 control (green line), *Hsp90aa1*-silenced TGFβ-stimulated NF1 compared with the TGFβ-stimulated control (blue line) and *Hsp90ab1*-silenced TGFβ-stimulated NF1 compared with the TGFβ-stimulated control (purple line). NES and FDR coefficients are also indicated. Where indicated, 5 ng/mL of TGFβ was added for 24h. *siC*: siRNA control. *siAA*: si*Hsp90aa1*. *siAB*: si*Hsp90ab1*. *+T*: +TGFβ. NES: Normalized Enrichment Score. FDR: False Discovery Rate.

#### 4.7. Proteomic analysis of *Hsp90aa1/ab1*-depleted CAFs and TGF $\beta$ -stimulated NFs

The transcriptomic analysis of *Hsp90aa1/ab1*-depleted CAFs and NFs stimulated with TGF $\beta$  demonstrated that the specific silencing of *Hsp90aa1* induces significant alterations in both systems at gene expression levels, modulating the activity of particular signaling cascades. Given the relevance of HSP90 in controlling the correct processing of proteins, we next investigated whether the observed changes in the transcriptional programs were the consequence of alterations of particular factors at protein level. For that, we next performed proteomic analysis in both CAF and TGF $\beta$ -stimulated NF systems after modulation of HSP90 $\alpha$  and HSP90 $\beta$ .

Contrary to the gene expression analysis, the analysis of the differentially expressed proteins (DEPs) for each transfected condition revealed no relevant differences in the number of dysregulated proteins in the *Hsp90aa1*-silenced conditions in comparison to the *Hsp90ab1*-silenced ones, for both CAFs and TGF $\beta$ -stimulated NFs (**Figure IV-7, A-B**). Still, there were relevant differences in the proteins affected by *Hsp90aa1* silencing compared to *hsp90ab1* depletion. Thus, the analysis of all DEPs derived from all the different conditions showed that *Hsp90aa1*-silencing in both CAFs and TGF $\beta$ -stimulated NFs induce a similar expression pattern. In fact, several proteins were commonly downregulated in both *Hsp90aa1*-silenced conditions, including Yap1 and its target proteins Diaph3 and Anln (**Figure IV-7, C**). Importantly, Diaph3 and Anln have

been previously described as cytoskeletal regulators with a notable influence over CAF functions<sup>105</sup>.

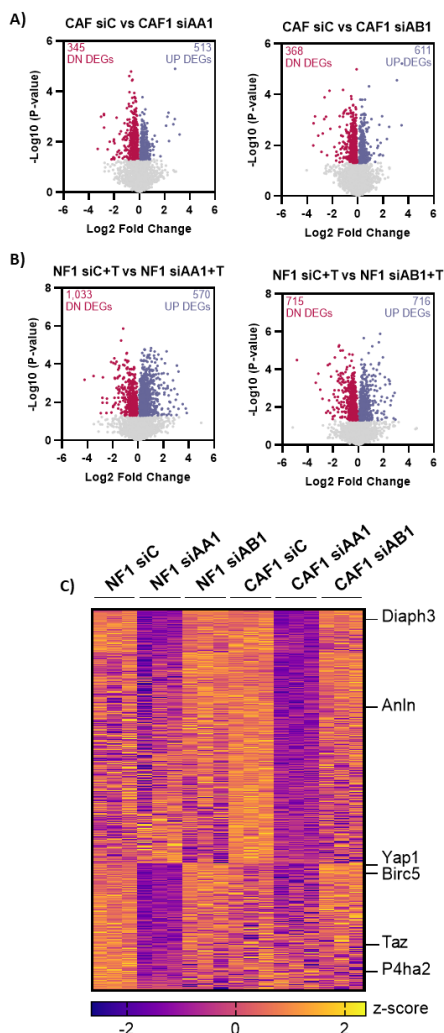


**Figure IV-7. Proteomic analysis of *Hsp90aa1*-silenced CAFs and TGF $\beta$ -stimulated NFs.** A-B. Graphs showing the upregulated (blue dots) and downregulated (red dots) DEPs as determined by their  $-\text{Log}_{10}$  P-value and the  $\text{Log}_2$  fold change, for the *Hsp90aa1/ab1*-silenced CAFs (A) and *Hsp90aa1/ab1*-silenced TGF $\beta$ -stimulated NFs (B), in comparison with the siRNA control transfected condition (siC). Each dot represents an individual protein identified in the analysis. (n=3 from 3 independent experiments). C. Heatmap showing the z-score values of the expression of relevant DEPs found in the different transfected conditions. Where indicated, 5 ng/mL of TGF $\beta$  was added for 24h. siC: siRNA control. siAA: si*Hsp90aa1*. siAB: si*Hsp90ab1*. +T: +TGF $\beta$ .

Similar to the strategy followed for the transcriptomic analysis, we performed a GSEA to study the molecular and biological consequences of the protein expression dysregulation promoted by *Hsp90aa1*-silencing in CAFs and TGF $\beta$ -stimulated NFs. Among the different signatures found to significantly downregulated in *Hsp90aa1*-silenced conditions, we found the YAP/TAZ signature without cell cycle regulators (“NON\_PROLIF\_B\_CAF\_YAPTAZ\_ALL\_UP”), the Src activation signature (“DASATINIB DN”) and the signature related to RhoA signaling (“BERENJENO\_TRANSFORMED\_BY\_RHOA\_UP”). These results indicate that at protein level, the dysregulation of YAP/TAZ and processes associated with Src and RhoA signaling as a result of HSP90 $\alpha$  modulation are also evident. Interestingly, at the level of protein expression we found that the TGF $\beta$  signature was diminished in both *Hsp90aa1* and *Hsp90ab1* conditions in TGF $\beta$ -stimulated NFs, but not CAFs (Figure IV-8, B).

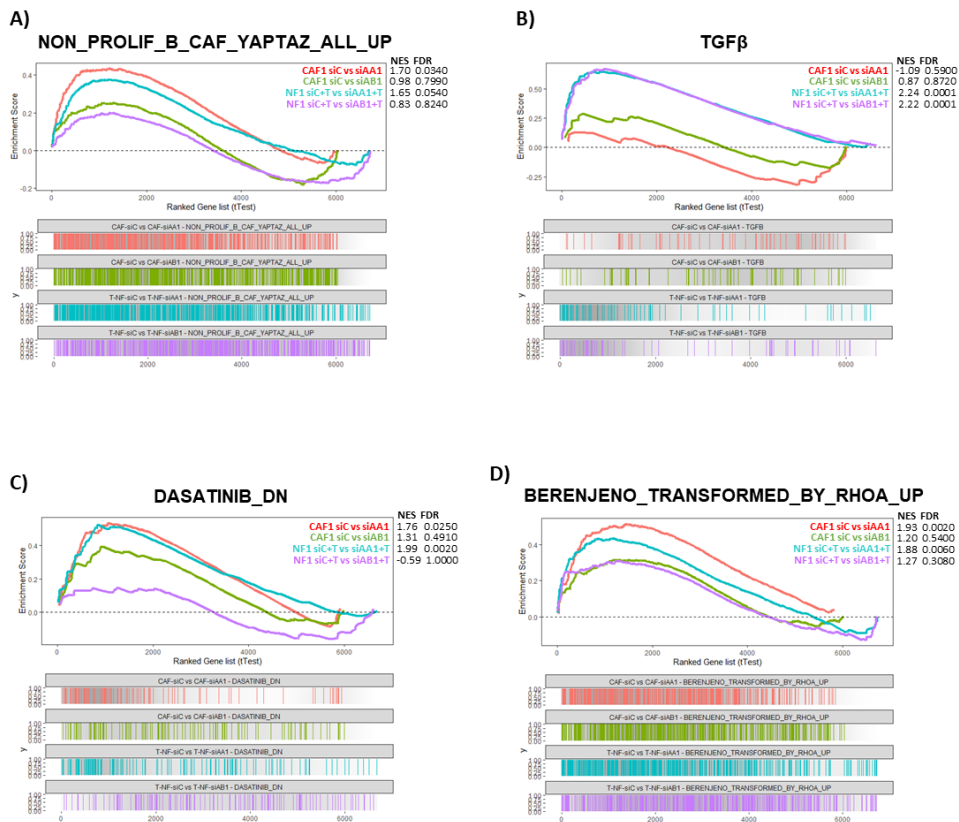


**Figure IV-8. GSEA of proteomic data from *Hsp90aa1/ab1*-silenced CAFs and TGFβ-stimulated NFs. A-D.** GSEA plots showing the activity of the indicated signatures in *Hsp90aa1*-silenced CAFs compared with the transfected control (red line), *Hsp90ab1*-silenced CAFs compared with the transfected control (green line), *Hsp90aa1*-silenced TGFβ-stimulated NFs compared with its control (blue line), and *Hsp90ab1*-silenced TGFβ-stimulated NFs compared with its control (purple line). NES and FDR coefficients are also indicated. Where indicated, 5 ng/mL of TGFβ was added for 24h. siC: siRNA control. siAA1: si*Hsp90aa1*. siAB1: si*Hsp90ab1*. +T: +TGFβ. NES: Normalized Enrichment Score. FDR: False Discovery Rate.

#### 4.8. Integrated analysis of transcriptomic and proteomic datasets for the understanding of the HSP90 $\alpha$ -YAP regulatory mechanisms in CAFs and TGF $\beta$ -stimulated NFs

The transcriptomic and proteomic analyses of HSP90 $\alpha/\beta$ -depleted CAFs and TGF $\beta$ -stimulated NFs pointed out to a specific regulatory mechanism of YAP/TAZ through the HSP90 $\alpha$  isoform. As TAZ has very limited functional relevance in CAFs<sup>105</sup>, our results suggested that YAP may be the main effector of HSP90 $\alpha$  in controlling the pro-tumor behavior of CAFs. Given the critical role of HSP90 in regulating the correct processing of client proteins, we speculated that HSP90 $\alpha$  may be controlling YAP activity by three different means: (1) HSP90 $\alpha$  regulates YAP activity through direct interaction, controlling its stability and correct processing; (2) HSP90 $\alpha$  controls the expression of YAP regulators, thus exerting an indirect influence over YAP activity; (3) both mechanisms are in place. Nevertheless, the mechanism regulating YAP function via HSP90 $\alpha$  in CAFs may operate over TAZ in a similar fashion, given the high regulatory similarities between both effectors.

To identify possible new regulators of YAP activity in CAFs that dependent on HSP90 $\alpha$  expression, we carried out a comprehensive analysis integrating the transcriptomic and proteomic data from the transfected CAFs and TGF $\beta$ -stimulated NFs (**Figure IV-9, A**). Using the BioGRID database<sup>193</sup>, we first generated a list containing all known HSP90 $\alpha$  interactors and a second list containing all YAP related proteins, including potential interactors as suggested by BioGRID. Next, we selected those proteins that belonged to both categories

and investigated their expression values in the proteomics dataset. Importantly, among the shortlisted candidates appeared YAP1 itself, as it has been reported to interact with HSP90 $\alpha$  in a high-throughput affinity capture–mass spectrometry approach<sup>214</sup>. On the other hand, TAZ was not included as there are no reports of potential HSP90 interaction. Using the different experimental points investigated extensively before, we analyzed the correlation between the protein expression levels of those candidates and YAP activity, as measured by the ssGSEA value of the signature “NON\_PROLIF\_B\_CAF\_YAPTAZ\_ALL\_UP” obtained from the transcriptomic dataset. In principle, this analysis will identify (i) YAP regulators that potentially interact with HSP90 $\alpha$ ; (ii) that are modulated at protein expression level in our system by HSP90 $\alpha$ ; and (iii) that their protein expression level is associated with YAP/TAZ activity.

The analysis showed a list of proteins with different levels of correlation with YAP/TAZ activity (**Figure IV–9, B**). Importantly, we observed that Yap1 was amongst the factors with most positive correlation but was not the highest, suggesting that possibly other factors may also be involved. Our analysis also identified a fraction of known YAP targets (*marked with asterisk in Figure IV–9, B*) that present different levels of correlation. Among these, Map2k3 and Rbbp7 showed a marked level of positive correlation and Prkca was negatively correlated. We decided to focus on the top proteins having the strongest correlation between expression levels and YAP/TAZ activity. Interestingly, we found a high correlation of factors such as Yes1 or Src, which are well-known activators of YAP commonly found in cancer and in the TME<sup>215,216</sup>. Thus, both Yes1 and

Src are kinases that promote the phosphorylation of key tyrosine residues in YAP necessary for the transcriptional activity<sup>217</sup>. On the other hand, the protein found to be least correlated with the YAP activity signature was Ctnnb1/ $\beta$ -catenin, which has also been described to have a prominent role in CAF functions<sup>79</sup>. Thus, our results suggested that Yap1, Yes1 and Src are potential HSP90 $\alpha$  clients whose expression levels are downregulated after *Hsp90aa1* depletion and that correlate with YAP/TAZ activities in our systems. When the factors with stronger correlation were analyzed together, we observed an interaction network dominated by Hsp90aa1, forming critical interactions with Yap1 and upstream regulators Yes1 and Src (Figure IV-9, C).

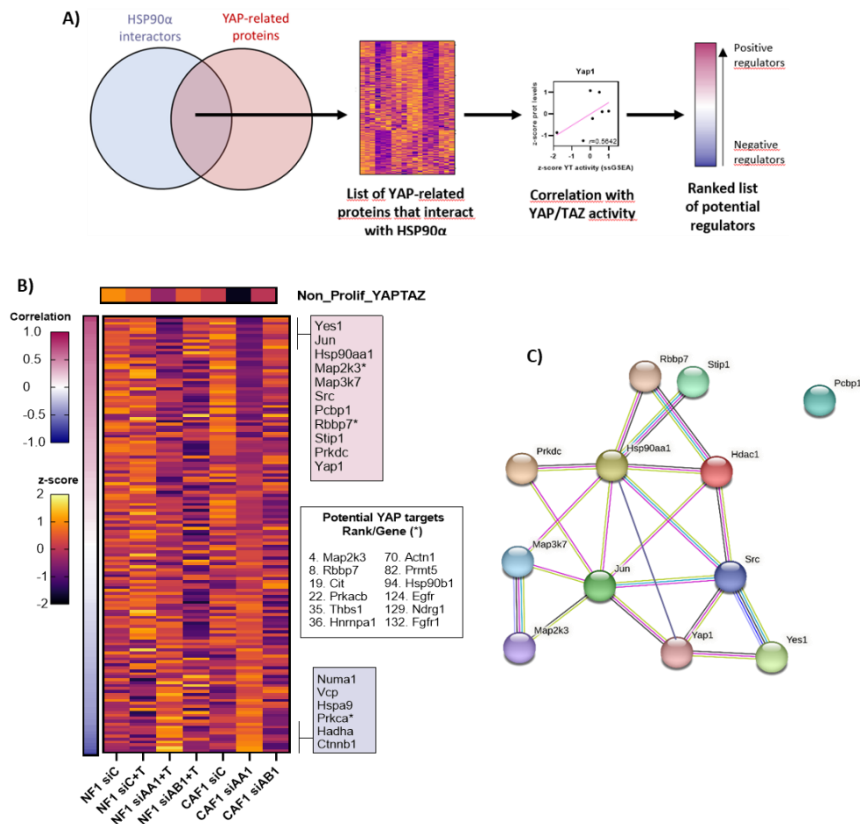


**Figure IV-9. Integrative analysis of transcriptomic and proteomic data derived from *Hsp90aa1/ab1*-silenced CAFs and TGF $\beta$ -stimulated NFs.** **A.** Schematic representation of the workflow followed for the integration of the transcriptomic and proteomic datasets. **B.** Heatmap showing z-score normalized protein expression of candidate genes (bottom), ranked based on their correlation values (red to green bar on left) with the “NON\_PROLIF\_B\_CAF\_YAPTAZ\_ALL\_UP” signature (Non\_Prolif\_YAPTAZ, ssGSEA values, z-score normalized, top heatmap). The top positive correlated factors are indicated in a green panel, whereas the top negative correlated factors are presented in a red panel. Some of the known YAP targets have been noted in the white right panel with their corresponding position in the rank; proteins from this group in the other lists (high/low correlation) are marked with (\*). The normalized z-score enrichment value for each protein/ssGSEA is also represented in a yellow-purple scale. siC: siRNA control. **C.** Diagram showing the interaction grid containing the top positive correlated proteins from the ranked list. Where indicated, 5 ng/mL of TGF $\beta$  was added for 24h (+T).

Even though TAZ was not within our shortlisted candidates (as it was not amongst the HSP90 $\alpha$  potential interactors from BioGrid), we decided to explore its protein expression values and correlation with YAP/TAZ activities. We hypothesized that given its high homology with YAP, TAZ may be similarly affected by HSP90 $\alpha$  and that this regulation may contribute to YAP/TAZ gene expression programs. First, we observed that TAZ protein levels were downregulated after *Hsp90aa1* silencing in TGF $\beta$ -stimulated NFs and in CAFs (**Figure IV-10, A**). Secondly, we observed that TAZ protein levels had a marginal level of correlation with YAP/TAZ activation, as inferred by the expression of YAP/TAZ signatures in our systems (**Figure IV-10, B**). On the other hand, TAZ protein levels and their modulation by HSP90 $\alpha/\beta$  perturbation had a significant level of correlation with TAZ activity, measured by the expression of TAZ-specific genesets, including those not affected by YAP (“ZHANG\_TAZ\_GENES\_NOT\_YAP”, **Figure IV-10, B**). Noteworthy, TAZ is also subjected to positive upstream regulation by Yes1 and Src<sup>216,218</sup>.

These results suggest that TAZ may be regulated by HSP90 in a similar fashion to YAP. Altogether, this integrated analysis suggests that HSP90 $\alpha$  might be directly regulating YAP/TAZ protein levels through its chaperone function. In addition, HSP90 $\alpha$  might be further potentiating YAP/TAZ activity by controlling the protein levels of Src and Yes1 and influencing its tyrosine phosphorylation required for its transcriptional regulation function. Noteworthy, our analyses did not identify any relevant association between HSP90 $\alpha$  and canonical Hippo regulators, such as LATS1/2 or MST1/2, among others (*not shown*).

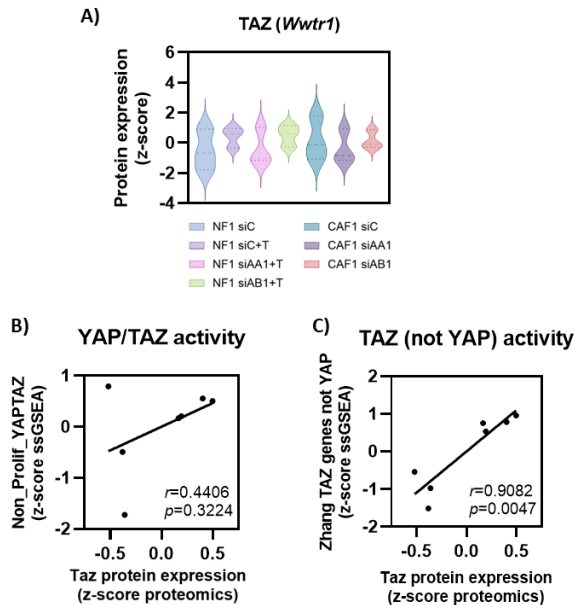


**Figure IV-10. TAZ expression in transfected CAFs and TGF $\beta$ -stimulated NFs, and correlation with YAP/TAZ activity.** **A.** Graph showing z-score of protein expression of TAZ in *Hsp90aa1* and *Hsp90ab1* silenced CAFs and TGF $\beta$ -stimulated NFs (n=3, from 3 independent experiments). **B-C.** Graphs showing correlation between the “Non\_Prolif\_YAPTAZ” signature (B) and “Zhang TAZ genes not YAP” signature (C) with TAZ protein expression. Both signatures “Non\_Prolif\_YAPTAZ” and “Zhang TAZ genes not YAP” were assessed by ssGSEA, and TAZ expression was obtained by proteomic analysis. Each point in the graph represents the average z-score of RNAseq data (triplicates) and proteomics data (triplicates) of experimental points as in (A). Where indicated, 5 ng/mL TGF $\beta$  was added for 24 h. *siC*: siRNA control. *siAA1*: *siHsp90aa1*. *siAB1*: *siHsp90ab1*. +T: +TGF $\beta$ .

# Results

5. HSP90 $\alpha$  regulates CAF  
pro-tumoral functions  
through YAP signaling



## 5.1. HSP90 effects over cell cycle and proliferation

The RNAseq analysis of silenced CAFs and TGF $\beta$ -stimulated NFs revealed an enrichment in genes related to cell cycle and cell proliferation signatures when HSP90 $\alpha/\beta$  was silenced. To further explore the possible consequences of HSP90 $\alpha/\beta$  over fibroblast proliferation in our *in vitro* murine systems, cell cycle progression after siRNA transfection was studied by flow cytometry analysis.

In the case of the transfected CAFs, there was an increase in the percentage of cells in G0-G1 stages after *Hsp90aa1/ab1*-silencing in comparison with the control transfected condition, but this difference was not significant (**Figure V-1, A**). No differences were observed either in the percentage of cells in the S phase after depletion of any of the HPS90 isoforms. However, there was a decrease in the percentage of *Hsp90aa1*-silenced CAFs in the G2 stage in comparison with the remaining conditions (**Figure V-1, A**), but this difference was again not significant. These results indicate that the depletion of either of the HSP90 isoforms does not affect the normal cell cycle progression of CAFs. More importantly, silencing of both isoforms resulted in similar trends, and therefore potential defects in cell cycle progression could not account for the reported functional differences between HSP90 $\alpha$  and HSP90 $\beta$  in CAFs.

In the case of the TGF $\beta$ -stimulated NFs, the silencing of *Hsp90aa1* induced an increase in the percentage of cells in G0-G1 stages, and a reduction of those in the S and G2 phase, although none of these differences were statistically significant (**Figure V-1, B**). Thus,

the depletion of HSP90 $\alpha/\beta$  in TGF $\beta$ -stimulated NFs does not appear to have any significant consequences for the normal progression of the cell cycle either

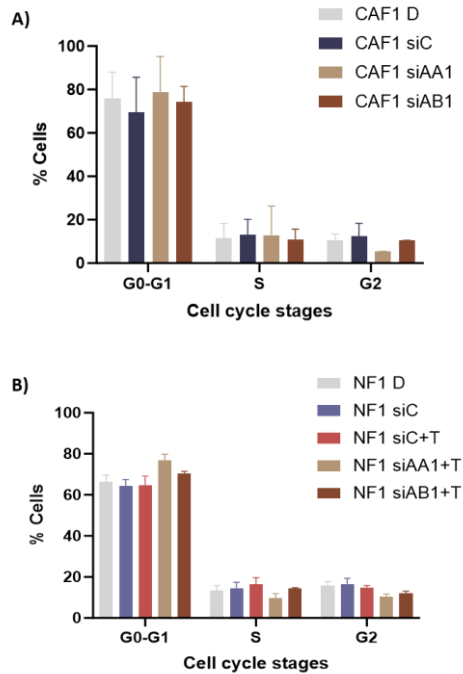


**Figure V-1. Cell cycle studies of *Hsp90aa1/ab1* silenced CAFs and TGF $\beta$ -stimulated NFs. A-B.** Graphs showing the percentage of cells included in each cell cycle stage for CAFs (A) and TGF $\beta$ -stimulated NFs (B) after transfection with control, *Hsp90aa1* or *Hsp90ab1* siRNAs (n=2, from 2 independent experiments). Where indicated, 5 ng/mL of TGF $\beta$  was added for 24h. *D*: DharmaFECT™ treated, not-transfected control condition. *siC*: siRNA control. *siAA1*: si*Hsp90aa1*. *siAB1*: si*Hsp90ab1*. *+T*: +TGF $\beta$ .

## 5.2. Modulation of Yap1 expression by HSP90 $\alpha$ in CAFs and TGF $\beta$ -stimulated NFs

The RNAseq analysis from CAFs and TGF $\beta$ -stimulated NFs showed a downregulation of signatures related to YAP/TAZ signaling after *Hsp90aa1*-silencing in both systems, indicating a potential role of HSP90 $\alpha$  in modulating YAP/TAZ functions. In addition, comprehensive analyses of proteomics and transcriptomics

datasets suggested that HSP90 $\alpha$  might be modulating YAP/TAZ by controlling their protein levels and the levels of upstream positive regulators Src and Yes1. Next, we proceeded to validate these possibilities employing orthogonal approaches.

To investigate if YAP/TAZ inhibition after *Hsp90aa1* silencing was a result of altered protein levels or the stability of these proteins, we first investigated the gene expression of these factors after *Hsp90aa1/ab1* silencing in CAFs. RT-qPCR analyses indicated that the gene expression levels of *Yap1* do not vary as a consequence of *Hsp90aa1/ab1* silencing (**Figure V-2, A**). No significant changes were found either in the gene expression levels of *Wwtr1* (encoding TAZ) after *Hsp90aa1/ab1* silencing (**Figure V-2, B**). Next, WB experiments were performed for YAP and TAZ in transfected CAFs and TGF $\beta$ -stimulated NFs. In both cases, the WB experiments showed a decrease in the protein levels of YAP and TAZ after depletion of HSP90 $\alpha$  (**Figure V-2, C-D**).

Similar results were obtained in the case of the *in vivo*-derived fibroblasts, in which the absence of Hsp90aa1 also affected negatively the protein expression of YAP and TAZ (**Figure V-2, E**). In addition, the expression of YAP and TAZ was maintained after *Hsp90ab1* silencing (**Figure V-2, C-D**), suggesting that their protein expression dysregulation is exclusive to the HSP90 $\alpha$  isoform. Even though the proteomic analysis suggested an upregulation of  $\beta$ -catenin, another important driver of the CAF pro-tumoral functions that shares certain regulatory mechanisms with YAP/TAZ, the depletion of *Hsp90aa1/ab1* did not affect its protein expression by WB

(Figure V-2, C-D). Taken together, these results show that HSP90 $\alpha$  regulates YAP and TAZ at the protein level in fibroblasts

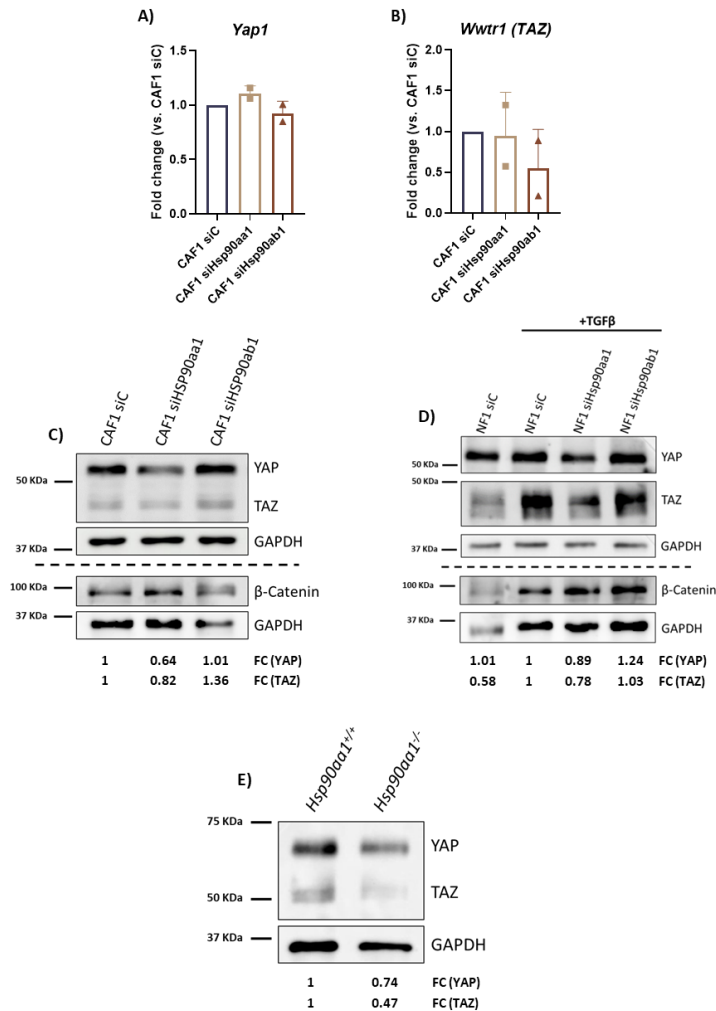


**Figure V-2. YAP/TAZ modulation through HSP90 $\alpha$  expression.** A-B. Graphs showing fold change gene expression of *Yap1* (A) and *Wwtr1* (TAZ, B) in *Hsp90aa1/ab1*-depleted CAF1 cells by qPCR (n=2). Each qPCR experiment was performed in triplicates. C-D. Images show a representative WB experiment for the expression of  $\beta$ -catenin, YAP, TAZ and GAPDH in transfected CAF1 (C) and TGF $\beta$ -stimulated NF1 cells (D). E. Images show a representative WB experiment for the expression of YAP, TAZ and GAPDH in *Hsp90aa1<sup>+/+</sup>* and *Hsp90aa1<sup>-/-</sup>* in vivo-derived mammary gland fibroblasts. Where indicated, 5 ng/mL of TGF $\beta$  was added for 24h. Below each image, the fold change (FC) expression vs. control condition (CAF1 siC, NF1 siC +TGF $\beta$  and *Hsp90aa1<sup>+/+</sup>*, respectively) is indicated for YAP and TAZ expression. All WB show indications for the molecular weight markers. Dashed lines separate independent WB experiments, each with their corresponding loading control. siC: siCtrl.

### 5.3. HSP90 $\alpha$ controls Yap1 protein stability

Given the chaperone nature of HSP90, the decrease in the protein levels of YAP/TAZ after *Hsp90aa1* silencing observed by WB could be the consequence of HSP90 $\alpha$  modulating YAP/TAZ protein stability. Thus, the depletion of HSP90 $\alpha$  could result in a more unstable form of YAP/TAZ, affecting their basal protein levels. To study this possibility, protein stability experiments were performed in which the *Hsp90aa1/ab1* silenced fibroblasts were treated with cycloheximide (CHX), a natural compound that functions as an inhibitor of the synthesis of new proteins. Then, the protein stability is studied by performing WB with samples collected at different time points after treatment with CHX. If protein stability is compromised, protein levels should be reduced after CHX treatment.

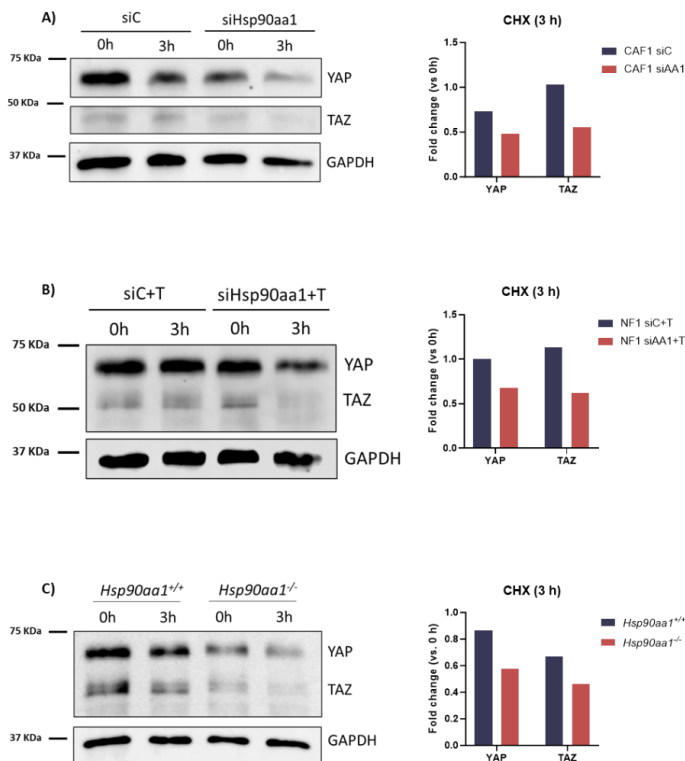


**Figure V-3. YAP/TAZ protein stability depends on HSP90 $\alpha$  expression. A-C.** Images show a representative WB experiment for the expression of YAP, TAZ and GAPDH before and after 3 h CHX treatment (10  $\mu$ g/mL) in transfected control (siC) and *Hsp90aa1*-silenced CAF1 (A) and TGF $\beta$ -stimulated NF1 cells (B), as well as in *Hsp90aa1*<sup>+/+</sup> and *Hsp90aa1*<sup>-/-</sup> *in vivo*-derived mammary gland fibroblasts (C). Graphs on the right show the fold change of normalized expression of the indicated proteins (against GAPDH expression) between 0 and 3 h of CHX treatment. All WB show indications for the molecular weight markers. Where indicated, 5 ng/mL of TGF $\beta$  was added for 24h. *siC*: siRNA control. *+T*: +TGF $\beta$ .

In the case of the *Hsp90aa1* silenced CAFs, there was a notable decrease in YAP and TAZ protein expression after 3h of CHX treatment in comparison with the control condition (**Figure V-3, A**). The silencing of *Hsp90aa1* also resulted in less YAP and TAZ expression after 3h of CHX treatment in the case of the TGF $\beta$ -stimulated NFs (**Figure V-3, B**). In addition, a similar reduction of the YAP and TAZ protein levels was observed when the CHX treatment was applied to our *Hsp90aa1*<sup>-/-</sup> murine breast NFs in comparison with the CHX-treated *Hsp90aa1*<sup>+/+</sup> control fibroblasts (**Figure V-3, C**). Altogether, these results indicate that YAP stability is dependent on HSP90 $\alpha$  expression.

#### 5.4. YAP as a “client” protein of HSP90 $\alpha$

The protein stability experiments demonstrated that YAP/TAZ protein stability is dependent on HSP90 $\alpha$  expression. However, they do not demonstrate that this observation is the consequence of the direct interaction of HSP90 $\alpha$  and YAP/TAZ, which is necessary for HSP90 $\alpha$  to function as a chaperone for YAP/TAZ.

To further elucidate if YAP directly interacts with HSP90 $\alpha$ , and thus could be one of its “client” proteins, we performed co-immunoprecipitation (co-IP) experiments of both proteins. For that, we used genetically engineered CAF and NF cell lines where a particular sequence was added in frame right after the *Yap1* gene. This sequence consisted of: (i) a V5 epitope tag sequence, which will be used for the endogenous immunoprecipitation of its protein product; and (ii) a degradation tag (dTAG) sequence, which allows for the precise degradation of the whole protein (YAP-V5-dTAG) after a specific chemical treatment (**Figure V-4, A**). Thanks to the V5 epitope, endogenous YAP can be precipitated using beads with the corresponding V5 antibody attached to it. Next, a WB experiment is performed to detect if our protein of interest is present in the precipitation as a readout of the interaction between that protein and YAP. However, if the fibroblasts are incubated with the corresponding dTAG molecule, which recognizes its specific site in the chimeric protein, YAP-V5-dTAG is ubiquitinated for proteasomal degradation and is no longer expressed. Thus, incubation with the V5 conjugated beads will not attach to anything, and the WB experiment will result empty. This condition was used as a negative control for the co-IP.

Noteworthy, our genetically engineered NFs and CAFs were only edited in one allele, resulting in the expression of both wild-type YAP and the engineered YAP-V5-dTAG at similar levels (**Figure V-4, E**). Upon dTAG treatment, only the YAP-V5-dTAG product disappears without compensating events in the wild-type allele. Although this results in less product available for V5-based immunoprecipitation,

it also enables the cell to maintain certain levels of YAP activity after dTAG molecule treatment. Otherwise, the treatment will be extremely toxic: complete removal of YAP may affect cell viability.

In both CAFs and NFs, the dTAG condition showed no V5 expression by WB, not in the total amount of protein nor in the IP, indicating that the dTAG condition successfully works in impeding YAP expression in these cells (**Figure V-4, B-C**). The YAP regulators LATS1 and 14-3-3 were used as positive controls for the co-IP, and thus both were detected in the control and TGF $\beta$ -treated condition in both NF1 and CAF1 cells, but not in the dTAG condition. Importantly, we could detect HSP90 interacting with YAP in both cell types, and the interaction was increased by TGF $\beta$  treatment. Importantly, since the HSP90 antibody is not able to discriminate between the HSP90 $\alpha$  and HSP90 $\beta$  isoforms, this experiment cannot determine if any of the isoform individually, or both of them at the same time, are interacting with YAP. However, since silencing *Hsp90ab1* did not affect YAP/TAZ expression or stability, it is unlikely that they are HSP90 $\beta$  clients.

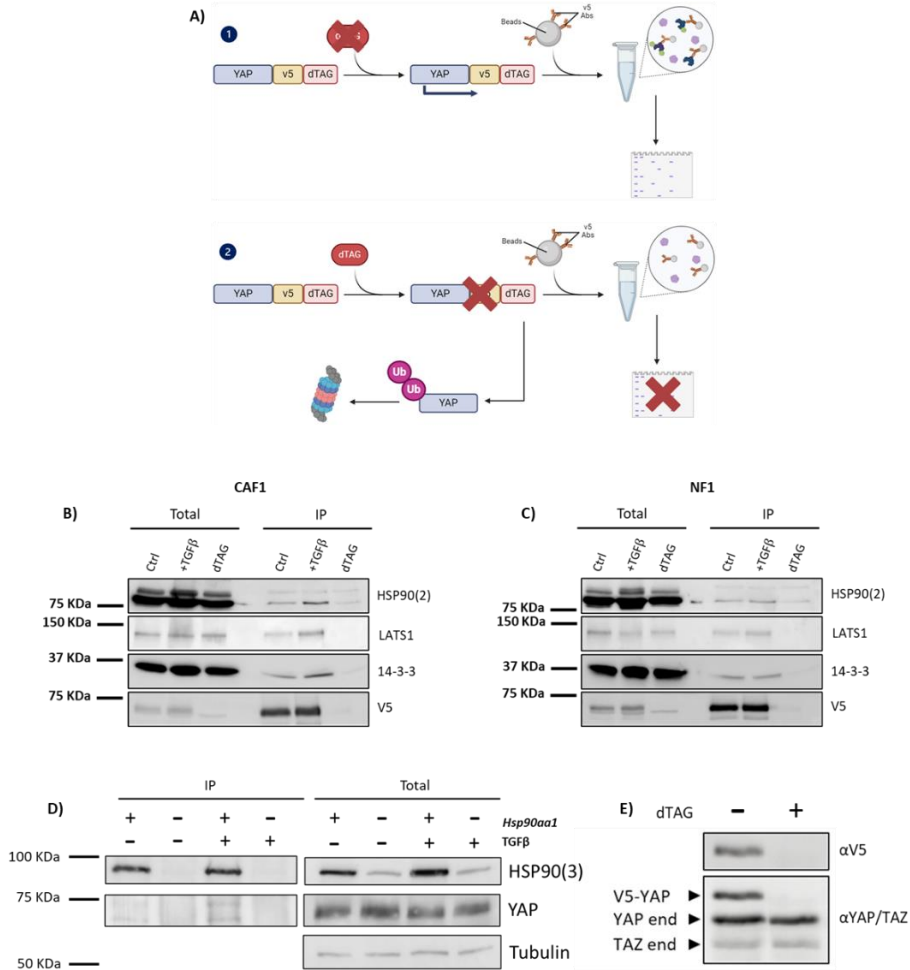


**Figure V-4. HSP90 interacts directly with YAP in CAFs and NFs.** **A.** Schematic representation of the immunoprecipitation strategy followed to determine whether HSP90 can interact directly with YAP. In the first case (1, upper panel), if the fibroblasts are not incubated with the dTAG enzyme, YAP can be immunoprecipitated by incubating with V5-conjugated beads. In the second (2, lower panel), if the fibroblasts are incubated with the dTAG enzyme, YAP is targeted for proteasomal degradation, and it cannot be detected by WB. *Abs*: antibodies. *Ub*: ubiquitin. Created on Biorender.com. **B-C.** Images of representative WB experiments for the expression of HSP90, LATS1, 14-3-3 and V5 in total lysates (total) and after V5 (YAP-V5-dTAG) immunoprecipitation (IP) in NF1-YAP-V5-dTAG (B) and CAF1-V5-dTAG (C) cells. **D.** Images of representative WB experiments for the expression of HSP90, YAP and Tubulin in total lysates (total) and after HSP90 immunoprecipitation (IP) in *Hsp90aa1*<sup>+/+</sup> and *Hsp90aa1*<sup>-/-</sup> *in vivo*-derived murine breast fibroblasts. Tubulin was used as loading control. **E.** Image of representative WB for the expression of V5-YAP and endogenous YAP and TAZ in CAF1-V5-dTAG cells, with and without dTAG treatment. Where indicated, 5 ng/mL of TGF $\beta$  or 300 nM dTAG were added for 24 h. All WB show indications for the molecular weight markers.

To further elucidate the possible specificity of the YAP interaction with the HSP90 $\alpha$  isoform, we performed co-IP experiments with the *Hsp90aa1<sup>+/+</sup>* and *Hsp90aa1<sup>-/-</sup>* *in vivo*-derived murine breast fibroblasts. In the case of the *Hsp90aa1<sup>+/+</sup>* fibroblasts, we were able to detect YAP after immunoprecipitation of HSP90 (Figure V-4, D). However, we were not able to immunoprecipitate HSP90 in the *Hsp90aa1<sup>-/-</sup>* fibroblasts, and in this case, YAP was not detected (Figure V-4, D). These observations further suggest a specific interaction of YAP with the HSP90 $\alpha$  isoform. The stimulation of both fibroblast cell lines with TGF $\beta$  did not appear to have significant effects over this interaction. However, these are preliminary results and further investigation is pending in order to confirm if this interaction is exclusive to the HSP90 $\alpha$  isoform and does not occur with HSP90 $\beta$ .

Altogether, these results demonstrate for the first time that HSP90, and more likely HSP90 $\alpha$ , interacts directly with YAP, and this interaction could be responsible for HSP90-dependent YAP regulator in fibroblasts. Thus, YAP could be a “client” protein of chaperone HSP90, and it could be exclusive to the HSP90 $\alpha$  isoform

## 5.5. Effects of HSP90 inhibitors over CAF functions and YAP expression

Given the important role of HSP90 in cancer cells, numerous HSP90i have been developed over the years to be potentially used in the clinic and have proved to be really effective in depleting HSP90. Thus, we decided to study if the use of HSP90i could be used

to target CAFs, and if they could have similar effects to those observed when silencing *Hsp90aa1/ab1* using siRNAs. For that, we chose to treat our CAF *in vitro* murine fibroblasts with two of the most traditionally used HSP90i: Geldanamycin and its derivative Tanespimycin. Both inhibitors have a similar mechanism of action, targeting the ATPase site in the N-terminal domain to impede the dimerization of HSP90 and impeding its chaperone function. This will end in dysfunctional HSP90 that will be targeted for proteasomal degradation. Importantly, given the great similarity in this specific site between the different HSP90 isoforms, both inhibitors are not able to discriminate between HSP90 $\alpha$  and HSP90 $\beta$ , so they target both isoforms simultaneously.

First, given the previously described results that indicate a direct interaction between HSP90 and YAP, suggesting that YAP could be a client protein of HSP90, we hypothesized that the treatment of CAFs with HSP90i would have similar effects on YAP expression to those observed when silencing *Hsp90aa1/ab1* expression by siRNA. Surprisingly, preliminary WB results after treating CAFs with two different concentrations of Geldanamycin and Tanespimycin showed no change in the protein expression of HSP90 (**Figure V-5, A**). However, and despite the low protein charge of the corresponding controls, there was a decrease in the protein expression of YAP after treatment with both HSP90i (**Figure V-5, B-C**). In addition, preliminary studies of YAP stability after the treatment with Geldanamycin and Tanespimycin show that it was not severely affected by any of these HSP90i (**Figure V-5, D-E**).

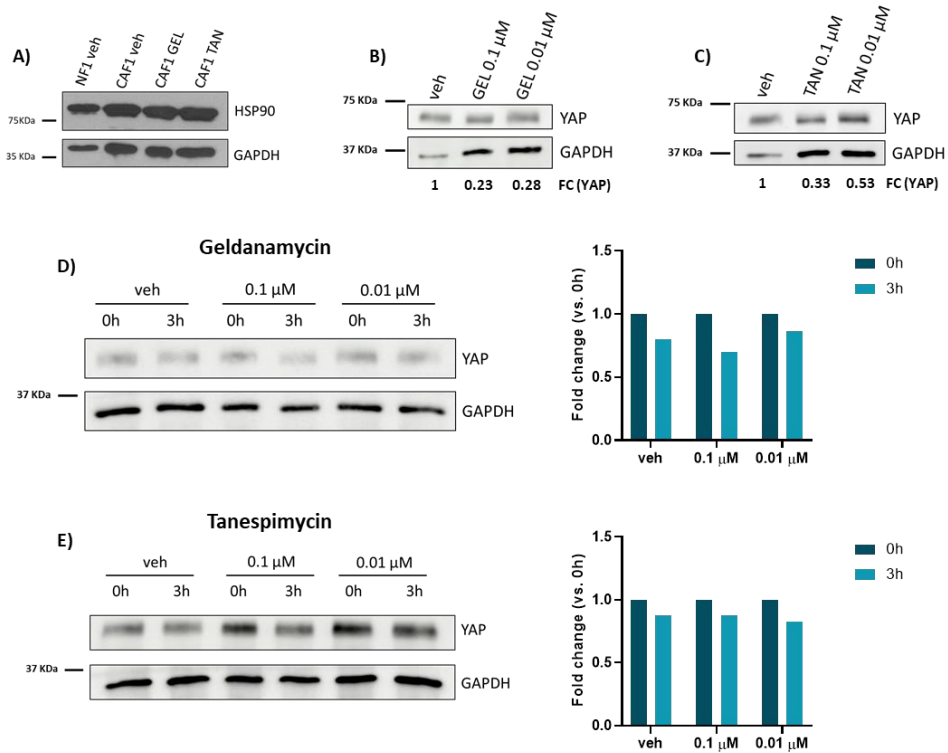


**Figure V-5. Effect of HSP90 inhibitors over YAP expression in CAFs.** **A.** Representative WB experiment of HSP90 expression in NF1 and CAF1 treated with vehicle, 0.01  $\mu$ M Geldanamycin or 0.01  $\mu$ M Tanespimycin, respectively. **B-C.** Representative WB experiments of YAP expression in CAFs treated with vehicle, 0.1 or 0.01  $\mu$ M of Geldanamycin (**B**) or Tanespimycin (**C**), respectively. **D-E.** Representative WB experiments of YAP expression in Geldanamycin (**D**) or Tanespimycin (**E**) treated CAF1 fibroblasts (left panel) and their corresponding 3 h CHX treatment expression levels quantification in comparison to 0 h (right panel). GAPDH was used as loading control. Molecular weight indicators are also shown. In all cases, cells were treated with the corresponding vehicle or inhibitor 24 h prior performing the experiment. *Veh*: vehicle. *GEL*: Geldanamycin. *TAN*: Tanespimycin.

The silencing of *Hsp90aa1* severely affected some important CAF functions *in vitro*, including their gel contraction capacity. To study if the treatment with HSP90i could have similar effects over CAF functions, we performed similar experiments with CAFs treated with Geldanamycin and Tanespimycin. Surprisingly, the treatment did not reduce the gel contraction abilities of these CAFs (**V-6, A**).

Thus, we increased 10 times the treatment concentration, but the gel contraction capacity of the CAFs remained invariable (V-6, B).

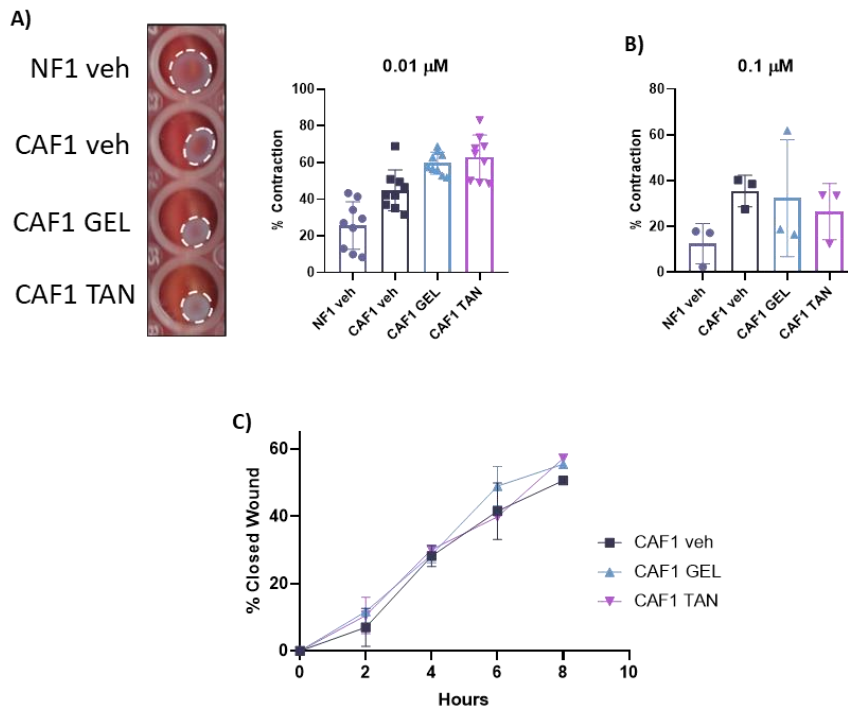


**Figure V-6. Functional effects of anti-HSP90 inhibitors in CAFs.** **A.** Image of a representative gel contraction experiment of NF1 and CAF1 fibroblasts treated with vehicle, 0.01  $\mu$ M Geldanamycin or 0.01  $\mu$ M Tanespimycin, respectively (left panel), and graph showing the percentage of gel contraction for each condition after 48 h (n=9, from 3 independent experiments). **B.** Graph showing the percentage of contraction of NF1 and CAF1 fibroblasts treated with vehicle, 0.1  $\mu$ M Geldanamycin or 0.1  $\mu$ M Tanespimycin, respectively, after 48 h (n=3, from 1 experiment). All gel contraction experiments were performed in technical triplicates. **C.** Graph showing the percentage of closed wound (n=2) of CAF1 treated with vehicle, 0.01  $\mu$ M Geldanamycin or 0.01  $\mu$ M Tanespimycin, respectively. In all cases, cells were treated with the corresponding vehicle or inhibitor 24 h prior performing the experiment. *Veh:* vehicle. *GEL:* Geldanamycin. *TAN:* tanespimycin.

Next, we decided to study if the treatment with HSP90i could have any effect over other CAF functions that were previously observed to be affected by *Hsp90aa1/ab1* silencing, such as wound healing. In this case, the treatment of CAFs with both Geldanamycin

and Tanespimycin did not have any significant effect either over this particular CAF function (**Figure V-6, C**). Although these preliminary results suggest that the treatment of CAFs with HSP90i does not have any functional effects, further experiments are needed in order to elucidate whether this is the consequence of a suboptimal approach or treatment.

Another possibility is that the treatment with HSP90i triggers different molecular programs to those from *Hsp90aa/ab1* silencing using siRNAs. Given that both Geldanamycin and Tanespimycin are known to target both HSP90 isoforms likewise, we studied the *in vitro* effects of transfecting CAFs with the siRNAs for both isoforms simultaneously. First, the effectiveness of this approach was tested by performing a qPCR for the expression of both *Hsp90aa1* and *Hsp90ab1*. The results showed that the transfection of CAFs with the combination of both siRNA smart pools effectively reduced the expression of both HSP90 isoforms (**Figure V-7, A**). This reduction in gene expression also translated in depleted HSP90 protein expression (**Figure V-7, B**). However, gel contraction experiments with the *Hsp90aa1/ab1* silenced CAFs showed that the simultaneous depletion of both HSP90 isoforms did not have any consequences for the ability of CAFs to contract the gels (**Figure V-7, C**). In fact, it did not reduce the protein levels of  $\alpha$ -SMA (**Figure V-7, B**). These results confirm the possibility that complete HSP90 depletion in CAFs triggers a compensatory mechanism that masks the potential consequences of HSP90 silencing. Thus, further molecular

characterization is needed in order to find the molecular mechanisms behind these observations.

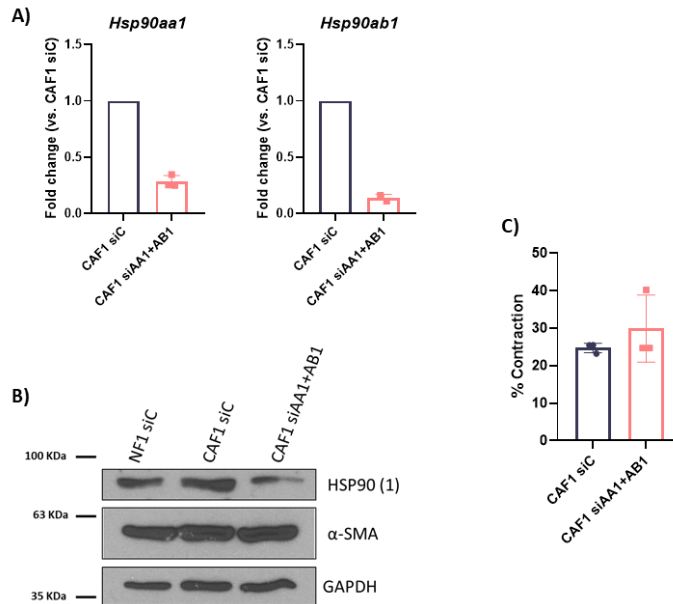


**Figure V-7. Silencing *Hsp90aa1* and *Hsp90ab1* simultaneously in CAFs.** **A.** Graphs showing fold change expression of *Hsp90aa1* (left) and *Hsp90ab1* (right) in CAF1 cells transfected with control siRNA or a mix of all available siRNAs for both HSP90 isoforms (n=3, from 1 experiment). **B.** Representative WB experiment for the expression of HSP90 and  $\alpha$ -SMA in NF1 and CAF1 cells transfected with control siRNA or a mix of all available siRNAs for both HSP90 isoforms. GAPDH was used as loading control. Molecular weight indicators are also shown. **C.** Graph showing percentage of gel contraction of CAF1 cells transfected with control siRNA or a mix of all available siRNAs for both HSP90 isoforms (n=3, from 1 experiment). siC: siCtrl. siAA1+AB1: all siRNAs mix for *Hsp90aa1* and *Hsp90ab1*.

## 5.6. Modulation of YAP/TAZ upstream regulators by HSP90 $\alpha$ / $\beta$

Results from the previous section also suggested that HSP90 $\alpha$  may be modulating the positive YAP/TAZ regulators SRC and YES1. These are kinases that regulate YAP/TAZ activity, and may interact with HSP90. They can phosphorylate and activate YAP and TAZ, inducing their translocation into the nucleus and interaction

with transcriptional factors such as TEAD1-4, leading to target gene expression<sup>215,216</sup>. To further study this possibility, we first performed WB experiments to check the protein expression levels of SRC and YES1 after *Hsp90aa1* or *Hsp90ab1* silencing. The WB results revealed that the depletion of HSP90 $\alpha$  did not affect the protein expression of SRC in CAFs, nor in TGF $\beta$ -stimulated NFs (Figure V-8, A-B). However, *Hsp90aa1* silencing decreased the expression of YES1 in both systems (Figure V-8, A-B). The silencing of *Hsp90ab1* did not have any consequences for the protein expression of either SRC or YES1 in CAFs or TGF $\beta$ -stimulated NFs, indicating that depletion of YES1 protein levels is an exclusive effect of *Hsp90aa1* silencing. Thus, these results suggest that HSP90 $\alpha$  could modulate YAP/TAZ expression through regulation of YES1.

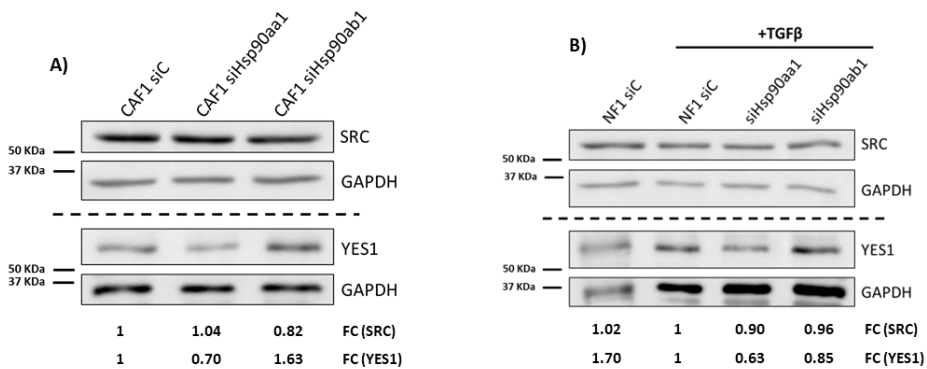


**Figure V-8. Modulation of SRC and YES1 protein levels by HSP90 $\alpha$ / $\beta$ .** A-B. Images show a representative WB experiment for the expression of Src and Yes1 protein levels after control (siC) or *Hsp90aa1/ab1* siRNA/mediated silencing in CAFs (A) and TGF $\beta$ -stimulated NFs (B). Below each image, the fold change (FC) expression vs. control condition (CAF1 siC and NF1 siC+T, respectively) is indicated for SRC and YES1 expression. Dashed lines separate two independent sets of WB experiments. Where indicated, 5 ng/mL of TGF $\beta$  was added for 24h. Gapdh was used as loading control for all WB experiments, and all WB show indications for the molecular weight markers. *siC*: *siCtrl*. *FC*: *Fold Change*.

## 5.7. HSP90 controls YAP expression and function in YAP-overexpressing NFs

Our results suggested that HSP90 $\alpha$  modulated YAP function by controlling its stability, and possibly also its activated status through Yes1-mediated phosphorylation. Thus, in systems where YAP activity is high (like for example CAFs compared to NFs)<sup>185</sup>, HSP90 activity is required to maintain its proper function. To further confirm this and to check whether constitutive activation of YAP is capable of bypassing HSP90 regulation, we employed genetically engineered NF cell lines that constitutively express an active form of YAP (NF1-YAP<sup>MUT</sup>). This mutant form consists of the modification of 5 key serine residues to alanine (YAP-S5A). Thus, this mutant cannot be phosphorylated by LATS kinases and the negative regulation exerted by the Hippo pathway is lost, rendering YAP more active. In NFs, constitute expression of this mutant leads to increased gel remodeling activities and represent an activated fibroblast model independent of TGF $\beta$  stimulation<sup>79</sup>.

Analysis of gel contraction ability of NF1-YAP<sup>MUT</sup> cells after silencing of *Hsp90aa1/ab1* indicated that this mutant still requires HSP90 $\alpha$  activity to stimulate this particular function (**Figure V-9, A**), confirming that HSP90 $\alpha$  mainly operates at the level of YAP or downstream, but not through Hippo signaling modulation.

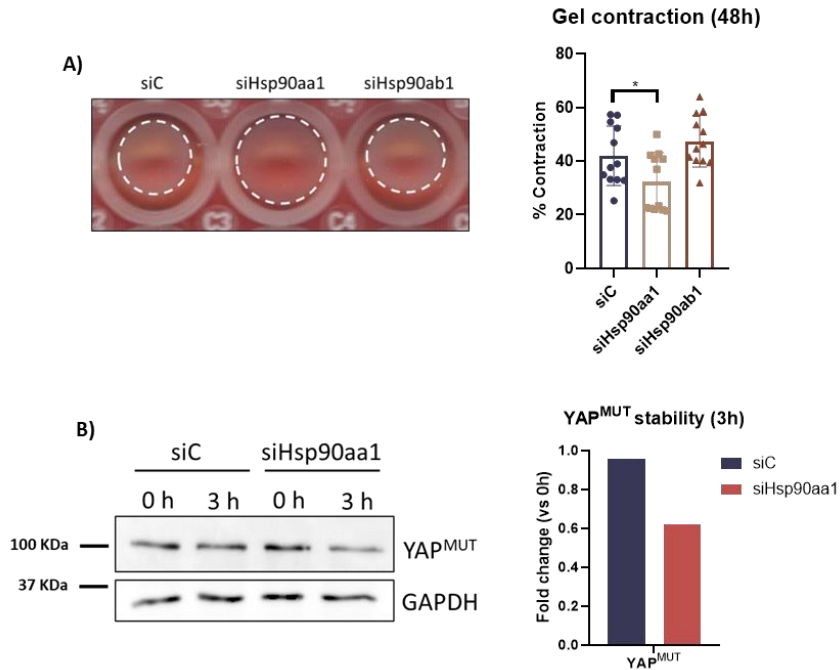


**Figure V-9. HSP90 $\alpha$  regulates YAP in activated NFs independently of TGF $\beta$ .** **A.** Images show representative images of gel contraction at 48 h of NF1-YAP<sup>MUT</sup> cells after transfection with control (siC), *Hsp90aa1* or *Hsp90ab1* siRNAs. Graph on the right shows quantification (n=9, from 3 independent experiments performed in technical triplicates). **B.** Images show a representative WB experiment for the expression of the constitutively active mutant form of YAP<sup>MUT</sup>-YFP (anti-YAP) and GAPDH before and after 3 h CHX treatment (10  $\mu$ g/mL) in transfected control (siC) and *Hsp90aa1*-silenced NF1-YAP<sup>MUT</sup> cells. Graph on the right shows quantification of normalized expression levels.

Furthermore, protein stability experiments with CHX revealed that there was a decrease in YAP<sup>MUT</sup> expression after 3 h of treatment in the *Hsp90aa1*-silenced condition in comparison with the control, similar to experiments with the wild-type form in CAFs and TGF $\beta$ -stimulated NFs (Figure V-9, B). Overall, these results indicate that HSP90 $\alpha$  controls YAP function and that it is particularly relevant in systems with high YAP activity.

## 5.8. Correlation of YAP and HSP90 $\alpha$ signatures with human scRNAseq datasets

To further study the implications of HSP90 and YAP activities in human cancer, we analyzed the possible correlations between HSP90-related signatures and YAP signatures in cancer stroma and CAF subpopulations from human cancer transcriptomic datasets. For assessing YAP activities, we employed a CAF-specific YAP/TAZ signature containing the top downregulated genes after YAP/TAZ silencing in mCAF1<sup>79</sup>. HSP90 $\alpha$  and HSP90 $\beta$  specific signatures were generated by selecting the top downregulated genes after *Hsp90aa1* and *Hsp90ab1* depletion in mCAF1, respectively (*see methods for further details*).

First, we found a high correlation between the CAF-specific YAP signature (“CAF-spec YAP”) and HSP90 $\alpha$  activities in CAFs (“CAF-spec HSP90AA1”) in breast cancer stroma datasets (GSE8977 and GSE26910) (**Figure V-10, A**). In the same stromal datasets, the “CAF-spec HSP90AA1” signature also had a high level of correlation with signatures related to RhoA and TGF $\beta$ , in line with our in vitro results (**Figure V-10, B**). Similar findings were obtained for HSP90i-related signatures. However, none of these signatures correlated with the one derived from silencing *Hsp90ab1* in our CAFs (“CAF-spec HSP90AB1”).

Furthermore, we also studied the expression of the previous signatures in CAFs extracted from human breast cancers and profiled by scRNAseq subtypes<sup>198</sup>. In this case, we found that all studied signatures except for the “CAF-spec HSP90AB1” were mostly

expressed by myCAFs (**Figure V-10, C**). In addition, there was a high correlation between the two “HSP90i” and the “CAF-spec HSP90AA1” signatures and the “CAF-spec YAP” and “F-TBRS” ones in the CAFs from this breast cancer dataset (**Figure V-10, D**). Similar correlations were found in the case of the CAFs from the previously analyzed bladder cancer dataset<sup>199</sup>, where they also correlated with the “BRENJENO\_RHOA\_UP” signature (**Figure V-10, D**). Importantly, the “CAF-spec HSP90AB1” signature did not correlate with any of the other signatures in breast CAFs nor in bladder CAFs (**Figure V-10, D**).

Since our “CAF-spec HSP90AA1” signature correlated with important CAF-related signatures in different human cancer datasets, we wanted to study its possible prognostic value. Thus, we stratified patients from breast, colon and ovarian datasets based on their high or low expression of the “CAF-spec HSP90AA1” signature. Results showed a significant decrease in survival in patients with high “CAF-spec HSP90AA1” signature expression, suggesting a relevant association between this signature and poorer prognosis in these cancer types (**Figure V-10, E**).

Taken together, these analyses indicate that the specific phenotype promoted by *Hsp90aa1* silencing in CAFs correlates with important CAF phenotypes in human patients and has prognostic value in different cancer types, suggesting that HSP90 activities in CAFs are key in human cancer development.

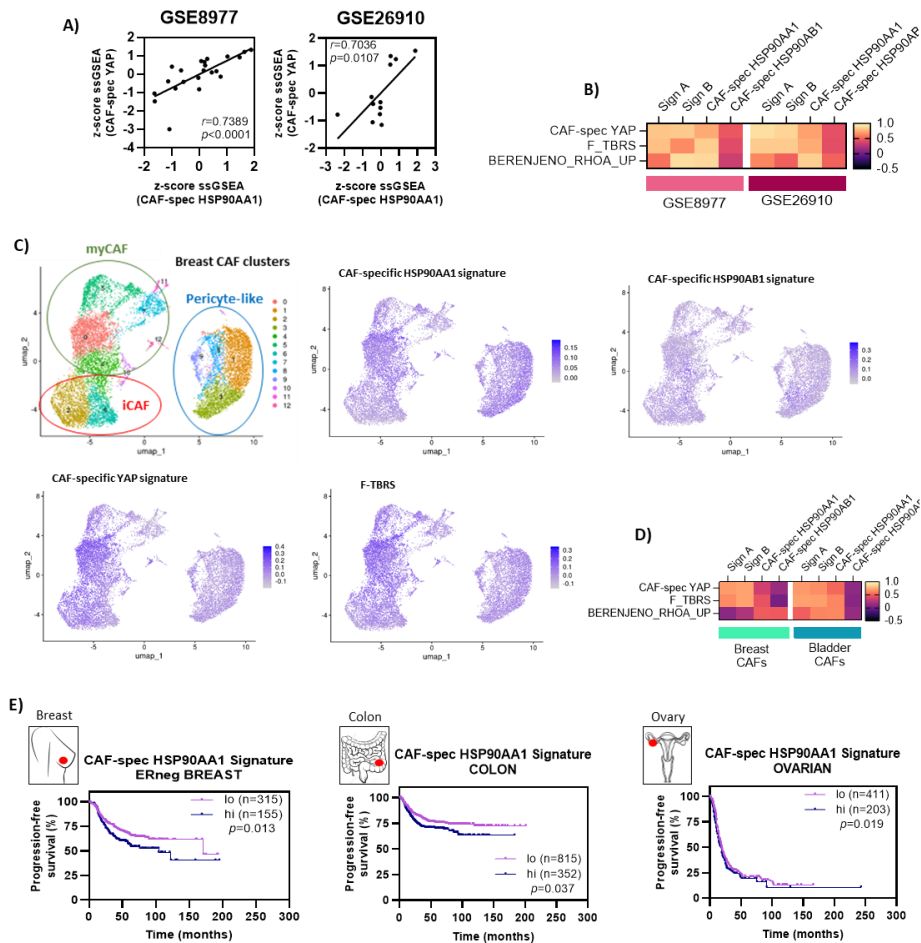


**Figure V-10. Correlation of YAP and HSP90 related signatures with different human datasets and prognostic value.** **A.** Graphs showing correlation between the “CAF-spec YAP” and “CAF-spec HSP90AA1” signatures in breast cancer stroma datasets GSE8977 (left) and GSE26910 (right). Signatures were assessed by ssGSEA and then z-score normalized. Each point in the graph represents an individual patient. **B.** Heatmap showing correlation coefficients between the indicated signatures in both breast cancer datasets (GSE8977 and GSE26910). **C.** UMAP of CAF subtypes found in the studied breast cancer dataset<sup>198</sup> as informed by scRNAseq analysis. Plots show the expression levels of the indicated signatures in each cell type. **D.** Heatmap showing correlation coefficients between the indicated signatures in CAFs derived from breast and bladder cancer datasets<sup>198,199</sup>. **E.** Graphs showing percentage of progression-free survival over time of the patients included in the ER negative breast, colorectal and ovarian datasets, based on their high or low expression of the “CAF-spec HSP90AA1” signature.



## Discussion



Cancer cells are permanently exposed to external insults, causing severe stress. In addition, cancer cells have the continuous necessity of expressing their pro-tumoral effectors to maintain their functions. However, these proteins usually present severe defects: they are usually misfolded and have the risk to aggregate, becoming severely dysfunctional and prone to degradation<sup>219</sup>. Thus, cancer cells suffer from proteostasis stress, as their protein homeostasis is severely compromised. To successfully resolve this stressful situation, cancer cells are characterized by a high expression of molecular chaperones, which are in charge of the correct protein folding and maintaining the functionality of these proteins. Not only this increases cancer cell survival, but the expression of chaperones also increases the tolerance of cancer cells to new protein modifications that could otherwise compromise the viability of the cells<sup>220,221</sup>. Consequently, cancer cells are highly dependent on chaperones such as HSP90.

The role of HSP90 in the chaperoning of cancer has historically been largely studied<sup>222,223</sup>, and it has been found significantly overexpressed in multiple cancer cell lines<sup>222,224</sup>. In this scenario, HSP90 modulates migration, invasion, survival, and angiogenesis in cancer cells through the regulation and stabilization of client proteins implicated in the signaling pathways that control such pro-tumoral functions, including RAF, AKT, HIF-1 $\alpha$ , VEGF, among many others<sup>225,226</sup>. Thus, HSP90 is implicated in all hallmarks of cancer through the stabilization of their main effectors.

Our results from bioinformatic analysis of publicly available datasets, as well as from *in vitro* experiments, show that there are no significant differences in the expression of HSP90 between NFs and CAFs, suggesting that the differences may be occurring at the functional level. Importantly, there are also cancer cell lines in which HSP90 expression levels were not found to be significantly higher to those in normal cells. However, in these cases, a higher HSP90 overall activity was found due to a significant increase in their affinity for HSP90 inhibitors in comparison with that from normal cells<sup>227</sup>. As previously mentioned, the increased activity of HSP90 in cancer cells in comparison to normal cells responds to an intracellular proteostatic stress caused by an excess in the expression of numerous pro-tumoral proteins. Due to CAFs representing an over-activated fibroblasts state, in which there is also overexpression of numerous effectors of the CAF pro-tumoral phenotype, questions arise on whether CAFs could also be under a similar proteostatic stress that could lead to similar increase in HSP90 activities in comparison with normal fibroblasts. Thus, CAFs could become dependent on HSP90 to maintain their malignant phenotype, similarly to the cancer cells. However, we have not explored yet the proteostatic state of our CAFs, or if this could be a possible mechanism underlying HSP90 functions in CAFs.

The chaperone role of HSP90 in maintaining protein homeostasis in cancer cells has been traditionally attributed to intracellular HSP90, composed by both HSP90 $\alpha$  and HSP90 $\beta$  pools. However, this is not the only HSP90 role found in cancer. More recently, extracellular HSP90 (eHSP90) has increasingly gained

attention in cancer studies. eHSP90 has only been found to be expressed by normal cells under stressful conditions such as heat, radiation, hypoxia, nutrient starvation and presence of reactive oxygen species<sup>142,226</sup>, which are also typical characteristics of the TME. In fact, constitutive expression of eHSP90 has been reported in a number of different cancer cell lines, including breast, colorectal and prostate, among others<sup>228,229</sup>, suggesting that secretion of eHSP90 is a conserved cancer feature. Importantly, the isoform that is mostly secreted is HSP90 $\alpha$ , whose expression is also enhanced in some cancer types in comparison with the HSP90 $\beta$  isoform<sup>230,231</sup>. This indicates an exclusive role of the HSP90 $\alpha$  isoform in the context of cancer.

In addition, extracellular HSP90 $\alpha$  (eHSP90 $\alpha$ ) has also been described to have important implications in cancer cell activation, promoting cancer cell growth, migration and even participating in therapy resistance<sup>142,232</sup>. As an example, eHSP90 $\alpha$  has been reported to induce cancer cell migration through the AKT signaling pathway<sup>233</sup>. In cancer cells, this HSP90 $\alpha$  behavior differs from its typical intracellular role as guardian of protein homeostasis. However, the molecular mechanisms through which eHSP90 $\alpha$  exert its functions remains unclear. On one hand, eHSP90 $\alpha$  could associate with important cell surface receptors to stabilize intracellular signaling. This particular effect has also been reported to happen in the context of fibrosis, where eHSP90 has been described to stabilize TGF $\beta$  signaling within activated fibroblasts through direct interaction with the TGF $\beta$  receptor I (TGF $\beta$ RI)<sup>234</sup>. Nevertheless, it is still uncertain if this effect is dependent on the ATPase chaperone function of HSP90, or

if there are other molecular mechanisms mediating this interaction. On the other hand, eHSP90 $\alpha$  has also been reported to act as a typical secreted ligand that binds to its receptor and triggers an intracellular response<sup>142</sup>. In this sense, LRP-1 has been found to be the main receptor of eHSP90 $\alpha$  in cancer cells<sup>233</sup>.

Our bioinformatic analysis of publicly available datasets revealed HSP90 as a possible regulator of pro-tumoral functions in the stroma, due to HSP90-related signatures found to be significantly upregulated in the stroma of various tumors in comparison with their normal counterparts. Importantly, these signatures had prognostic value, suggesting that patients could benefit from anti-HSP90 therapies targeted to the tumor stroma. In addition, our *in vivo* experiments with *Hsp90aa1*<sup>-/-</sup> KO mice indicate a role of stromal HSP90 $\alpha$  in tumor growth and in the early stages of tumor development. Importantly, since the *Hsp90aa1*<sup>-/-</sup> mice lack HSP90 $\alpha$  expression in their whole anatomy, the anti-tumoral effect cannot be solely attributed to CAFs as other stromal components also lack HSP90 activity in this model. Thus, our results thus far cannot rule out a possible role of endothelial or immune *Hsp90aa1* in the observed *in vivo* effect. We are still performing further histopathology analysis in order to study more profoundly the stromal composition of the *Hsp90aa1*<sup>-/-</sup> breast cancer tumors. Furthermore, a follow up *in vivo* experiment co-injecting *Hsp90aa1*<sup>-/-</sup> fibroblasts with *Hsp90aa1*<sup>+/+</sup> cancer cells is also needed to confirm the pro-tumorigenic relevance of HSP90 $\alpha$  in CAFs.

Besides our current finding about the implications of HSP90 $\alpha$  in the tumor stroma, little is known about the role of HSP90 in the TME, particularly about the role of intracellular HSP90 in the different ECM components. Some studies have pointed out the relevance of HSP90 in immune cells, in which it has been reported to have different roles, such as inducing the interferon response or promoting AKT signaling activation in T-cells<sup>235,236</sup>. Importantly, HSP90 has also been found to have relevance in other TME components with CAF-like phenotypes, such as pancreatic stellate cells<sup>237</sup>. However, most of these studies base their findings in the treatment with HSP90i, which could have off-target effects over other components of the TME. Thus, the particular role of HSP90 in each TME component individually needs further study.

Nevertheless, it has been reported that eHSP90 participate in the activation of immune cells, endothelial cells and CAFs. In fact, many of the TME cellular components have been found to express receptors for eHSP90<sup>238</sup>. In the case of the immune cells, eHSP90 can play as tumor suppressor by facilitating antigen presentation from malignant cells to the immune system<sup>238</sup>; or as pro-tumorigenic, due to eHSP90 $\alpha$  activating the polarization of macrophages into the M2 pro-tumoral phenotype<sup>239</sup>. In addition, eHSP90 $\alpha$  mediates migration and tubulogenesis of the endothelial cells in the TME<sup>240,241</sup>. In fact, in other context such as wound healing, endothelial cells also secrete eHSP90 $\alpha$  to induce angiogenesis<sup>229</sup>. Finally, eHSP90 has also been described to directly interact with some ECM components, including the MMP2 metalloproteinase<sup>229,242</sup> and fibronectin<sup>243</sup>. This suggests a possible role of HSP90 in ECM remodeling.

eHSP90 has also been demonstrated to activate fibroblasts in different pathological contexts. In wound healing, eHSP90 induces the activation of fibroblasts into the myofibroblastic phenotype, and promotes ECM remodeling and migration<sup>244,245</sup>. In fibrosis, eHSP90 $\alpha$  promotes fibroblasts activation through the PI3K/AKT signaling pathway<sup>246</sup>. In cancer, the activation of CAFs through eHSP90 is mediated by similar molecular mechanisms. eHSP90 promotes migration and cell motility in CAFs<sup>241</sup>. Our studies indicate a clear role of HSP90 $\alpha$  in modulating several relevant CAF functions, and some of those effects could be explained by the chaperone nature of HSP90 and its role in stabilizing CAF effector proteins such as YAP or TAZ. However, given the fact that the majority of the eHSP90 pool found in tumors correspond to the HSP90 $\alpha$  isoform, it would also be interesting to explore whether any of our observations are the consequence of this particular HSP90 form.

On the other hand, information is very scarce about the role of intracellular HSP90 in CAFs. However, many of the molecular regulators of CAF functions that have been described in the literature are also well-known HSP90 clients, and have actually been found to be regulated by HSP90 in cancer cells. This is the case of proteins such as RAF<sup>247</sup>, AKT<sup>248</sup> and HIF1 $\alpha$ <sup>249</sup>, among others. This suggest that similar regulatory mechanisms could also be at play in CAFs. In addition, our transcriptional and proteomic data indicates that there is a reduction in the expression of HSP90 interactors after HSP90 $\alpha$  silencing in CAFs and TGF $\beta$ -stimulated NFs. Whether these proteins are modulated by the classical chaperone function of HSP90 $\alpha$  or if they are regulated by additional mechanisms remains unsolved.

Given the chaperone nature of HSP90 and the long list of client proteins whose activity depends on its expression, HSP90 typically functions as a protein node that forms multimolecular complexes with numerous clients and co-chaperones. Thus, in cancer cells it has already been demonstrated that the silencing of *Hsp90aa1/ab1*, or the inhibition of its ATPase function using anti-HSP90 drugs, has consequences in various independent molecular processes, ending in the collapse of multiple signaling pathways simultaneously. Similar effects were observed in our transcriptomic and proteomic data from *Hsp90aa1/ab1*-silenced CAFs and TGF $\beta$ -stimulated NFs, in which the depletion of HSP90 expression caused the simultaneous downregulation of several important CAF-related pathways, as well as other pathways related with biological processes, such as cell cycle, DNA repair mechanisms and metabolic processes, among others. Interestingly, the silencing of *Hsp90aa1/ab1* did not cause a depletion in markers usually related with the CAF phenotype in any of our *in vitro* systems, including  $\alpha$ -SMA and S100A4. This indicates that HSP90 does not regulate CAF identity, rather it is more implicated in CAF functions.

Interestingly, although the silencing of HSP90 $\alpha$  in both CAFs and TGF $\beta$ -stimulated NFs had similar consequences at the functional level, our transcriptomic and proteomic data indicate that different expression programs are promoted in each system. In fact, the HSP90 $\alpha$  effect over the TGF $\beta$  pathway was only observed in the stimulated-NFs, but not in our CAF cell line. This suggests that HSP90 $\alpha$  could potentially have different roles depending on the activated status of the fibroblasts. Thus, it could have a specific role

in the acquisition of the pro-tumoral phenotype, whereas it can have a different role in well-established CAFs, in which more signaling pathways besides the TGF $\beta$  pathway are at play. In addition, given the importance of stromal HSP90 $\alpha$  in tumor progression at the primary site and in the establishment of new secondary malignancies observed in our *in vivo* experiments, it would also be interesting to study the synergies of HSP90 molecular mechanisms in different stages of the disease.

Among the numerous alterations caused by *Hsp90aa1* silencing in CAFs and TGF $\beta$ -stimulated NFs, there is the downregulation of YAP and several of their regulators and related proteins. As previously mentioned, YAP is a transcriptional factor that control important CAF functions, mostly related with mechanotransduction, ECM remodeling and migration<sup>79,185,250</sup>. Thus, given the usual upregulation of YAP functions found in CAFs, and the numerous processes they regulate in this context, its downregulation causes the collapse of several important CAF functions. Most of these we found to be severely affected by HSP90 $\alpha$  depletion, including their gel contraction ability, ECM architecture, wound healing, and migration capacities. Importantly, many of these functions rely on the activity of the acto-myosin cytoskeleton, which was also found to be altered upon HSP90 $\alpha$  depletion. Thus, one proposed mechanism of HSP90 $\alpha$  action in CAFs is through the control of YAP activities (either directly, as a “client” protein, or indirectly, through the regulation of upstream modulators such as YES1), which in turn modulates CAF functions through the expression and activity of their cytoskeleton. However, further work is required

to delineate the relevance of the observed role of HSP90 $\alpha$  over YES1 stability, and its effect in YAP phosphorylation and activity. In addition, the possibility of YAP being an exclusive “client” protein of the HSP90 $\alpha$  could also explain the specific effects of this isoform over the CAF phenotype, and not HSP90 $\beta$ . In addition, transcriptomic and proteomic results from HSP90 $\alpha$  modulation in CAFs revealed that there are other molecular programs at play, such as RhoA/ROCK, which are also important regulators of the cytoskeleton mechanics<sup>251</sup>. Further investigation is required in order to understand how YAP/TAZ and RhoA/ROCK activities interconnect with each other under the regulation of HSP90 in CAFs. In particular, it needs to be assessed whether the modulation of RhoA is downstream of the effect of HSP90 over YAP (via the regulation of cytoskeletal genes potentiating actomyosin contractility and cytoskeletal rearrangements) or whether it is a direct effect over RhoA or upstream regulators (**Figure 9**). Importantly, TAZ activities have not yet been described to be directly related to CAF functions<sup>185</sup>, but our data indicates that its expression is also modulated by HSP90 $\alpha$ . Further studies are needed to investigate the potential role of TAZ in CAFs, and if its possible modulation by HSP90 $\alpha$  could add to the effects of YAP.

Furthermore, YAP/TAZ also play important roles in other malignant contexts, in which they mediate tumor growth, metastasis and resistance<sup>252</sup>. Given our *in vivo* results, which point out to an important role of HSP90 $\alpha$  in the TME, further investigation would be necessary to investigate whether these effects are also mediated by YAP/TAZ modulation *in vivo*, and thus if the *in vitro* observed effects derived of YAP/TAZ modulation by HSP90 could be translated into *in*

*in vivo* effects over cancer cell growth and metastasis. In addition, it would be interesting to investigate if anti-HSP90 strategies also modulate YAP/TAZ in cancer cells or other TME components, or if these regulatory mechanisms and interactions between HSP90 and YAP/TAZ are exclusive to CAFs.

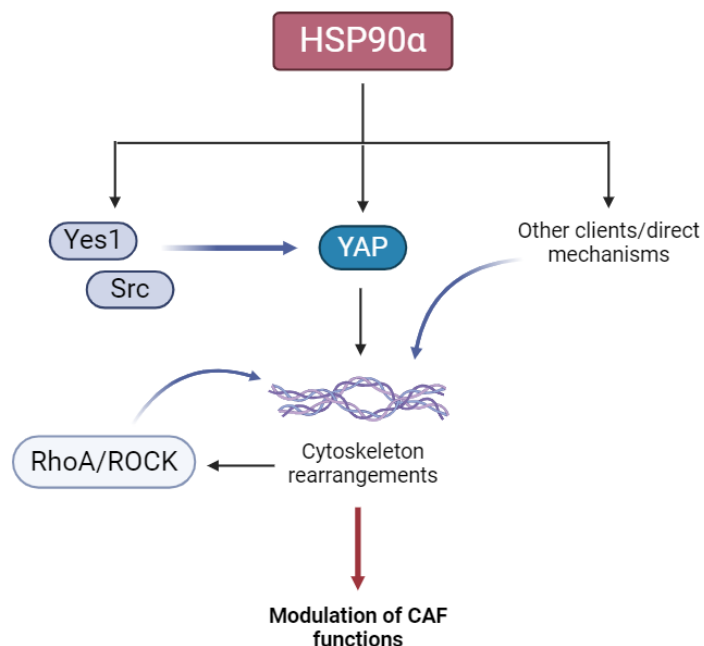


**Figure 9. Proposed mechanism of action of HSP90α in CAFs.** Our data indicates a role of HSP90 in regulating YAP, either directly (as a “client” protein) or indirectly (through modulation of some of their most important regulators, including Src or Yes1. YAP activities in turn induce changes in the cytoskeleton of CAFs, which will ultimately lead to the activation of other molecular programs, such as RhoA/ROCK, and the ultimate modulation of CAF functions. The same results could be achieved by regulation of other HSP90α clients or other direct unknown mechanisms.

Surprisingly, the treatment with HSP90i did not have any functional effect in CAFs. These particular drugs target the ATPase site at the N-terminal domain of both HSP90α and HSP90β, as they are not able to distinguish between the two isoforms. Similarly, the silencing of both HSP90 isoforms simultaneously with both siRNA

smart pools did also not have any effect over the *in vitro* functions we tested. These results suggest that there could be compensatory mechanisms that are activated when neither of the HSP90 isoforms is active in the cell.

Complete absence of HSP90 could influence the expression of other factors that could ultimately neutralize YAP effects. It has been known for a long time that HSP90 stabilizes Heat Shock Factor 1 (HSF1) in the cytoplasm, preventing its translocation into the nucleus and impeding the transcriptional activation of its target genes<sup>253–255</sup>. Given the recently found role of HSF1 in modulating CAF pro-tumoral activities<sup>79</sup>, we hypothesized that the compensatory regulatory mechanism activated by HSP90 inhibition was carried out through HSF1 functions. Preliminary data in this line discards this possibility, as we observed a reduction in the active form of HSF1 in HSP90-depleted CAFs (*not shown*). Further investigation is needed in order to elucidate the reasons behind this lack of effect of anti-HSP90 drugs in CAFs. Moreover, analyses of HSP90i in *in vivo* contexts and CAF biological activity are required, given the clear correlation between CAF aggressive phenotypes and HSP90i signatures in clinical samples obtained at the beginning of this work.

Altogether, our findings describe a novel role of HSP90, and particularly HSP90 $\alpha$ , in modulating the CAF phenotype through regulation of the stability of YAP/TAZ and one of their most important regulators, Yes1. Further studies are needed in order to find if YAP/TAZ and Yes1 are actual HSP90 client proteins, or if there are additional regulatory mechanisms at play. In addition, we described the importance of stromal HSP90 $\alpha$  in tumor growth and metastasis, although further studies are needed to elucidate which one of the stromal components are responsible for these HSP90 $\alpha$ -driven effects.

## Conclusions



1. Bioinformatic analyses of public datasets identified HSP90 as a possible driver of pro-tumoral processes associated with tumor stroma and CAF with prognostic value.
2. The silencing of HSP90, and specially the *Hsp90aa1* isoform, in CAFs and TGF $\beta$ -stimulated NFs, alters the gene and protein expression of key regulators of the CAF phenotype, with important consequences at the functional level.
3. The *Hsp90aa1* isoform regulates CAF functions through modulation of the actomyosin cytoskeleton, and its silencing in CAFs and TGF $\beta$ -stimulated NFs impedes their contractile capacity, migration and motility.
4. The *Hsp90aa1* isoform regulates the architecture of CAFs-derived ECM, which impacts the behavior of cancer cells.
5. *Hsp90aa1* impacts the TGF $\beta$  pathway in TGF $\beta$ -stimulated NFs, but these regulatory mechanisms are not present or does not have any relevance for pro-tumoral functions in pathologically activated CAFs.
6. The knock-out of stromal *Hsp90aa1* in vivo reduces collagen deposition, cancer cell growth and metastatic colonization.
7. *Hsp90aa1* in CAFs regulates important transcriptional programs. It controls cell cycle, RhoA-related functions and YAP/TAZ.
8. *Hsp90aa1* modulates CAF functions through regulation of the stability of YAP/TAZ and key upstream regulators, including Yes1.
9. Co-IP experiments demonstrate a direct interaction of *Hsp90aa1* with YAP.
10. HSP90 inhibitors Geldanamycin and Tanespimycin affect YAP protein levels.
11. Altogether, these observations indicate that YAP is a client protein of HSP90 $\alpha$ , and that HSP90 $\alpha$  promotes pro-tumoral behaviors in CAFs by potentiating YAP activity.



# Bibliography



1. McDowell, Sandy, Ludwig Rausch, Sarah & Simmons, Kenna. Cancer Research Insights from the Latest Decade, 2010 to 2020. *American Cancer Society* (2019). Available from: <https://www.cancer.org/research/acs-research-news/cancer-research-insights-from-the-latest-decade-2010-to-2020.html>. (Accessed 11 June, 2023)
2. Guevara, M. *et al.* Cancer Survival in Adults in Spain: A Population-Based Study of the Spanish Network of Cancer Registries (REDECAN). *Cancers* **14**, 2441 (2022).
2. World Health Organization. Cancer: key facts. *World Health Organization (WHO)* (2022). Available from: <https://www.who.int/news-room/fact-sheets/detail/cancer>. (Accessed 11 June, 2023)
4. Hanahan, D. & Weinberg, R. A. Hallmarks of Cancer: The Next Generation. *Cell* **144**, 646–674 (2011).
5. Jin, H., Wang, L. & Bernards, R. Rational combinations of targeted cancer therapies: background, advances and challenges. *Nat Rev Drug Discov* **22**, 213–234 (2023).
6. Hanahan, D. Hallmarks of Cancer: New Dimensions. *Cancer Discovery* **12**, 31–46 (2022).
7. Hinshaw, D. C. & Shevde, L. A. The Tumor Microenvironment Innately Modulates Cancer Progression. *Cancer Research* **79**, 4557–4566 (2019).
8. Hanahan, D. & Coussens, L. M. Accessories to the Crime: Functions of Cells Recruited to the Tumor Microenvironment. *Cancer Cell* **21**, 309–322 (2012).
9. Oliver, A. J. *et al.* Tissue-Dependent Tumor Microenvironments and Their Impact on Immunotherapy Responses. *Front. Immunol.* **9**, 70 (2018).
10. Junttila, M. R. & de Sauvage, F. J. Influence of tumour micro-environment heterogeneity on therapeutic response. *Nature* **501**, 346–354 (2013).
11. Kidd, S. *et al.* Origins of the Tumor Microenvironment: Quantitative Assessment of Adipose-Derived and Bone Marrow-Derived Stroma. *PLoS ONE* **7**, e30563 (2012).

12. Bussard, K. M., Mutkus, L., Stumpf, K., Gomez-Manzano, C. & Marini, F. C. Tumor-associated stromal cells as key contributors to the tumor microenvironment. *Breast Cancer Res* **18**, 84 (2016).
13. Balkwill, F. R., Capasso, M. & Hagemann, T. The tumor microenvironment at a glance. *Journal of Cell Science* **125**, 5591–5596 (2012).
14. Trimm, E. & Red-Horse, K. Vascular endothelial cell development and diversity. *Nat Rev Cardiol* **20**, 197–210 (2023).
15. Siemann, D. W. The unique characteristics of tumor vasculature and preclinical evidence for its selective disruption by Tumor-Vascular Disrupting Agents. *Cancer Treatment Reviews* **37**, 63–74 (2011).
16. Nagl, L., Horvath, L., Pircher, A. & Wolf, D. Tumor Endothelial Cells (TECs) as Potential Immune Directors of the Tumor Microenvironment – New Findings and Future Perspectives. *Front. Cell Dev. Biol.* **8**, 766 (2020).
17. Georganaki, M., Van Hooren, L. & Dimberg, A. Vascular Targeting to Increase the Efficiency of Immune Checkpoint Blockade in Cancer. *Front. Immunol.* **9**, 3081 (2018).
18. Fang, J. *et al.* Exploring the crosstalk between endothelial cells, immune cells, and immune checkpoints in the tumor microenvironment: new insights and therapeutic implications. *Cell Death Dis* **14**, 586 (2023).
19. Lopes-Coelho, F., Martins, F., Pereira, S. A. & Serpa, J. Anti-Angiogenic Therapy: Current Challenges and Future Perspectives. *IJMS* **22**, 3765 (2021).
20. Lei, X. *et al.* Immune cells within the tumor microenvironment: Biological functions and roles in cancer immunotherapy. *Cancer Letters* **470**, 126–133 (2020).
21. Tanaka, H. *et al.* Successful Adoptive Immunotherapy of Murine *Poorly Immunogenic* Tumor with Specific Effector Cells Generated from Gene-Modified Tumor-Primed Lymph Node Cells. *The Journal of Immunology* **162**, 3574–3582 (1999).
22. Li, C., Jiang, P., Wei, S., Xu, X. & Wang, J. Regulatory T cells in tumor microenvironment: new mechanisms, potential therapeutic strategies and future prospects. *Mol Cancer* **19**, 116 (2020).

23. Wu, X. *et al.* Reprogramming of Treg cells in the inflammatory microenvironment during immunotherapy: a literature review. *Front. Immunol.* **14**, 1268188 (2023).
24. Bluestone, J. A., McKenzie, B. S., Beilke, J. & Ramsdell, F. Opportunities for Treg cell therapy for the treatment of human disease. *Front. Immunol.* **14**, 1166135 (2023).
25. Gao, L. *et al.* CCL2/EGF positive feedback loop between cancer cells and macrophages promotes cell migration and invasion in head and neck squamous cell carcinoma. *Oncotarget* **7**, 87037–87051 (2016).
26. Kaneda, M. M. *et al.* Macrophage PI3K $\gamma$  Drives Pancreatic Ductal Adenocarcinoma Progression. *Cancer Discovery* **6**, 870–885 (2016).
27. Pathria, P., Louis, T. L. & Varner, J. A. Targeting Tumor-Associated Macrophages in Cancer. *Trends in Immunology* **40**, 310–327 (2019).
28. Postow, M. A., Callahan, M. K. & Wolchok, J. D. Immune Checkpoint Blockade in Cancer Therapy. *JCO* **33**, 1974–1982 (2015).
29. Brassart-Pasco, S. *et al.* Tumor Microenvironment: Extracellular Matrix Alterations Influence Tumor Progression. *Front. Oncol.* **10**, 397 (2020).
30. Karamanos, N. K. *et al.* A guide to the composition and functions of the extracellular matrix. *The FEBS Journal* **288**, 6850–6912 (2021).
31. Socovich, A. M. & Naba, A. The cancer matrisome: From comprehensive characterization to biomarker discovery. *Seminars in Cell & Developmental Biology* **89**, 157–166 (2019).
32. Popova, N. V. & Jücker, M. The Functional Role of Extracellular Matrix Proteins in Cancer. *Cancers* **14**, 238 (2022).
33. Öhlund, D., Franklin, O., Lundberg, E., Lundin, C. & Sund, M. Type IV collagen stimulates pancreatic cancer cell proliferation, migration, and inhibits apoptosis through an autocrine loop. (2013).
34. Tian, C. *et al.* Proteomic analyses of ECM during pancreatic ductal adenocarcinoma progression reveal different contributions by tumor and stromal cells. *Proc. Natl. Acad. Sci. U.S.A.* **116**, 19609–19618 (2019).

35. Best, S. L. *et al.* Collagen organization of renal cell carcinoma differs between low and high grade tumors. *BMC Cancer* **19**, 490 (2019).
36. Zhou, Z.-H. *et al.* Reorganized Collagen in the Tumor Microenvironment of Gastric Cancer and Its Association with Prognosis. *J. Cancer* **8**, 1466–1476 (2017).
37. Provenzano, P. P. *et al.* Collagen reorganization at the tumor-stromal interface facilitates local invasion. *BMC Med* **4**, 38 (2006).
38. Boyd, D. F. & Thomas, P. G. Towards integrating extracellular matrix and immunological pathways. *Cytokine* **98**, 79–86 (2017).
39. Yuan, Z. *et al.* Extracellular matrix remodeling in tumor progression and immune escape: from mechanisms to treatments. *Mol Cancer* **22**, 48 (2023).
40. Kalluri, R. The biology and function of fibroblasts in cancer. *Nature Reviews Cancer* **16**, 582–598 (2016).
41. Plikus, M. V. *et al.* Fibroblasts: Origins, definitions, and functions in health and disease. *Cell* **184**, 3852–3872 (2021).
42. Nurmik, M., Ullmann, P., Rodriguez, F., Haan, S. & Letellier, E. In search of definitions: Cancer-associated fibroblasts and their markers. *Int. J. Cancer* **146**, 895–905 (2020).
43. Shiga, K. *et al.* Cancer-Associated Fibroblasts: Their Characteristics and Their Roles in Tumor Growth. *Cancers* **7**, 2443–2458 (2015).
44. Belhabib, I., Zaghdoudi, S., Lac, C., Bousquet, C. & Jean, C. Extracellular Matrices and Cancer-Associated Fibroblasts: Targets for Cancer Diagnosis and Therapy? *Cancers* **13**, 3466 (2021).
45. Calvo, F. *et al.* Cdc42EP3/BORG2 and Septin Network Enables Mechano-transduction and the Emergence of Cancer-Associated Fibroblasts. *Cell Reports* **13**, 2699–2714 (2015).
46. Kim, D. K., Kim, E. K., Jung, D.-W. & Kim, J. Cytoskeletal alteration modulates cancer cell invasion through RhoA-YAP signaling in stromal fibroblasts. *PLoS ONE* **14**, e0214553 (2019).

47. O'Connell, J. T. *et al.* VEGF-A and Tenascin-C produced by S100A4<sup>+</sup> stromal cells are important for metastatic colonization. *Proc. Natl. Acad. Sci. U.S.A.* **108**, 16002–16007 (2011).
48. Monteran, L. & Erez, N. The Dark Side of Fibroblasts: Cancer-Associated Fibroblasts as Mediators of Immunosuppression in the Tumor Microenvironment. *Front. Immunol.* **10**, 1835 (2019).
49. Chen, Y., McAndrews, K. M. & Kalluri, R. Clinical and therapeutic relevance of cancer-associated fibroblasts. *Nat Rev Clin Oncol* **18**, 792–804 (2021).
50. Saw, P. E., Chen, J. & Song, E. Targeting CAFs to overcome anticancer therapeutic resistance. *Trends in Cancer* **8**, 527–555 (2022).
51. Klemm, F. & Joyce, J. A. Microenvironmental regulation of therapeutic response in cancer. *Trends in Cell Biology* **25**, 198–213 (2015).
52. Manoukian, P., Bijlsma, M. & Van Laarhoven, H. The Cellular Origins of Cancer-Associated Fibroblasts and Their Opposing Contributions to Pancreatic Cancer Growth. *Front. Cell Dev. Biol.* **9**, 743907 (2021).
53. Sahai, E. *et al.* A framework for advancing our understanding of cancer-associated fibroblasts. *Nature Reviews Cancer* **20**, 174–186 (2020).
54. Gabbiani, G., Ryan, G. B. & Majno, G. Presence of modified fibroblasts in granulation tissue and their possible role in wound contraction. *Experientia* **27**, 549–550 (1971).
55. Pakshir, P. *et al.* The myofibroblast at a glance. *Journal of Cell Science* **133**, jcs227900 (2020).
56. El Ayadi, A., Jay, J. W. & Prasai, A. Current Approaches Targeting the Wound Healing Phases to Attenuate Fibrosis and Scarring. *IJMS* **21**, 1105 (2020).
57. Chandler, C., Liu, T., Buckanovich, R. & Coffman, L. G. The double edge sword of fibrosis in cancer. *Translational Research* **209**, 55–67 (2019).
58. Dvorak, H. F. Tumors: Wounds That Do Not Heal. *N Engl J Med* **315**, 1650–1659 (1986).

59. Gunaydin, G. CAFs Interacting With TAMs in Tumor Microenvironment to Enhance Tumorigenesis and Immune Evasion. *Front. Oncol.* **11**, 668349 (2021).
60. Hosaka, K. *et al.* Pericyte–fibroblast transition promotes tumor growth and metastasis. *Proc. Natl. Acad. Sci. U.S.A.* **113**, (2016).
61. Miyazaki, Y. *et al.* Adipose-derived mesenchymal stem cells differentiate into heterogeneous cancer-associated fibroblasts in a stroma-rich xenograft model. *Sci Rep* **11**, 4690 (2021).
62. Raz, Y. *et al.* Bone marrow–derived fibroblasts are a functionally distinct stromal cell population in breast cancer. *Journal of Experimental Medicine* **215**, 3075–3093 (2018).
63. Helms, E. J. *et al.* Mesenchymal Lineage Heterogeneity Underlies Nonredundant Functions of Pancreatic Cancer–Associated Fibroblasts. *Cancer Discovery* **12**, 484–501 (2022).
64. Zeisberg, E. M., Potenta, S., Xie, L., Zeisberg, M. & Kalluri, R. Discovery of Endothelial to Mesenchymal Transition as a Source for Carcinoma-Associated Fibroblasts. *Cancer Research* **67**, 10123–10128 (2007).
65. Radisky, D. C., Kenny, P. A. & Bissell, M. J. Fibrosis and cancer: Do myofibroblasts come also from epithelial cells via EMT? *J. Cell. Biochem.* **101**, 830–839 (2007).
66. Yeh, H.-W., Lee, S.-S., Chang, C.-Y., Lang, Y.-D. & Jou, Y.-S. A New Switch for TGF $\beta$  in Cancer. *Cancer Research* **79**, 3797–3805 (2019).
67. Nilsson, U. W., Jönsson, J. A. & Dabrosin, C. Tamoxifen decreases extracellular TGF- $\beta$ 1 secreted from breast cancer cells — A post-translational regulation involving matrix metalloproteinase activity. *Experimental Cell Research* **315**, 1–9 (2009).
68. Yoon, H. *et al.* TGF- $\beta$ 1-mediated transition of resident fibroblasts to cancer-associated fibroblasts promotes cancer metastasis in gastrointestinal stromal tumor. *Oncogenesis* **10**, 13 (2021).
69. Hawinkels, L. J. A. C. *et al.* Interaction with colon cancer cells hyperactivates TGF- $\beta$  signaling in cancer-associated fibroblasts. *Oncogene* **33**, 97–107 (2014).

70. Ringuette Goulet, C. *et al.* Exosomes Induce Fibroblast Differentiation into Cancer-Associated Fibroblasts through TGF $\beta$  Signaling. *Molecular Cancer Research* **16**, 1196–1204 (2018).
71. Erez, N., Truitt, M., Olson, P. & Hanahan, D. Cancer-Associated Fibroblasts Are Activated in Incipient Neoplasia to Orchestrate Tumor-Promoting Inflammation in an NF- $\kappa$ B-Dependent Manner. *Cancer Cell* **17**, 135–147 (2010).
72. Wu, H., Ma, S., Xiang, M. & Tong, S. HTRA1 promotes transdifferentiation of normal fibroblasts to cancer-associated fibroblasts through activation of the NF- $\kappa$ B/bFGF signaling pathway in gastric cancer. *Biochemical and Biophysical Research Communications* **514**, 933–939 (2019).
73. Fang, Z. *et al.* Signaling pathways in cancer-associated fibroblasts: recent advances and future perspectives. *Cancer Communications* **43**, 3–41 (2023).
74. Shah, M. A. & Rogoff, H. A. Implications of reactive oxygen species on cancer formation and its treatment. *Seminars in Oncology* **48**, 238–245 (2021).
75. Martinez-Outschoorn, U. E. *et al.* Cell Cycle Oxidative stress in cancer associated fibroblasts drives tumor-stroma co-evolution A new paradigm for understanding tumor metabolism, the field effect and genomic instability in cancer cells. (2010) doi:10.4161/cc.9.16.12553.
76. Zhou, W. *et al.* Oxidative stress induced autophagy in cancer associated fibroblast enhances proliferation and metabolism of colorectal cancer cells. *Cell Cycle* **16**, 73–81 (2017).
77. Gumilar, K. E. *et al.* Heat Shock Factor 1 Inhibition: A Novel Anti-Cancer Strategy with Promise for Precision Oncology. *Cancers* **15**, (2023).
78. Wang, Q. *et al.* Heat shock factor 1 in cancer-associated fibroblasts is a potential prognostic factor and drives progression of oral squamous cell carcinoma. *Cancer Sci* **110**, 1790–1803 (2019).
79. Ferrari, N. *et al.* Dickkopf-3 links HSF1 and YAP/TAZ signalling to control aggressive behaviours in cancer-associated fibroblasts. *Nature Communications* **10**, (2019).

80. Öhlund, D. *et al.* Distinct populations of inflammatory fibroblasts and myofibroblasts in pancreatic cancer. *Journal of Experimental Medicine* **214**, 579–596 (2017).
81. Yamaguchi, H. & Sakai, R. Direct Interaction between Carcinoma Cells and Cancer Associated Fibroblasts for the Regulation of Cancer Invasion. *Cancers* **7**, 2054–2062 (2015).
82. Strell, C. *et al.* Impact of Epithelial–Stromal Interactions on Peritumoral Fibroblasts in Ductal Carcinoma in Situ. *JNCI: Journal of the National Cancer Institute* **111**, 983–995 (2019).
83. Fisher, K. E. *et al.* MT1-MMP- and Cdc42-dependent signaling co-regulate cell invasion and tunnel formation in 3D collagen matrices. *Journal of Cell Science* **122**, 4558–4569 (2009).
84. Walker, C., Mojares, E. & Del Río Hernández, A. Role of Extracellular Matrix in Development and Cancer Progression. *IJMS* **19**, 3028 (2018).
85. Pankova, D. *et al.* Cancer-Associated Fibroblasts Induce a Collagen Cross-link Switch in Tumor Stroma. *Molecular Cancer Research* **14**, 287–295 (2016).
86. Hasan, S. & Buechler, M. B. What’s in a name? An emerging framework for cancer-associated fibroblasts, myofibroblasts, and fibroblasts. *Cancer Cell* **40**, 1273–1275 (2022).
87. Lee, H.-O. *et al.* FAP-overexpressing fibroblasts produce an extracellular matrix that enhances invasive velocity and directionality of pancreatic cancer cells. *BMC Cancer* **11**, 245 (2011).
88. Zhang, H., Lin, F., Huang, J. & Xiong, C. Anisotropic stiffness gradient-regulated mechanical guidance drives directional migration of cancer cells. *Acta Biomaterialia* **106**, 181–192 (2020).
89. Jain, R. K., Martin, J. D. & Stylianopoulos, T. The Role of Mechanical Forces in Tumor Growth and Therapy. *Annu. Rev. Biomed. Eng.* **16**, 321–346 (2014).
90. Lakins, M. A., Ghorani, E., Munir, H., Martins, C. P. & Shields, J. D. Cancer-associated fibroblasts induce antigen-specific deletion of CD8 + T Cells to protect tumour cells. *Nat Commun* **9**, 948 (2018).

91. Zhang, C. *et al.* CAFs orchestrates tumor immune microenvironment— A new target in cancer therapy? *Front. Pharmacol.* **14**, 1113378 (2023).
92. Koppensteiner, L., Mathieson, L., O'Connor, R. A. & Akram, A. R. Cancer Associated Fibroblasts - An Impediment to Effective Anti-Cancer T Cell Immunity. *Front. Immunol.* **13**, 887380 (2022).
93. Comito, G. *et al.* Cancer-associated fibroblasts and M2-polarized macrophages synergize during prostate carcinoma progression. *Oncogene* **33**, 2423–2431 (2014).
94. Martinez-Outschoorn, U. E., Lisanti, M. P. & Sotgia, F. Catabolic cancer-associated fibroblasts transfer energy and biomass to anabolic cancer cells, fueling tumor growth. *Seminars in Cancer Biology* **25**, 47–60 (2014).
95. Li, Z., Sun, C. & Qin, Z. Metabolic reprogramming of cancer-associated fibroblasts and its effect on cancer cell reprogramming. *Theranostics* **11**, 8322–8336 (2021).
96. Sousa, C. M. *et al.* Pancreatic stellate cells support tumour metabolism through autophagic alanine secretion. *Nature* **536**, 479–483 (2016).
97. Pavlides, S. *et al.* The reverse Warburg effect: Aerobic glycolysis in cancer associated fibroblasts and the tumor stroma. *Cell Cycle* **8**, 3984–4001 (2009).
98. Schoppmann, S. F. *et al.* Podoplanin expressing cancer associated fibroblasts are associated with unfavourable prognosis in adenocarcinoma of the esophagus. *Clinical & Experimental Metastasis* **30**, 441–446 (2013).
99. Suzuki, H. *et al.* Podoplanin in cancer cells is experimentally able to attenuate prolymphangiogenic and lymphogenous metastatic potentials of lung squamoid cancer cells. *Mol Cancer* **9**, 287 (2010).
100. Matsuo, Y. *et al.* CXCL8/IL-8 and CXCL12/SDF-1 $\alpha$  co-operatively promote invasiveness and angiogenesis in pancreatic cancer. *Intl Journal of Cancer* **124**, 853–861 (2009).
101. Ganguly, D. *et al.* Cancer-associated fibroblasts: Versatile players in the tumor microenvironment. *Cancers* **12**, 1–35 (2020).

102. Aizawa, T. *et al.* Cancer-associated fibroblasts secrete Wnt2 to promote cancer progression in colorectal cancer. *Cancer Medicine* **8**, 6370–6382 (2019).
103. Straussman, R. *et al.* Tumour micro-environment elicits innate resistance to RAF inhibitors through HGF secretion. *Nature* **487**, 500–504 (2012).
104. Lamprecht, S. *et al.* Teaming Up for Trouble: Cancer Cells, Transforming Growth Factor- $\beta$ 1 Signaling and the Epigenetic Corruption of Stromal Naïve Fibroblasts. *Cancers* **10**, 61 (2018).
105. Calvo, F. *et al.* Mechanotransduction and YAP-dependent matrix remodelling is required for the generation and maintenance of cancer-associated fibroblasts. *Nature Cell Biology* **15**, 637–646 (2013).
106. Santolla, M. F. *et al.* G Protein-coupled Estrogen Receptor Mediates the Up-regulation of Fatty Acid Synthase Induced by 17 $\beta$ -Estradiol in Cancer Cells and Cancer-associated Fibroblasts. *Journal of Biological Chemistry* **287**, 43234–43245 (2012).
107. Albanito, L. *et al.* Effects of Atrazine on Estrogen Receptor  $\alpha$  – and G Protein–Coupled Receptor 30–Mediated Signaling and Proliferation in Cancer Cells and Cancer-Associated Fibroblasts. *Environ Health Perspect* **123**, 493–499 (2015).
108. Ishii. Fibroblasts associated with cancer cells keep enhanced migration activity after separation from cancer cells: A novel character of tumor educated fibroblasts. *Int J Oncol* **37**, (2010).
109. Erdogan, B. & Webb, D. J. Cancer-associated fibroblasts modulate growth factor signaling and extracellular matrix remodeling to regulate tumor metastasis. *Biochemical Society Transactions* **45**, 229–236 (2017).
110. Sanz-Moreno, V. *et al.* ROCK and JAK1 Signaling Cooperate to Control Actomyosin Contractility in Tumor Cells and Stroma. *Cancer Cell* **20**, 229–245 (2011).
111. Conciatori, F. *et al.* Role of mTOR Signaling in Tumor Microenvironment: An Overview. *IJMS* **19**, 2453 (2018).

112. Barone, I. *et al.* Activation of Farnesoid X Receptor impairs the tumor-promoting function of breast cancer-associated fibroblasts. *Cancer Letters* **437**, 89–99 (2018).
113. Tian, G. & Ren, T. Mechanical stress regulates the mechanotransduction and metabolism of cardiac fibroblasts in fibrotic cardiac diseases. *European Journal of Cell Biology* **102**, 151288 (2023).
114. Kuehlmann, B., Bonham, C. A., Zucal, I., Prantl, L. & Gurtner, G. C. Mechanotransduction in Wound Healing and Fibrosis. *JCM* **9**, 1423 (2020).
115. Levental, K. R. *et al.* Matrix Crosslinking Forces Tumor Progression by Enhancing Integrin Signaling. *Cell* **139**, 891–906 (2009).
116. Balaban, N. Q. *et al.* Force and focal adhesion assembly: a close relationship studied using elastic micropatterned substrates. *Nature Cell Biology* **3**, 466–472 (2001).
117. Meng, Z., Moroishi, T. & Guan, K.-L. Mechanisms of Hippo pathway regulation. *Genes Dev.* **30**, 1–17 (2016).
118. Harvey, K. F., Zhang, X. & Thomas, D. M. The Hippo pathway and human cancer. *Nat Rev Cancer* **13**, 246–257 (2013).
119. Zanconato, F., Cordenonsi, M. & Piccolo, S. YAP and TAZ: a signalling hub of the tumour microenvironment. *Nat Rev Cancer* **19**, 454–464 (2019).
120. Wei, Y. *et al.* YAP/TAZ: Molecular pathway and disease therapy. *MedComm* **4**, e340 (2023).
121. Park, H. W. *et al.* Alternative Wnt Signaling Activates YAP/TAZ. *Cell* **162**, 780–794 (2015).
122. Kim, N. H., Lee, Y. & Yook, J. I. Dishevelving Wnt and Hippo. *BMB Rep.* **51**, 425–426 (2018).
123. Lavie, D., Ben-Shmuel, A., Erez, N. & Scherz-Shouval, R. Cancer-associated fibroblasts in the single-cell era. *Nat Cancer* **3**, 793–807 (2022).
124. Roulis, M. *et al.* Paracrine orchestration of intestinal tumorigenesis by a mesenchymal niche. *Nature* **580**, 524–529 (2020).

125. Affo, S. *et al.* Promotion of cholangiocarcinoma growth by diverse cancer-associated fibroblast subpopulations. *Cancer Cell* **39**, 866-882.e11 (2021).
126. Biffi, G. *et al.* IL1-Induced JAK/STAT Signaling Is Antagonized by TGF $\beta$  to Shape CAF Heterogeneity in Pancreatic Ductal Adenocarcinoma. *Cancer Discovery* **9**, 282–301 (2019).
127. Darby, I. A., Zakuan, N., Billet, F. & Desmoulière, A. The myofibroblast, a key cell in normal and pathological tissue repair. *Cell. Mol. Life Sci.* **73**, 1145–1157 (2016).
128. Nicolas, A. M. *et al.* Inflammatory fibroblasts mediate resistance to neoadjuvant therapy in rectal cancer. *Cancer Cell* **40**, 168-184.e13 (2022).
129. Geng, X. *et al.* Cancer-Associated Fibroblast (CAF) Heterogeneity and Targeting Therapy of CAFs in Pancreatic Cancer. *Front. Cell Dev. Biol.* **9**, 655152 (2021).
130. Elyada, E. *et al.* Cross-Species Single-Cell Analysis of Pancreatic Ductal Adenocarcinoma Reveals Antigen-Presenting Cancer-Associated Fibroblasts. *Cancer Discov* **9**, 1102–1123 (2019).
131. Bartoschek, M. *et al.* Spatially and functionally distinct subclasses of breast cancer-associated fibroblasts revealed by single cell RNA sequencing. doi:10.1038/s41467-018-07582-3.
132. Froeling, F. E. M. *et al.* Retinoic Acid–Induced Pancreatic Stellate Cell Quiescence Reduces Paracrine Wnt– $\beta$ -Catenin Signaling to Slow Tumor Progression. *Gastroenterology* **141**, 1486-1497.e14 (2011).
133. Sherman, M. H. *et al.* Vitamin D Receptor-Mediated Stromal Reprogramming Suppresses Pancreatitis and Enhances Pancreatic Cancer Therapy. *Cell* **159**, 80–93 (2014).
134. Gieniec, K. A., Butler, L. M., Worthley, D. L. & Woods, S. L. Cancer-associated fibroblasts—heroes or villains? *Br J Cancer* **121**, 293–302 (2019).
135. Ritossa, F. Discovery of the heat shock response. *Cell Stress Chaperones* **1**, 97–98 (1996).

136. Biebl, M. M. & Buchner, J. Structure, Function, and Regulation of the Hsp90 Machinery. *Cold Spring Harb Perspect Biol* **11**, a034017 (2019).
137. Schopf, F. H., Biebl, M. M. & Buchner, J. The HSP90 chaperone machinery. *Nature reviews. Molecular cell biology* **18**, 345–360 (2017).
138. Khurana, N. & Bhattacharyya, S. Hsp90, the concertmaster: Tuning transcription. *Frontiers in Oncology* **5**, (2015).
139. Echeverría, P. C., Bernthaler, A., Dupuis, P., Mayer, B. & Picard, D. An Interaction Network Predicted from Public Data as a Discovery Tool: Application to the Hsp90 Molecular Chaperone Machine. *PLOS ONE* **6**, e26044 (2011).
140. Obermann, W. M. J., Sondermann, H., Russo, A. A., Pavletich, N. P. & Hartl, F. U. In Vivo Function of Hsp90 Is Dependent on ATP Binding and ATP Hydrolysis. *The Journal of Cell Biology* **143**, 901–910 (1998).
141. Röhl, A., Rohrberg, J. & Buchner, J. The chaperone Hsp90: changing partners for demanding clients. *Trends in Biochemical Sciences* **38**, 253–262 (2013).
142. Sager, R. A. *et al.* Targeting extracellular Hsp90: A unique frontier against cancer. *Front. Mol. Biosci.* **9**, 982593 (2022).
143. Wayne, N. & Bolon, D. N. Dimerization of Hsp90 Is Required for in Vivo Function. *Journal of Biological Chemistry* **282**, 35386–35395 (2007).
144. Meyer, P. *et al.* Structural and Functional Analysis of the Middle Segment of Hsp90: Implications for ATP Hydrolysis and Client Protein and Cochaperone Interactions. *Molecular Cell* **11**, 647–658 (2003).
145. Harris, S. F., Shiau, A. K. & Agard, D. A. The Crystal Structure of the Carboxy-Terminal Dimerization Domain of htpG, the Escherichia coli Hsp90, Reveals a Potential Substrate Binding Site. *Structure* **12**, 1087–1097 (2004).
146. Hessling, M., Richter, K. & Buchner, J. Dissection of the ATP-induced conformational cycle of the molecular chaperone Hsp90. *Nat Struct Mol Biol* **16**, 287–293 (2009).
147. Baker, J. D., Ozsan, I., Ospina, S. R., Gulick, D. & Blair, L. J. Hsp90 Heterocomplexes Regulate Steroid Hormone Receptors: From Stress

- Response to Psychiatric Disease. *International journal of molecular sciences* **20**, (2018).
148. Wrighton, K. H., Lin, X. & Feng, X.-H. Critical regulation of TGF $\beta$  signaling by Hsp90. *Proceedings of the National Academy of Sciences* **105**, 9244–9249 (2008).
  149. García, R. *et al.* Extracellular heat shock protein 90 binding to TGF $\beta$  receptor I participates in TGF $\beta$ -mediated collagen production in myocardial fibroblasts. *Cellular Signalling* **28**, 1563–1579 (2016).
  150. Hunter, M. C. *et al.* Hsp90 Binds Directly to Fibronectin (FN) and Inhibition Reduces the Extracellular Fibronectin Matrix in Breast Cancer Cells. *PLOS ONE* **9**, e86842 (2014).
  151. Cheng, C.-F. *et al.* Transforming Growth Factor  $\alpha$  (TGF $\alpha$ )-Stimulated Secretion of HSP90 $\alpha$ : Using the Receptor LRP-1/CD91 To Promote Human Skin Cell Migration against a TGF $\beta$ -Rich Environment during Wound Healing. *Molecular and Cellular Biology* **28**, 3344–3358 (2008).
  152. Picard, D. Hsp90 invades the outside. *Nat Cell Biol* **6**, 479–480 (2004).
  153. Lancaster, G. I. & Febbraio, M. A. Exosome-dependent Trafficking of HSP70: A NOVEL SECRETORY PATHWAY FOR CELLULAR STRESS PROTEINS\*. *Journal of Biological Chemistry* **280**, 23349–23355 (2005).
  154. Lees-Miller, S. P. & Anderson, C. W. Two human 90-kDa heat shock proteins are phosphorylated in vivo at conserved serines that are phosphorylated in vitro by casein kinase II. *Journal of Biological Chemistry* **264**, 2431–2437 (1989).
  155. Marzec, M., Eletto, D. & Argon, Y. GRP94: An HSP90-like protein specialized for protein folding and quality control in the endoplasmic reticulum. *Biochimica et Biophysica Acta (BBA) - Molecular Cell Research* **1823**, 774–787 (2012).
  156. Altieri, D. C., Stein, G. S., Lian, J. B. & Languino, L. R. TRAP-1, the mitochondrial Hsp90. *Biochimica et Biophysica Acta (BBA) - Molecular Cell Research* **1823**, 767–773 (2012).
  157. Maiti, S. & Picard, D. Cytosolic Hsp90 Isoform-Specific Functions and Clinical Significance. *Biomolecules* **12**, 1166 (2022).

158. Millson, S. H. *et al.* Expressed as the sole Hsp90 of yeast, the  $\alpha$  and  $\beta$  isoforms of human Hsp90 differ with regard to their capacities for activation of certain client proteins, whereas only Hsp90 $\beta$  generates sensitivity to the Hsp90 inhibitor radicicol: Human Hsp90 $\alpha$  and Hsp90 $\beta$  expressed in yeast. *FEBS Journal* **274**, 4453–4463 (2007).
159. Kim, S.-H. *et al.* High-level expression of Hsp90 $\beta$  is associated with poor survival in resectable non-small-cell lung cancer patients. *Histopathology* **67**, 509–519 (2015).
160. Meng, J. *et al.* Hsp90 $\beta$  promoted endothelial cell-dependent tumor angiogenesis in hepatocellular carcinoma. *Mol Cancer* **16**, 72 (2017).
161. Voss, A. K., Thomas, T. & Gruss, P. Mice lacking HSP90 $\beta$  fail to develop a placental labyrinth. *Development* **127**, 1–11 (2000).
162. Echeverría, P. C., Briand, P.-A. & Picard, D. A Remodeled Hsp90 Molecular Chaperone Ensemble with the Novel Cochaperone Aarsd1 Is Required for Muscle Differentiation. *Molecular and Cellular Biology* **36**, 1310–1321 (2016).
163. Jing, R., Duncan, C. B. & Duncan, S. A. A small molecule screen reveals that HSP90 $\beta$  promotes the conversion of iPSC-derived endoderm to a hepatic fate and regulates HNF4A turnover. *Development dev.146845* (2017) doi:10.1242/dev.146845.
164. Zheng, Z.-G. *et al.* Inhibition of HSP90 $\beta$  Improves Lipid Disorders by Promoting Mature SREBPs Degradation via the Ubiquitin-proteasome System. *Theranostics* **9**, 5769–5783 (2019).
165. Zuehlke, A. D., Beebe, K., Neckers, L. & Prince, T. Regulation and function of the human HSP90AA1 gene. *Gene* **570**, 8–16 (2015).
166. Grad, I. *et al.* The Molecular Chaperone Hsp90 $\alpha$  Is Required for Meiotic Progression of Spermatocytes beyond Pachytene in the Mouse. *PLoS ONE* **5**, e15770 (2010).
167. Quanz, M. *et al.* Heat Shock Protein 90 $\alpha$  (Hsp90 $\alpha$ ) Is Phosphorylated in Response to DNA Damage and Accumulates in Repair Foci. *Journal of Biological Chemistry* **287**, 8803–8815 (2012).
168. Pennisi, R., Antocchia, A., Leone, S., Ascenzi, P. & di Masi, A. Hsp90 $\alpha$  regulates ATM and NBN functions in sensing and repair of DNA double-strand breaks. *The FEBS Journal* **284**, 2378–2395 (2017).

169. Eustace, B. K. *et al.* Functional proteomic screens reveal an essential extracellular role for hsp90 $\alpha$  in cancer cell invasiveness. *Nat Cell Biol* **6**, 507–514 (2004).
170. Li, W. *et al.* Extracellular heat shock protein-90 $\alpha$ : linking hypoxia to skin cell motility and wound healing. *The EMBO Journal* **26**, 1221–1233 (2007).
171. Whitesell, L. & Lindquist, S. L. HSP90 and the chaperoning of cancer. *Nature Reviews Cancer* **5**, 761–772 (2005).
172. Liu, H. *et al.* Plasma HSP90AA1 Predicts the Risk of Breast Cancer Onset and Distant Metastasis. *Front. Cell Dev. Biol.* **9**, 639596 (2021).
173. Kim, S. W. *et al.* Casein Kinase 2 (CK2)-mediated Phosphorylation of Hsp90 $\beta$  as a Novel Mechanism of Rifampin-induced MDR1 Expression. *Journal of Biological Chemistry* **290**, 17029–17040 (2015).
174. Li, Z.-N. & Luo, Y. HSP90 inhibitors and cancer: Prospects for use in targeted therapies (Review). *Oncol Rep* **49**, 6 (2022).
175. Henderson, N. C., Rieder, F. & Wynn, T. A. Fibrosis: from mechanisms to medicines. *Nature* **587**, 555–566 (2020).
176. Peng, Y.-F. *et al.* Heat shock protein 90 inhibitor ameliorates pancreatic fibrosis by degradation of transforming growth factor- $\beta$  receptor. *Cellular Signalling* **84**, 110001 (2021).
177. RuizdelRio, J. *et al.* Profibrotic Role of Inducible Heat Shock Protein 90 $\alpha$  Isoform in Systemic Sclerosis. *The Journal of Immunology* **209**, 38–48 (2022).
178. Cáceres, R. A. *et al.* Reduction of cardiac TGF $\beta$ -mediated profibrotic events by inhibition of Hsp90 with engineered protein. *Journal of Molecular and Cellular Cardiology* **123**, 75–87 (2018).
179. Tomcik, M. *et al.* Heat shock protein 90 (Hsp90) inhibition targets canonical TGF- $\beta$  signalling to prevent fibrosis. *Ann Rheum Dis* **73**, 1215–1222 (2014).
180. Yu, J., Zhang, C. & Song, C. Pan- and isoform-specific inhibition of Hsp90: Design strategy and recent advances. *European Journal of Medicinal Chemistry* **238**, 114516 (2022).

181. Ochel, H.-J., Eichhorn, K. & Gademann, G. Geldanamycin: the prototype of a class of antitumor drugs targeting the heat shock protein 90 family of molecular chaperones. *Cell Stress Chaper* **6**, 105 (2001).
182. Bhatia, S. *et al.* Targeting HSP90 dimerization via the C terminus is effective in imatinib-resistant CML and lacks the heat shock response. *Blood* **132**, 307–320 (2018).
183. Bhatia, S. *et al.* Development of a First-in-Class Small-Molecule Inhibitor of the C-Terminal Hsp90 Dimerization. *ACS Cent. Sci.* **8**, 636–655 (2022).
184. Sontake, V. *et al.* Hsp90 regulation of fibroblast activation in pulmonary fibrosis. *JCI Insight* **2**, (2017).
185. Calvo, F. *et al.* Mechanotransduction and YAP-dependent matrix remodelling is required for the generation and maintenance of cancer-associated fibroblasts. *Nature Cell Biology* **15**, 637–646 (2013).
186. Calvo, F., Hooper, S. & Sahai, E. Isolation and Immortalization of Fibroblasts from Different Tumoral Stages. *BIO-PROTOCOL* **4**, (2014).
187. Kaukonen, R., Jacquemet, G., Hamidi, H. & Ivaska, J. Cell-derived matrices for studying cell proliferation and directional migration in a complex 3D microenvironment. *Nature Protocols* **12**, 2376–2390 (2017).
188. Kopylova, E., Noé, L. & Touzet, H. SortMeRNA: fast and accurate filtering of ribosomal RNAs in metatranscriptomic data. *Bioinformatics* **28**, 3211–3217 (2012).
189. Dobin, A. *et al.* STAR: ultrafast universal RNA-seq aligner. *Bioinformatics* **29**, 15–21 (2013).
190. Patro, R., Duggal, G., Love, M. I., Irizarry, R. A. & Kingsford, C. Salmon provides fast and bias-aware quantification of transcript expression. *Nat Methods* **14**, 417–419 (2017).
191. Smith, T., Heger, A. & Sudbery, I. UMI-tools: modeling sequencing errors in Unique Molecular Identifiers to improve quantification accuracy. *Genome Res.* **27**, 491–499 (2017).

192. Love, M. I., Huber, W. & Anders, S. Moderated estimation of fold change and dispersion for RNA-seq data with DESeq2. *Genome Biol* **15**, 550 (2014).
193. Oughtred, R. *et al.* The BioGRID database: A comprehensive biomedical resource of curated protein, genetic, and chemical interactions. *Protein Science* **30**, 187–200 (2021).
194. Zhang, H. *et al.* TEAD Transcription Factors Mediate the Function of TAZ in Cell Growth and Epithelial-Mesenchymal Transition. *Journal of Biological Chemistry* **284**, 13355–13362 (2009).
195. Kovács, S. A., Fekete, J. T. & Gyórfy, B. Predictive biomarkers of immunotherapy response with pharmacological applications in solid tumors. *Acta Pharmacol Sin* **44**, 1879–1889 (2023).
196. Gyórfy, B. Discovery and ranking of the most robust prognostic biomarkers in serous ovarian cancer. *GeroScience* **45**, 1889–1898 (2023).
197. Gyórfy, B. Survival analysis across the entire transcriptome identifies biomarkers with the highest prognostic power in breast cancer. *Computational and Structural Biotechnology Journal* **19**, 4101–4109 (2021).
198. Cords, L. *et al.* Cancer-associated fibroblast classification in single-cell and spatial proteomics data. *Nat Commun* **14**, 4294 (2023).
199. Chen, Z. *et al.* Single-cell RNA sequencing highlights the role of inflammatory cancer-associated fibroblasts in bladder urothelial carcinoma. *Nat Commun* **11**, 5077 (2020).
200. Wershof, E. *et al.* A FIJI macro for quantifying pattern in extracellular matrix. *Life Science Alliance* **4**, (2021).
201. Lazard, D. *et al.* Expression of smooth muscle-specific proteins in myoepithelium and stromal myofibroblasts of normal and malignant human breast tissue. *Proc. Natl. Acad. Sci. U.S.A.* **90**, 999–1003 (1993).
202. Hanks, S. K. & Polte, T. R. Signaling through focal adhesion kinase. *BioEssays* **19**, 137–145 (1997).

203. Tamada, M., Sheetz, M. P. & Sawada, Y. Activation of a Signaling Cascade by Cytoskeleton Stretch. *Developmental Cell* **7**, 709–718 (2004).
204. Park, D. *et al.* Extracellular matrix anisotropy is determined by TFAP2C-dependent regulation of cell collisions. *Nat. Mater.* **19**, 227–238 (2020).
205. Zhang, Z., Zhang, Y. & Zhang, R. P4HA3 promotes clear cell renal cell carcinoma progression via the PI3K/AKT/GSK3 $\beta$  pathway. *Med Oncol* **40**, 70 (2023).
206. Ma, Z. *et al.* Interferon-dependent SLC14A1+ cancer-associated fibroblasts promote cancer stemness via WNT5A in bladder cancer. *Cancer Cell* **40**, 1550-1565.e7 (2022).
207. Hirashima, T. *et al.* Wnt5a in cancer-associated fibroblasts promotes colorectal cancer progression. *Biochemical and Biophysical Research Communications* **568**, 37–42 (2021).
208. Ray, A. *et al.* Anisotropic forces from spatially constrained focal adhesions mediate contact guidance directed cell migration. *Nature Communications* **8**, (2017).
209. Strand, D. W. *et al.* TGF- $\beta$  induction of FGF-2 expression in stromal cells requires integrated Smad3 and MAPK pathways.
210. Grad, I. *et al.* The Molecular Chaperone Hsp90 $\alpha$  Is Required for Meiotic Progression of Spermatocytes beyond Pachytene in the Mouse. *PLoS ONE* **5**, e15770 (2010).
211. Fu, M. *et al.* The Hippo signalling pathway and its implications in human health and diseases. *Sig Transduct Target Ther* **7**, 376 (2022).
212. Fetiva, M. C. *et al.* Oncogenic YAP mediates changes in chromatin accessibility and activity that drive cell cycle gene expression and cell migration. *Nucleic Acids Research* **51**, 4266–4283 (2023).
213. Zheng, Y. & Pan, D. The Hippo Signaling Pathway in Development and Disease. *Developmental Cell* **50**, 264–282 (2019).
214. Liu, Y. *et al.* CCT3 acts upstream of YAP and TFCP2 as a potential target and tumour biomarker in liver cancer. *Cell Death Dis* **10**, 644 (2019).

215. Dasgupta, I. & McCollum, D. Control of cellular responses to mechanical cues through YAP/TAZ regulation. *Journal of Biological Chemistry* **294**, 17693–17706 (2019).
216. Lamar, J. M. *et al.* SRC tyrosine kinase activates the YAP/TAZ axis and thereby drives tumor growth and metastasis. *Journal of Biological Chemistry* **294**, 2302–2317 (2019).
217. Zaidi, S. K. *et al.* Tyrosine phosphorylation controls Runx2-mediated subnuclear targeting of YAP to repress transcription. *EMBO J* **23**, 790–799 (2004).
218. Guégan, J.-P. *et al.* Signaling by the tyrosine kinase Yes promotes liver cancer development. *Sci. Signal.* **15**, eabj4743 (2022).
219. Brancolini, C. & Iuliano, L. Proteotoxic Stress and Cell Death in Cancer Cells. *Cancers (Basel)* **12**, (2020).
220. Calderwood, S. K. & Gong, J. Heat Shock Proteins Promote Cancer: It's a Protection Racket. *Trends in Biochemical Sciences* **41**, 311–323 (2016).
221. Zabinsky, R. A., Mason, G. A., Queitsch, C. & Jarosz, D. F. It's not magic – Hsp90 and its effects on genetic and epigenetic variation. *Seminars in Cell & Developmental Biology* **88**, 21–35 (2019).
222. Isaacs, J. S., Xu, W. & Neckers, L. Heat shock protein 90 as a molecular target for cancer therapeutics. *Cancer Cell* **3**, 213–217 (2003).
223. Trieb, K. *et al.* Antibodies to heat shock protein 90 in osteosarcoma patients correlate with response to neoadjuvant chemotherapy. *Br J Cancer* **82**, 85–87 (2000).
224. Birbo, B., Madu, E. E., Madu, C. O., Jain, A. & Lu, Y. Role of HSP90 in Cancer. *IJMS* **22**, 10317 (2021).
225. Miyata, Y., Nakamoto, H. & Neckers, L. The Therapeutic Target Hsp90 and Cancer Hallmarks. *Current Pharmaceutical Design* **19**, 347–365 (2013).
226. Li, W. *et al.* Extracellular Hsp90 (eHsp90) as the Actual Target in Clinical Trials. Intentionally or Unintentionally. in *International Review of Cell and Molecular Biology* vol. 303 203–235 (Elsevier Inc., 2013).

227. Kamal, A. *et al.* A high-affinity conformation of Hsp90 confers tumour selectivity on Hsp90 inhibitors. *Nature* **425**, 407–410 (2003).
228. McCready, J., Sims, J. D., Chan, D. & Jay, D. G. Secretion of extracellular hsp90 $\alpha$  via exosomes increases cancer cell motility: a role for plasminogen activation. (2010).
229. Song, X. & Luo, Y. The regulatory mechanism of Hsp90 $\alpha$  secretion from endothelial cells and its role in angiogenesis during wound healing. *Biochemical and Biophysical Research Communications* **398**, 111–117 (2010).
230. Zuehlke, A. D., Beebe, K., Neckers, L. & Prince, T. Regulation and function of the human HSP90AA1 gene. *Gene* **570**, 8–16 (2015).
231. Liu, W. *et al.* A novel pan-cancer biomarker plasma heat shock protein 90 $\alpha$  and its diagnosis determinants in clinic. *Cancer Science* **110**, 2941–2959 (2019).
232. Liu, H. *et al.* Plasma HSP90AA1 Predicts the Risk of Breast Cancer Onset and Distant Metastasis. *Front. Cell Dev. Biol.* **9**, 639596 (2021).
233. Lillis, A. P., Van Duyn, L. B., Murphy-Ullrich, J. E. & Strickland, D. K. LDL Receptor-Related Protein 1: Unique Tissue-Specific Functions Revealed by Selective Gene Knockout Studies. *Physiological Reviews* **88**, 887–918 (2008).
234. García, R. *et al.* Extracellular heat shock protein 90 binding to TGF $\beta$  receptor I participates in TGF $\beta$ -mediated collagen production in myocardial fibroblasts. *Cellular Signalling* **28**, 1563–1579 (2016).
235. Mbofung, R. M. *et al.* HSP90 inhibition enhances cancer immunotherapy by upregulating interferon response genes. *Nat Commun* **8**, 451 (2017).
236. Song, K.-H. *et al.* HSP90A inhibition promotes anti-tumor immunity by reversing multi-modal resistance and stem-like property of immune-refractory tumors. *Nat Commun* **11**, 562 (2020).
237. Zhang, Y. *et al.* Heat shock protein-90 inhibition alters activation of pancreatic stellate cells and enhances the efficacy of PD-1 blockade in pancreatic cancer. HHS Public Access. *Mol Cancer Ther* **20**, 150–160 (2021).

238. Calderwood, S. K., Gong, J. & Murshid, A. Extracellular HSPs: The Complicated Roles of Extracellular HSPs in Immunity. *Front. Immunol.* **7**, (2016).
239. Fan, C.-S. *et al.* Extracellular HSP90 $\alpha$  Induces MyD88-IRAK Complex-Associated IKK $\alpha$ / $\beta$ -NF- $\kappa$ B/IRF3 and JAK2/TYK2-STAT-3 Signaling in Macrophages for Tumor-Promoting M2-Polarization. *Cells* **11**, 229 (2022).
240. Hou, Q. *et al.* Extracellular Hsp90 $\alpha$  Promotes Tumor Lymphangiogenesis and Lymph Node Metastasis in Breast Cancer. *IJMS* **22**, 7747 (2021).
241. Joshi, S. *et al.* Extracellular HSP90 Machineries Build Tumor Microenvironment and Boost Cancer Progression. (2021) doi:10.3389/fcell.2021.735529.
242. Baker-Williams, A. J. *et al.* Co-chaperones TIMP2 and AHA1 Competitively Regulate Extracellular HSP90:Client MMP2 Activity and Matrix Proteolysis. *Cell Reports* **28**, 1894-1906.e6 (2019).
243. Chakraborty, A., Marie-Eraïne Boel, N. & Edkins, A. L. HSP90 Interacts with the Fibronectin N-terminal Domains and Increases Matrix Formation. doi:10.3390/cells9020272.
244. Li, W., Sahu, D. & Tsen, F. Secreted Heat Shock Protein-90 (Hsp90) in Wound Healing and Cancer. (2011) doi:10.1016/j.bbamcr.2011.09.009.
245. Hance, M. W., Nolan, K. D. & Isaacs, J. S. The double-edged sword: Conserved functions of extracellular Hsp90 in wound healing and cancer. *Cancers* **6**, 1065–1097 (2014).
246. Zhang, J. *et al.* Extracellular HSP90 $\alpha$  Interacts With ER Stress to Promote Fibroblasts Activation Through PI3K/AKT Pathway in Pulmonary Fibrosis. *Front. Pharmacol.* **12**, 708462 (2021).
247. Liu, T., Zhou, L., Xiao, Y., Andl, T. & Zhang, Y. BRAF Inhibitors Reprogram Cancer-Associated Fibroblasts to Drive Matrix Remodeling and Therapeutic Escape in Melanoma. *Cancer Res* **82**, 419–432 (2022).
248. Takahashi, H. *et al.* AKT3 Is a Novel Regulator of Cancer-Associated Fibroblasts in Head and Neck Squamous Cell Carcinoma. *Cancers (Basel)* **13**, (2021).

249. Kim, I., Choi, S., Yoo, S., Lee, M. & Kim, I.-S. Cancer-Associated Fibroblasts in the Hypoxic Tumor Microenvironment. *Cancers (Basel)* **14**, (2022).
250. Dupont, S. *et al.* Role of YAP/TAZ in mechanotransduction. *Nature* **474**, 179–183 (2011).
251. Shahbazi, R. *et al.* Targeting ROCK signaling in health, malignant and non-malignant diseases. *Immunology Letters* **219**, 15–26 (2020).
252. Zanconato, F., Cordenonsi, M. & Piccolo, S. YAP/TAZ at the Roots of Cancer. *Cancer Cell* **29**, 783–803 (2016).
253. Kijima, T. *et al.* HSP90 inhibitors disrupt a transient HSP90-HSF1 interaction and identify a noncanonical model of HSP90-mediated HSF1 regulation. *Scientific Reports* **8**, 6976 (2018).
254. Chen, Y. *et al.* Targeting HSF1 sensitizes cancer cells to HSP90 inhibition. *Oncotarget* **4**, 816–829 (2013).
255. Zou, J., Guo, Y., Guettouche, T., Smith, D. F. & Voellmy, R. Repression of Heat Shock Transcription Factor HSF1 Activation by HSP90 (HSP90 Complex) that Forms a Stress-Sensitive Complex with HSF1. *Cell* **94**, 471–480 (1998).







# Agradecimientos

Dicen que el doctorado es un camino que, además de largo y complicado, normalmente se hace muy solitario. Yo he tenido la inmensa suerte de que mi realidad ha sido totalmente distinta, y esta tesis no habría sido posible sin todas estas personas e instituciones:

Gracias a la Asociación Española Contra el Cáncer (AECC), especialmente a su sede de Cantabria, por concederme la ayuda que ha financiado esta tesis durante 4 años y haberme invitado a tantos eventos que me han ayudado a divulgar este trabajo. Gracias también a todos los voluntarios que colaboran con la AECC, a los pacientes y al resto de asociaciones locales que también aportan su granito de arena. Gracias a vosotros es posible hacer una investigación contra el cáncer de calidad en este país.

Thanks to the European Association for Cancer Research (EACR), who funded my international stay for 3 months at the Institute of Genetics and Cancer (Edinburgh), and the lab of Dr. Alexander von Kriegsheim, for being my hosts during those months. Thank you, Alex, for being such an amazing tutor and for all the help the following months. Thanks also to all the lab members, specially Najeeb, Jair and Amber, for the guidance and help, and for treating me as one of yours.

To my little children from Edinburgh: Zaid, Chartinun, Dan, Chinmayi, Ana, Xinhao, Harold, Lily and Hongfei. You're the kindest people I've ever met. Thank you for adopting me since day one and all the moments we shared. I wish you the best of lucks in your

careers and I'm sure you'll be amazing scientists because you already are amazing people. You know I already have you forever in my skin (literally).

A mi Alaó, la mejor compañera de piso que podía tener y que vio nacer este manuscrito en directo. Tengo claro que sin ti la experiencia de Edimburgo no habría sido tan buena. Eres maravillosa y vas a ser una doctora increíble, porque no hay persona que trabaje y se lo merezca más que tú. Te echo muchísimo de menos.

Gracias al grupo de la Dra. María Caffarel (Biodonosti), por el training en la técnica de la cirugía mamaria en ratones.

Gracias al personal del Animalario del IBBTEC, por su ayuda y su disposición en todo momento.

Gracias a Víctor Manuel Campa, del departamento de microscopía (IBBTEC), por toda tu ayuda estos años con las CDM.

Al laboratorio de la Dra. Ana Victoria Villar Ramos (IBBTEC), en especial a Jorge, David y Helena. Gracias Anavi, por resolver todas nuestras dudas, por tus sugerencias y por tus ánimos todos estos años. Gracias Jorge por introducirme al maravilloso mundo de los ratones y por enseñarme todo lo necesario para llevar la colonia.

Al laboratorio del Dr. Ignacio Varela (IBBTEC), en especial a Laurita y David, por enseñarme a pinchar en la cola, sois unos auténticos cracks. ¡Te echamos muchísimo de menos Laurita! Gracias Nacho por resolver todas mis dudas estos últimos meses y ayudarme con todo el proceso de depósito.

Al laboratorio del Dr. Piero Crespo (IBBTEC), "los Piero", por los anticuerpos, los reactivos, los cristales del WB, los pedidos... En definitiva, por todo el apoyo sin el cual la mitad de los experimentos no habrían salido. En especial gracias a Lorena, por los ánimos, las sugerencias y por preocuparte por mí todos estos años, no solo como evaluadora. Gracias Ana, por tus valiosísimas lecciones de vida todos los días a la hora de comer. Eres mi ejemplo a seguir. Laura, eres la brisilla de poniente que se levanta milagrosamente un día de agosto a las 17:00 en Sevilla a más de 40°C, esa que querrías que fuera para siempre.

Gracias a la que ha sido mi casa durante estos años: laboratorio 01.05 de Microambiente Tumoral, Dr. Fernando Calvo González. Fer, gracias en primer lugar por darme esta oportunidad, por tu guía, tu ayuda y, especialmente, por tu apoyo y tu paciencia, y por darme todo por esta tesis estos últimos meses. Espero haber estado a la altura. Mil millones de gracias a la familia sin la cual nada hubiera sido igual:

Bea, gracias por todos los "tú me has entendido, ¿verdad?". Ya quisiera para mí la mitad de la fuerza y valentía que tú tienes para afrontar las cosas. De mayor quiero ser como tú.

Cata, gracias por ser mi asesora de moda personal, por escucharme y por entenderme. No tengo palabras para explicarte lo esencial que ha sido tu apoyo para mí. No sé cómo habría sobrevivido a estos últimos meses sin ti. Gracias.

Carmen, tienes más calle que un bordillo. Ojalá ir por la vida pisando tan fuerte como lo haces tú (y no me refiero a tus plataformas). Somos los mayores los que tenemos que aprender de ti.

Diane, miarma, thank you for your friendship and for always being there for me, no matter what. I know the future that awaits you is at least as brilliant as you are, and my only hope is to continue to be there to see you shine.

Francesca, no es que hables poco, es que el que no te conoce no sabe que solo necesitas un suspiro profundo para decirlo todo. Gracias por los ataques de risa espontáneos en mitad del lab.

Javi, si solo pudiera pedir un deseo, sería encontrarme a alguien como tú en cada trabajo que tenga. Eres la persona de la que más he aprendido. Gracias por ser tan buen profe y tan buen compañero.

María, eres una reina con todas las letras, y aunque hayas nacido en el sitio y la cuenta bancaria equivocadas, nos haces la vida más divertida al resto de los mortales. Por alegrarme los días desde el primero que llegué, gracias, ¡loca!

Miguel, a pesar del poco respeto que te tenemos, en realidad sabemos que no te merecemos. Eres el mejor en lo tuyo, o sea, en la bioinformática y en contar tu vida como si fuera una sitcom. Ojalá seguir teniendo algún cameo en las próximas temporadas.

Patri, mi compañera de aduanas, la que siempre dice que sí a todos mis caprichos, la que siempre está cuando la necesito, la que escucha, la que aconseja, la que no te deja caer pase lo que pase. Las gracias se quedan muy cortas.

Gracias a mis amigos. A los incondicionales: Andrea, Marcos, Lucía, Pedro, por preocuparos por mí e interesaros por esto, aunque no entendáis muy bien lo que hago. Andrea, no tengo dudas de que en un futuro no muy lejano serás tú la que esté escribiendo estas palabras. A mis Cinnamomum, por estar siempre, aunque sea de lejos. Y a mis "et al.": Andrea, Laura y María Elena. La vida es simplemente mejor porque os tengo a vosotras.

A mis amigos Irene y Alonso, por ser mi sur en el norte. Sin vosotros no sé cómo hubiera sobrevivido todos estos años a 800 km de casa.

A Toñi y Eduardo, por todos los "¿y cómo está Silvia?" que escuché desde la otra habitación y que no pude contestar por estar delante del ordenador. Gracias.

Gracias a mi familia. A mis abuelas, a las que es un auténtico privilegio tener.. A mis padres, que me apoyaron a pesar de las dudas y, cuando ya no las hubo, lo hicieron con más fuerza todavía. Sin vuestro cariño y apoyo nunca hubiera llegado hasta aquí. A mi hermana, créeme, soy yo la que está orgullosa de ti.

Y a mis compañeros de vida. A mi gatito–soporte–emocional, Miyo, por echarse siempre a dormir en la cama detrás de mí mientras escribía, y llamarme con su patita a la hora de comer o cenar, por si se me olvidaba. Y a mi marido, Eduardo, por ayudarme a cumplir todos mis sueños desde el día que te conocí y todos los sacrificios que has tenido que hacer para ello. Por sufrir esta tesis conmigo cada día y cuidar de mí. Por haber reído conmigo cada momento, llorado conmigo cada lágrima y preocupado por cada problema como si también fuera tuyo. Me pasaré el resto de la vida intentando devolverte todo lo que me das.



